Site Characterization for CO_2 Storage from Coal-fired Power Facilities in the Black Warrior Basin of Alabama

Type of Report:	Final
Reporting Period Start Date:	2010
Reporting Period End Date:	August 31, 2013
Principal Author(s)	Peter E. Clark, Oklahoma State University Jack Pashin, Oklahoma State University Eric Carlson, University of Alabama Andrew Goodliffe, University of Alabama Marcella McIntyre-Redden, Geological Survey of Alabama Steven D. Mann, Geological Survey of Alabama Mason Thompson, Rice University
Report Issue Date	11/29/2013
DOE Award Number:	DE-FE0001910
Submitting Organization:	University of Alabama 152 Rose Administration Building Tuscaloosa, AL 35487-0104 Geological Survey of Alabama Rice University
Submitted to:	U.S. Department of Energy National Energy Technology Laboratory DOE Project Manager, Karen Kluger

DISCLAIMER

ABSTRACT

Coal-fired power plants produce large quantities of carbon dioxide. In order to mitigate the greenhouse gas emissions from these power plants, it is necessary to separate and store the carbon dioxide. Saline formations provide a potential sink for carbon dioxide and delineating the capacity of the various known saline formations is a key part of building a storage inventory. As part of this effort, a project was undertaken to access the storage capacity of saline reservoirs in the Black Warrior Basin of Alabama.

This basin has been a productive oil and gas reservoir that is well characterized to the west of the two major coal-fired power plants that are north of Birmingham. The saline zones were thought to extend as far east as the Sequatchie Anticline which is just east of the power plants. There is no oil or gas production in the area surrounding the power plants so little is known about the formations in that area.

A geologic characterization well was drilled on the Gorgas Power Plant site, which is the farthest west of two power plants in the area. The well was planned to be drilled to approximately 8,000 feet, but drilling was halted at approximately 5,000 feet when a prolific freshwater zone was penetrated. During drilling, a complete set of cores through all of the potential injection zones and the seals above these zones were acquired. A complete set of openhole logs were run along with a vertical seismic profile (VSP). Before drilling started two approximately perpendicular seismic lines were run and later correlated with the VSP.

While the zones that were expected were found at approximately the predicted depths, the zones that are typically saline through the reservoir were found to be saturated with a light crude oil. Unfortunately, both the porosity and permeability of these zones were small enough that no meaningful hydrocarbon production would be expected even with carbon dioxide flooding.

While this part of the basin was found to be unsuitable for carbon dioxide injection, there is still a large storage capacity in the basin to the west of the power plants. It will, however, require pipeline construction to transport the carbon dioxide to the injection sites.

TABLE OF CONTENTS

Illustrations

Tables

EXECUTIVE SUMMARY

The Black Warrior Basin of Alabama contains two coal-fired power facilities that emit more than 27 megatonnes (Mt) of CO_2 annually. Options for management of these emissions include the implementation of CCUS technology, and so the a multi-year evaluation of the geologic storage potential in the basin was conducted. Activities included regional evaluation of capacity, the development of an exploratory borehole and test site at the Gorgas steam plant, reservoir simulation, containment analysis, and risk assessment. Results of this program were synthesized to identify best practices that can be applied to sedimentary basins in similar geologic settings, particularly the Paleozoic basins of the eastern United States.

Opportunities for geologic storage exist in Cambrian through Devonian carbonate rocks and in Mississippian-Pennsylvanian siliciclastic rocks. Volumetric assessment of storage capacity indicates that the basin has gigaton-class storage potential. The P_{50} storage estimate for carbonate rocks of the Cambrian-Ordovician Knox Group is about 650 Mt, and an additional 812 Mt of capacity was assessed in Ordovician-Devonian carbonate rocks of the Stones River Group, Red Mountain Formation, and an unnamed Devonian limestone interval. About 380 Mt of capacity was identified in Mississippian sandstone and carbonate that includes the major conventional oil and gas reservoirs in the basin. Nearly half of the capacity in the basin is in Pennsylvanian-age sandstone units of the lower Pottsville Formation, which is estimated to P_{50} capacity exceeding 1,350 Mt. Although regional capacity is high, however, widespread implementation of CCUS technology will need to employ drilling and well completion techniques designed for tight, heterogeneous formations in which natural fracture systems account for a significant portion of the available storage and injectivity.

The Gorgas #1 borehole was drilled to a depth of 4,915 feet and reached total depth in the Copper Ridge Dolomite of the Knox Group. A diverse geophysical log suite was obtained from the well, and sidewall cores and whole cores were retrieved from selected intervals in the Cambrian-Pennsylvanian section. Results of core analysis indicate that porosity and permeability are anomalously low in the Gorgas area. Low-salinity water was discovered at depth, indicating at a protected aquifer may exist in the Copper Ridge Dolomite that was fed by meteoric recharge in the Appalachian thrust belt. Analysis of reservoir fluids indicates that saline water is present in younger strata and that a large oil resource is in the Hartselle Sandstone. In addition, the cores revealed many open natural fractures in the Hartselle, which can be characterized as a fractured tight oil prospect. Oil saturation of the Hartselle Sandstone in the Gorgas #1 borehole, the amount of oil in place is estimated to be 9,000 barrels per acre, or 360,000 barrels per 40-acre tract of land. Directional drilling may be help unlock this oil resource, and CO_2 flooding may be promising as a technology that can mobilize the oil.

Simulation activities focused on modeling CO_2 injection in the Knox Group. A combination of continuum and DFN modeling was used, and new techniques were developed to merge discrete element models with cellular flow models. Results indicate that natural fracturing is a major source of permeability anisotropy in the Knox Group. This anisotropy affects the geometry of the injected CO_2 plume, as well as the pressure footprint associated with the plume. Zones containing weakly fractured carbonate function as confining units at the scale of the injection modeling, although the sealing integrity of these zones over geologic timespans is unknown.

Analysis of shale properties helped identify factors that influence geologic containment of CO_2. Shale seals in the Gorgas area have a range of compositional, porosity, and fluid saturation values; the shale units have nanodarcy-type permeability and thus major sealing capacity. The

principal factor influencing shale permeability is total organic carbon, and organic-lean shale forms better reservoir seals than organic-rich shale. Sealing capacity is enhanced by adsorption, which serves as a buffer where formations lie above capillary entry pressure. An important outcome of this research is that hydrolysis of CO_2 by clay-bound water augments monolayer storage by adsorption.

Five basic geologic risk factors were identified for the Black Warrior Basin. These are capacity, injectivity, seals, faults, and risk to underground sources of drinking water (USDWs). Although regional capacity is high, it is concentrated in tight formations in which natural fractures support injectivity. Multiple widespread shale units make seal risk negligible in the Black Warrior Basin, and normal faults pose the most serious containment risk in the region. Therefore, sequestration wells should be located in internally coherent structural panels, and plume modeling should be used to ensure that CO_2 does not migrate into fault zones at the millennial time scale. Identification of the deep USDW in the Copper Ridge Dolomite precludes commercial injection in the Cambrian-Ordovician carbonate in the Gorgas area, but opportunities exist farther southwest where Knox strata contain saline fluid. The widespread shale units in the Mississippian-Pennsylvanian section are proven reservoir seals the protect shallow USDWs. Hence, minimizing fault risk is a central aspect of aquifer protection in the Black Warrior basin.

INTRODUCTION

The Black Warrior basin of Alabama contains two major coal-fired power plants that emitted 27.45 megatonnes (Mt) of CO_2 to the atmosphere in 2008 from the combustion of pulverized coal (Figure 1). These are the William C. Gorgas (7.53 Mt) and James. H. Miller, Jr. (19.92 Mt) electric generating plants, which serve the Birmingham-Tuscaloosa corridor—an area of significant population growth and industrial development. The Black Warrior basin of Alabama hosts diverse coal, coalbed methane, and conventional oil and gas resources and has significant CO_2 storage capacity (e.g., Pashin et al., 2004, 2009; Pashin and Payton, 2005). However, only the capacity of coal seams has been assessed in detail, and this assessment indicates that only about 6 years of storage capacity exists in proven reservoir coal seams at current emission rates (Pashin et al., 2004, 2009). Therefore, additional capacity must be identified and validated to ensure that a long-term carbon storage solution can be deployed as a low-carbon option for these power plants.

Multiple stacked saline formations that include mature conventional petroleum reservoirs are in the Mississippian-Pennsylvanian section of the Black Warrior basin, and most of the saline formations underlie the Gorgas and Miller steam plants (e.g., Thomas, 1972, 1988; Pashin, 1993, 1994) (Figures 1, 2). The diverse saline formations in the region indicate significant potential for sequestration of CO_2 emissions. Saline reservoirs provide the greatest potential for long-term storage, particularly in the immediate area of the steam plants, and additional opportunities exist in mature oil and gas fields, which are west of the plants. Most oil fields in the Black Warrior basin, although of limited size, contain oil with API gravity higher than 30° and are thus prospective for miscible CO_2 flooding (Pashin and Payton, 2005). Pressure maintenance through injection of CO_2 in the aging conventional gas fields of the Black Warrior basin also may add

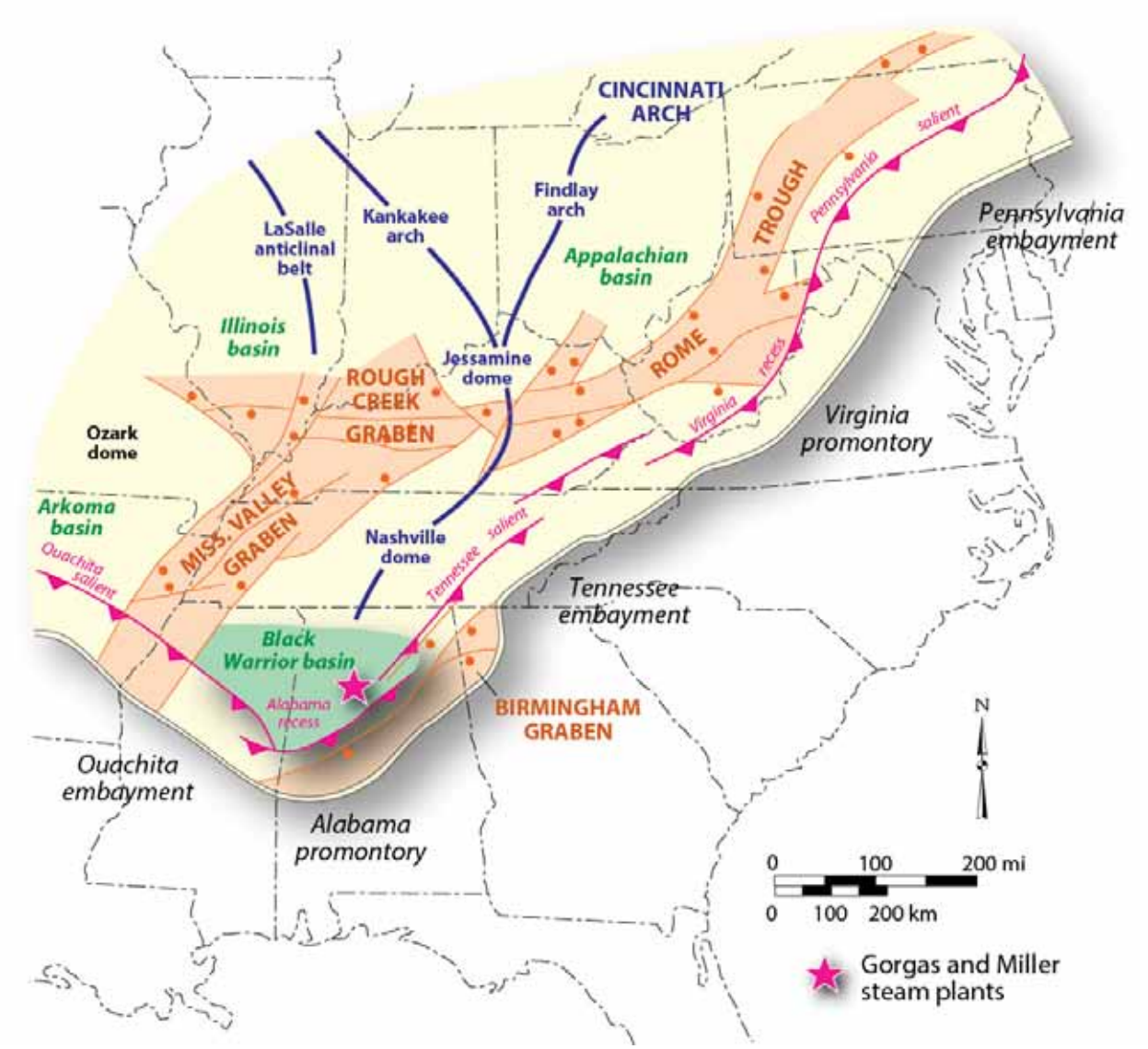

Figure 1.—Regional tectonic setting of the Black Warrior Basin (modified from Thomas, 1988).

value to carbon storage operations by prolonging the life of these fields. Multiple regional seals, moreover, exist within the carbon sequestration target interval and protect underground sources of drinking water in the upper part of the Pennsylvanian-age coal-bearing section.

In partnership with the University of Alabama (UA), Rice University, Southern Company Services, and Schlumberger Carbon Services, and the Southeastern Regional Carbon Sequestration Partnership (SECARB), the Geological Survey of Alabama (GSA) participated in

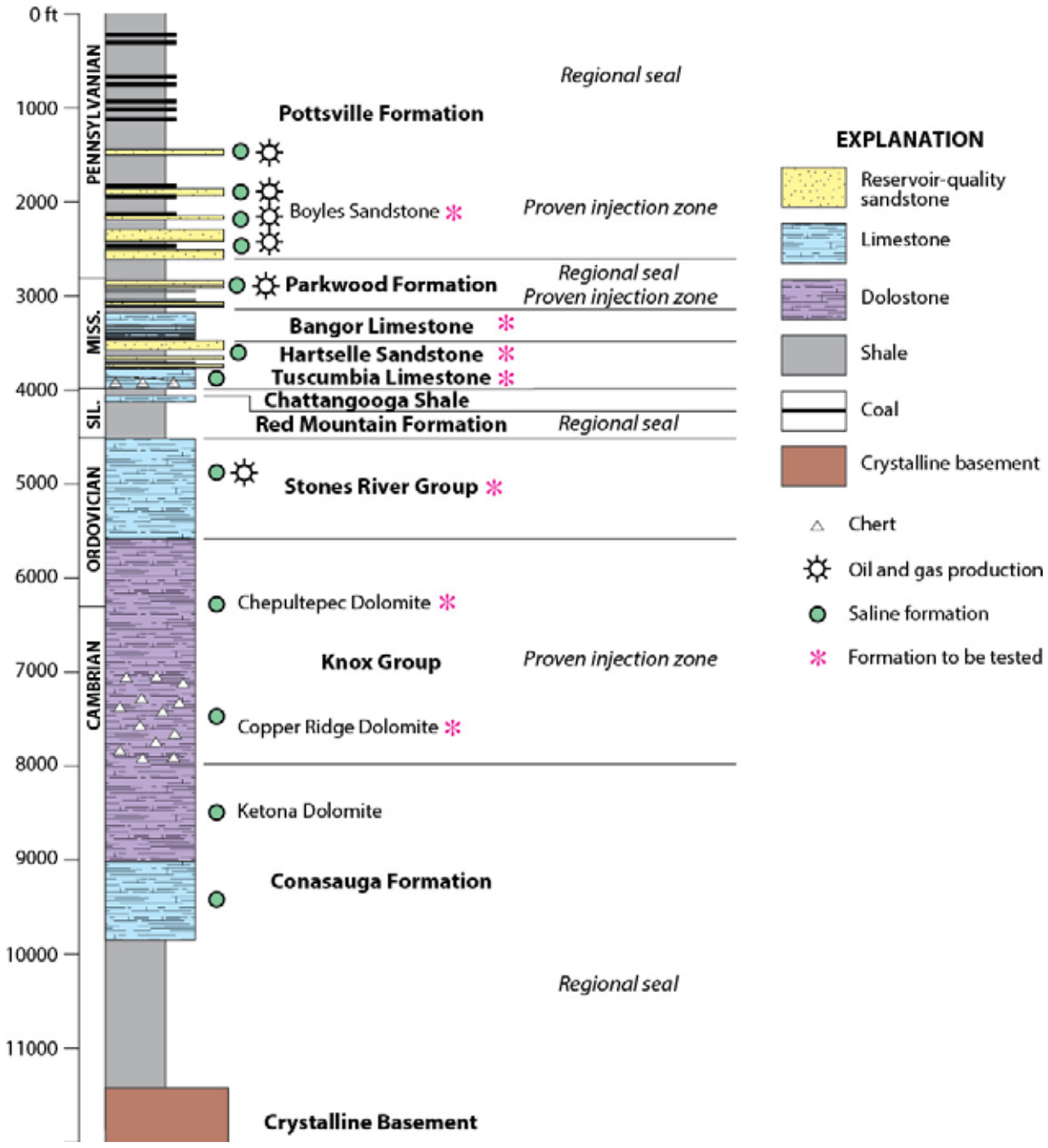

Figure 2.—Generalized stratigraphic column showing major Paleozoic formations in the Black Warrior Basin of Alabama.

a four-year study to determine the capacity and viability of carbon storage in saline formations and mature conventional hydrocarbon reservoirs in the Black Warrior basin of Alabama. This research was funded as part of the American Reinvestment and Recovery Act (ARRA) and is part of a major initiative to identify and implement next-generation energy infrastructure.

This study employed a multidisciplinary approach that was directed toward quantifying the regional significance of saline formations and mature hydrocarbon reservoirs. This program included the development and characterization of a test site at Plant Gorgas (Figure 3), which Alabama Power - a Southern Company - made available. This plant, in service since 1917, was chosen because flue-gas desulfurization (FGD) units facilitate application of carbon capture, utilization, and storage (CCUS) technology; local geology is highly favorable; and no deep wells are nearby to pose leakage risk. Site characterization included drilling and coring a test well; quantifying reservoir properties using an array of petrophysical and geophysical techniques; and analyzing seal integrity and containment using petrophysical, geophysical, well testing, and simulation techniques.

The results of these activities were used to assess risks associated with geologic carbon storage in the Black Warrior basin and to develop a regional plan for the application of carbon sequestration technology to the Gorgas and Miller steam plants. This project has contributed greatly to the knowledge of best practices for storage site selection and site characterization. Accordingly, this report includes a best practices manual on the characterization of stacked geologic formations within well-consolidated Paleozoic strata of the southeastern U.S. The knowledge gained from this project, moreover, is an important component of a national framework for site characterization. A vigorous technology transfer program was conducted

Figure 3.—Photograph of the William Crawford Gorgas Electrical Generating Plant showing location of the Gorgas #1 borehole (photo courtesy of Alabama Power Company).

throughout this study to ensure stakeholder input on the progress and direction of the project and to facilitate timely dissemination of results to stakeholders and the public at large.

This report begins with a discussion of the approach and methodology used in this investigation. The discussion then focuses on the regional significance of this research, which includes delineation of the regional geologic framework and assessment of storage capacity and injectivity. The next section discusses characterization of the test site at Plant Gorgas. The results of regional analysis and test site characterization were used to analyze the containment potential of the geologic formations in the Black Warrior Basin of Alabama and to assess risks associated with the implementation of CCUS technology in the region. The results of all project activities

were synthesized into a best practices manual that identifies the characterization techniques that proved useful, as well as the key lessons learned from the project.

APPROACH AND METHODOLOGY

An array of scientific methods was used to assess and characterize the CO_2 storage potential in the Black Warrior Basin and at the Gorgas test site. Regional assessment required the compilation and analysis of the available subsurface data in the Black Warrior basin of Alabama (Figure 4). These data include geophysical well logs, core analyses, published records, and the file data of the GSA and the State Oil and Gas Board of Alabama (OGB). Header data, including permit number, fee name, well location, structural datum, and bottom-hole temperature, were recorded from the geophysical well logs. The data were compiled in a database using Petra software, which is a petroleum-based geographic information system that is designed specifically to store and analyze subsurface data.

Well logs were correlated, stratigraphic boundaries were identified, and stratigraphic tops were entered into the Petra database. Porosity and permeability data from 1,495 conventional core analyses in the GSA and OGB files were compiled from Mississippian and Pennsylvanian strata. These data were analyzed statistically to determine mean porosity for the Mississippian and Pennsylvanian reservoirs. Porous zones also were identified using spontaneous potential, resistivity, micrologs, density porosity, neutron porosity, and photoelectric logs. These logs were used to define CO_2 storage reservoir zones, and a porosity cutoff of 3 percent was used to delimit zones that have potential to store CO_2 over geologic time. Data from 1,552 wells (Figure 4) were used to construct grids and maps of measured depth, net reservoir thickness, and geologic structure. Data were organized and maps were gridded and contoured using Petra software,

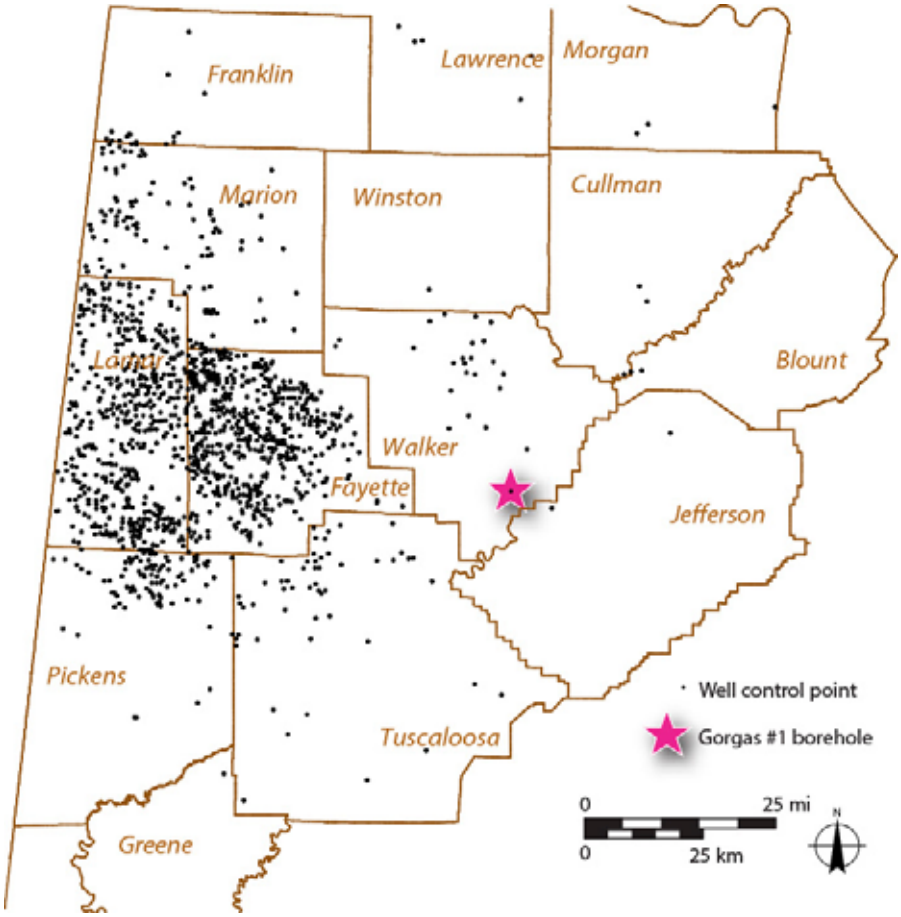

Figure 4.—Map showing well control used to assess CO_2 storage capacity in Paleozoic strata of the Black Warrior Basin.

which is widely used in the oil and gas industry to organize subsurface data, construct maps and cross sections, and develop hydrocarbon prospects.

For each unit only wells with tops below 2,500 feet below sea level were used to construct the measured depth and thickness maps. Grids were constructed using the least squares method and a grid cell size of 1,320 feet. The measured depth grid was then exported to the ArcMap software package to be converted into a polygon showing the extent of the potential reservoir. The polygons were then used to quantify the storage capacity of each pay zone on the basis of areal extent, average reservoir thickness, porosity, CO_2 density, and storage efficiency (P_{15}, P_{50}, and P_{85}) using the assessment methods described by NETL (2010).

Activities at the Gorgas test site included drilling, logging, and coring the Gorgas #1 borehole. The Gorgas #1 is an exploratory borehole that was drilled to increase understanding of the storage capacity and seal integrity of strata in the Black Warrior Basin. The borehole was drilled using an air-foam system and hammer bit until a significant quantity of water was encountered at a depth of 4,855 feet. The remainder of the well was drilled with a rotary bit and drilling mud, and the well reached total depth of 4,915 feet.

Drill cuttings were captured at 10- to 30-foot intervals, and a mud log was compiled by Geosearch Logging, Incorporated. Washed cuttings were described and are stored in the core warehouse of the Geological Survey of Alabama. A diverse suite of geophysical well logs was run by Schlumberger Carbon Services, which include a basic suite of spontaneous potential (SP), resistivity, caliper, gamma ray, density porosity, neutron porosity, and sonic logs. Advanced logs were run, including a formation microimager (FMI) log an electron capture spectroscopy (ECS) log, and a variety of other computed montage logs that display automated interpretations of mineralogy, rock types, and reservoir fluids.

Cores were retrieved from numerous stratigraphic intervals in the wellbore to characterize potential geologic carbon sinks and sealing strata. H-gauge (4-inch diameter) cores were retrieved from selected stratigraphic intervals between depths of 1,220 and 3,013 feet using a drill-stem barrel operated by Devilbiss Coring Service. Rotary sidewall cores were recovered by Schlumberger Carbon Services from a range of stratigraphic units between depths of 1,098 and 4,820 feet. All drill-stem and sidewall cores were described and logged using standard laboratory procedures for the determination of rock type, grain size, texture, sedimentary structures, fossil content, and natural fractures. Billets were cut from the cores, and thin sections were made to

perform basic petrographic analysis of rock composition and fabric. Thin sections were stained with alizarin red to identify calcite and with cobalt nitrite to identify feldspar.

In sandstone and carbonate units, 1-inch core plugs were recovered from the H-gauge cores at 1-foot intervals. These and the sidewall cores were sent to PTS Laboratories for conventional (i.e., Dean-Stark) core analysis, which included the determination of grain density, porosity, air permeability, oil saturation, water saturation, and sample fluorescence. In shale units, 4-inch core segments were sent to TerraTek for tight rock analysis. This analytical suite includes quantitative x-ray diffraction analysis to determine mineralogy, determination of total organic carbon (TOC) content, rock-eval pyrolysis, pressure-decay permeability analysis, and Dean-Stark analysis to determine grain density, porosity, and fluid saturation.

Simulation activities at the GSA focused on modeling the influence of natural fractures on geologic storage. Fracture architecture was analyzed using outcrop data and an interpretation of the FMI log from the Gorgas #1 borehole. Discrete fracture network (DFN) models were then built using DFNModeler software (see Pashin et al., 2008). The main challenge was developing multi-phase flow simulations that are not only capable of integrating complex, multi-layer DFN models with cellular models of matrix porosity and permeability, but also provide computational results quickly and efficiently. To meet this goal, a method was developed that analyzes the variability of permeability tensors across a range of cell sizes. This approach proved useful for optimizing cell dimensions to simulate fracture-related reservoir heterogeneity while maintaining adequate computational performance when modeling flow in large geologic models. Once the optimal grid size was determined, the geologic model, boundary conditions, fluid properties, and injection rates were parameterized, and the flow models were run.

Containment analysis concentrated on characterization of shale sealing properties, the distribution of candidate CO_2 sinks relative to reservoir seals, and the influence of fracture architecture on sink and seal integrity. This analysis required integration of the sedimentologic, structural, and petrologic data collected during the study to develop a conceptual framework of the geologic factors affecting containment. The analysis was further informed by the results of simulation, which provide graphic representations of plume geometry, reservoir heterogeneity, and reservoir integrity.

Risk assessment centered on the technical risks associated with geologic CO_2 storage in the Black Warrior Basin, and the procedure used is similar to those outlined by DNV (2003), IEA (2009), and NETL (2013). Individual risks associated with reservoir properties and seal properties (e.g., porosity, permeability, heterogeneity, fracturing, faulting, geochemical processes, and leakage mechanisms) were identified and described. Risks were then compiled in a matrix that ranks each risk by severity and probability. This approach enabled the identification of unacceptable risks that must be addressed before proceeding with storage operations and minor risks that, while of concern, do not necessarily impede the implementation of geologic storage technology. The result of this analysis is a ranking of storage risks and the development of a risk management strategy that identifies specific mitigation and remediation approaches that may be effective for mitigating or eliminating those risks.

REGIONAL SIGNIFICANCE

Opportunities for geologic carbon storage in the Black Warrior Basin are diverse in terms of geographic distribution, rock type, geologic age, depositional environment, structural setting, and reservoir characteristics. Therefore, assessing these opportunities requires a regional approach.

This section begins by characterizing the basic geologic framework and continues with a discussion of the reservoir and sealing properties of the major geologic units in the basin. The section concludes with assessment of the storage capacity and injectivity of each prospective CO_2 sink in the basin.

Geologic Framework

Structural and tectonic framework.—The Black Warrior Basin is a late Paleozoic foreland basin that formed adjacent to the syntaxis of the Appalachian and Ouachita orogenic belts (Figure 1). These orogenic belts parallel the margins of the Alabama promontory, which was a protuberance of ancestral North America that formed during late Precambrian-Early Cambrian Iapetan rifting (e.g., Thomas, 1988, 1991, 1995). The southeastern margin of the basin parallels the Appalachian thrust belt, whereas the southwestern margin parallels the Ouachita thrust belt. The basin also is framed partially by two northeast-trending Iapetan rifts: the Mississippi Valley graben and the Birmingham graben. The Mississippi Valley graben bounds the northwestern edge of the basin in Mississippi and strikes at a high angle to the Ouachita orogenic belt. By comparison, the Birmingham graben follows the southeastern margin of the Black Warrior Basin in Alabama. The graben parallels regional strike of the Appalachian orogen and underlies a large part of the thrust belt (Thomas, 1985, 2001; Thomas and Bayona, 2005).

Regional dip of the Paleozoic strata within the basin is southwest toward the Ouachita orogenic belt and along the regional plunge of the Appalachian orogenic belt. In the broadest sense, the basin can be defined as a southwest-dipping homocline. A structural contour map of the top of the Mississippian-age Tuscumbia Limestone in Alabama shows that the homocline is broken by a series of normal faults that generally strike northwest (Figure 5). These fault

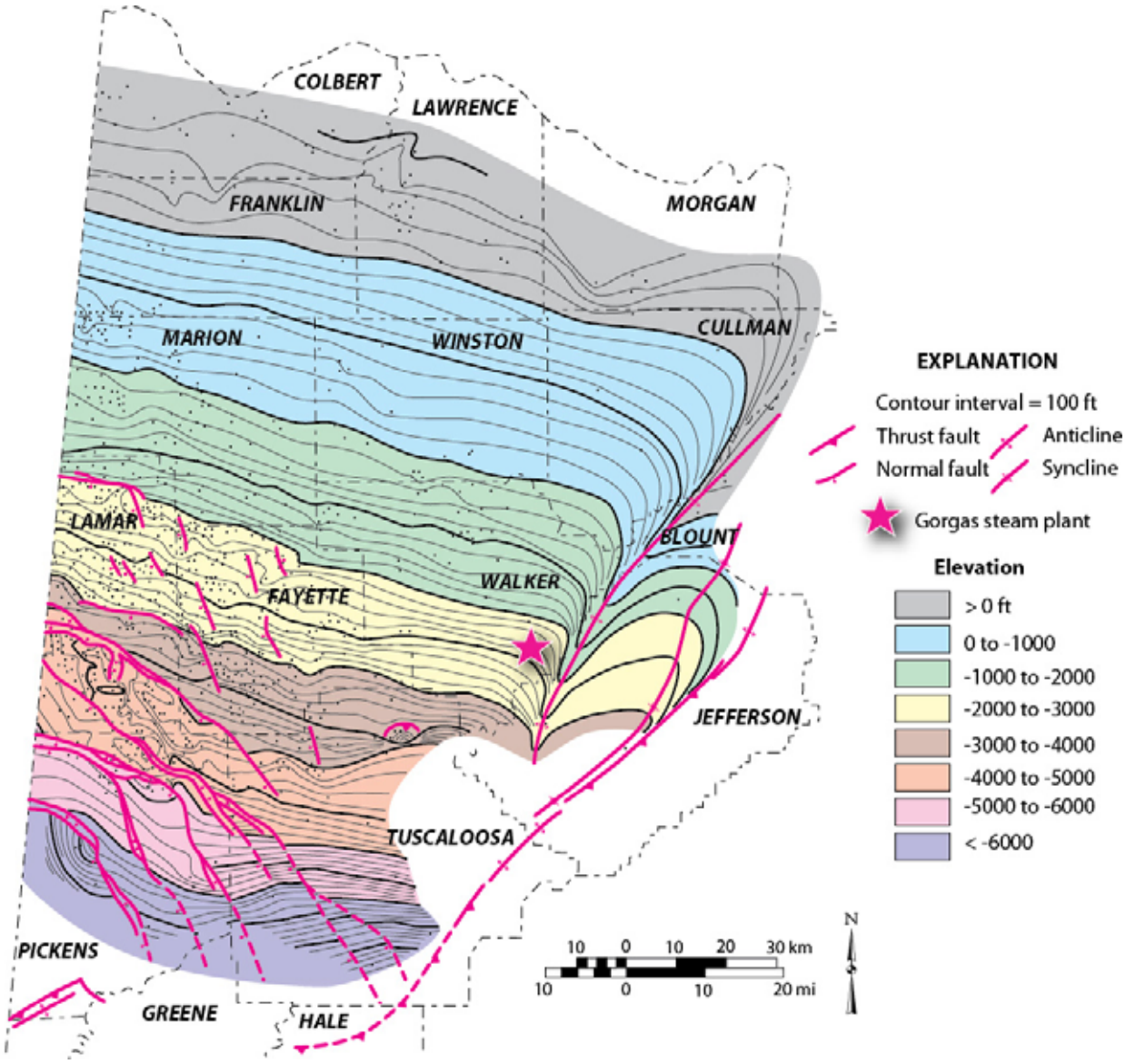

Figure 5.—Structural contour map of the top of the Tuscumbia Limestone in the Black Warrior Basin of Alabama showing locations of major folds and faults (modified from Pashin, 1993).

networks are geometrically complex and include thick- and thin-skinned structural elements; they are thought to have formed by flexural extension related to emplacement of the Ouachita allochthon (e.g., Pashin and Groshong, 1998; Groshong and others, 2010). Appalachian folds are superimposed on the southeastern margin of the homocline and include thin-skinned folds and

thrust faults that are detached in Cambrian shale (e.g., Rodgers, 1950; Thomas, 1985; Thomas and Bayona, 2005).

Stratigraphic and sedimentologic framework.—The sedimentary cover in the Black Warrior Basin consists of carbonate and siliciclastic strata ranging in age from Cambrian through Pennsylvanian (Figure 2). Crystalline basement has been penetrated by only two wells, which penetrated Grenvillian granitic rocks in the northeastern part of the basin (Neathery and Copeland, 1983). Basement is overlain nonconformably by about 1,200 feet of shale and carbonate assigned to the Cambrian-age Rome and Conasauga Formations, which were deposited during the late stages of Iapetan rifting (Thomas, 1988). The Iapetan succession is overlain by a thick section of dolostone, limestone, and sandstone assigned to the Knox Group, which was deposited in a passive margin setting.

The Middle Ordovician through Lower Mississippian section forms a northeast-thinning wedge of sediment that contains numerous disconformities and contains a heterogeneous assemblage of limestone, shale, and ironstone assigned to the Stones River Group (Middle Ordovician), the Sequatchie Formation (Upper Ordovician), the Red Mountain Formation (Silurian), the Chattanooga Shale (Middle-Upper Devonian), the Fort Payne Chert (Lower Mississippian), and the Tuscumbia Limestone (Lower Mississippian) (Kidd, 1975). This section is considered part of a passive margin succession that was deposited on a southwest-sloping shelf that was open to the Ouachita embayment. Unconformities and facies changes within this succession also may reflect the far-field effects of the Taconic and Acadian orogenic events in the ancestral Appalachians (Thomas, 1988).

Upper Mississippian and Lower Pennsylvanian strata constitute the synorogenic basin fill that was deposited during Appalachian-Ouachita orogenesis (Thomas, 1974). These strata include the Pride Mountain Formation, the Hartselle Sandstone, the Bangor Limestone, and the Parkwood Formation (Figure 2). The Mississippian-Pennsylvanian boundary is in the Parkwood. Pride Mountain-Parkwood strata were deposited during the initial stages of Ouachita orogenesis and contain a mixed carbonate-siliciclastic assemblage with complex facies relationships. Interpretations of source areas and depositional systems have long been controversial (e.g., Thomas, 1974, 1995; Cleaves and Broussard, 1980; Cleaves, 1983; Stapor and Cleaves, 1992; Pashin, 1993, 1994; Pashin and Gastaldo, 2009). Several sandstone units in this section produce oil and natural gas and include the Lewis sandstone (Pride Mountain), the Hartselle Sandstone, the Carter sandstone (Parkwood), Gilmer sandstone (Parkwood), and Coats sandstone (Parkwood). Most conventional hydrocarbons are produced from the Lewis and the Carter, and the Hartselle contains one of the largest tar sand deposits in North America (Wilson, 1982). The Pottsville Formation is the youngest stratigraphic unit in the Black Warrior Basin and is mainly of Early Pennsylvanian age. The Pottsville contains shale, sandstone, and economic coal seams and is locally thicker than 6,500 feet. The Alabama Pottsville has been interpreted as a cyclic, fluvial-deltaic clastic wedge that was deposited in response to advancing thrust and sediment loads in the Appalachian orogen (e.g., Pashin, 2004).

The southwestern part of the basin is overlain with pronounced angular unconformity by Cretaceous strata of the Gulf of Mexico basin and the Mississippi Embayment. Cretaceous strata form a southwest-thickening wedge of sediment that is locally thicker than 900 feet and contains major fresh-water aquifers in Alabama (Kidd, 1976; Pashin, 2007). These strata were deposited

during a prolonged episode of southwestward tilting and regional flexure that post-dated all folding and faulting in the Black Warrior Basin and the Appalachian-Ouachita orogen.

Candidate Sinks and Seals

Knox Group.—The Knox Group in the Black Warrior Basin comprises the Upper Cambrian Copper Ridge Dolomite and the Lower Ordovician Chepultepec Dolomite. Additional stratigraphic units that are younger than the Chepultepec may be present locally but have not been identified in the basin. The Knox Group was deposited on a broad carbonate ramp that covered much of the continental United States during Late Cambrian and Early Ordovician time (Thomas, 1988). The top of the Knox Group increases with depth in the Black Warrior Basin to the southwest (Figure 6), reaching depth greater than 10,000 feet in southern Pickens, and northern Greene and Hale Counties, Alabama. The Copper Ridge is composed of finely to medium-crystalline limestone, chert, and dolomite (Kidd, 1975; Osborne and Raymond, 1992). Thin (<20 feet) quartzose sandstone units also occur in the Copper Ridge and have a patchy distribution.

Wells penetrating the Copper Ridge Dolomite in the Black Warrior Basin are few, and only two penetrate the full thickness of the Copper Ridge. The Copper Ridge is 2,666 feet thick in the Mother 13-15 #1 well (OGB Permit 4100)and 2,462 feet thick in the F. W. Smith 26-6 #1 well (OGB Permit 1689). Southeast of the basin in the Appalachian thrust belt, the Copper Ridge has been measured to be between 1,150 and 1,475 feet thick (Batchelder, 1984; Osborne and Raymond, 1992). Hence, the Copper Ridge appears to be substantially thicker in the Black Warrior Basin than in the adjacent thrust belt.

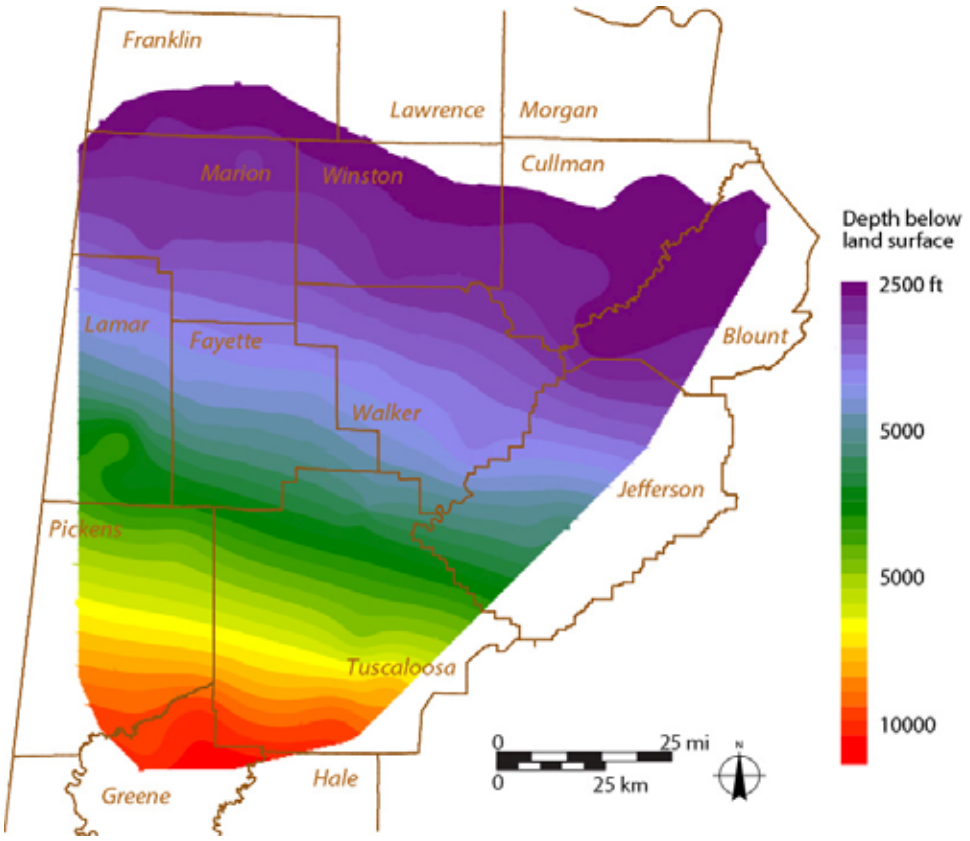

Figure 6.—Regional map showing depth of the top of the Knox Group in the Black Warrior basin of Alabama.

Records from the Mother 13-15 #1 well (OGB Permit 4100) in southern Morgan County indicate that dolomite and cherty dolomite are the dominant rock types; chert is most abundant near the base of the formation. Limestone units are few and range in thickness from 1 to 5 feet. Siliceous units, including sandstone and chert, also are thin, ranging from 1 to 4 feet thick. Porous zones in the Copper Ridge are restricted to dolomitic intervals and range in thickness from 4 to 8 feet. The F. W. Smith 26-6 #1 well (OGB Permit 1689), located in northeastern Cullman County, indicates that dolomite is again the dominant rock type in the Copper Ridge and that chert is most abundant in the lower part of the formation. Individual porosity zones in the Smith well range from 5 to 13 feet thick. The cumulative thickness of the porous zones in the

Mother well is 116 feet and in the Smith well is 67 feet; porosity averages about 6percent in each well.

A few well logs have recorded the upper part of the Copper Ridge in the southern part of the Black Warrior Basin. The Republic Steel Corp. 5-5 #1well (OGB Permit 2574) and the Republic Steel Corp. #9-13 (OGB Permit 2583) are both in Tuscaloosa County. The upper 250 feet of the Copper Ridge was penetrated in Republic Steel Corp. 5-5 #1 well in what is now Wiley Dome Field. The neutron and density porosity logs indicate that the lithology is mostly limestone with matrix porosity higher than 3percent in many zones. The upper 100 feet of the Copper Ridge was penetrated in the Republic Steel Corp. #9-13 well. As in the Republic Steel Corp, 5-5 #1 well, the neutron density log indicates that the lithology is mostly limestone, suggesting that the limestone content of the upper Copper Ridge increases toward the deep part of the basin.

The Chepultepec Dolomite overlies the Copper Ridge Dolomite, and the basal contact of the Chepultepec can be difficult to identify and pick with consistency in drillers logs and in geophysical logs. The Chepultepec is most easily distinguished from the Copper Ridge by a lack of sandstone and substantially lower chert content. For practical purposes, the to base of the Chepultepec was picked at the top of the uppermost sandstone interval in the Copper Ridge. Like the Copper Ridge, the Chepultepec is dominated by chert-bearing dolomite in the northern part of the Black Warrior Basin (Franklin, Morgan, and Cullman Counties). In the southern part of the basin (Walker, Tuscaloosa, and Lamar Counties), the Chepultepec is dominated by limestone, with dolomitic shale intervals occurring near the base of the formation, and massive dolomite occurring at the top. The upper contact of the Chepultepec is sharp and marks a regional disconformity that defines the top of the Knox Group throughout the eastern United States (Thomas, 1988; Osborne and Raymond, 1992).

The Chepultepec appears to thin toward the south. It is approximately 1,297 feet thick in the Glenn 28-12 #1 (OGB Permit 15417) well in Lawrence County and is approximately 1,023 feet thick in the Mother 13-15 #1 well (OGB Permit 4100) in Morgan County. About 32 miles farther south, the Chepultepec is only about 840 feet thick in the Harrell 26-13 #1 well (OGB Permit 3803) in Cullman County and is only 359 feet thick in the Republic Steel #9-13 well in Jefferson County. Defining the Copper Ridge-Chepultepec contact is extremely difficult in Fayette, Lamar, and Pickens Counties, and a lack of confidence in the log correlations makes the thickness of the Chepultepec uncertain.

Matrix porosity in the Chepultepec Dolomite is concentrated in thin zones in limestone and dolostone and has an erratic stratigraphic distribution. The highest cumulative thickness of porous zones in the Chepultepec is 168 feet. Because of uncertainty in the location of the Copper Ridge-Chepultepec contact, net reservoir thickness was mapped only for the Knox Group as a whole (Figure 7). Accordingly, the cumulative thickness of porous strata in the Knox Group averages 106 feet. Porosity is concentrated in the lower part of the Copper Ridge Dolomite and, to a lesser extent, in the Chepultepec Dolomite, although sparse well control makes the distribution of porosity uncertain. The thickest known porous section in the Knox Group is in northern Tuscaloosa County, but regional undersampling indicates that more exploratory wells need to be drilled before the extent of porosity can be characterized with any degree of confidence. Experience from brine disposal operations, moreover, indicates that considerable fracture porosity exists in the Knox Group (Ortiz and others, 1993) and that fracture porosity is much more widespread and predictable than matrix porosity. Importantly, the Knox Group underlies the entirety of the Black Warrior Basin and occurs at depths exceeding 2,500 feet throughout the region (Figure 6). Indeed, at least some Knox strata are deeper than 2,500

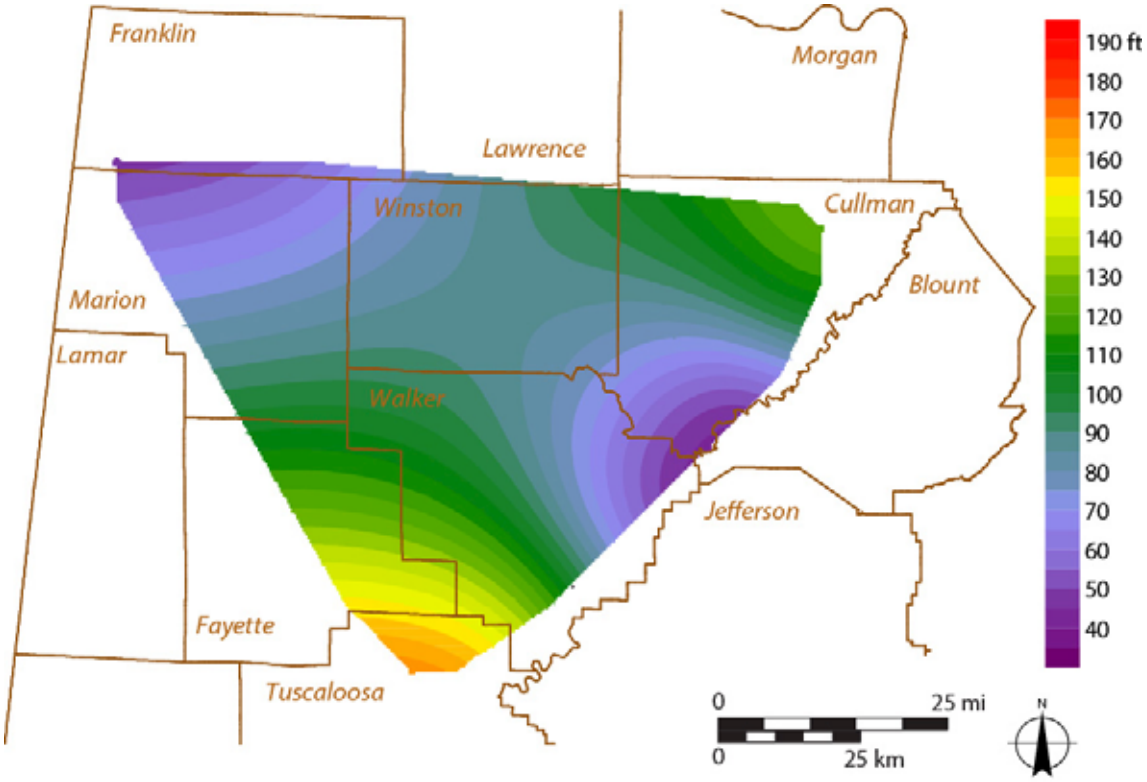

Figure 7.—Net reservoir thickness in the Knox Group in the Black Warrior Basin of Alabama.

throughout the basin, and the upper contact of the Knox Group is deeper than 2,500 feet in all but the northern tier of counties in an area encompassing more than 7,350 mi^2 (19,040 km^2).

Stones River Group.—The Stones River Group is primarily of Middle Ordovician age and consists mainly limestone with minor amounts of dolostone and shale (Jewell, 1950). The Stones River can be interpreted as the product of continued carbonate ramp deposition during the early Paleozoic. As in the Knox Group, wells penetrating the Stones River Group are few, and only 33 wells penetrate the full thickness of the Stones River. In the Mother 13-15 #1 well (OGB Permit 4100) in southern Morgan County, the Stones River contains mainly limestone and argillaceous limestone with some interbeds of dolostone and shale. In the Bedford Estate 2-1 #1 (OGB Permit 4697) located in Marion County, Alabama, log data indicates that the Stones River is

predominantly limestone to dolomitic limestone, becoming more argillaceous in the lower part of the formation. In the Champion International 35-13 #1 well (OGB Permit 13384), located on the Wiley Dome in northeastern Tuscaloosa County, Alabama, the upper part of the Stones River is predominantly limestone with a few shale interbeds.

Thickness of the Stones River is relatively uniform in the study area. In most wells, the Stones River is between 747 and 805 feet thick. Notable thickness anomalies are 543 feet in the Webber Wyer Massey 29-10 #1 well (OGB Permit 3083) in Franklin County and 263 feet in the Gorgas #1 borehole. Porous zones constitute a larger part of the Stones River Group than the Knox Group. Cumulative porous carbonate thickness in the Stones River averages 106 feet and has a maximum value of 327 feet in the Champion International 35-13 #1 well (OGB Permit 13384). Nearly all of the porosity in the Champion International well is in limestone within the upper part of the Stones River. The lower half of the Stones River in this well is dominated by dolomite and contains several argillaceous zones.

The Stones River Group is deeper than 2,500 feet throughout most of the study area and is thus potentially capable of storing supercritical CO_2 over an area exceeding 4,200 mi^2 (11,000 km^2) (Figure 8). In the southern part of the study area, the top of the Stones River is deeper than 10,000 feet. Of 33 wells studied, 22 contain porous zones. Average porosity is 5 percent, and porosity is locally as high as 11 percent (F. W. Smith 26-6 #1 well, OGB Permit 1689). The net reservoir thickness map reveals a patchy distribution of porosity (Figure 9). The net thickness of porous strata in the Stones River has a bimodal distribution. Five wells have net reservoir thickness ranging from 148 feet to 327 feet, whereas 17 wells contain less than 75 feet of porous carbonate. Although well control is limited, subsurface mapping suggests that porosity is developed primarily in the eastern part of the study area. Overall, reservoir quality in the Stones

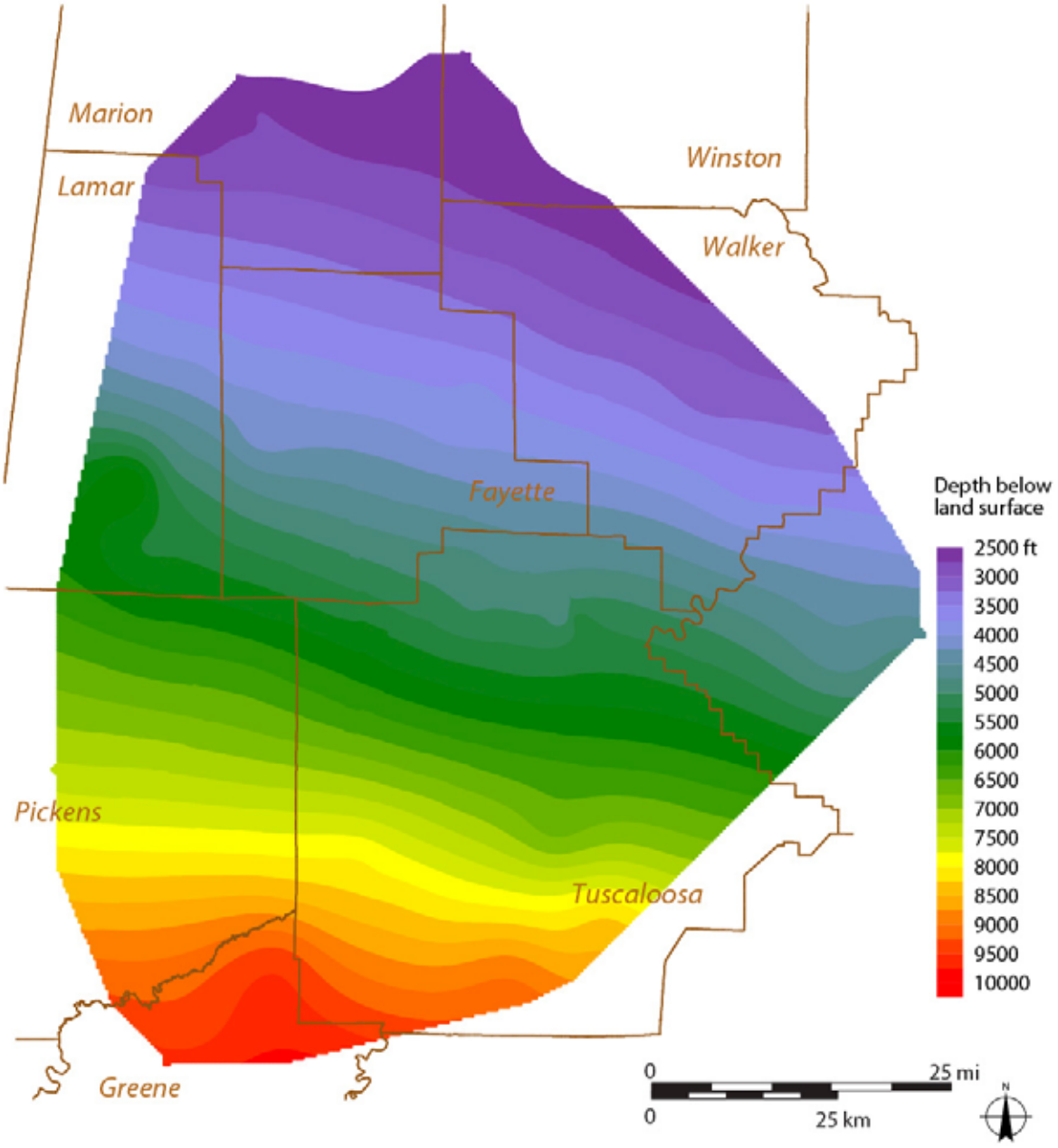

Figure 8.—Depth to the top of the Stones River Group in the Black Warrior Basin of Alabama.

River Group tends to be marginal, and so the interval is not considered a major target for geologic carbon sequestration.

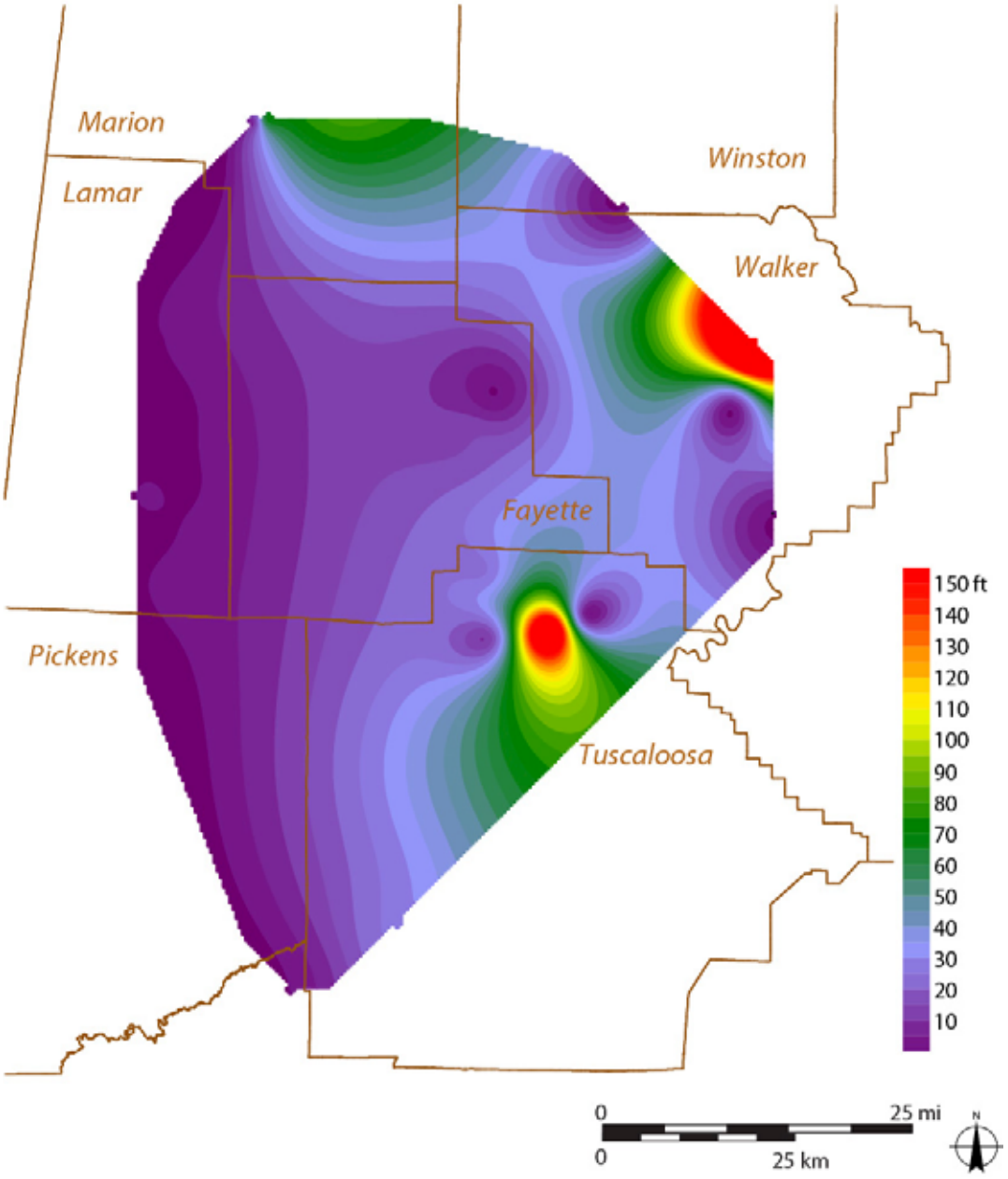

Figure 9.—Net reservoir thickness in the Stones River Group in the Black Warrior Basin of Alabama.

Sequatchie Formation.—The Sequatchie Formation sharply overlies the Stones River Group and contains primarily Upper Ordovician strata (Kidd, 1975; Thomas, 1988). The formation is quite heterogeneous, consisting of interbedded shale, limestone, and dolostone. Overall, the Sequatchie Formation represents continued carbonate ramp deposition coupled with the first

introduction of muddy sediment associated with uplift of the ancestral Appalachian Mountains during the Taconic Orogeny. The geophysical log suite for the Carnes 17-9 #1 well (OGB Permit 4350) in Marion County indicates that the basal 100 feet of the Sequatchie is composed of interbedded dolostone and shale with some chert. The middle 110 feet is mainly interbedded limestone and shale. The upper 75 feet of the section is primarily shale with some thin interbeds of dolostone. Most of porosity is developed in the basal dolostone. The Gorgas #1 borehole contains mainly limestone and argillaceous limestone. The geophysical log suite from the Dodson-Unger #1 well (OGB Permit 2393) in western Fayette County suggests that the lithology is predominantly argillaceous limestone and chert.

The Sequatchie Formation is deeper than 2,500 feet in a large part of the study area and reaches a maximum depth of about 10,000 feet in southern Tuscaloosa and northern Greene Counties (Figure 10). Thus, the area in which the formation has potential to store supercritical CO_2 is about 3,750 mi^2 (9,700 km^2). The thickness of the Sequatchie Formation in the Black Warrior Basin is variable, ranging from 122 feet in northern Tuscaloosa County to 524 feet in Lamar County. In general, the Sequatchie thickens westward and is thinnest in the southeastern part of the study area.

Forty wells penetrate the full thickness of the Sequatchie Formation, and only 22 of those wells contain evidence for significant porosity development. Reservoir quality is generally low, with porosity averaging 4 percent, but porosity is locally as high as 15 percent. The net thickness of porous carbonate in the Sequatchie Formation averages 67 feet and reaches a maximum thickness of 122 feet in Fayette County. In general, porosity is best developed in the northwestern part of the area where enough data are available to facilitate mapping (Figure 11). Mapping indicates that net porous reservoir thickness exceeds 50 feet in much of Fayette

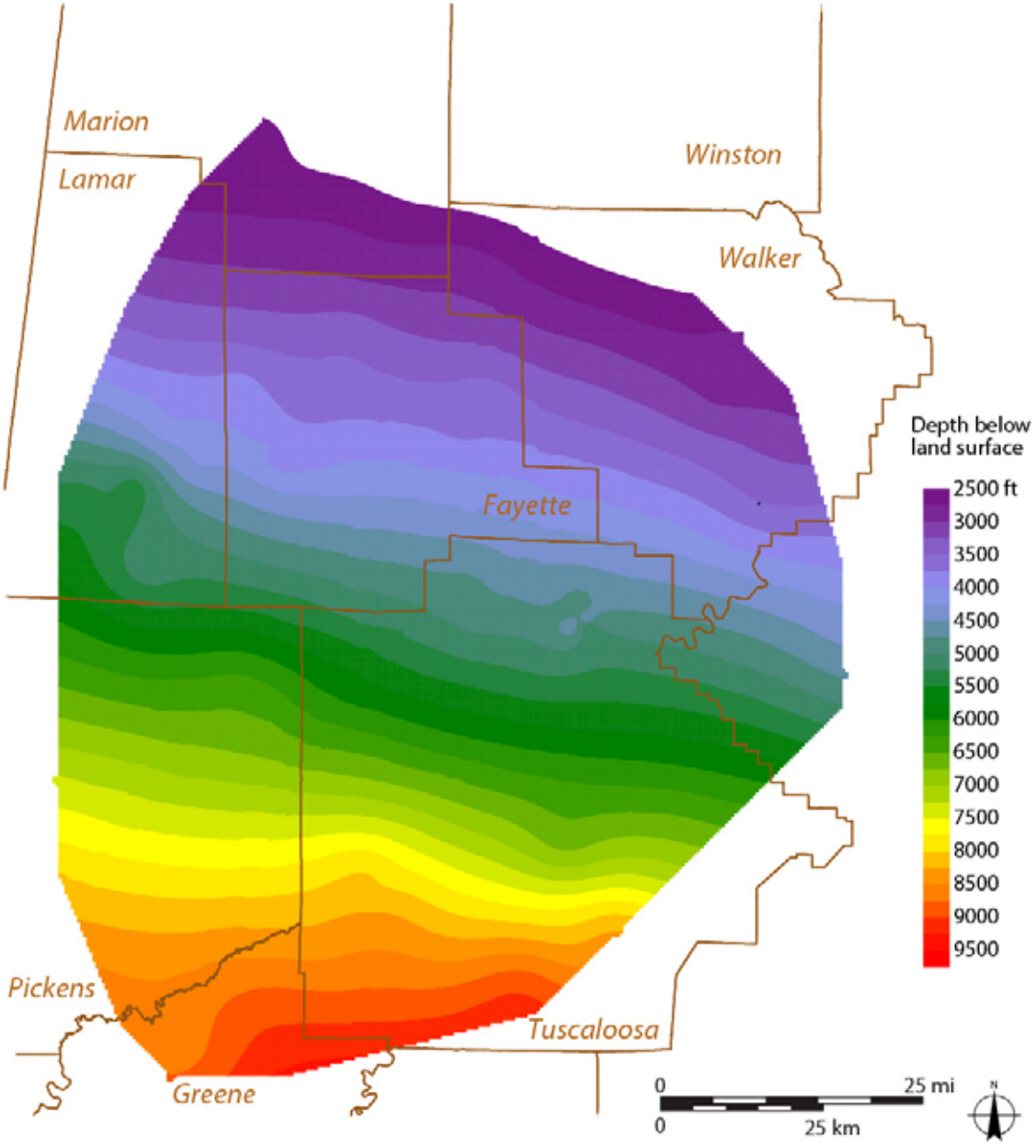

Figure 10.—Depth to the top of the Sequatchie Formation in the Black Warrior Basin in Alabama.

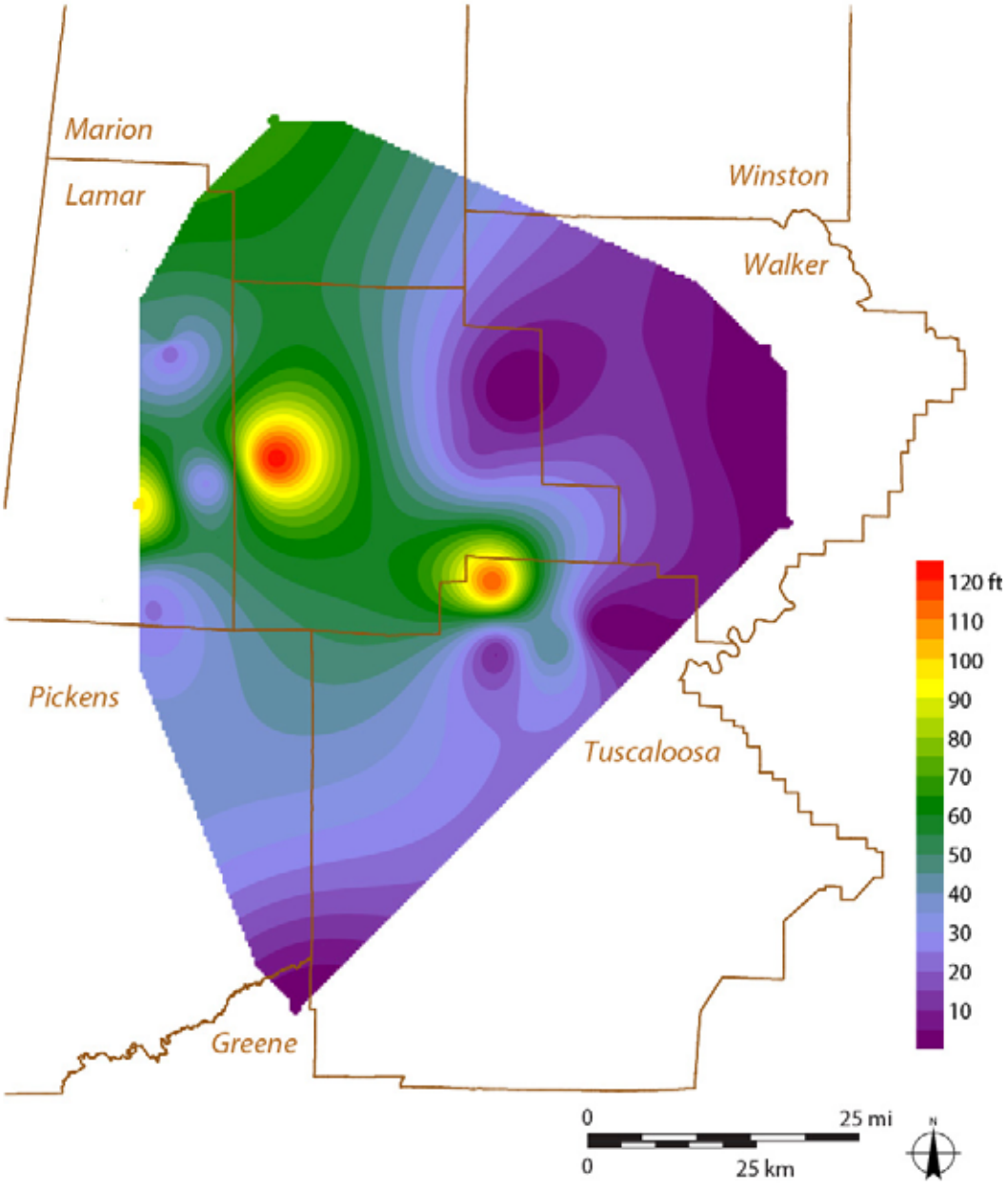

Figure 11.—Net reservoir thickness in the Sequatchie Formation in the Black Warrior Basin in Alabama.

County, and this trend appears to extend northward into Marion County. Overall, opportunities for CO_2 storage in the Sequatchie Formation appear limited, although modest potential exists in parts of Fayette and Marion Counties. The abundance of shaly strata in the upper part of the Sequatchie, moreover, may indicate significant sealing capacity in the eastern part of the Black Warrior Basin.

Red Mountain Formation.—The Red Mountain Formation is of Silurian age and contains a spectrum of carbonate and siliciclastic rock types in the Black Warrior Basin. The classic Red Mountain rock types are shale, sandstone, conglomerate, oolitic ironstone, limestone, and dolostone (e.g., Bearce, 1973; Thomas, 1988; Chowns, 2006). A regional cross section shows that the Silurian section is dominated by siliciclastic rock in the northeast and by chert-bearing carbonate rocks in the southwest (Pashin et al., 2010) (Figure 12). The siliciclastic and ferruginous rock types are thought to have been deposited in beach-barrier and oolitic shoal environments, whereas the chert-bearing carbonate units represent a carbonate ramp.

Thickness of the Red Mountain Formation increases southward, ranging between 300 and 600 feet in where it is deep enough to be considered as a storage target or reservoir seal. However, the formation thins northward is absent along much of the northern rim of the basin, where Devonian strata rest disconformably on Ordovician strata (Kidd, 1975). Depth to the top of the Red Mountain exceeds 2,500 feet in the central and southern parts of the study area in an area encompassing 4,119 mi^2 (10,669 km^2) (Figure 13). Maximum depth is greater than 9,500 feet in southwestern Tuscaloosa and northeastern Greene Counties.

Porosity exceeding 3 percent in the siliciclastic-dominated lower Red Mountain Formation was identified in only 5 of the 20 wells that penetrated the full thickness of the Red Mountain

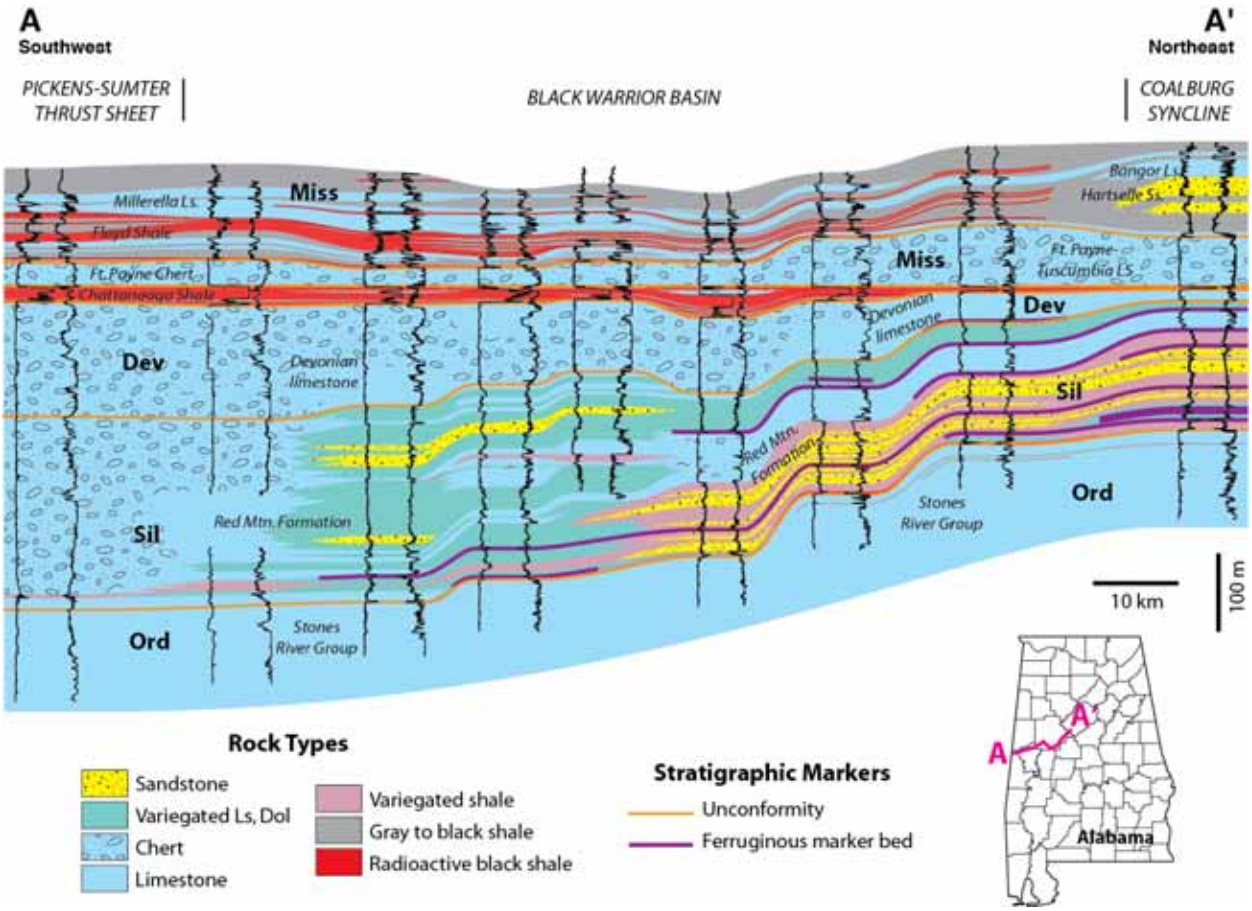

Figure 12.—Regional cross section showing facies relationships in Silurian through Mississippian section in the Black Warrior Basin of Alabama.

Formation, and all of this porosity is in thin ironstone and limestone intervals (Figure 14). The greatest reservoir thickness is in the Dodson-Unger #1 well (OGB Permit 2393) in west-central Fayette County. The lower Red Mountain in this well contains four porosity zones totaling 36 feet thick. Average net porous carbonate thickness is only 22 feet, and the localized nature of porosity development indicates limited potential for CO_2 storage in the lower Red Mountain. The abundance of shale in the lower Red Mountain, moreover, suggests that many beds have significant sealing capacity.

Siliceous limestone and dolostone in the upper part of the Red Mountain constitute the bulk of the formation in the southern and western parts of the study area. Whereas porosity is poorly

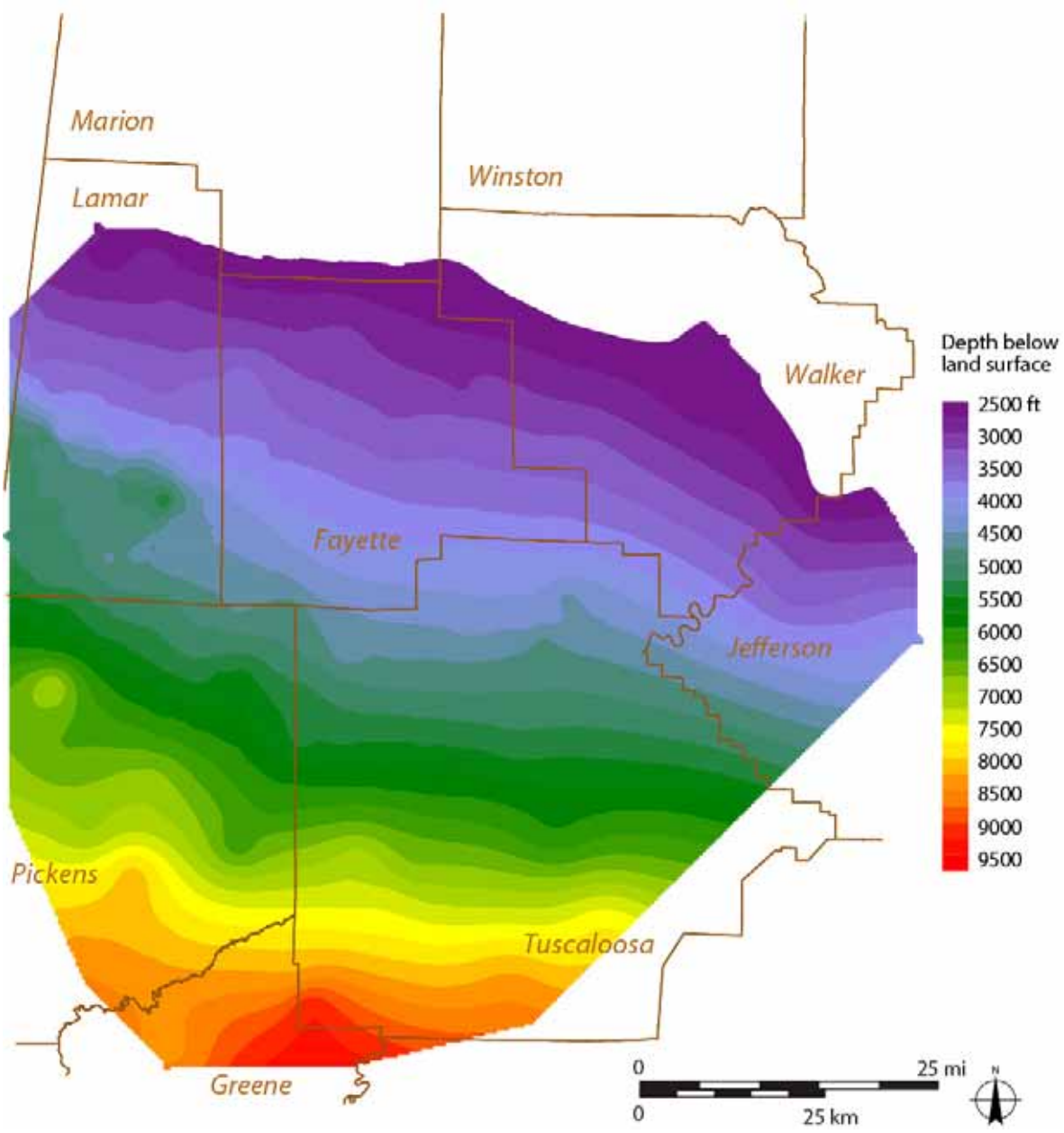

Figure 13.—Depth to the top of the Red Mountain Formation in the Black Warrior Basin of Alabama.

developed in the siliciclastic-dominated lower Red Mountain Formation, 25 wells penetrating the carbonate-dominated upper Red Mountain intersect porous zones. Maximum porosity, however, is only 8 percent, and average porosity is only 4 percent. The net thickness of porous carbonate increases southwestward, reaching a maximum thickness exceeding 320 feet in western

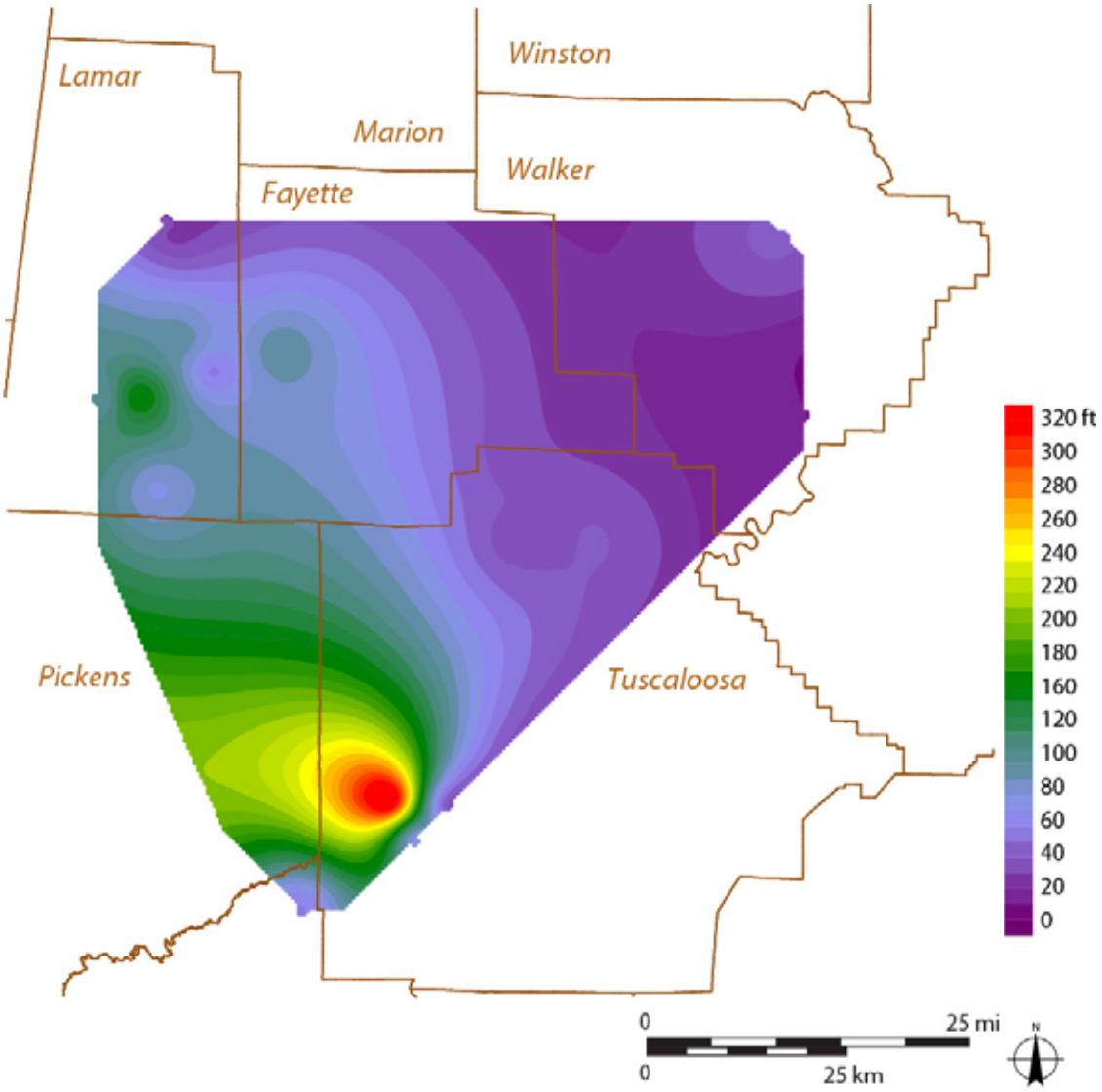

Figure 14.—Net reservoir thickness in the Red Mountain Formation of the Black Warrior Basin in Alabama.

Tuscaloosa County (Figure 13). The net thickness of porous carbonate is greater than 100 feet in much of Pickens and Lamar Counties, indicating modest storage potential in the southwestern part of the study area.

Devonian undifferentiated.—Devonian strata in the Black Warrior Basin are dominated by a northeast-thinning wedge of limestone and shale (Kidd, 1975; Thomas, 1988; Pashin and others,

2010) (Figure 12). The limestone unit is unnamed and forms the bulk of the Devonian section in much of the basin; it is absent in the northeastern part of the basin, where Mississippian strata disconformably overlie Silurian and older formations. The limestone contains principally Middle Devonian strata and locally includes some Lower Devonian carbonate. Maximum thickness of the Devonian carbonate is greater than 600 feet. The Chattanooga Shale is largely Upper Devonian and forms a thin veneer of organic-rich shale that extends throughout the study area, save for parts of Lamar and Pickens Counties (Rheams and Neathery, 1988; Pashin and others, 2010). The Chattanooga Shale is typically between 20 and 40 feet thick and reaches a maximum thickness of 80 feet in southwestern Tuscaloosa and northeastern Greene Counties.

The Devonian limestone is rich in chert and contains a minor amount of dolostone; it is the principal storage target in the Devonian of Alabama. The limestone is deeper than 2,500 feet in an area exceeding 3,175 mi^2 (8,225 km^2) and is deeper than 9,000 feet in southwestern Tuscaloosa and northeastern Greene Counties (Figure 15). Forty five wells penetrate the full Devonian section, and the geophysical well logs indicate that porosity is developed principally in chert-bearing intervals. Thirty six of the wells contain porous zones, and these zones correlate across large areas. Maximum porosity is 20 percent, and average porosity is greater than 5 percent. Net reservoir thickness averages about 80 feet and locally exceeds 200 feet (Figure 16). Net reservoir thickness increases markedly toward the southwest, indicating significant carbon storage potential in Lamar, Pickens, Tuscaloosa, and Greene Counties.

The Chattanooga Shale has matrix permeability on the order of 0.1 microdarcies (μD) and is a target for shale gas development in Blount, Tuscaloosa, and Greene Counties (Pashin and others, 2010). The low permeability indicates significant sealing potential, but the shale is intensely jointed, particularly where it lies in the thermogenic gas window. Accordingly, the

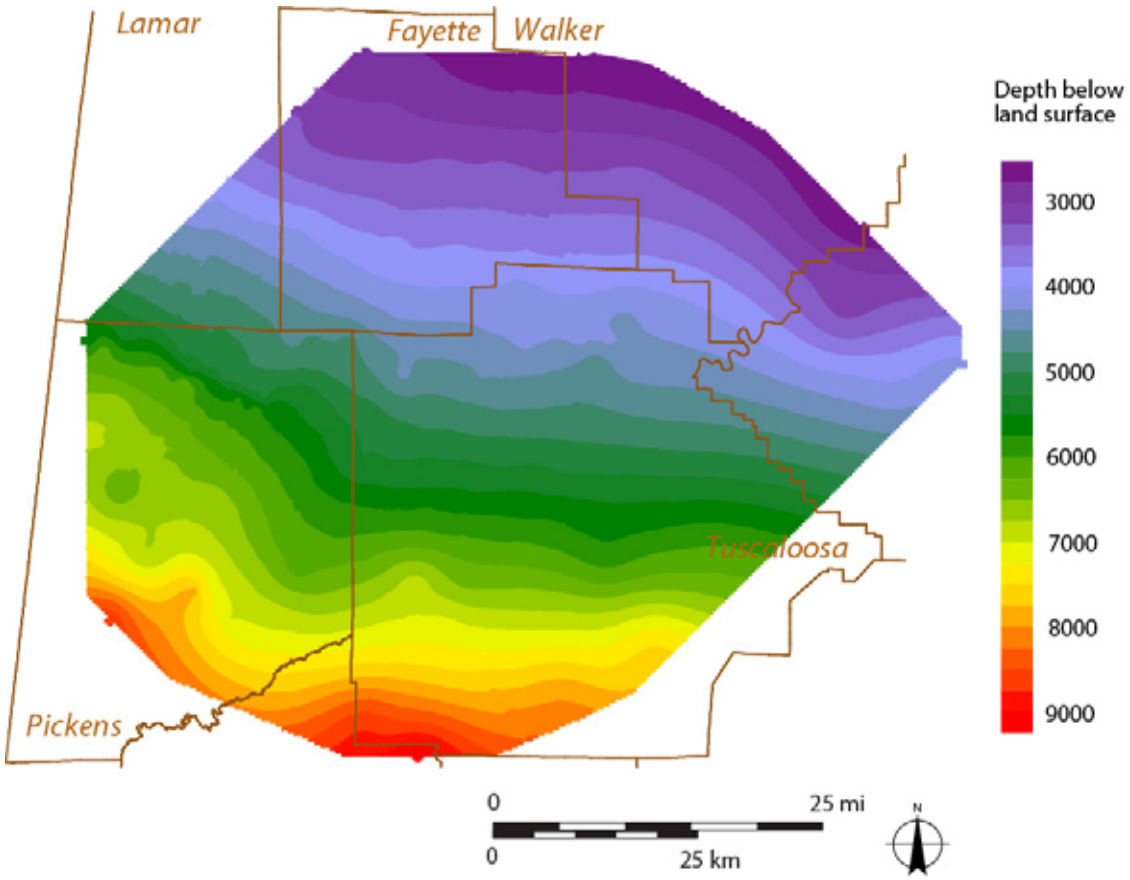

Figure 15.—Depth to the top of the Devonian limestone in the Black Warrior Basin in Alabama.

Chattanooga is not considered to be a significant reservoir seal in the Black Warrior Basin because it is thinner than 100 feet and is highly fractured.

Maury Shale, Fort Payne Chert, and Tuscumbia Limestone.—The Maury Shale forms the base of the Mississippian System in the Black Warrior basin and disconformably overlies the Chattanooga Shale (Thomas, 1972; Pashin, 1993) (Figure 17). The Maury typically is only 2-4 feet thick and thins to a feather edge in the western part of the basin. The shale is generally gray and contains phosphate nodules and glauconite in places. The Maury is less fractured than the Chattanooga and may contribute slightly to the sealing capacity of the Devonian-Mississippian shale section.

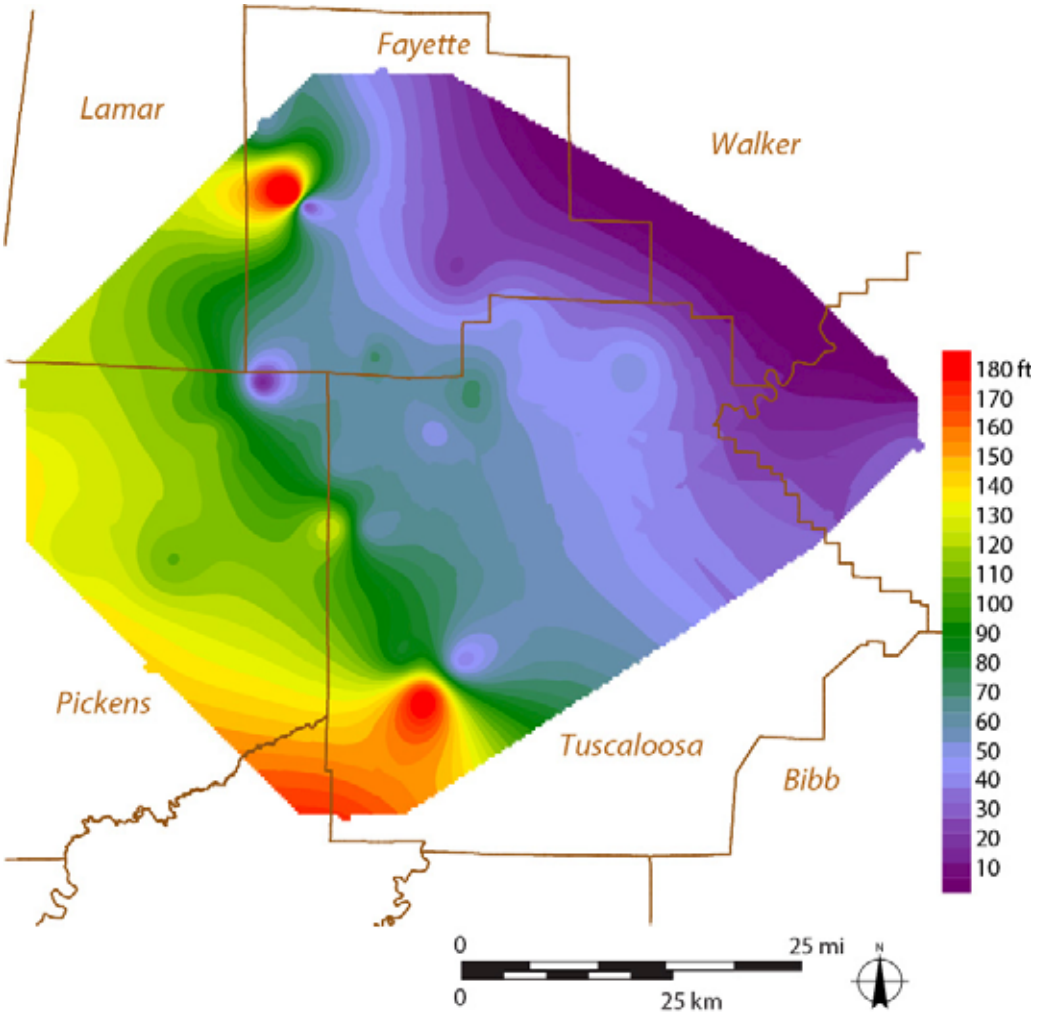

Figure 16.—Net reservoir thickness in the unnamed Devonian limestone in the Black Warrior Basin in Alabama.

The Fort Payne Chert constitutes the Osagean Series in Alabama; it sharply overlies the Maury Shale and is composed principally of dark gray micrite with abundant chert nodules in the Black Warrior Basin. The Fort Payne grades upward into the Tuscumbia Limestone, which contains interbedded gray micrite and light gray skeletal calcarenite. The Fort Payne-Tuscumbia contact is extremely difficult to define in well logs, and so the units are typically mapped together. Moreover, the Tuscumbia grades southwestward into a chert-rich facies that is indistinguishable from the Fort Payne. Overall, the Fort Payne-Tuscumbia interval is interpreted

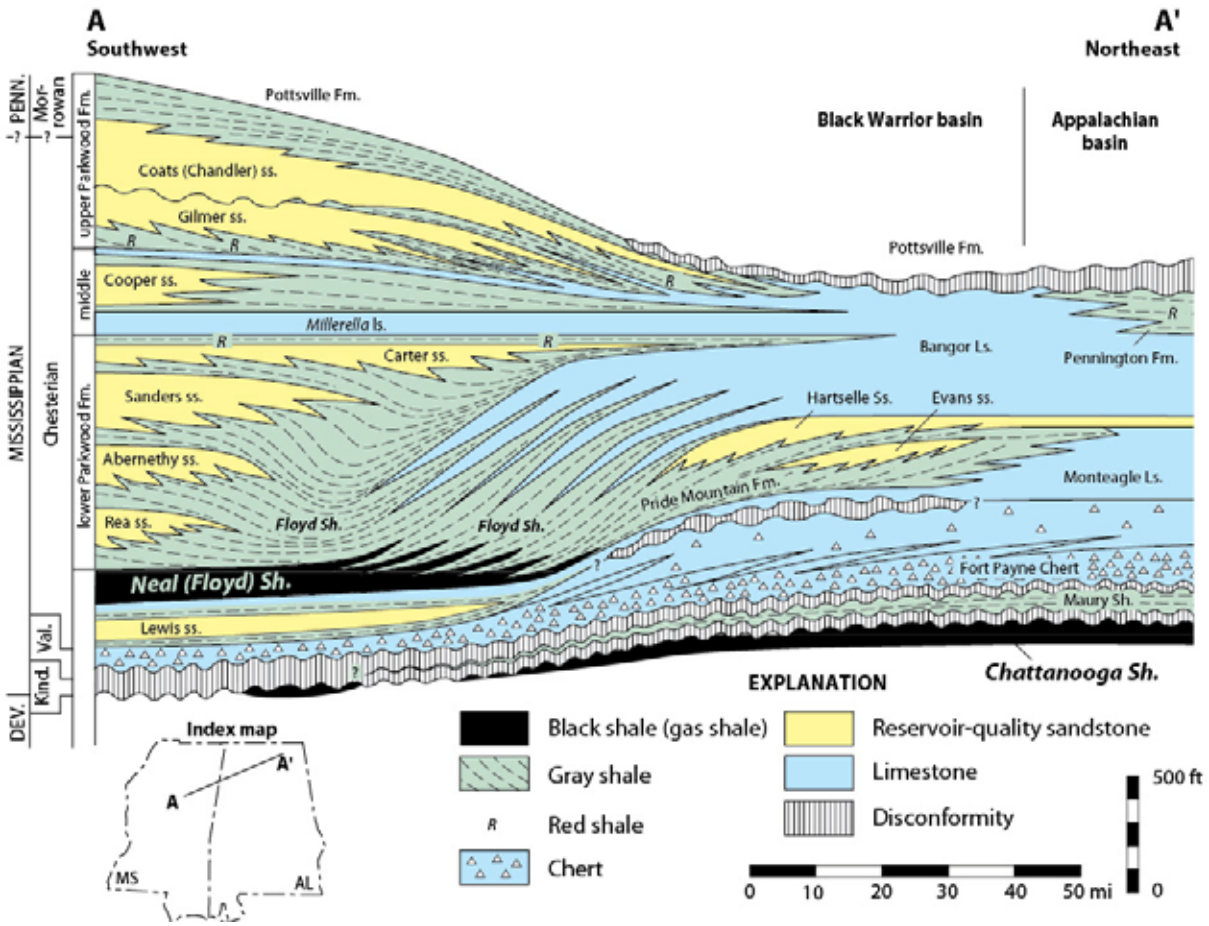

Figure 17.—Schematic cross section showing stratigraphic architecture of the Mississippian System in Alabama (after Pashin, 1994).

as a shoaling-upward succession that was deposited on a carbonate ramp (e.g., Thomas, 1972; Kopaska-Merkel and others, 2013). The combined Fort Payne-Tuscumbia interval thins southwestward from more than 450 feet to less than 100 feet (Figure 18). In parts of Lamar County, the Fort Payne-Tuscumbia is less than 25 feet thick.

Most conventional oil and gas wells in the Black Warrior Basin penetrate the top of the Fort Payne-Tuscumbia interval, but relatively few penetrate the base. As in most other formations, the top of the Tuscumbia Limestone dips south-southwest. The formation is deeper than 2,500 feet in an area covering 2,949 mi^2 (7,638 km^2) and is deeper than 7,000 feet in southern Tuscaloosa and

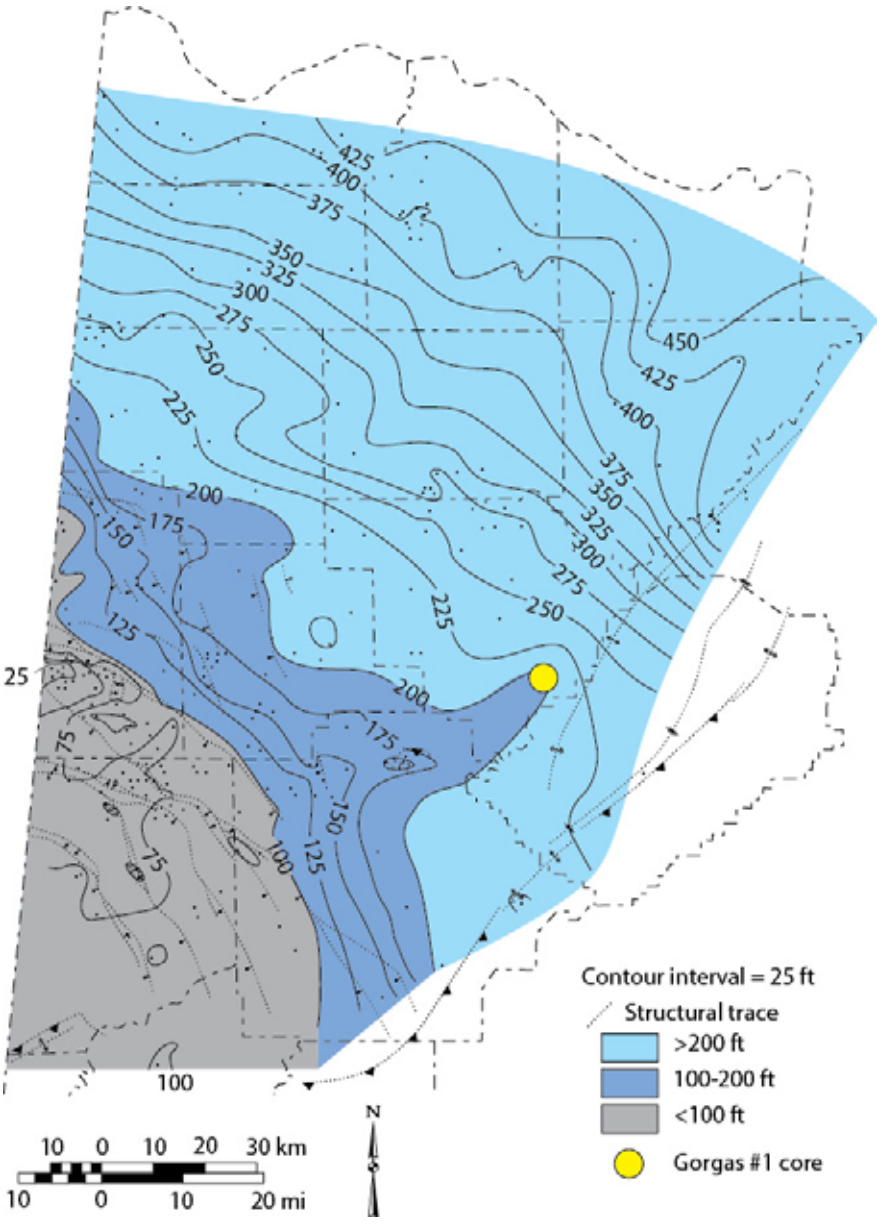

Figure 18.—Isopach map of the Fort Payne Chert and Tuscumbia Limestone (after Pashin, 1993; Kopaska-Merkel and others, 2013).

Pickens Counties (Figure 19). Porosity is developed mainly in the upper part of the Tuscumbia Limestone, averages less than 5 percent, and rarely exceeds 8 percent. Analysis of well logs indicates that net porous limestone thickness locally exceeds 100 feet in parts of Tuscaloosa and

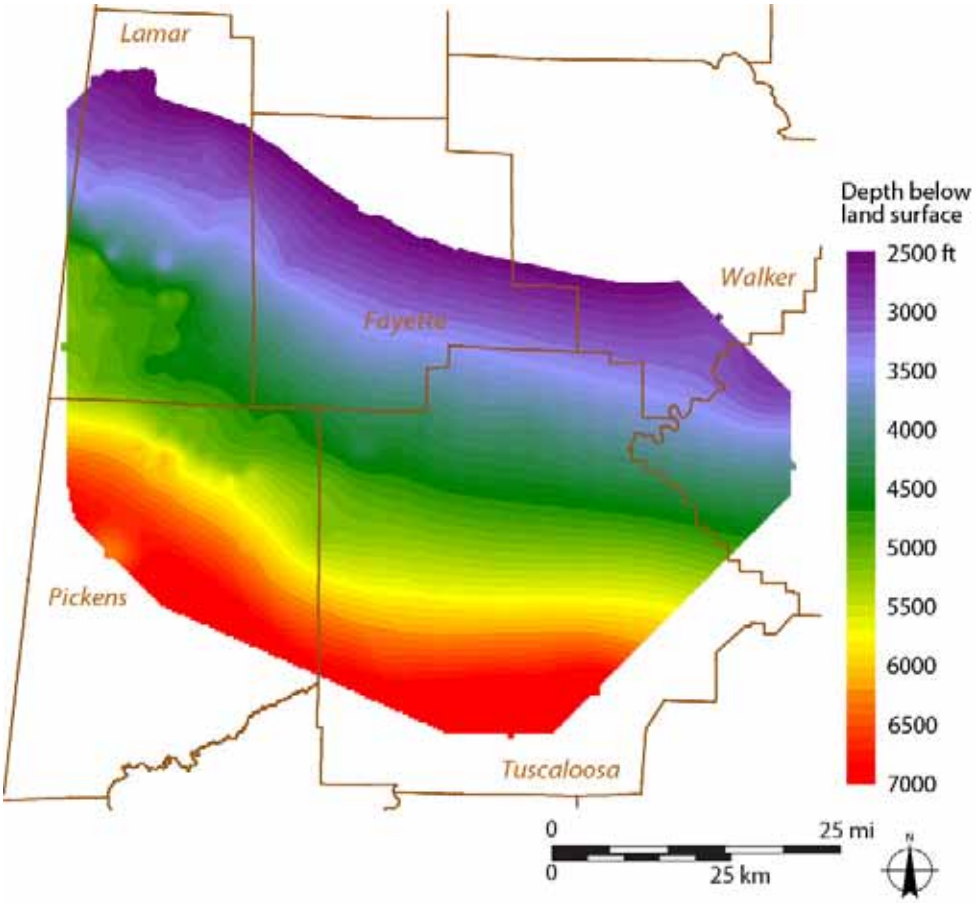

Figure 19.—Depth to the top of the Tuscumbia Limestone in the Black Warrior Basin of Alabama.

Jefferson Counties (Figure 20). Mapping indicates that the distribution of porosity is quite patchy, and the low values indicate that the Tuscumbia has limited sequestration potential.

Pride Mountain Formation and Hartselle Sandstone.—The Pride Mountain Formation, along with the Hartselle Sandstone, comprises three shale-sandstone-limestone cycles known as the Lewis, Evans, and Hartselle cycles (Pashin, 1993; Pashin and Rindsberg, 1993). The Lewis cycle forms the base of the Chesterian Series in Alabama. The Lewis sandstone is the second most productive conventional gas reservoir in the Black Warrior Basin (Pashin and Rindsberg, 1993), and the Hartselle Sandstone hosts the third largest tar sand deposit in the United States (Wilson,

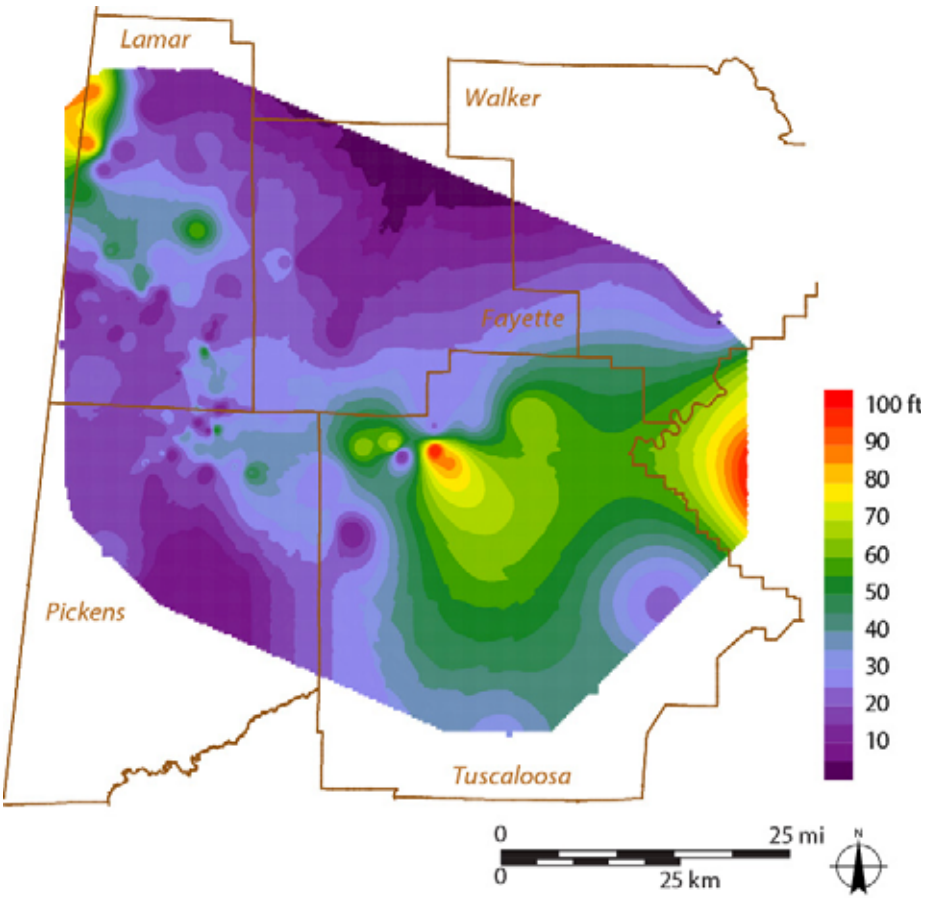

Figure 20.—Net reservoir thickness in the Tuscumbia Limestone in the Black Warrior Basin of Alabama.

1987). Shale in the Pride Mountain-Hartselle interval is gray and clay-rich, whereas the sandstone is quartzarenite. The carbonate units in this interval contain a spectrum of rock types from micrite to calcirudite. The Lewis interval is generally thinner than 125 feet, forming a widespread blanket of sedimentary rock that extends across most of the basin, and the Lewis sandstone has been interpreted as part of a lowstand wedge that was deposited in shelf and beach-barrier environments above the Fort Payne-Tuscumbia outer ramp (Pashin and Rindsberg, 1993). The Evans sandstone and Hartselle Sandstone, by comparison, represent barrier-strandplain deposits that are part of a prograding sediment wedge that was deposited mainly in the northeastern part of the basin. The Evans-Hartselle interval is thicker than 200 feet in the

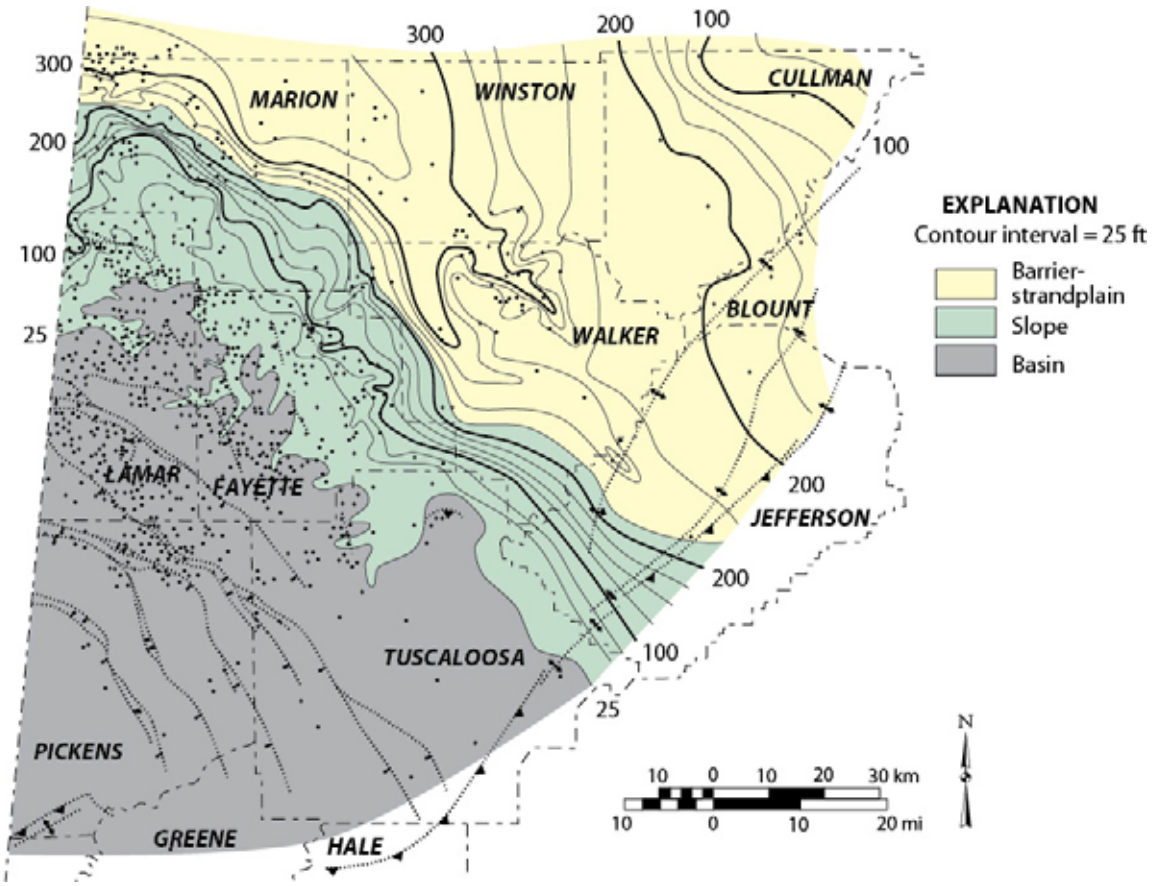

Figure 21.—Isopach map of the Evans-Hartselle interval in the Black Warrior Basin in Alabama (after Pashin, 1993).

northeastern part of the basin and passes rapidly southwestward into a condensed section of organic-rich shale that is assigned to the Floyd (Neal) Shale (Figures 17, 21).

The Lewis sandstone is deeper than 2,500 feet in an area encompassing 1,489 mi^2 (3,857 km^2) in Lamar, Fayette, northern Pickens, and northwestern Tuscaloosa Counties (Figure 22). By comparison, the Hartselle Sandstone is deeper than 2,500 feet in an area of only about 220 mi^2 (571 km^2) (Figure 23). Although this is a small area, it is important to note that this area includes the Miller and Gorgas steam plants.

Whereas estimates of porosity are based primarily on analysis of geophysical well logs, laboratory core analyses are available for 807 samples of Mississippian reservoir sandstone in

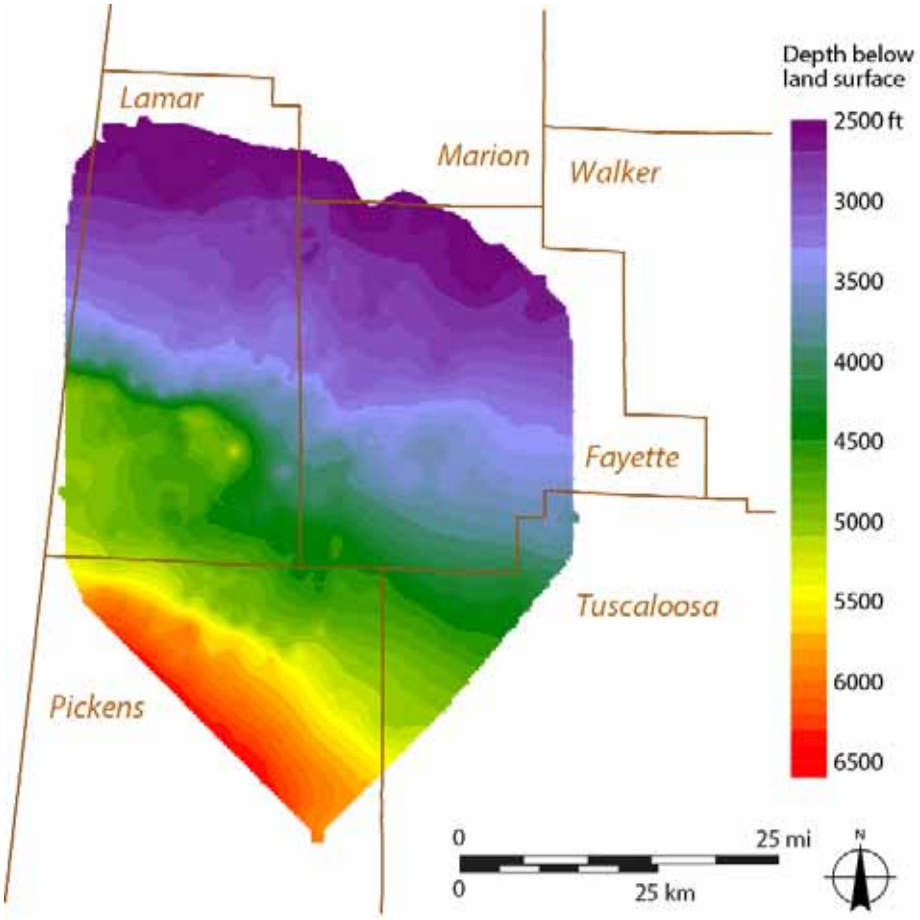

Figure 22.—Depth to the top of the Lewis cycle in the Black Warrior Basin of Alabama.

Table 1. Porosity and permeability of sandstone in the Black Warrior basin.

Interval	Porosity			Permeability		
	Maximum %	Minimum %	Mean %	Maximum mD	Minimum mD	Mean mD
All data	28.3	3.0	9.9	663.00	0.01	29.15
Mississippian-age Lewis, Carter, Gilmer, and Chandler sandstone	27.7	3.0	9.6	663.00	0.01	26.24
Pennsylvanian-age Pottsville Formation sandstone	28.3	10.2	19.2	471.00	1.20	89.45

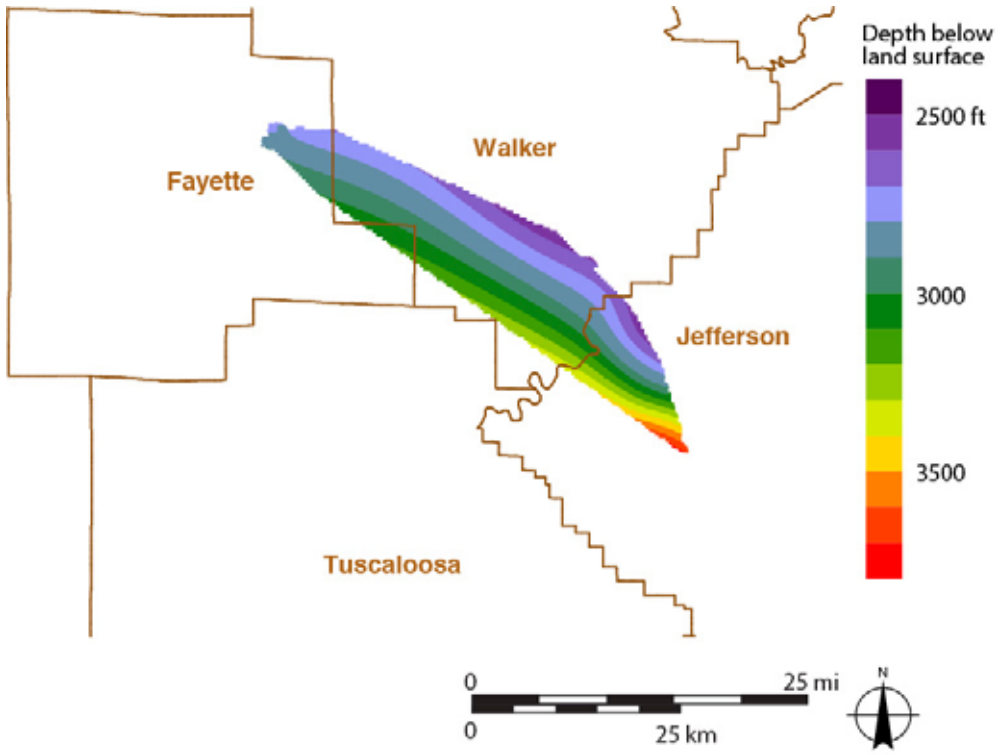

Figure 23.—Depth to the top of the Hartselle Sandstone in the Black Warrior Basin of Alabama.

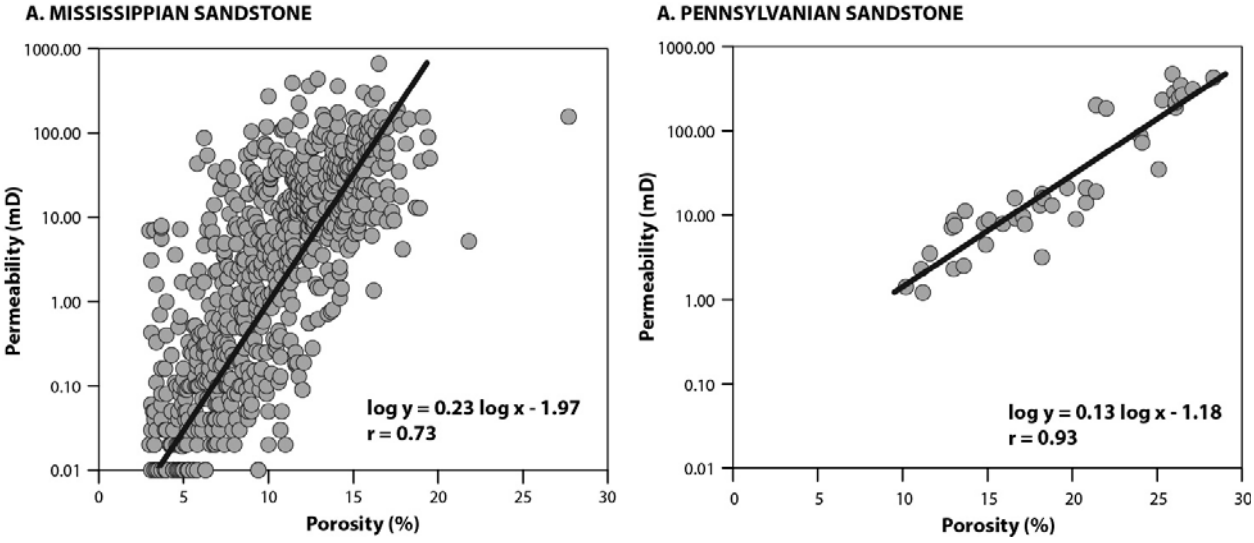

Figure 24.—Plots of porosity versus permeability based on conventional core analysis Mississippian and Pennsylvanian sandstone in the Black Warrior Basin of Alabama.

the Black Warrior Basin of Alabama (Figure 24; table 1). Porosity in Mississippian sandstone has a mean value of 9.6 percent and has a maximum value of 27.7 percent. Permeability, by comparison, has a mean value of 26.24 millidarcies (mD) and has a maximum value of 663 mD. Importantly, shale units in the Pride Mountain-Hartselle interval form proven reservoir seals that have trapped natural gas over geologic time. The net thickness of Lewis reservoir sandstone is between 20 and 70 feet in the gas producing parts of Lamar, Fayette, and Pickens Counties (Figure 25). The abundant wells in this area, moreover, may provide useful entry points for CO_2 storage operations. Net reservoir thickness in the Hartselle sandstone is locally greater than 70 feet but is severely constrained by the southwestward limit of the formation (Figure 26). Therefore, the Hartselle Sandstone my provide viable sequestration opportunities around the Gorgas and Miller steam plants, but the formation is of limited significance regionally.

Bangor Limestone.—The Bangor Limestone is a major part of the Chesterian Series in Alabama and is composed of gray limestone with rock types ranging from micrite to calcirudite. Oolitic limestone is the signature Bangor rock type. The Bangor represents the establishment of a major shoal-rimmed carbonate ramp in the northern part of the Black Warrior Basin (Thomas, 1972; Pashin, 1993). The Bangor interval is generally 300 to 500 feet thick in the northern part of the Black Warrior Basin, and the formation is thickest in the area of the shoal rim along the margin of the inner ramp (Figure 27). Like the Pride Mountain-Hartselle interval, the Bangor Limestone passes basinward into the organic-rich shale of the Floyd (Neal) Shale, which thins southwestward to less than 100 feet (Figures 17, 27).

The Bangor Limestone is deeper than 2,500 feet in an area covering 794 mi^2 (2,058 km^2) in Lamar, Fayette, and northern Tuscaloosa Counties (Figure 28). Log analysis indicates that

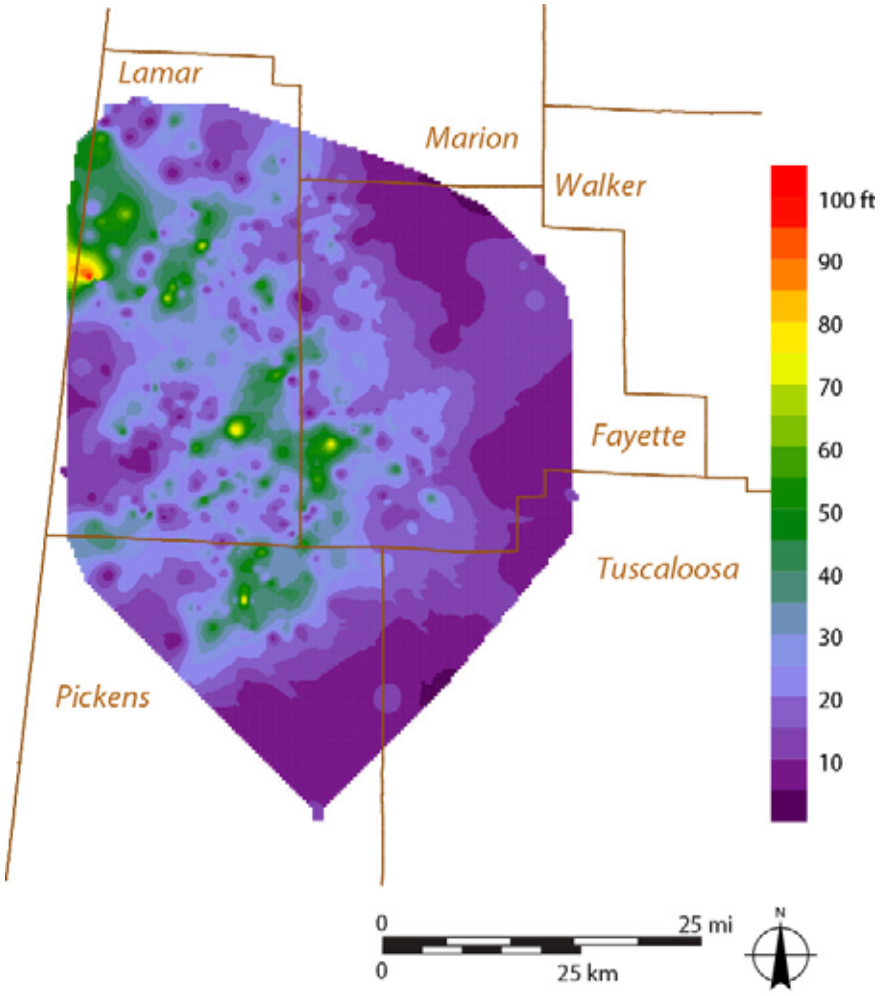

Figure 25.—Net reservoir thickness in the Lewis cycle in the Black Warrior Basin of Alabama.

porosity is generally less than 8 percent in the Bangor and averages only 4 percent. Net porous reservoir thickness increases northeastward, and only locally exceeds 70 feet (Figure 29). Hence, the storage capacity that exists in the Bangor is restricted to a small part of Fayette County near the updip limit of where natural conditions may support supercritical CO_2 storage.

Parkwood Formation.—The Parkwood Formation contains a complex array of siliciclastic and carbonate rock types and spans the Mississippian-Pennsylvanian boundary (Thomas, 1972, 1988, 1995). The formation can be subdivided into three parts, namely the lower, middle, and

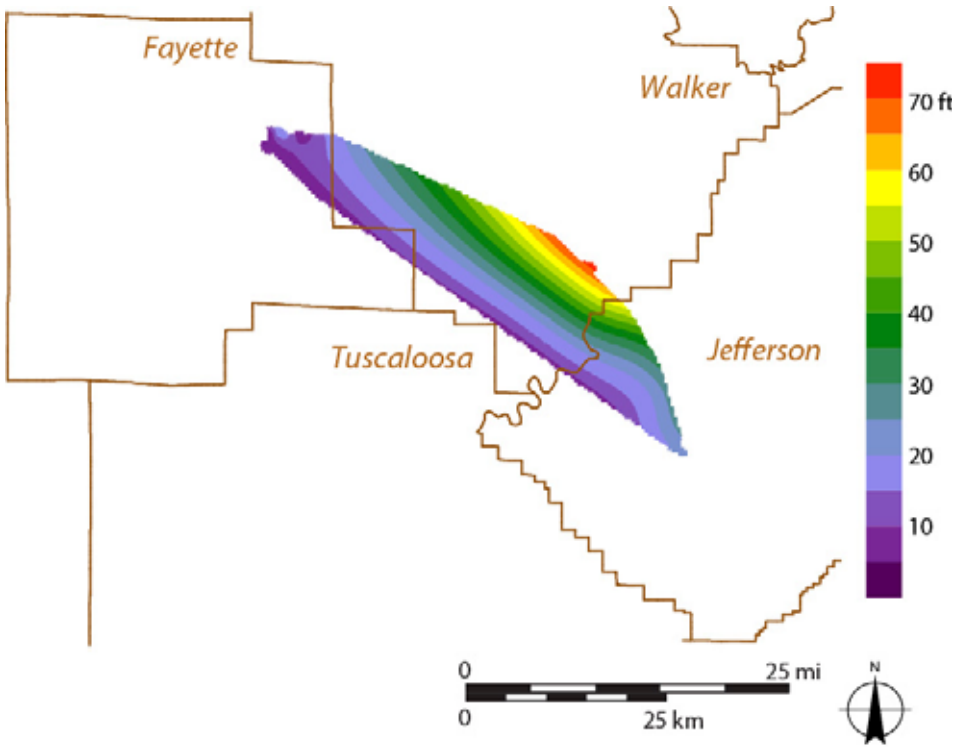

Figure 26.—Net reservoir thickness in the Hartselle Sandstone in the Black Warrior Basin of Alabama.

upper Parkwood (Pashin, 1993). The lower Parkwood is composed of shale and quartzose sandstone. The Carter sandstone occurs near the top of the lower Parkwood and is the most prolific conventional reservoir in the Black Warrior basin, accounting for the vast majority of the proven oil and gas reserves. The lower Parkwood fills part of the basin area south of the Bangor carbonate bank and overlaps the bank rim in Fayette and Lamar Counties (Figures 27, 30). A constructive delta lobe prograded eastward into the basin in Lamar and Pickens Counties, and destructive, shoal-water delta deposits, which include the major oil reservoirs in the basin, accumulated above the bank rim (e.g., Pashin and Kugler, 1992, 1996).

The Parkwood Formation contains strata deep enough to store supercritical CO_2 in an area covering about 1,765 mi^2 (4,570 km^2). Lower Parkwood strata containing porous sandstone are present in southern Lamar, southern Fayette, northern Pickens, and northwestern Tuscaloosa

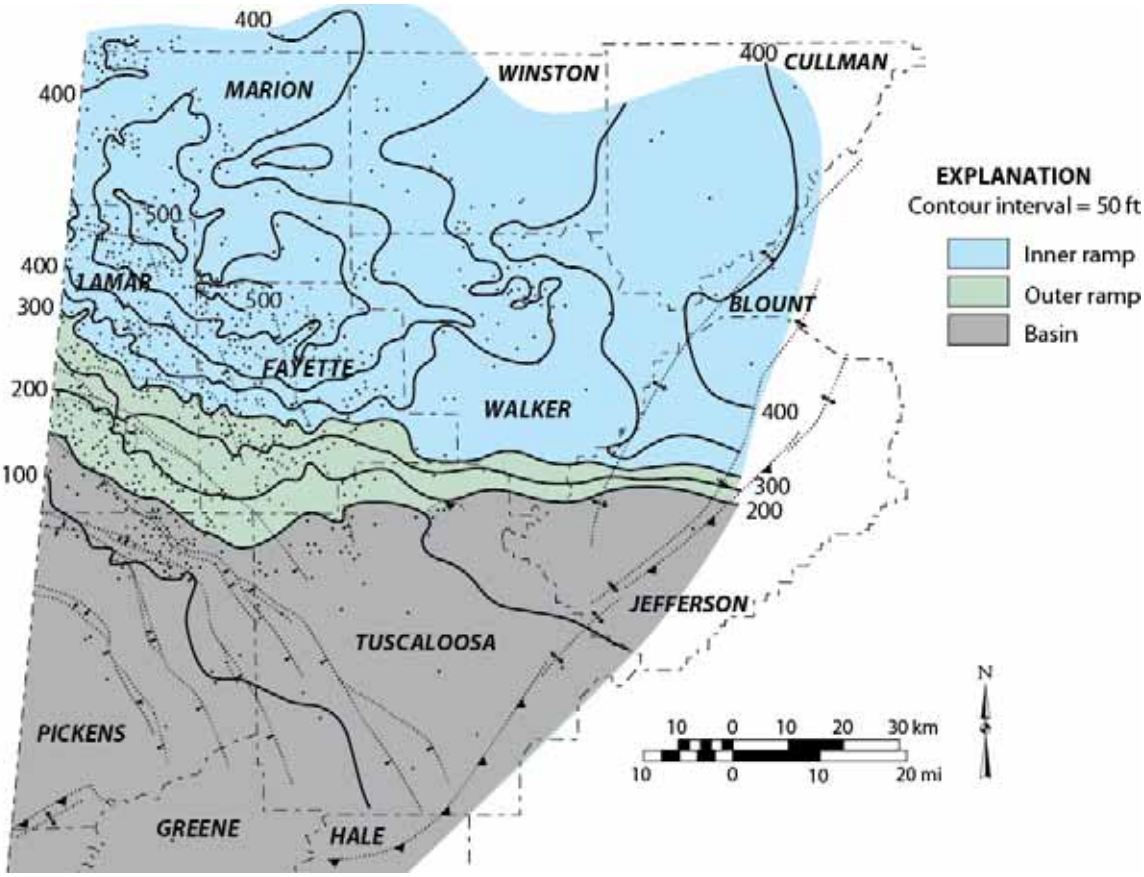

Figure 27.—Isopach map of the Bangor Limestone and equivalent strata in the Floyd (Neal) Shale in the Black Warrior Basin of Alabama (after Pashin, 1993).

Counties and are locally deeper than 6,000 feet in Pickens County (Figure 31). Net reservoir thickness locally exceeds 80 feet in parts of Lamar and Pickens Counties (Figure 32). However, some significant opportunities for CO_2 storage exist where reservoir thickness is less than 30 feet. For example oil production is concentrated in north-central Fayette and east-central Lamar Counties, and the API gravity of the oil is about 40°, suggesting that potential exists for CO_2 enhanced oil recovery.

The middle Parkwood contains numerous thin limestone, sandstone, and shale units, including the Millerella limestone, a prominent regional stratigraphic marker. Within this interval are numerous thin, discontinuous sandstone units, which are called the Millerella

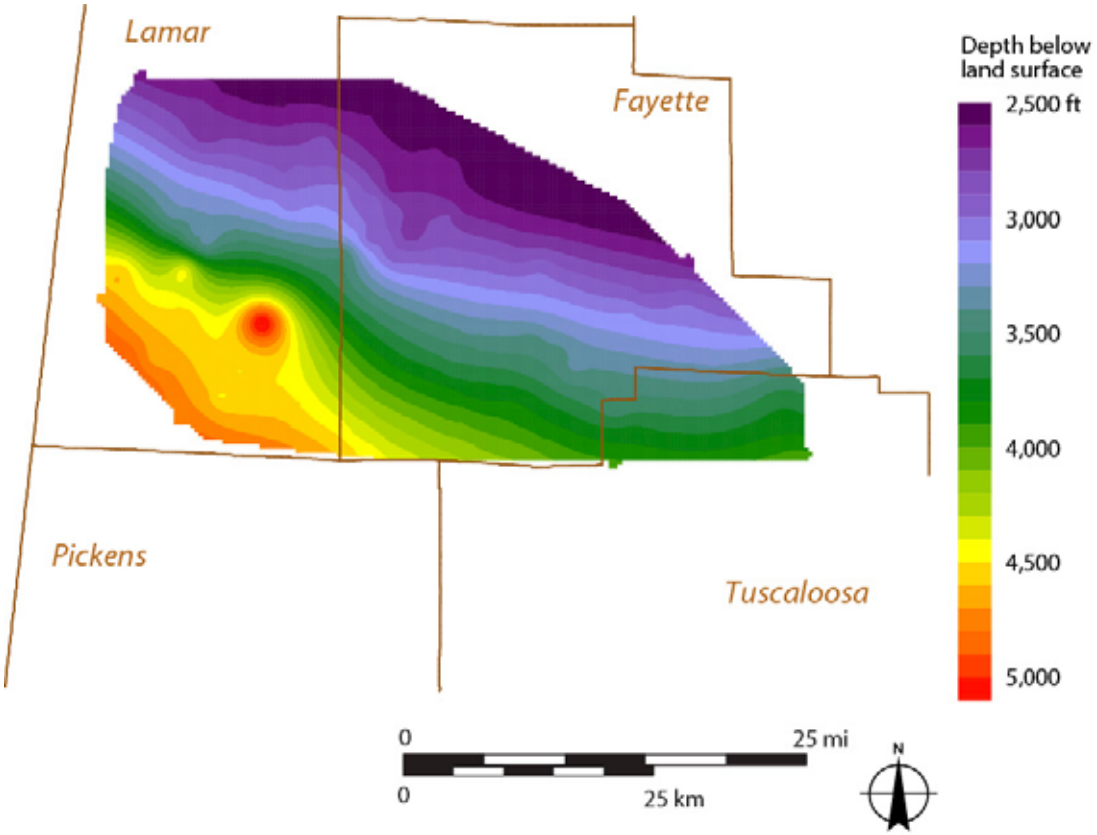

Figure 28.—Depth to the top of the Bangor Limestone in the Black Warrior Basin of Alabama.

sandstone. The Millerella sandstone is a significant producer of oil and gas in Lamar and Fayette Counties. The middle Parkwood ranges in thickness from less than 50 feet in the northeastern part of the basin to more than 700 feet in the southern part of the basin (Figure 33). Where this interval overlies the Bangor carbonate bank and thick lower Parkwood deltaic clastics, the middle Parkwood is thinner than 250 feet. The thicker middle Parkwood deposits fill the portion of the basinal area that remained after lower Parkwood deposition. Most Millerella sandstone overlies lower Parkwood deltaic deposits, whereas the middle Parkwood contains mainly limestone and shale in other parts of the basin. The middle Parkwood has been interpreted largely as a transgressive interval recording widespread shoal-water sedimentation during the late stages of delta destruction (Pashin, 1993, 1994).

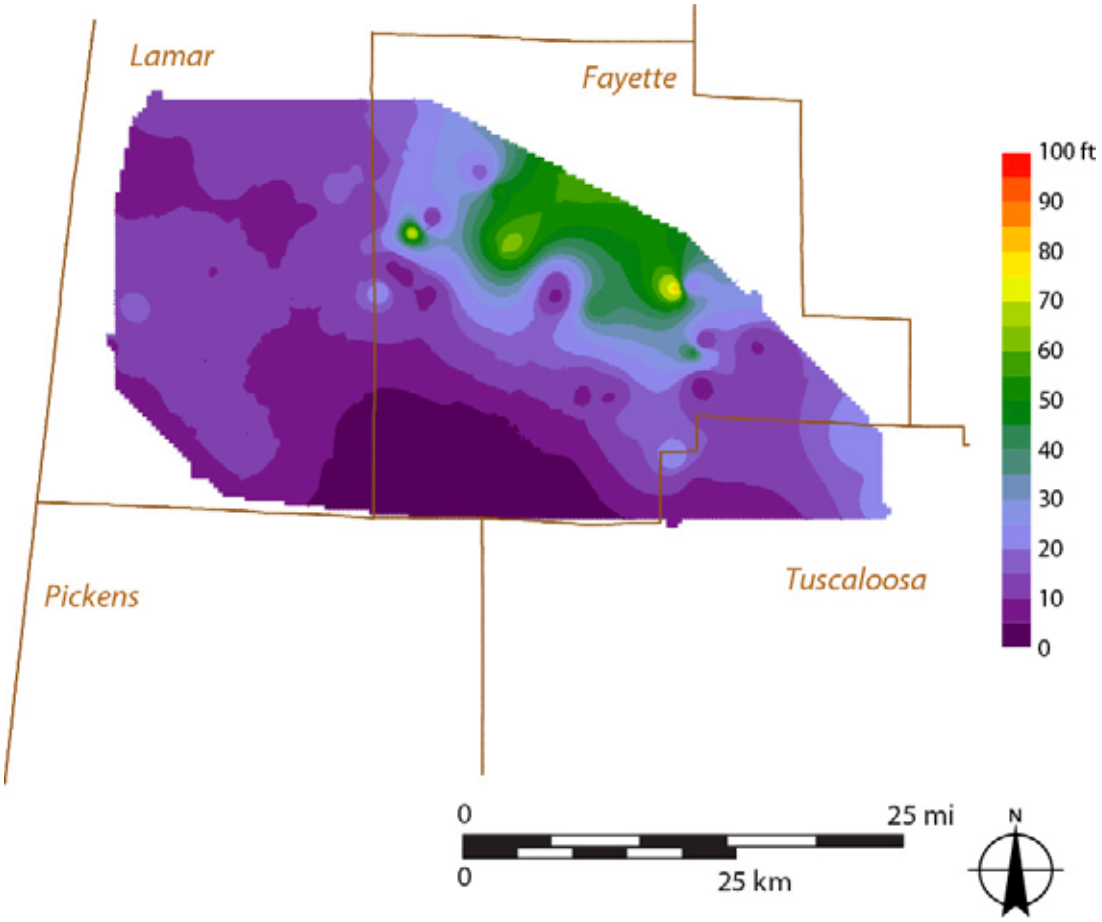

Figure 29.—Net reservoir thickness in the Bangor Limestone Black Warrior Basin of Alabama.

Middle Parkwood strata have some storage potential in large parts of Lamar, Fayette, Pickens, and Tuscaloosa Counties (Figure 34). Here, the depth of the top of the interval ranges from 2,500 to more than 7,000 feet. The maximum reservoir thickness in the middle Parkwood is only 35 feet (Figure 35), and most storage potential is in the Millerella sandstone in Lamar and Fayette Counties. Outside of this area, porosity is restricted to limestone.

The upper Parkwood Formation is composed mainly of sandstone and shale and contains some limestone that merges with the uppermost part of the Bangor Limestone toward the northeast (Thomas, 1972, 1974, 1988) (fig. 17). The upper Parkwood contains two reservoir

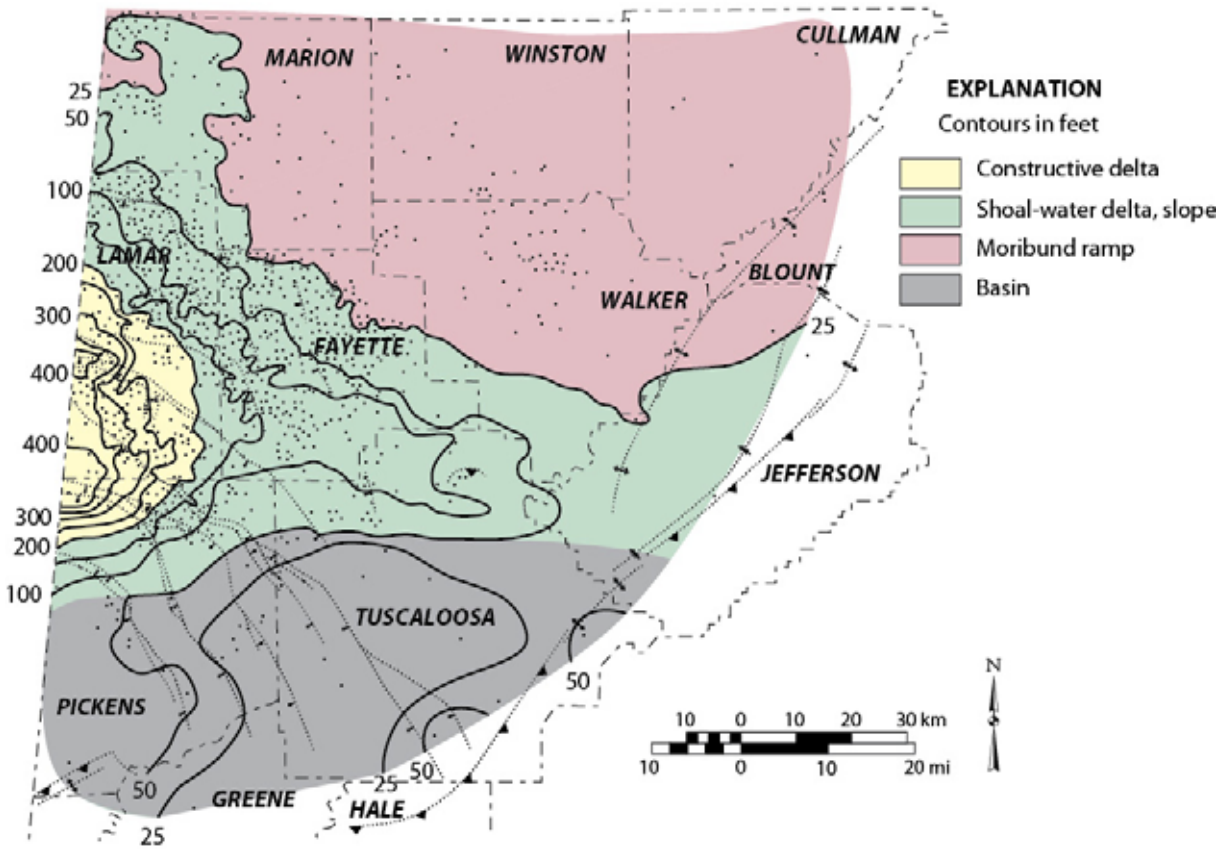

Figure 30.—Isopach map of the lower Parkwood Formation in the Black Warrior Basin of Alabama (after Pashin, 1993).

sandstone units called the Gilmer sandstone and the Coats sandstone. The Chandler sandstone, which produces in Pickens County, is equivalent to the Coats (Pashin, 1993). Upper Parkwood strata constitute a southwest-thickening wedge of sedimentary rock that includes fluvial-deltaic deposits. The upper Parkwood is locally absent in the northeastern Black Warrior Basin and thickens southwestward to more than 900 feet in Pickens County (Figure 36). The Gilmer sandstone has been interpreted as constructive deltaic deposits, whereas the Coats sandstone appears to contain incised valley fills defining the fluvial axes that fed the Gilmer deltaic systems (Pashin, 1993).

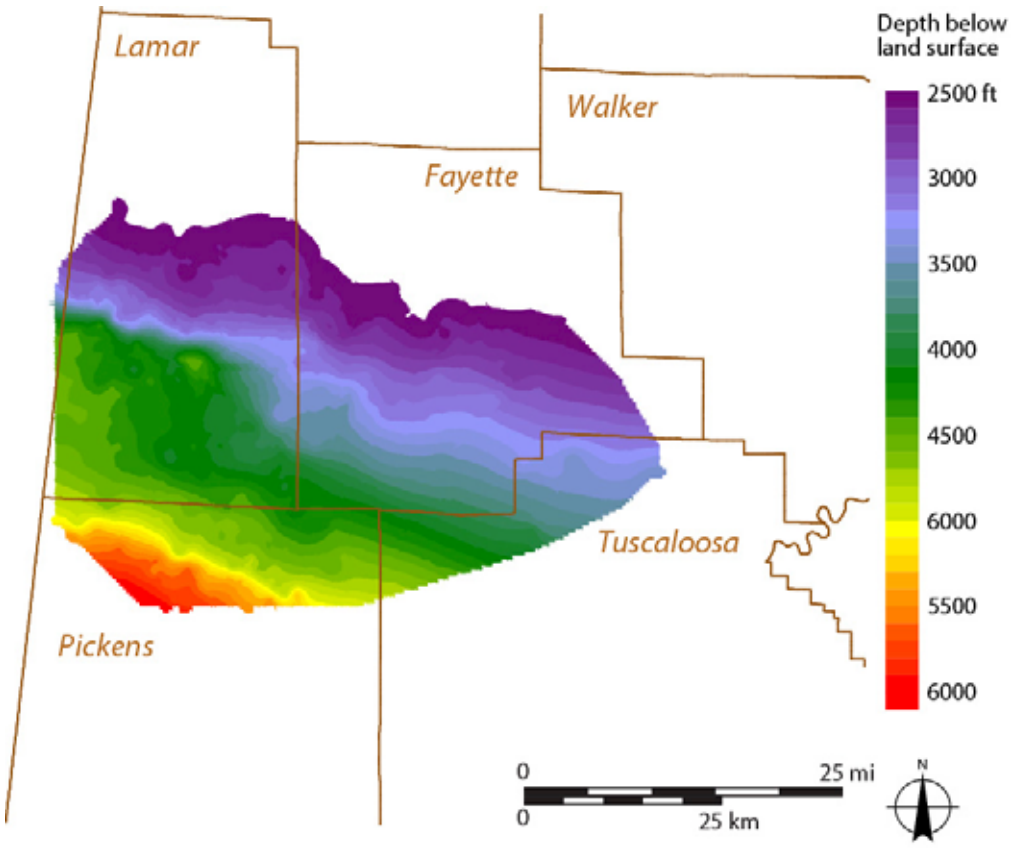

Figure 31.—Depth to the top of the lower Parkwood Formation in the Black Warrior Basin of Alabama.

Candidate reservoirs for CO^2 storage in the upper Parkwood are present in southern Lamar, southern Fayette, northern Pickens, and northwestern Tuscaloosa Counties (Figure 37). Potential CO_2 sinks are shallower than 4,000 feet in Lamar and Fayette Counties and locally deeper than 6,000 feet in Pickens County. Reservoir thickness is highly variable, reflecting the heterogeneity of Gilmer-Coats depositional systems, and ranges from less than 5 to more than 90 feet (Figure 38). Average reservoir thickness is 37 feet. Reservoir thickness is negligible in Fayette County, and so sandstone thickness patterns indicate that the principal storage potential is in Lamar and Pickens Counties.

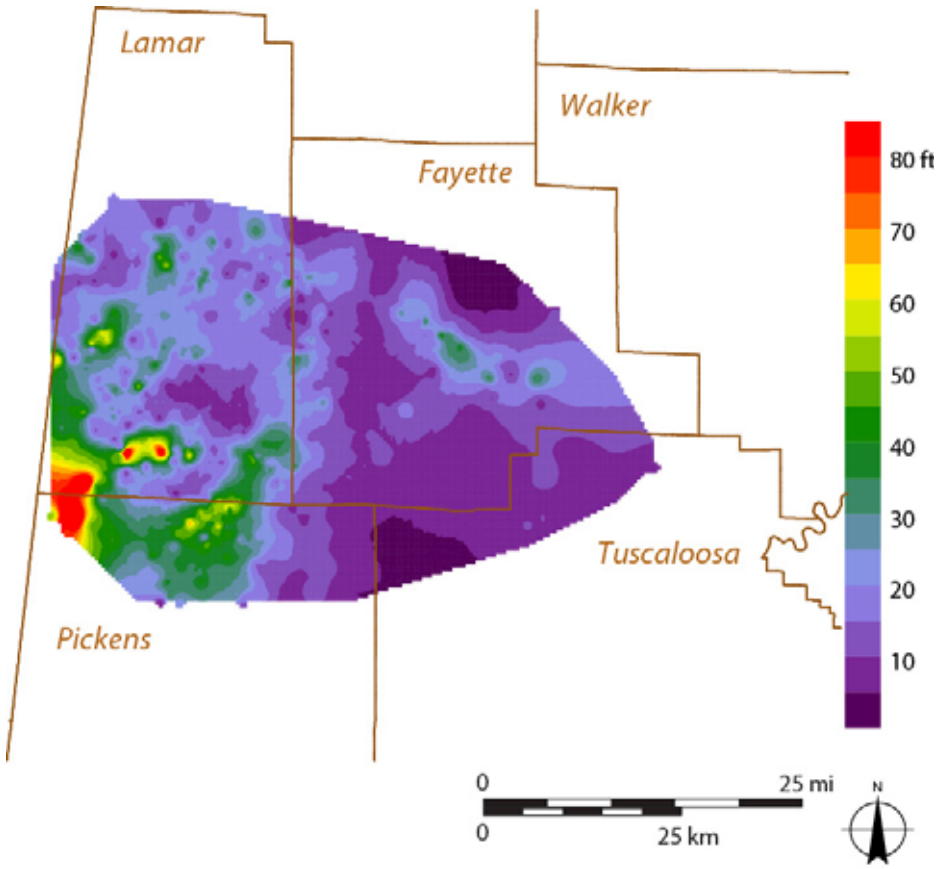

Figure 32.—Net reservoir thickness in the lower Parkwood Formation in the Black Warrior Basin of Alabama.

Pottsville Formation.—The Pottsville Formation disconformably overlies the Parkwood Formation and constitutes the bulk of the Pennsylvanian System in Alabama. The Pottsville is typically subdivided into lower and upper parts. The lower Pottsville is dominated by thick, quartzose sandstone units (Figure 39), whereas the upper Pottsville contains cyclic successions of shale, impermeable sandstone, and coal. Lower Pottsville sandstone contains some significant conventional gas reservoirs, whereas the upper Pottsville contains nearly all of the commercial coal and coalbed methane resources in the Black Warrior Basin (e.g., Pashin, 1994, 2004; Pashin and others, 2009). Hence, this study is focused on the stacked quartzose sandstone in the lower Pottsville. The Pottsville has been interpreted as a fluvial-deltaic succession, and the quartzose

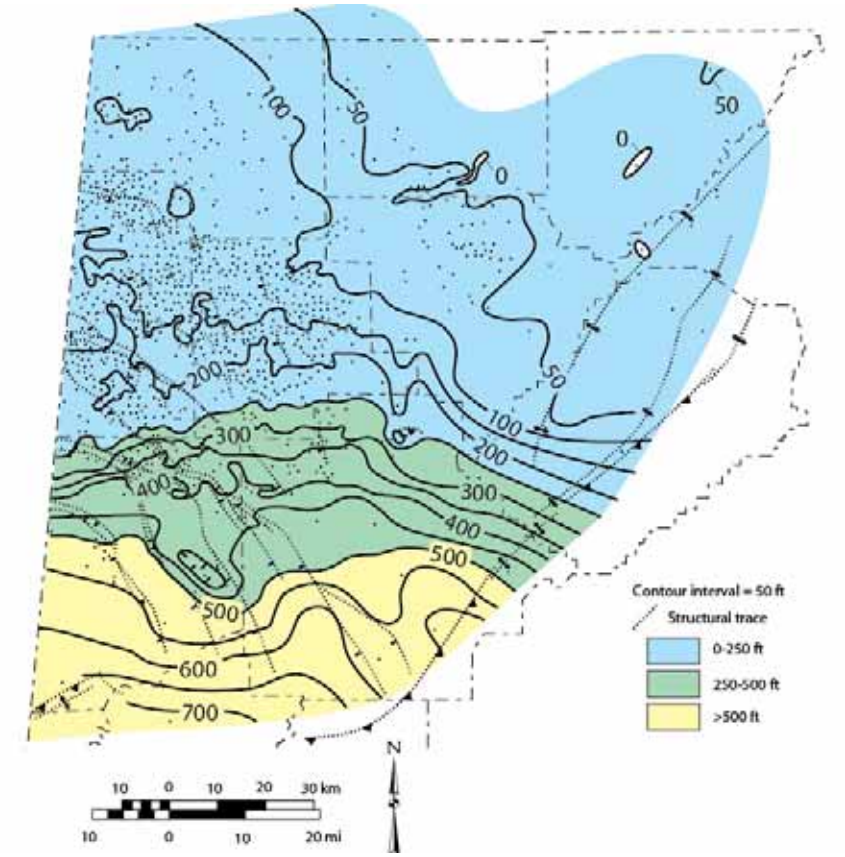

Figure 33.—Isopach map of the middle Parkwood Formation in the Black Warrior Basin of Alabama (after Pashin, 1993).

sandstone units have been interpreted as delta-destructive beach barrier and tidal shoal deposits (Hobday, 1974; Gastaldo and others, 1993; Pashin, 1994, 2004).

The lower Pottsville contains three major depositional cycles: the lower Boyles, upper Boyles, and Fayette cycles (Figure 39). Each cycle is readily correlated across the study area and contains quartzose sandstone bodies that are at least locally productive of natural gas. The Boyles Sandstone Member of the Pottsville Formation forms the bulk of the lower Boyles cycle and consists primarily of quartzarenitic sandstone and conglomerate with pebbles of vein quartz. The sandstone tends to fine upward into thinly interbedded shale and sandstone, and the cycle is capped by the Bear Creek coal zone. The upper Boyles contains numerous stacked sandstone

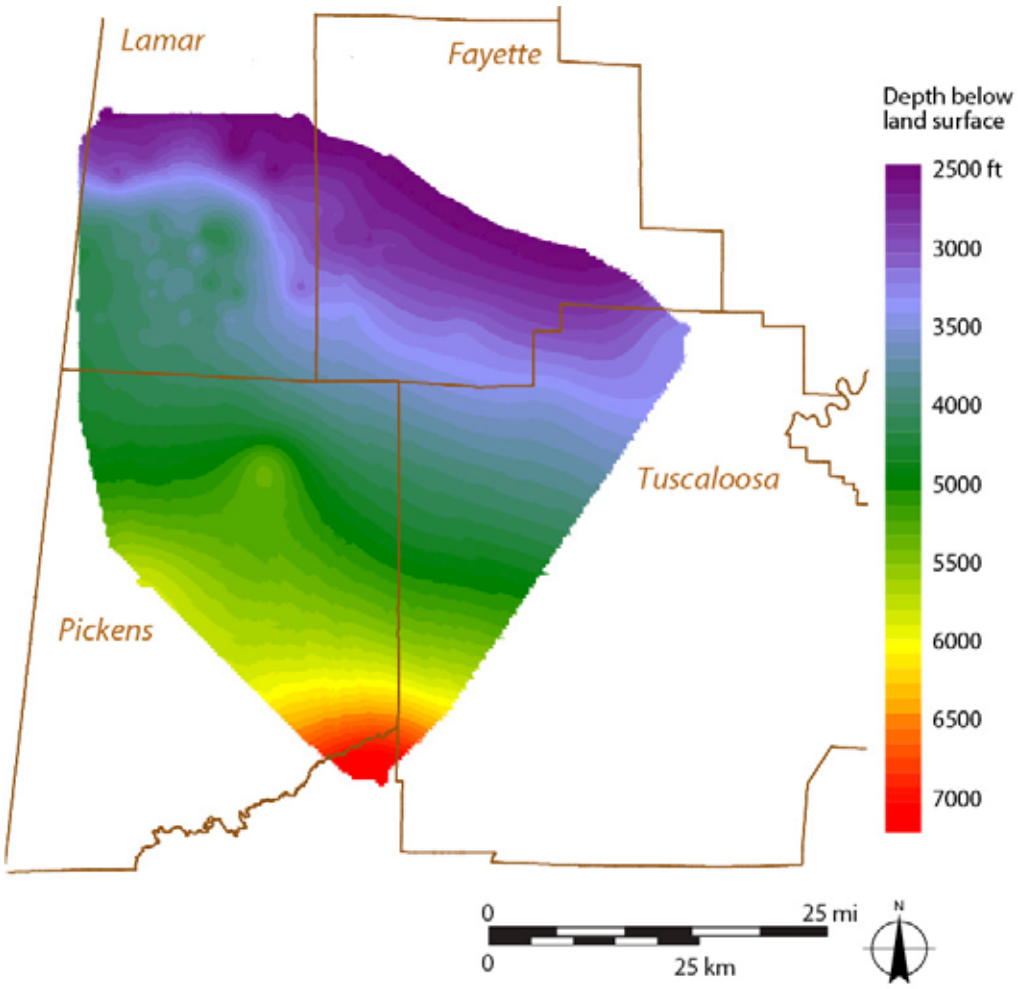

Figure 34.—Depth to the top of the middle Parkwood Formation in the Black Warrior Basin of Alabama.

units, and the thickest sandstone bodies are clustered in the middle part of the interval (Figure 40). The Fayette cycle contains a thick marine shale unit at the base that can be correlated across most of the basin and is thus a significant reservoir seal. The Fayette sandstone sharply overlies the marine shale and is a significant natural gas reservoir. Another thick marine shale unit forms the base of the upper Pottsville and provides a regional topseal for the lower Pottsville sandstone units. In addition to the regional seals, the lower Pottsville contains thick successions of interbedded shale and sandstone that provide baffles and barriers, as well as local seals, and thus help contain fluids in the target sandstone bodies.

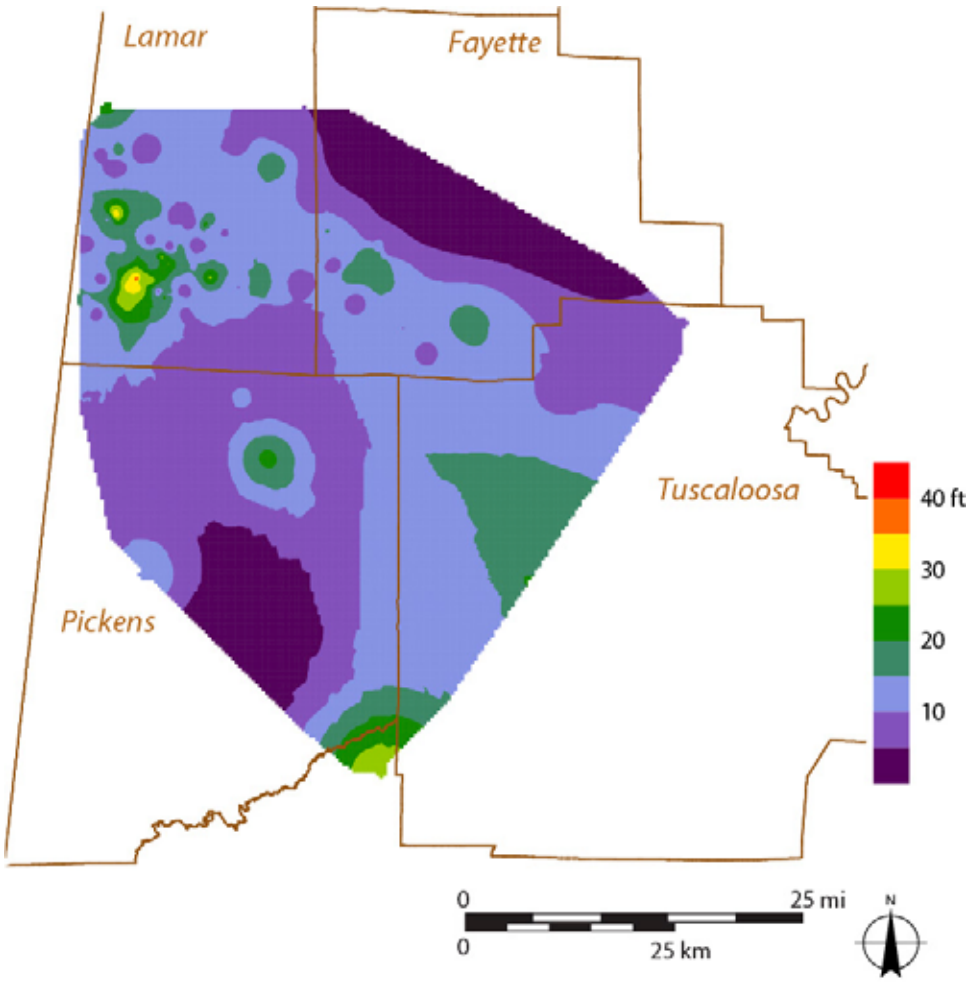

Figure 35.—Net reservoir thickness in the middle Parkwood Formation in the Black Warrior Basin of Alabama.

Conventional core analyses are available from 43 samples of reservoir sandstone and indicate that the lower Pottsville can store significant amounts of CO_2 (Figure 24, Table 1). Porosity ranges from 10.2 to 28.3 percent and averages 192 percent, whereas permeability ranges from 1.8 to 471 mD and has a log normal mean of 89 mD. Subsurface mapping indicates that the Pottsville Formation has storage potential in a large part of the Black Warrior Basin in an area covering more than 2,300 mi^2 (5,960 km^2). The lower Boyles is deeper than 2,500 feet in much of Lamar, Pickens, and Tuscaloosa Counties (Figure 41). Mapping the thickness of porous sandstone reveals significant heterogeneity, and net thickness exceeds 200 feet in many areas

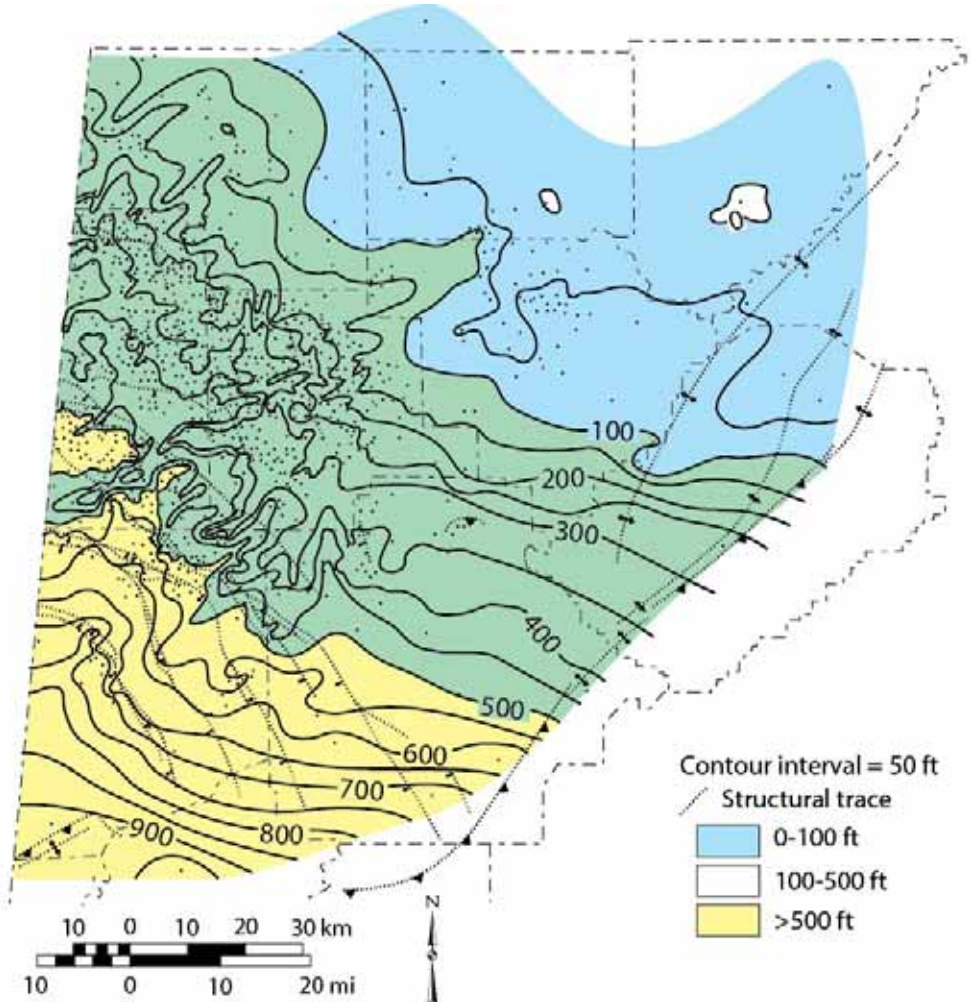

Figure 36.—Isopach map of the upper Parkwood Formation in the Black Warrior Basin of Alabama (after Pashin, 1993).

(Figure 42). The upper Boyles cycle is deeper than 2,500 feet in an area similar to that of the lower Boyles and is locally deeper than 5,500 feet (Figure 43). Net reservoir thickness in the upper Boyles is highly variable and is greater than 100 feet in many areas. Fayette sandstone is deeper than 2,500 feet mainly in Lamar and Pickens Counties (Figure 44). Mapping net reservoir thickness indicates that heterogeneity is similar to that in the other Pottsville sandstone units, and that net reservoir thickness exceeds 75 feet in many areas (Figure 45). Results indicate that the lower Pottsville is one of the most attractive targets for CO_2 storage in the Black Warrior Basin

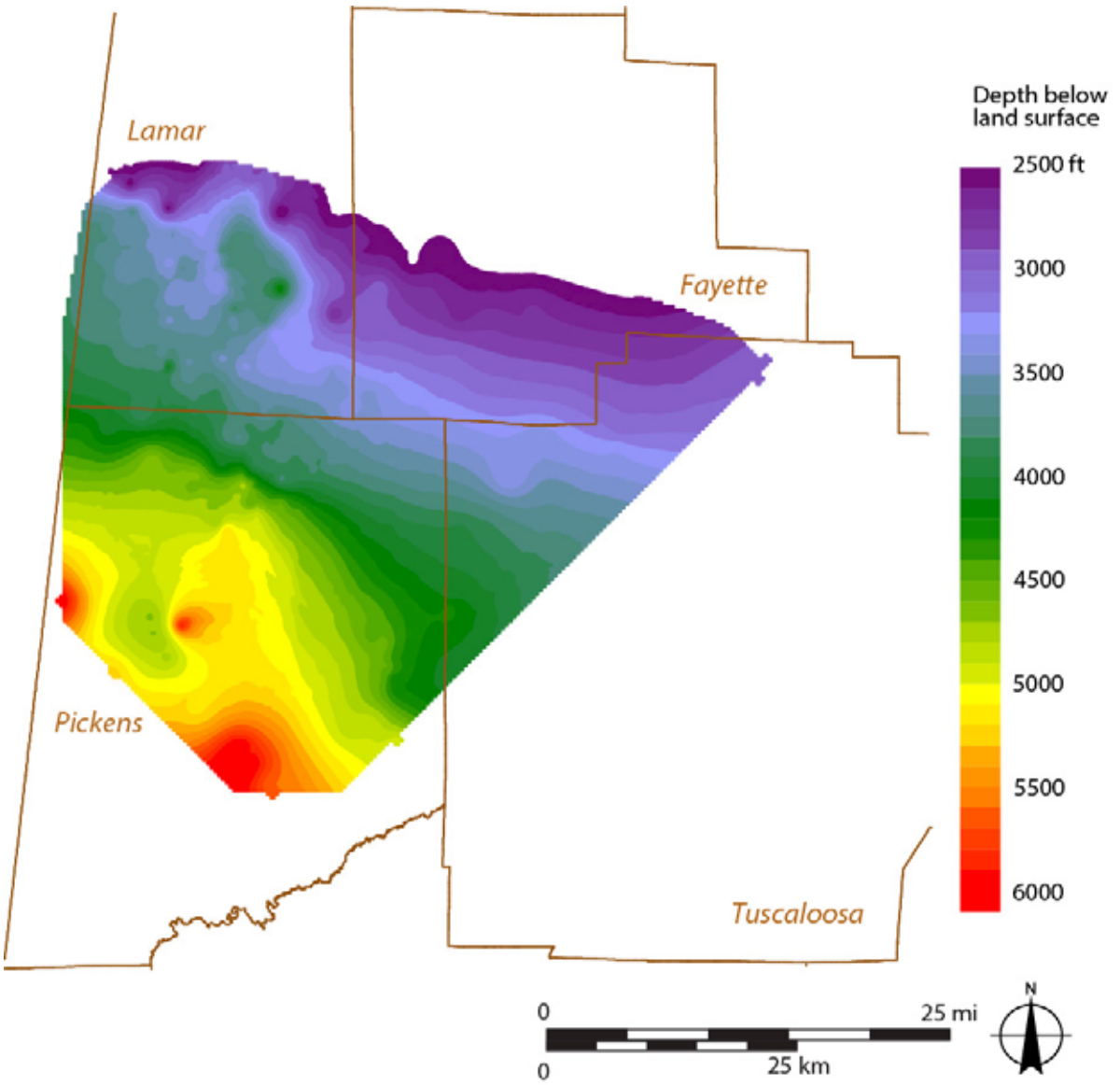

Figure 37.—Depth to the top of the upper Parkwood Formation in the Black Warrior Basin of Alabama.

on the bases of reservoir quality, reservoir thickness, and the presence of widespread seals. This leads us to the discussion of capacity and injectivity, which is critical for evaluating each target storage interval.

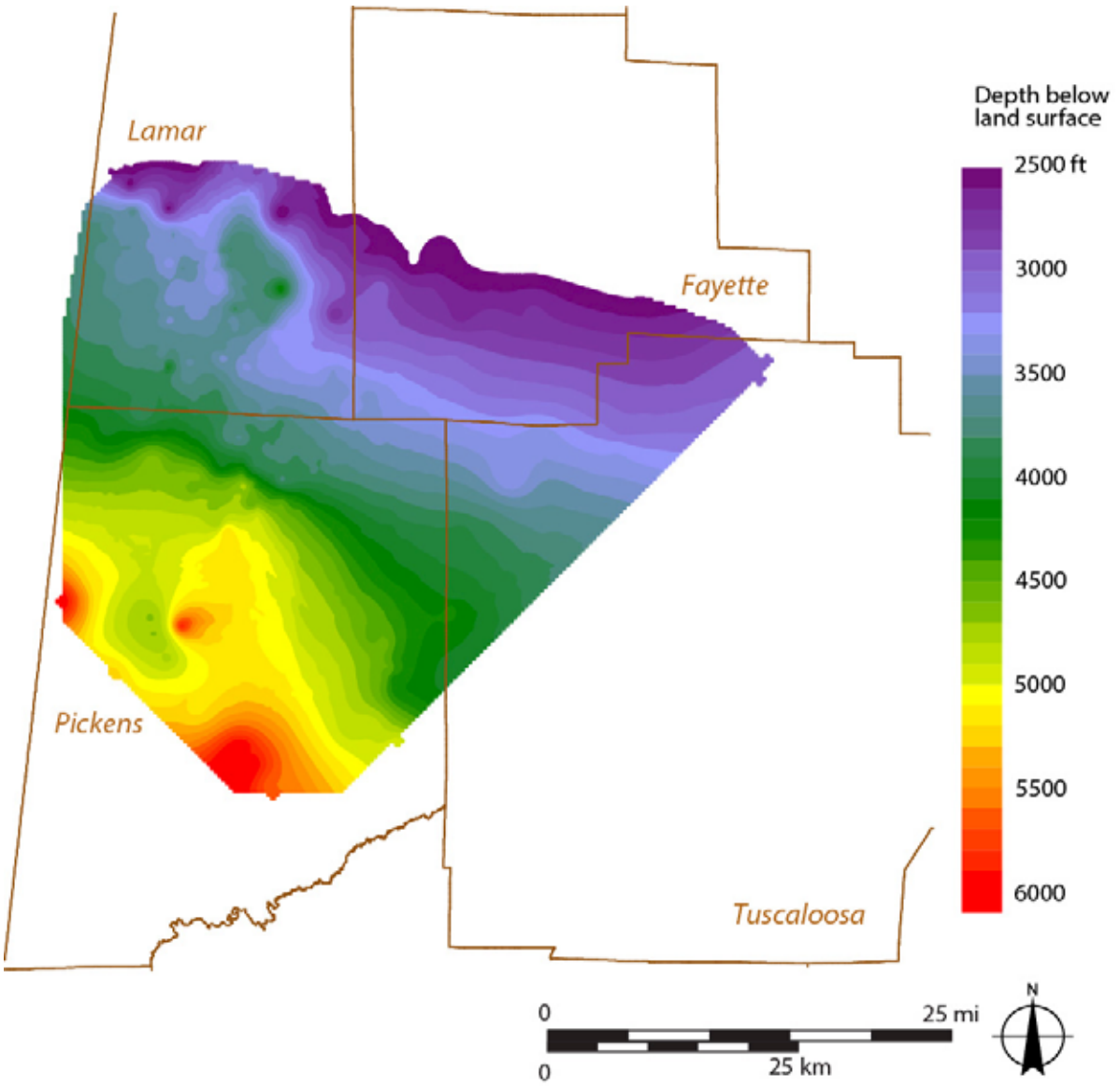

Figure 38.—Net reservoir thickness in the upper Parkwood Formation in the Black Warrior Basin of Alabama.

Capacity and Injectivity Assessment

The distribution and geologic characteristics of potential geologic carbon sinks in the Black Warrior Basin is highly variable. The major parameters used to quantify capacity were potential sink area, average porosity, reservoir thickness, and CO_2 density (table 2). The capacity estimates for each stratigraphic unit analyzed were calculated for three scenarios of storage efficiency (P_{15},

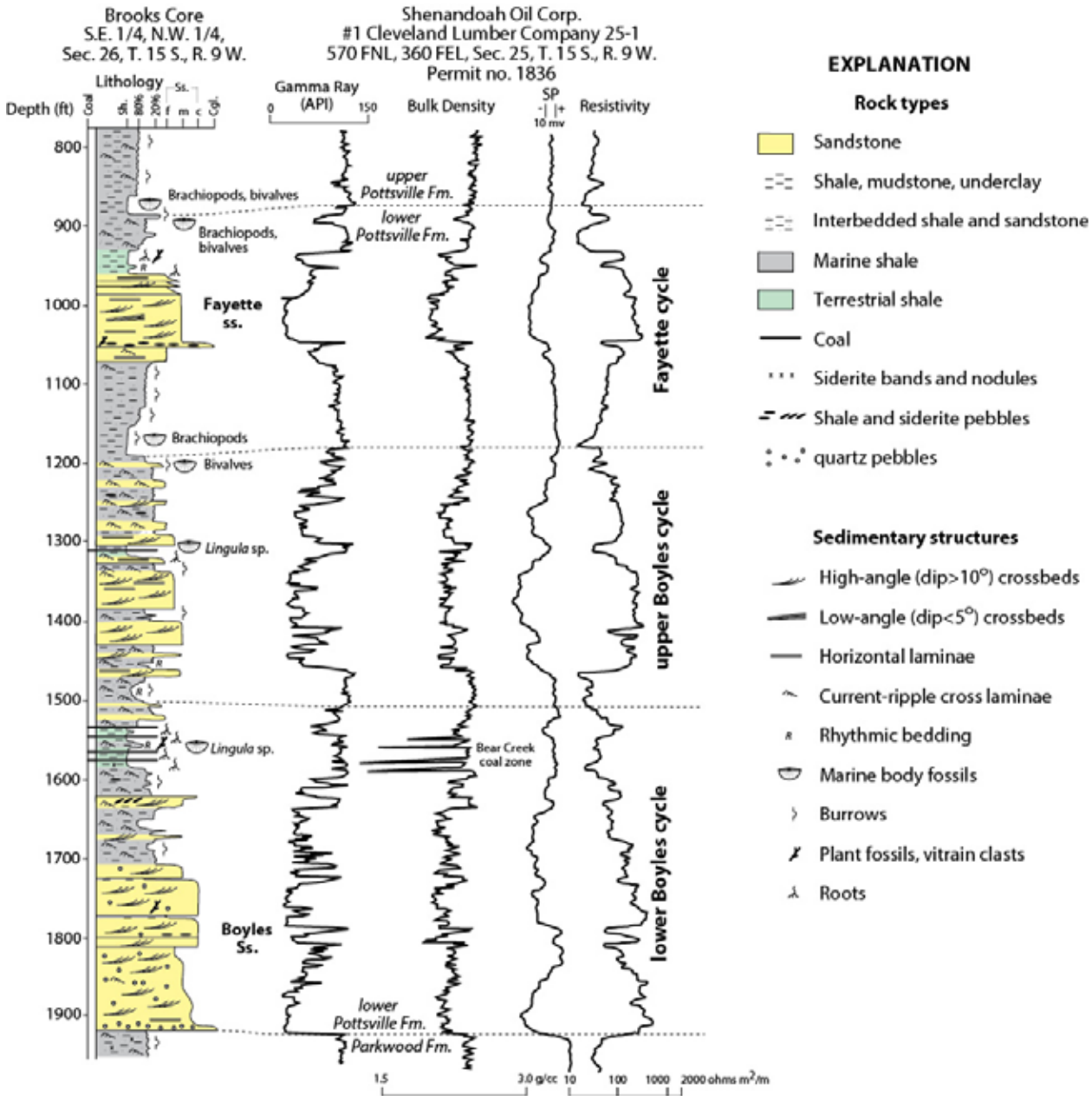

Figure 39.—Measured section of the lower Pottsville Formation in the Brooks core, Walker County, Alabama (after Pashin, 2004).

P_{50}, P_{85}) and are summarized in Table 3. Estimates of capacity also include the number of years of emissions that can be stored by each unit based on the available estimates of emission rates for the Gorgas and Miller steam plants (27.45 Mt/yr), as well as the estimated P_{50} capacity of each

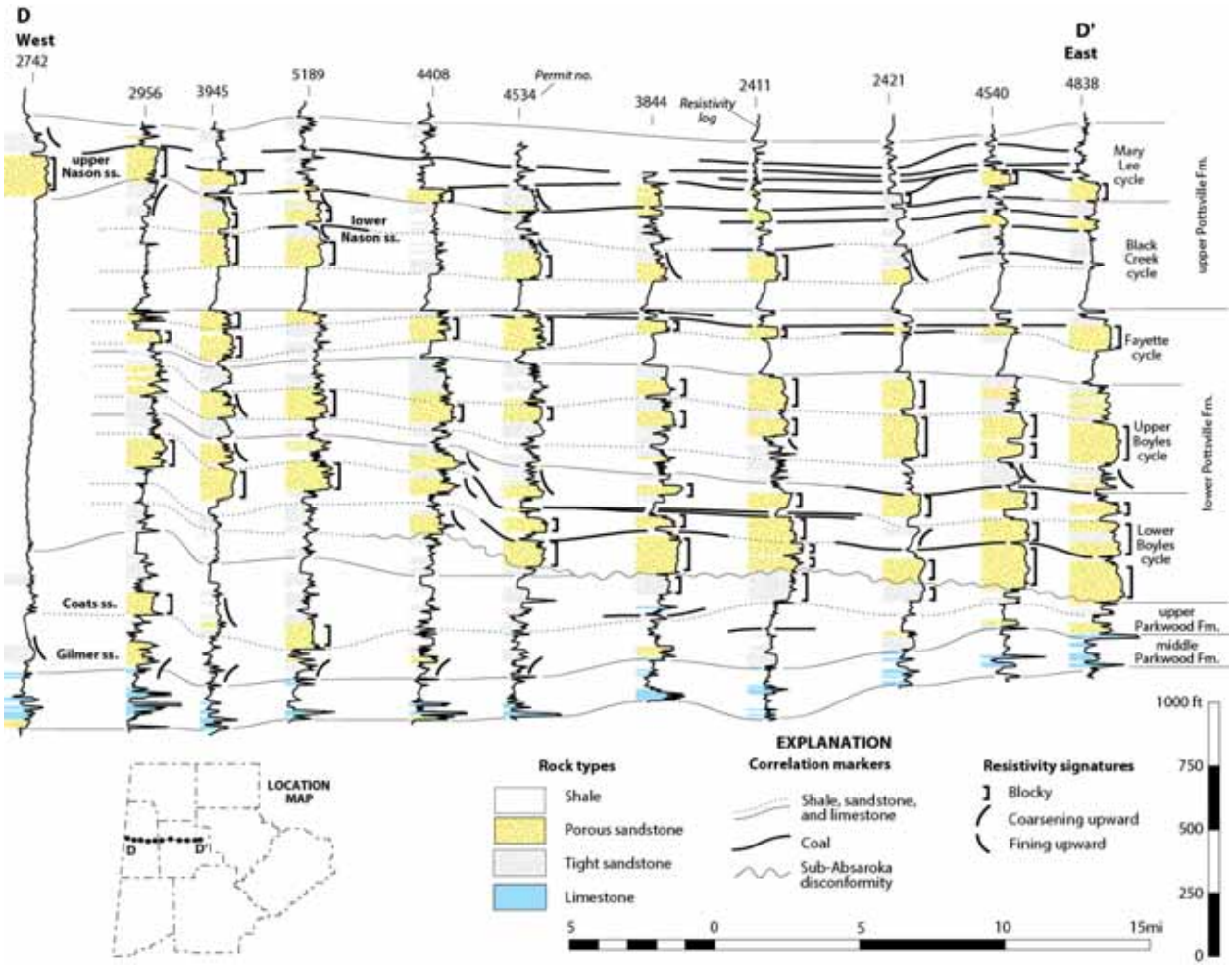

Figure 40.—Regional cross section showing the distribution of reservoir sandstone and sealing shale units in the lower Pottsville Formation.

unit (Table 3). Information on injectivity comes mainly from saltwater disposal operations in the Black Warrior basin and is summarized in Table 4. This information provides the best available baseline indication of the reservoir performance that can be expected during the implementation of sequestration operations.

The results of capacity analysis reflect differences in geologic characteristics and areal extent of the candidate sinks in the Black Warrior Basin of Alabama (Table 3). The Knox Group ranks second among the stratigraphic units analyzed in terms of capacity, with a P_{50} value of about 650 megatonnes (Mt). This estimate is conservative, because it does not consider the impact of

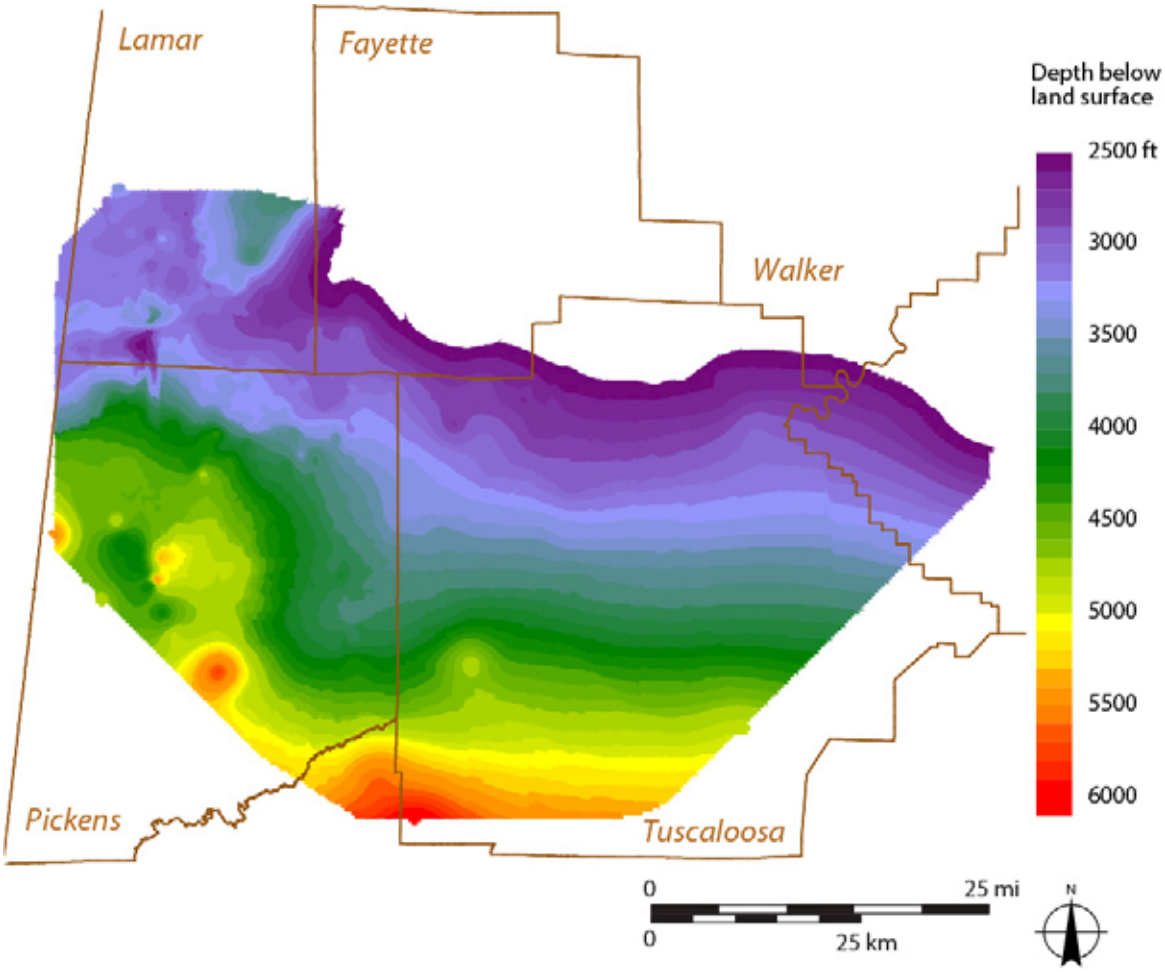

Figure 41.—Depth to the top of the lower Boyles cycle of the lower Pottsville Formation in the Black Warrior Basin of Alabama.

natural fracture networks, which are an important source of injectivity and storage in the Knox Group (Ortiz and others, 1993). Storage capacity in Ordovician carbonate strata of the Stones River Group and the Sequatchie Formation together are about 230 Mt, but low porosity and permeability make the viability of utilizing this potential questionable. Capacity in the Silurian Red Mountain Formation is about half of that in the Knox Group, and concerns about limited injectivity because of low porosity and permeability are similar to those in older rocks. Devonian carbonate has similar capacity to the Red Mountain Formation, but porosity and permeability are

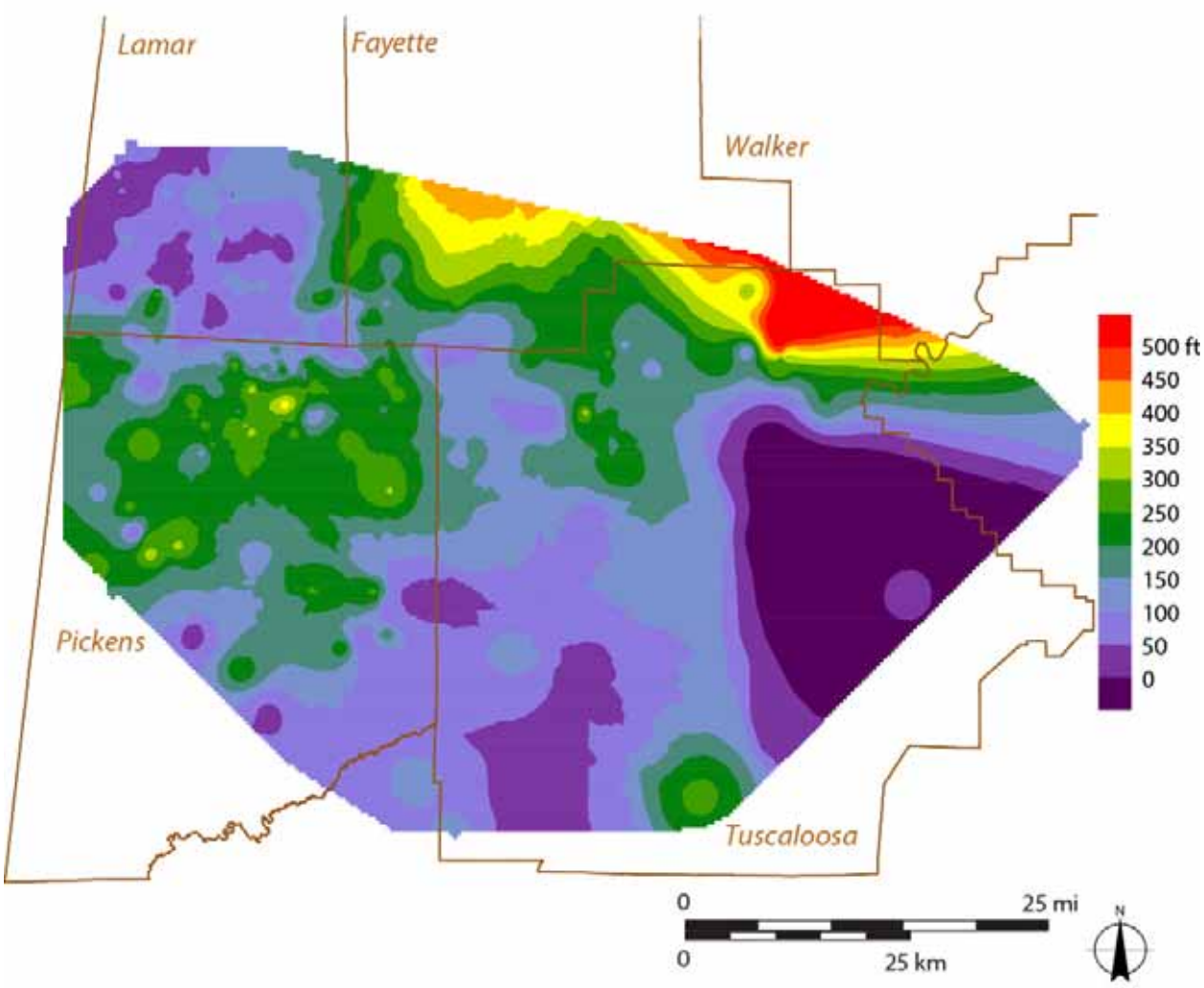

Figure 42.—Net reservoir thickness in lower Boyles sandstone in the lower Pottsville Formation of the Black Warrior Basin in Alabama.

significantly higher. As in the Knox Group, natural fractures in Devonian carbonate are thought to have facilitated saltwater disposal operations.

The Mississippian System has an estimated P_{50} capacity of about 380 Mt of CO_2. Of this, 141 Mt of capacity is in the Tuscumbia Limestone. However, limited porosity and permeability in the Tuscumbia make utilization of this unit questionable, and this zone has not been used for underground injection in the past. The P_{50} capacity of the Bangor Limestone is estimated to be only 24 Mt, and poor reservoir characteristics give the Bangor low priority as a geologic carbon

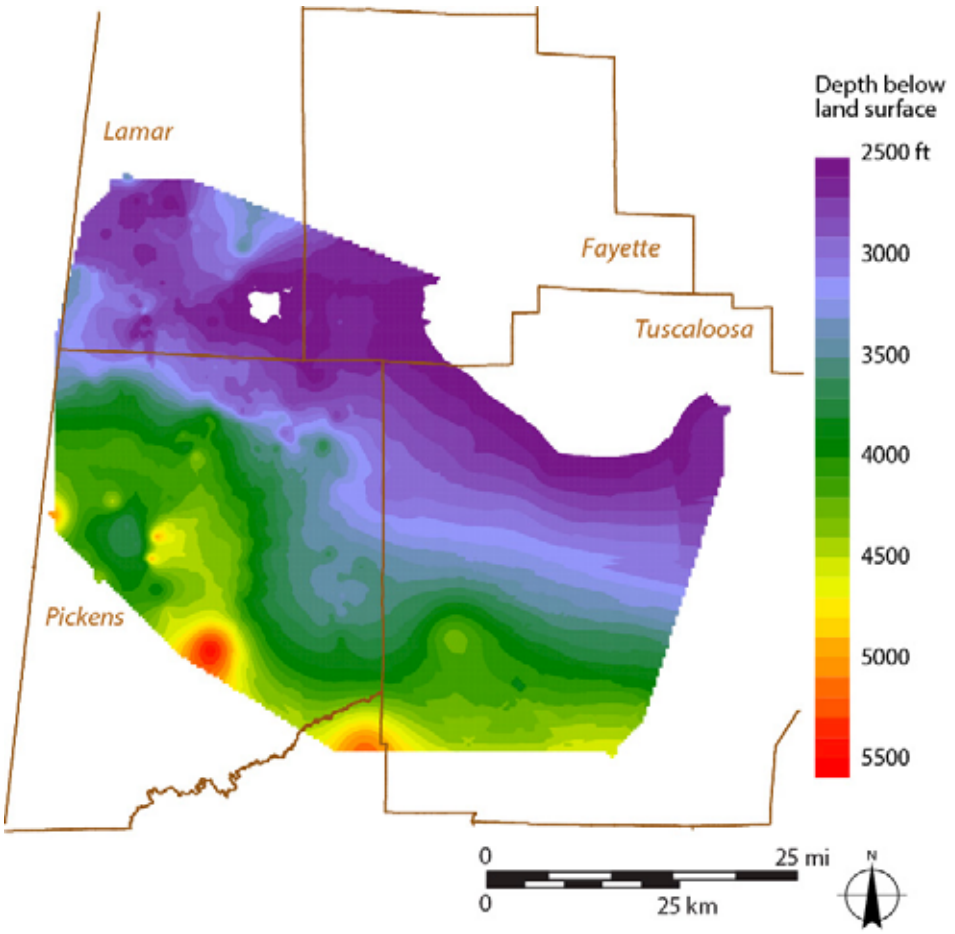

Figure 43.—Depth to the top of the upper Boyles cycle of the lower Pottsville Formation in the Black Warrior Basin of Alabama.

sink. Whereas the potential of Mississippian carbonate units is limited, that of the sandstone units is more promising. The Lewis sandstone has capacity on the order of 58 Mt, and natural gas production from this interval demonstrates that the bounding strata have significant sealing capacity. Although capacity and the available area in the Hartselle Sandstone are limited, potential is greatest at the locations of the steam plants. Hence, although the Hartselle does not provide a long-term opportunity, it does provide the best opportunity to begin operations on or near plant property. The Parkwood Formation has P_{50} capacity of about 150 Mt, and with proven oil and gas production, is among the most attractive storage intervals in the Black Warrior Basin.

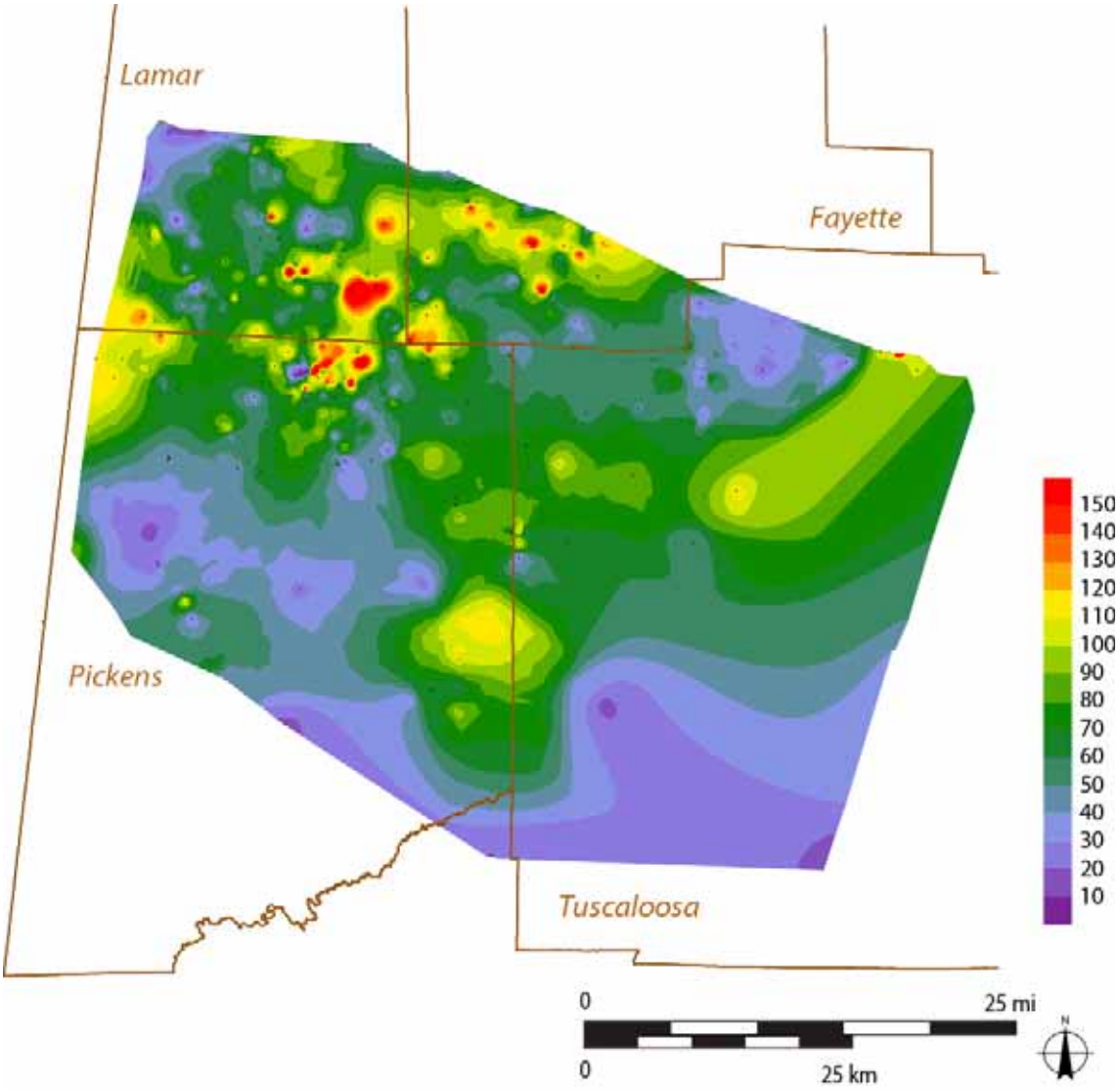

Figure 44.—Net reservoir thickness in the upper Boyles cycle of the lower Pottsville Formation in the Black Warrior Basin of Alabama.

The lower Parkwood, moreover, has been utilized for underground gas storage in East Detroit Field in northern Lamar County, suggesting that this interval can be used safely for CO_2 storage.

Pottsville reservoir sandstone makes a superior target for geologic CO_2 storage in the Black Warrior basin because it has the highest porosity and permeability of any unit characterized (tables 2 and 3). In addition, the Pottsville is shallower than the other sinks in any given area, which can help control drilling and injection costs. Estimated P_{50} capacity in the lower Pottsville

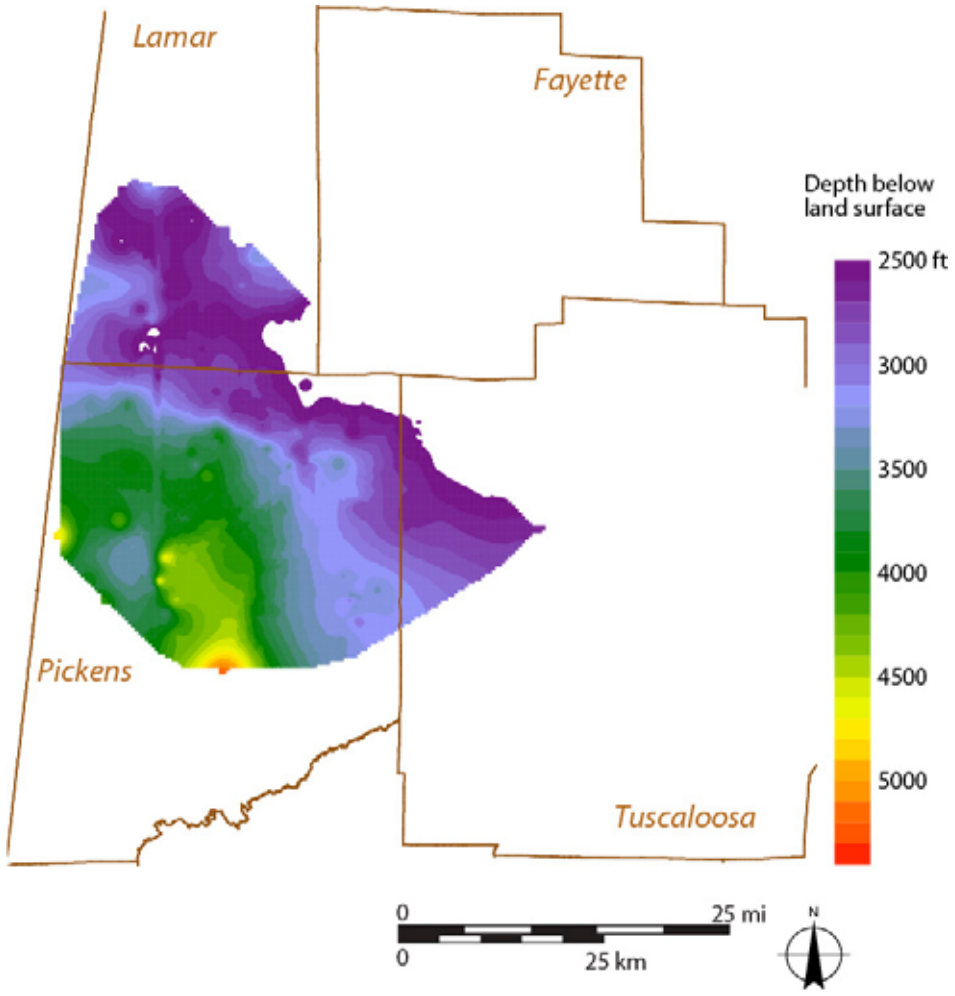

Figure 45.—Depth to the top of the Fayette cycle of the lower Pottsville Formation in the Black Warrior Basin of Alabama.

is estimated to be greater than 1,350 Mt, which is equivalent to nearly 50 years of emissions from the Miller and Gorgas steam plants. More than 70 percent of this capacity is in sandstone and conglomerate of the lower Boyles cycle, whereas 22 percent is in the middle Boyles and 8 percent is in the Fayette sandstone. At least two of these intervals contain reservoir quality sandstone in most areas, indicating that Pottsville strata provide the best potential for stacked geologic storage in the Black Warrior Basin. The lower Pottsville, moreover, has been used for

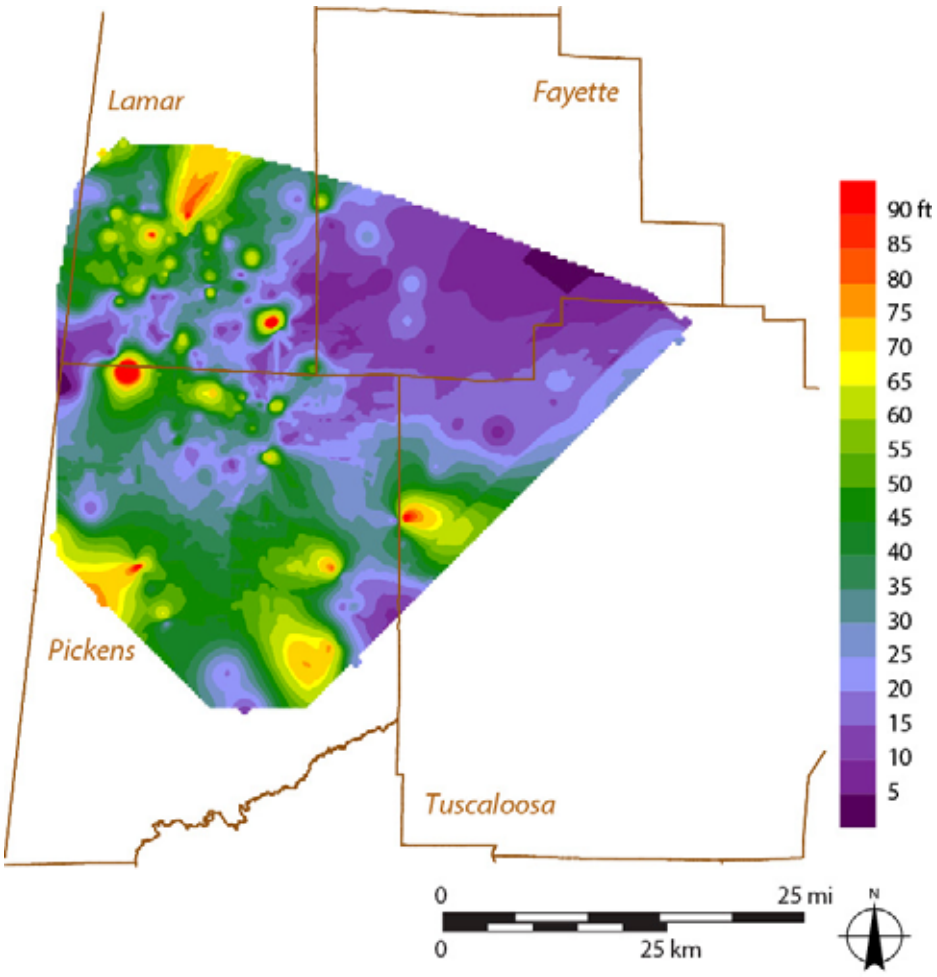

Figure 46.—Net reservoir thickness in the Fayette cycle of the lower Pottsville Formation in the Black Warrior Basin of Alabama.

underground injection, and the occurrence of regional seals above the lower Boyles and Fayette sandstone units can facilitate secure storage.

Underground injection operation have been performed for the disposal of subsurface brine at depths between 2,400 and more than 10,000 feet in the Black Warrior basin in formations ranging in age from Cambrian through Pennsylvanian (Table 4). These formations have had maximum allowable injection rates between 1,350 and 10,800 bbl/d and maximum allowable wellhead injection pressures between 350 and 1,750 psig. Based on these numbers, the maximum injectivity of these zones ranges from 0.8 to 11.8 bbl/d/psig.

Table 2. Summary of parameters used to assess capacity of candidate CO_2 sinks in the Black Warrior Basin, Alabama.

Formation or Group	Member	Age	Sink area (mi^2)	Porosity (%)	Reservoir thickness (ft)	CO_2 density (lb/ft^3)
Pottsville	Fayette	Pennsylvanian	894	19	60	31
Pottsville	U. Boyles	Pennsylvanian	1,806	19	70	34
Pottsville	L. Boyles	Pennsylvanian	2,485	19	145	37
Parkwood	U. Parkwood	Mississippian	1,430	10	40	37
Parkwood	M. Parkwood	Mississippian	1,600	10	15	37
Parkwood	L. Parkwood	Mississippian	1,138	10	25	37
Bangor		Mississippian	859	8	20	37
Hartselle		Mississippian	234	10	25	28
Pride Mountain	Lewis	Mississippian	1,589	10	25	39
Tuscumbia		Mississippian	3,153	8	30	40
Devonian		Devonian	3,176	7	80	42
Red Mountain		Silurian	4,119	6	80	41
Sequatchie		Ordovician	3,769	4	30	41
Stones River		Ordovician	4,226	5	50	41
Knox		Cambrian-Ordovician	7,353	6	105	41

The two injection wells in the Knox Group were completed at depths of 8,800 feet and 10,000 feet and injected into up to 1,000 feet of section (Table 4). The high rate achieved by the well in Hale County reflects a combination of great reservoir thickness coupled with abundant natural fractures. The well in Tuscaloosa County was drilled to dispose of brine from coalbed methane operations and supported rates exceeding 3,000 bbl/d with half of the injectivity reported from the Hale County well. Devonian carbonate also was used for disposal of produced water from coalbed methane operations and had about half of the injectivity of the Tuscaloosa County Knox well.

Two wells completed in Parkwood sandstone were used for brine disposal in Fayette and Tuscaloosa Counties (table 4). These wells were injected at depths of 2,400 and 3,600 feet and had maximum allowable injection rates of 1,350 and 3,600 bbl/d. Significantly higher pressure

Table 3. Estimates of CO_2 capacity in candidate geologic carbon sinks in the Black Warrior Basin, Alabama.

Formation or Group	Member	Age	Depositional Environment	Low (P15; Mt)	Medium (P50; Mt)	High (P85: Mt)	Capacity (yr at P_{50})
Pottsville	Fayette	Pennsylvanian	Deltaic, beach	16.0	117.9	219.8	4.3
Pottsville	U. Boyles	Pennsylvanian	Deltaic, beach	41.3	304.7	568.0	11.1
Pottsville	L. Boyles	Pennsylvanian	Deltaic, beach	128.1	945.0	1,761.9	34.4
Pottsville total				*185.4*	*1,367.6*	*2,549.7*	*49.8*
Parkwood	U. Parkwood	Mississippian	Deltaic	10.7	78.9	147.2	2.9
Parkwood	M. Parkwood	Mississippian	Deltaic, beach	4.5	33.1	61.8	1.2
Parkwood	L. Parkwood	Mississippian	Deltaic, beach	5.3	39.3	73.2	1.4
Bangor		Mississippian	Carbonate shelf	3.2	23.7	44.2	0.9
Hartselle		Mississippian	Beach	0.8	6.1	11.4	0.2
Pride Mountain	Lewis	Mississippian	Beach	7.8	57.8	107.7	2.1
Tuscumbia		Mississippian	Carbonate shelf	19.1	141.2	263.2	5.1
Mississippian total				*51.4*	*380.1*	*708.7*	*13.8*
Devonian		Devonian	Carbonate shelf	37.8	278.6	519.5	10.1
Red Mountain		Silurian	Carbonate shelf	41.0	302.4	564.0	11.0
Sequatchie		Ordovician	Carbonate shelf	9.4	69.2	129.0	2.5
Stones River		Ordovician	Carbonate shelf	21.9	161.6	301.3	5.9
Knox		Cambrian-Ordovician	Carbonate shelf	88.0	649.7	1,210.9	23.7
Grand Total				***414.5***	***3,058.5***	***5,702.2***	***111.4***

was required to achieve the lower of the two injection rates, and this is reflected in injectivity of only 0.8 bbl/d/psig. Injectivity in the Fayette County well was the same as that in the Tuscaloosa County Knox well.

The highest injectivity was reported from disposal wells in the lower Pottsville Formation in Pickens and Tuscaloosa Counties (table 4). Depth of the injection zones ranges from 4,500 to 5,150 feet, and wellhead injection pressures were only 350 to 787 psig. Injectivity is between 6.2

Table 4. Injectivity in saltwater disposal wells in the Black Warrior basin.

Permit	County	Geologic Unit	Depth (ft)	Maximum injection rate (bbl/d)	Injection Pressure (psig)	Injectivity (bbl/d/psig)
2617-A-SWD-89-2	Tuscaloosa	Pottsville	4,600	4,000	600	6.7
8467-SWD-90-5	Tuscaloosa	Pottsville	4,500	9,325	787	11.8
8376-SWD-90-13	Pickens	Pottsville	5,150	2,160	350	6.2
3475-A-SWD-90-2	Tuscaloosa	Parkwood	3,600	1,350	1,700	0.8
4791-A-SWD-88-5	Fayette	Parkwood	2,400	3,600	1,050	3.4
8864-SWD-90-9	Tuscaloosa	Devonian	7,200	2,435	1,500	1.6
6261-SWD-89-5	Tuscaloosa	Knox	10,000	3,350	995	3.4
8940-SWD-90-10	Hale	Knox	8,800	10,800	1,750	6.2

and 11.8 bbl/d/psig, reflecting the high reservoir quality of lower Pottsville sandstone relative to all other intervals evaluated during this project. Indeed, sandstone in on of the wells supported an injection rate exceeding 9,000 bbl/d, indicating that implementing storage operations in the lower Pottsville Formation.

Results of capacity and injectivity analysis indicate that significant CO_2 storage potential exists in the Cambrian through Pennsylvanian strata of the Black Warrior Basin (tables 3, 4). The greatest potential in terms of both capacity and injectivity lies in lower Pottsville sandstone, and deep Knox carbonate also provides significant storage opportunities. Importantly, wells in each interval support a broad range of injection rates and pressures, which is a direct reflection of reservoir heterogeneity. Lower and middle Paleozoic carbonate units, moreover, have limited matrix porosity and permeability, and so natural fractures play an important role in determining injection properties. The low porosity and permeability of many intervals, moreover, suggests

that accessing the capacity offered by most formations will require the application of drilling and completion technologies tailored specifically for tight geologic formations. Options include the drilling and completion of directional wells, which will help maximize injection rate and the volume of accessible reservoir.

TEST SITE CHARACTERIZATION

Site Selection, Design, and Development

An early decision point during the development of this program was whether to drill a test borehole at the Miller steam plant, which has a nameplate capacity of 2.8 gigawatts, or at the Gorgas steam plant, which has a smaller nameplate capacity of 1.4 gigawatts (Figure 47). Early geological characterization indicated that the Miller steam plant was located on a hinge in the backlimb of the Sequatchie anticline, which is a major frontal Appalachian fold. Plant Gorgas, by comparison, is located west of the anticline in the interior of the Black Warrior basin in an area with minimal structural dip. Experience from drilling coalbed methane wells in the backlimb of the Sequatchie anticline southwest of Plant Miller indicates that fold hinges are zones of enhanced fracturing (Pashin and Groshong, 1998). Because of this, the project team was concerned that similar fracturing posed a stratigraphic containment risk at the Miller steam plant. No such risk was identified at Gorgas, and so the test site was selected there.

The Gorgas #1 borehole was spudded at a surface elevation of 376 feet in the Pratt coal zone of the upper Pottsville Formation and drilled to a total depth of 4,915 feet, reaching bottom in the Copper Ridge Dolomite, which was the deepest objective of the program (Figure 48). The plan was to drill deeper into the Copper Ridge, but influx of fresh water into the well slowed the drilling. Fresh water (total dissolved solids content <10,000 mg/L), moreover, is protected by the

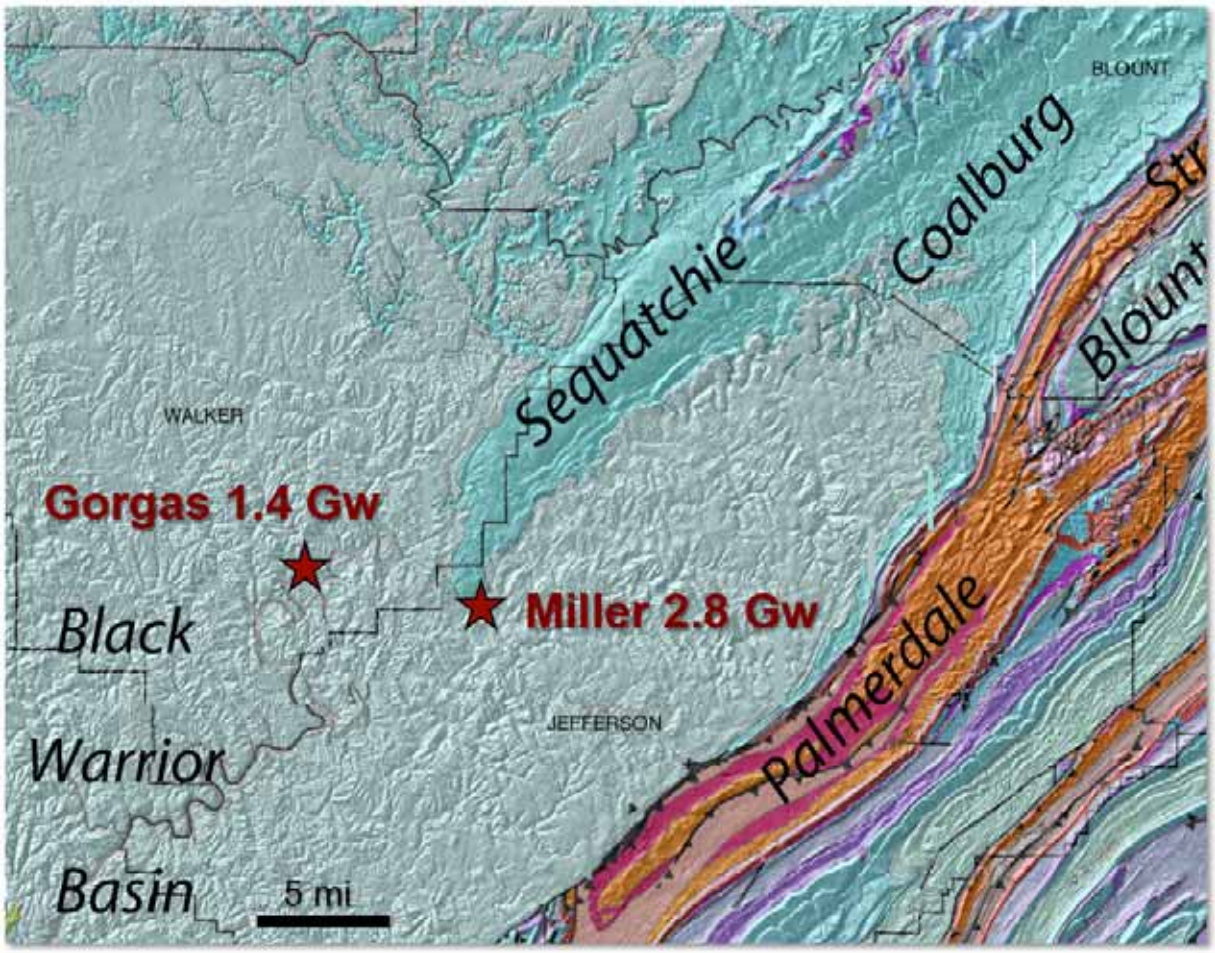

Figure 47.—Geologic map and digital elevation model showing locations of the Gorgas and Miller steam plants relative to the Sequatchie anticline.

Safe Drinking Water Act, precluding CO_2 injection into the Copper Ridge Dolomite. The following sections summarize the geologic formations in the Gorgas #1 borehole, the results of the coring program, and the implications for the application of CO_2 sequestration technology at the Gorgas steam plant, as well as the Black Warrior Basin at large.

Wellbore geology.—The top of the Copper Dolomite, which is the basal formation of the Knox Group in Alabama, was penetrated at a depth of 4,502 feet (Figure 48). The well logs record the upper 413 feet of the formation. The Copper Ridge contains thickly interbedded

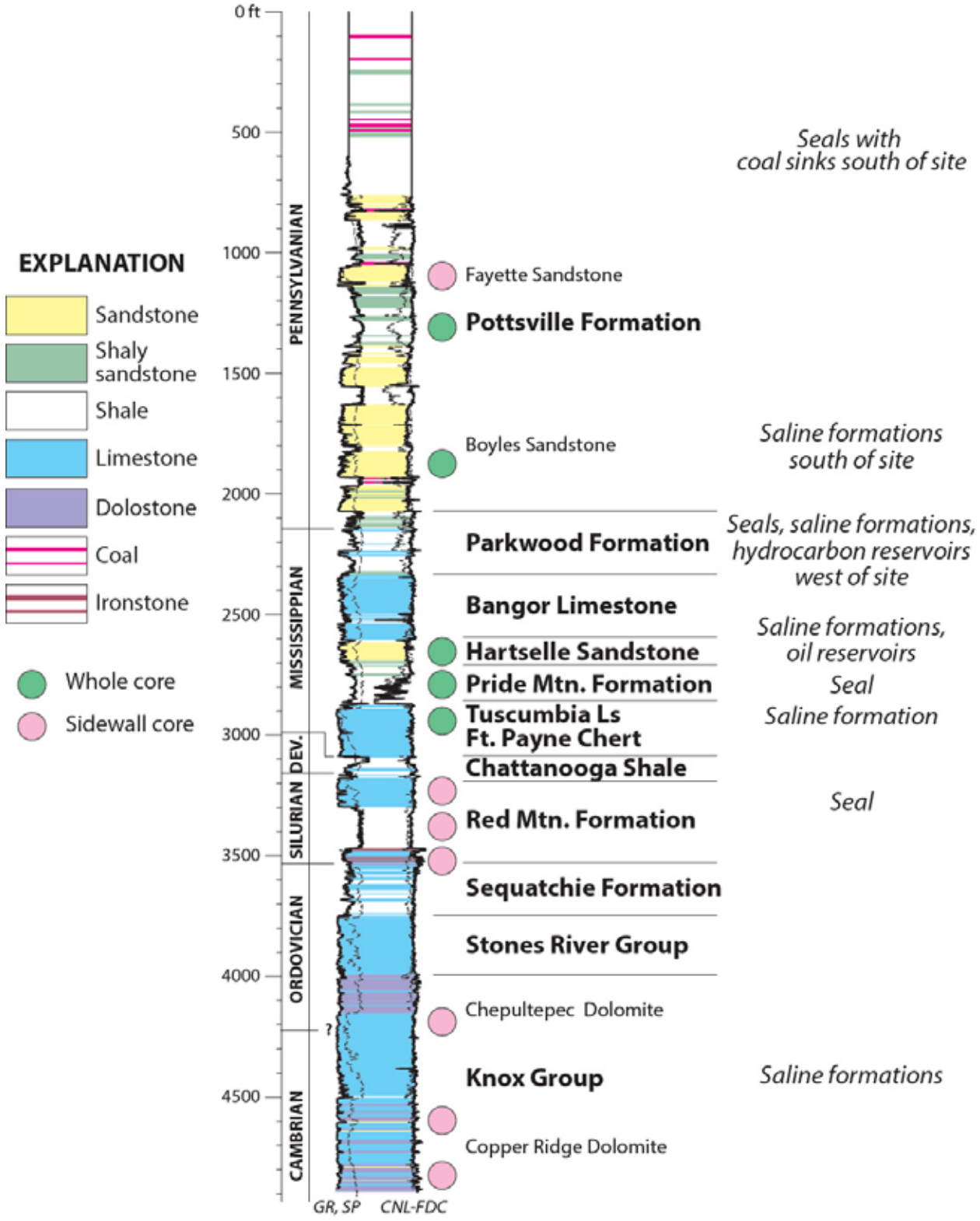

Figure 48.—Stratigraphic column and geophysical well logs of the Gorgas #1 borehole.

limestone and dolostone with some siliceous intervals. The siliceous intervals are locally thicker than 20 feet and include chert-bearing and arenaceous dolostone. Well cuttings and sidewall cores indicate that Copper Ridge carbonate is dominantly micritic.

The Copper Ridge is overlain sharply by the Chepultepec Dolomite, which extends from a depth of 4,010 feet to 4,502 feet, spanning a thickness of 492 feet. The lower 104 feet of the formation is composed of limestone that is argillaceous, weakly arenaceous, and dolomitic. The basal 14 feet of this interval can be classified as argillaceous dolostone, and the remainder can be classified as dolomitic limestone. Dolomite content approaches and locally exceeds 50 percent sporadically in the lower 180 feet of the formation. The middle part of the formation, which spans depths from 4,150 to 4,320 feet is dominated by limestone with less than 10 percent dolomite and negligible amounts of clay and silica. The upper 140 feet of the formation is dominated by dolostone with some thick interbeds of dolomitic limestone. This part of the Chepultepec also contains up to 20 percent clay and silica in places. Together, the Copper Ridge Dolomite and the Cheupultepec Dolomite in the Gorgas #1 borehole are typical of Knox carbonate shelf deposits in the Black Warrior Basin (Thomas, 1988; Osborne and Raymond, 1992). The dolostone at the top of the Chepultepec is interpreted to be the product of widespread exposure and dolomitization during development of the unconformity that marks the top of the Knox Group throughout the eastern United States.

The Stones River Group was logged between depths of 3,747 and 4,010 feet and thus is 263 feet thick (Figure 48). The Stones River overlies the Knox Group with sharp contact, and the basal 20 feet of the Stones River is composed of argillaceous dolostone that grades upward into limestone. Geophysical log analysis indicates that the limestone contains between 3 and 25 percent dolomite and less than 10 percent clay and silica. Well cuttings indicate that the

limestone is dominantly micrite. Skeletal material is common in the limestone between 3,910 and 3,950 feet and is dominated by brachiopods. The Stones River Group represents reestablishment of carbonate shelf sedimentation following regional exposure and development of the Knox unconformity.

The Sequatchie Formation was penetrated between depths of and 3,548 and 3,747 feet and sharply overlies the Stones River Group (Figure 48). The Sequatchie in the Gorgas #1 borehole is 199 feet thick and is composed of thinly interbedded limestone, dolostone, and shale. The formation contains slightly more calcite than dolomite. The shale is very silty, containing subequal amounts of clay and silica, and shale content exceeds 75 percent at depths of 3,670 to 3,676 feet and 3,688 to 3,700 feet. The Sequatchie Formation was deposited during the Taconic orogeny, and the composition of the formation reflects the encroachment of synorogenic sediment onto the carbonate shelf (Thomas, 1988).

The Red Mountain Formation was logged from 3,178 to 3,548 feet and consists of three parts (Figure 48). The basal Red Mountain is composed of interbedded limestone, dolostone, and ironstone and spans 79 feet of section from 3,469 to 3,548 feet. This interval is lithologically heterogeneous and includes intervals of calcareous, oolitic ironstone that has a distinctive reddish-brown color. The middle Red Mountain is composed of silty shale and spans 171 feet of section from 3,298 to 3,469 feet. The shale is dark greenish-gray and is composed of about 70 percent silica and 30 percent clay. The middle Red Mountain is remarkably homogeneous, save for an 11-foot calcareous zone at the top of the interval. The upper Red Mountain constitutes the remaining 120 feet of the formation and is composed principally of coarse-grained crinoidal calcarenite. The calcarenite is gray, although many of the grains have reddish hematite overgrowths. The upper Red Mountain contains some minor argillaceous and dolomitic zones

that are thinner than 10 feet. The Red Mountain Formation in the Gorgas #1 borehole records a diverse succession of depositional environments beginning with the formation of ferruginous oolite shoals. Inundation of the shoals apparently resulted in deposition of a widespread shelf mud blanket followed by deposition of crinoidal limestone in a younger shoal complex. Hematite coatings in the crinoidal limestone apparently reflect regional exposure and unconformity development following Red Mountain sedimentation.

The Devonian section at Plant Gorgas was penetrated between 3,092 and 3,178 feet and includes the unnamed Devonian limestone and the Chattanooga Shale (Figure 48). The Devonian limestone is 58 feet thick and is highly argillaceous. Above the limestone is 18 feet of Chattanooga Shale, which is composed primarily of black, fissile shale that is characterized by high organic content and elevated radioactivity. The Chattanooga Shale has been interpreted as the product of a muddy, oxygen-deficient shelf that extended throughout the Black Warrior Basin during the Late Devonian (Pashin and others, 2010).

No Maury Shale was identified in the Gorgas #1 borehole, and so the Fort Payne Chert appears to rest sharply upon the Chattanooga Shale (Figure 49). The top of the Fort Payne was picked at a depth of 3,020 feet and spans 72 feet of section. Cuttings indicate that the Fort Payne is composed principally of dark gray calcimicrite, dolomicrite, and chert, with chert forming 20 to 40 percent of the formation. The Tuscumbia Limestone spans 130 feet of section from 2,890 to 3,020 feet at Plant Gorgas. The basal 28 feet of the Tuscumbia is dominated by chert, which decreases in abundance upward in the Formation. The upper 50 feet of the formation lacks chert. Dolomite content is minimal in the Tuscumbia Limestone, and the formation records a transition from micritic rock types to crinoid-bryozoan calcarenite. The lithologic succession is typical of the progradational carbonate shelf deposits in the Fort Payne-Tuscumbia interval, although the

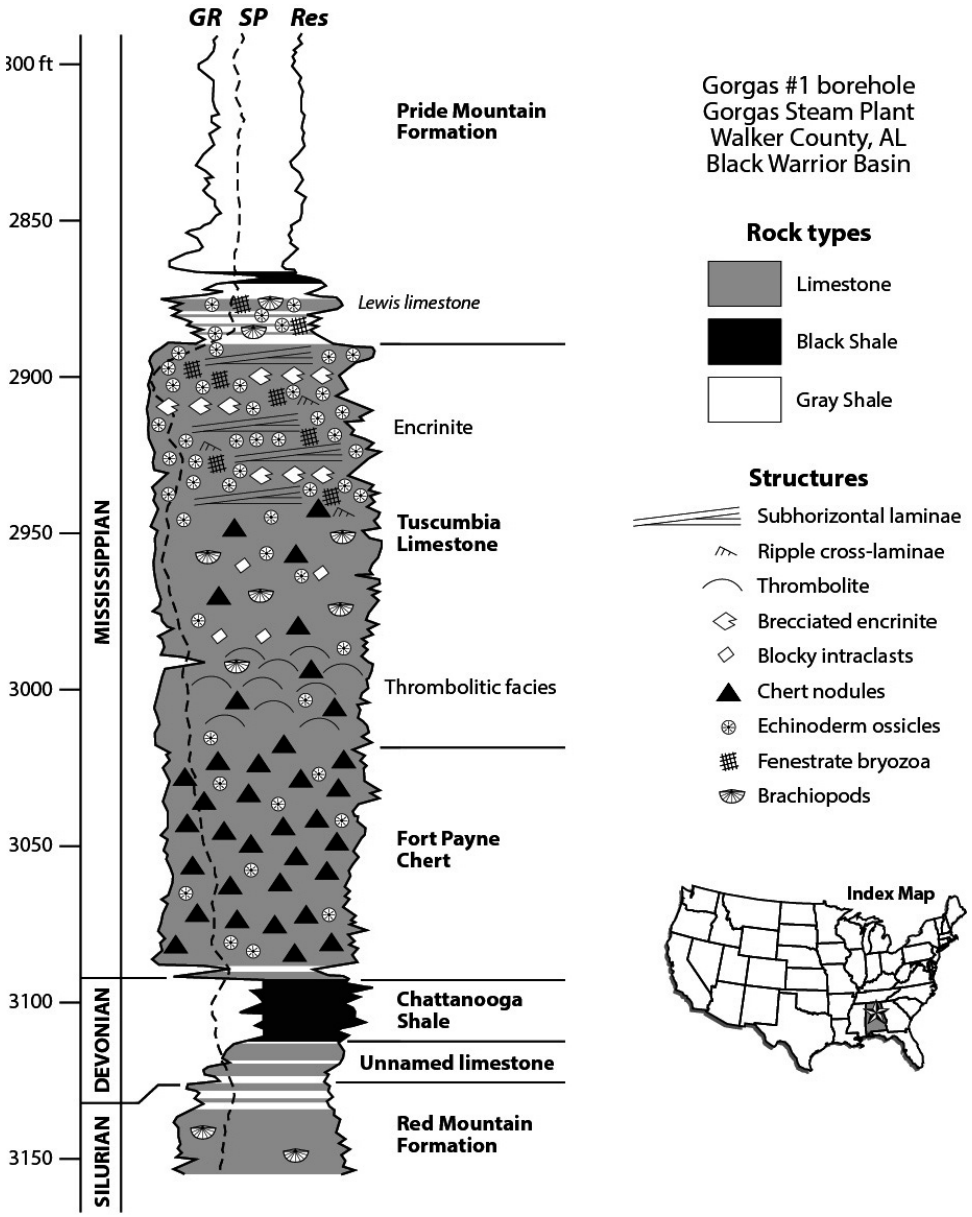

Figure 49.—Stratigraphic column and geophysical well logs of the Tuscmbia Limestone and Fort Payne Chert in the Gorgas #1 borehole.

Gorgas #1 borehole contains an unusual reefal facies near the base of the Tuscumbia, which has been studied in detail by Kopaska-Merkel et al. (2013).

The Tuscumbia Limestone is overlain sharply by the Pride Mountain Formation, which consists of the Lewis limestone and a thick shale section. The top of the Pride Mountain Formation is at a depth of 2,698 feet, and the formation has a total thickness of 192 feet. The

Lewis limestone forms the basal 18 feet of the formation and is composed of interbedded shale and calcarenite containing abundant crinoids, fenestrate bryozoans, and brachiopods. The remainder of the Pride Mountain Formation is silty shale that grades upward into thinly interbedded shale, siltstone, and sandstone. The lower 105 of the Pride Mountain shale caved extensively prior to logging, and so the log data are not reliable for interpreting rock properties. Examination of cuttings indicates that the shale is fairly homogeneous and lacks significant carbonate and siltstone-sandstone layers. Siltstone and sandstone content increase markedly above this interval, and silica constitutes more than 60 percent of the upper Pride Mountain shale. Characteristics of the Pride Mountain formation at Plant Gorgas are consistent with interpretations of a prograding muddy slope that culminated in deposition of the Hartselle Sandstone (e.g., Thomas, 1972; Pashin, 1993).

The Hartselle Sandstone gradationally overlies the Pride Mountain Formation and spans 93 feet of section, with the formation top having been penetrated at 2,605 feet (Figure 48). The Hartselle is composed mainly of very fine- to fine-grained quartz sandstone containing numerous shale partings. Well logs indicate that sandstone content is greater than 90 percent throughout the formation and that the purest sandstone is in the upper part of the formation between depths of 2,615 and 2,640 feet. The sandstone is oil-stained and has a strong petroliferous odor. The density and neutron porosity logs show significant gas-effect crossover and indicate that porosity is typically between 4 and 8 percent. The upper 9 feet of the Hartselle contains thinly interbedded sandstone and shale containing fragments of crinoids and brachiopods. The Hartselle has been interpreted as a barrier-strandplain succession (Thomas and Mack, 1982).

The Bangor Limestone spans depths from 2,338 to 2,605 feet and contains mainly limestone with subordinate quantities of shale and dolostone. Basal Bangor strata below 2,568 feet are rich

in crinoids and are argillaceous and dolomitic. This interval is overlain by 30 feet of micritic limestone, which is in turn overlain by 88 feet of thinly interbedded limestone and shale. The limestone content of this interval increases upward. The upper part of the limestone is dominated by oolitic rock types and contains few shale partings. Well logs indicate that the Bangor in the Gorgas #1 borehole is effectively nonporous. The Bangor limestone has an overall shoaling-upward signature and represents renewed establishment of carbonate shelf sedimentation in the Gorgas area.

The Parkwood Formation is 265 feet thick in the Gorgas #1 borehole, with the top at a depth of 2,073 feet. The lower Parkwood ranges in depth from 2,258 to 2,338 feet, having a thickness of 80 feet. This interval is dominated by silty shale and includes 10 feet of argillaceous, calcareous siltstone near the base. The middle Parkwood is 110 feet thick, with the top at 2,148 feet. The Millerella limestone constitutes the lower 24 feet of the middle Parkwood and has a crystalline texture. Above the Millerella is about 75 feet of silty gray shale, and the middle Parkwood is capped by a thin, argillaceous limestone marker. The upper Parkwood contains 75 feet of thinly interbedded dark gray shale and medium gray sandstone. Well logs indicate that the sandstone is effectively nonporous. Parkwood strata record alternating siliciclastic and carbonate sedimentation as deltaic sediment encroached on the carbonate shelf during the early stages of Appalachian-Ouachita orogenesis (Thomas, 1972, 1974).

Pottsville strata sharply overlie the Parkwood Formation. The lower Pottsville Formation is 1,095 feet thick, spanning depths of 978 to 2,073 feet (Figure 48). The lower Pottsville contains a complete section that includes the lower Boyles, upper Boyles, and Fayette cycles. The lower Boyles is 451 feet thick and is dominated by quartz sandstone and quartz-pebble conglomerate; the interval contains several intervals of thinly interbedded shale and sandstone. The top of the

lower Boyles is at 1,622 feet and is sharply overlain by the upper Boyles cycle. The top of the upper Boyles is at 1,332 feet, and the cycle is 290 feet thick. The basal 70 feet of the upper Boyles is a silty shale unit. The shale is overlain sharply by a about 140 feet of sandstone. The lower 76 feet of the sandstone lacks significant shale partings, whereas the upper part of the sandstone is increasingly shaly. The Fayette cycle is 354 feet thick and contains a basal shale that coarsens upward into thinly interbedded shale, siltstone. Some zones within the shale contain brachiopod valves. The shale interval is overlain by about 70 feet of quartz sandstone (i.e., the Fayette sandstone) that grades upward into shale that is overlain by a thin coal seam. The upper part of the Fayette cycle is composed of thinly interbedded shale, siltstone, and sandstone. Although a great thickness of lower Pottsville sandstone exists at Plant Gorgas, indicating major development of delta-destructive beaches and tidal banks in the area. Well logs indicate that porosity is lower than 9 percent, which is anomalously low for the Black Warrior Basin. However, neutron-density logs do record significant gas-effect crossover, and a gas show was recorded while drilling the Fayette sandstone.

The upper 978 feet of the Gorgas #1 borehole is in the coal-bearing strata of the upper Pottsville Formation (Figure 48). This interval contains thickly interbedded shale and nonporous sandstone, as well as several coal seams. Surface casing was set to a depth of 766 feet, and so mud logs provide the only record of much of the upper Pottsville section in the borehole. Conductor was set to a depth of 40 feet, and so no drilling record exists for the uppermost part of the borehole. The basal 110 feet of the upper Pottsville consists of dark gray silty shale. The shale coarsens upward into gray sandstone, and the Jefferson coal seam was observed at a depth of 828 feet. Another thick shale interval was encountered between depths of 520 and 760 feet. Seams of the Mary Lee coal zone were drilled between 445 and 492 feet, and the Jagger, Mary

Lee, and New Castle seams were identified. The Mary Lee coal zone is overlain by another thick shale interval spanning depths of 280 to 380 feet. A normal fault with an estimated vertical separation exceeding 150 feet was intersected near the top of the shale. The shale coarsens upward into gray sandstone, and above the sandstone is the Pratt coal zone, which extends to the surface at the Gorgas steam plant. The Gillespy coal is at a depth of 197 feet, and the American coal was intersected at 100 feet.

Coring results: geologic characteristics.—Core was retrieved from several intervals in the Gorgas #1 borehole, with rotary sidewall cores being taken in the Cambrian-Devonian and whole core taken in the Mississippian-Pennsylvanian section (Figure 48). The cores were taken from a variety of carbonate, sandstone, and shale units to analyze reservoir properties and sealing properties. Description and laboratory analysis of the cores further provided first-hand verification of the rock types and reservoir properties indicated by the geophysical well logs. Whole core is particularly useful because it provides a continuous record of rock types, sedimentary structures, and fossil content, which essential for analyzing depositional process and interpreting depositional environment. This section of the report summarizes the basic core descriptions.

Nineteen sidewall cores were recovered from the Knox Group. Of these, 11 samples are from the Copper Ridge Dolomite and include limestone, dolostone, and sandstone. The limestone and dolostone samples are mainly light gray peloidal micrite. One sample from 4,720 feet has gray-white mottling and has visible moldic porosity that appears to be derived from dissolution of skeletal material. Several of the samples had a distinct petroliferous smell and exhibited yellow-white fluorescence under the fluoroscope. Sandstone samples were retrieved from 4,760 and

4,790 feet. The lower sandstone sample is light gray, whereas the upper sample is light brownish gray and is oil-stained. The eight Chepultepec samples are all limestone consisting of peloidal micrite. Colors range from dark gray to light gray and include some greenish-gray and bluish-gray specimens near the base of the unit. Little structure was observed in most of the samples, save for fenestrae and stylolites. Two of the Chepultepec samples exhibited yellow fluorescence. The fine grain size and predominance of peloidal textures in the Knox carbonate samples suggest that sedimentation took place mainly in lagoonal and tidal flat environments.

Four sidewall cores were recovered from the Stones River Group, and two were recovered from the Sequatchie Formation. All six samples are limestone ranging in color from gray to dark gray. Rock types range from peloidal micrite to calcisiltite and calcarenite composed of skeletal wackestone and packstone. One sample contains a calcite vein, whereas another contains stylolites. One of the core specimens exhibited light yellow fluorescence under the fluoroscope. The grain-rich rock types of the Stones River Group and Sequatchie Formation in the Gorgas #1 borehole indicate sedimentation in higher energy environments that the Knox Group and suggest an association with carbonate shoal systems.

Sidewall cores were taken from the basal ironstone, middle shale, and upper limestone of the Red Mountain Formation. The two samples from the ironstone interval consist of weak red, fine- to medium-grained oolitic ironstone. The sample from 3,514 feet contains ironstone interlaminated with sparry limestone, whereas the sample from 3,476 feet contains ironstone with intergranular cement composed of calcite spar. Hence, the lower Red Mountain in the Gorgas #1 borehole is typical of the hematitic oolite shoal deposits that are widespread in Alabama. On the basis of 5 samples, the middle shale is technically composed of greenish-gray argillaceous siltstone containing sparse organic matter and pyrite crystals. Fossil material,

including a bryozoan and trilobite, was observed at 3,375 feet. The fossil content indicates sedimentation in marine environments and deposition on a muddy shelf. The upper Red Mountain is composed of coarse-grained crinoidal grainstone. The limestone is gray to light gray, and the crinoid ossicles exhibit partial to complete hematite coats. The sample from 3,200 feet had a faint yellow fluorescence, thus providing the only indication of oil in the Red Mountain Formation. The sparry crinoidal grainstone indicates the development of major skeletal shoals in the Gorgas area, and the hematite grain coats appear to be the product of regional exposure prior to deposition of the unnamed Devonian limestone.

One core sample was taken from the unnamed Devonian limestone. The core contains gray arenaceous limestone containing abundant stylolites. The limestone has a mottled texture and also contains irregular pyrite nodules. The thin and arenaceous nature of the Devonian limestone indicates condensed sedimentation on a carbonate shelf and foreshadows the widespread euxinic basin represented by the Chattanooga Shale.

The Fort Payne Chert was characterized using 4 sidewall cores. The sample from 3,082 consists of gray crinoidal packstone with chert nodules. At 3,070 feet, the Fort Payne is composed of gray micrite containing pyrite nodules. Samples from 3,035 and 3,050 feet contain dark gray to dark greenish-gray micrite containing glauconite grains. Features in the Fort Payne samples are typical of muddy outer ramp deposits, and the glauconitic material in the upper Fort Payne is transitional into a glauconitic facies identified in the lower part of the Tuscumbia Limestone.

Whole core was taken to assess reservoir properties in the Tuscumbia Limestone and the Lewis limestone between depths of 2,890 and 3,015 feet (Figure 50). The lower part of the limestone contains sponge-microbial boundstone that is dolomitic, siliceous, and has a distinctive

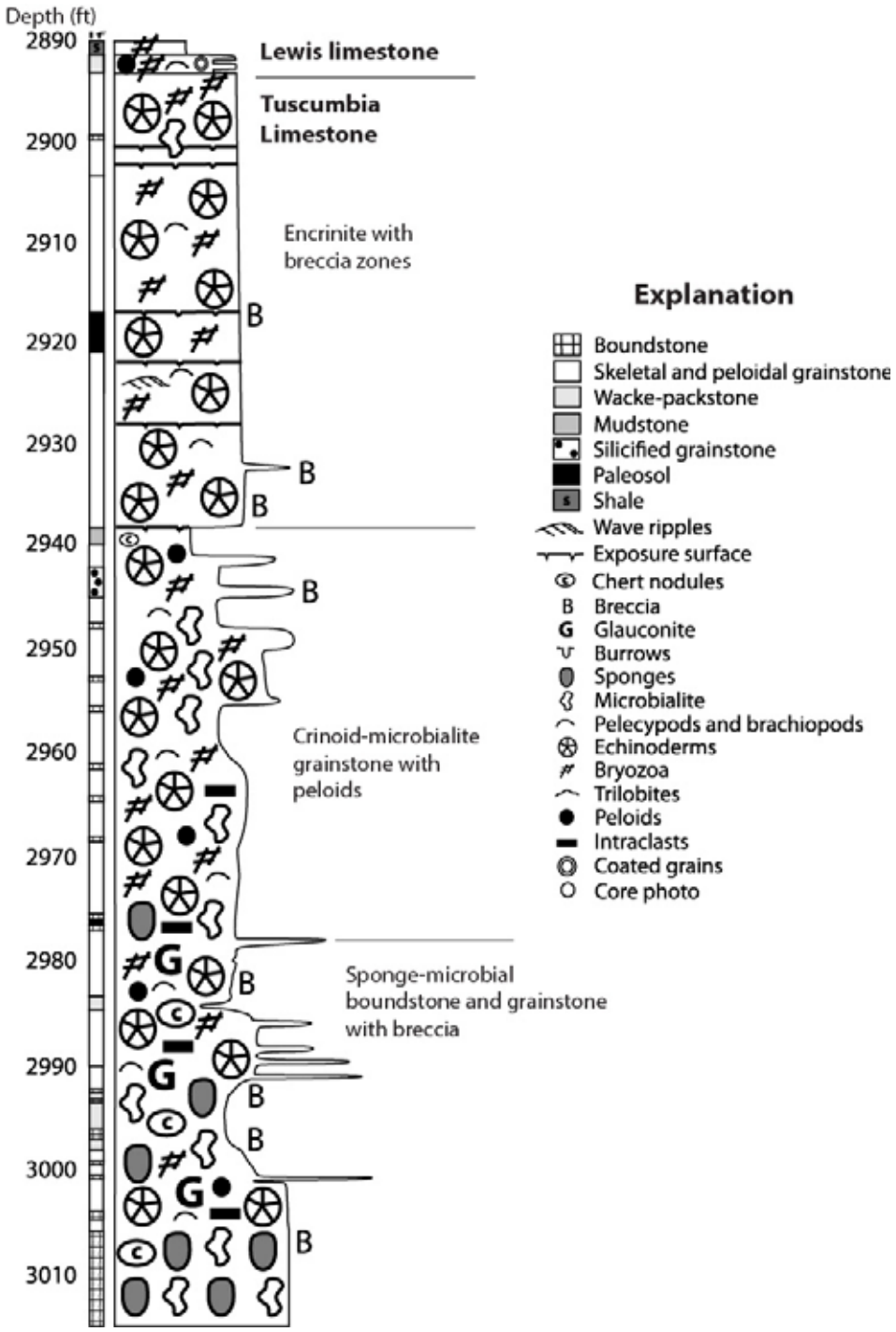

Figure 50.—Graphic core log of the Tuscumbia Limestone in the Gorgas #1 borehole.

thrombolitic texture (Figure 51A). This part of the core also contains glauconitic grainstone, packstone, and wackestone with abundant crinoids and intraclasts. Parts of the limestone include pale micrite that is intensely brecciated; dolostone and microbial boundstone fills the interstices between the breccia clasts (Figure 51B). The middle part of the limestone from 2,978 to 2,938 feet is composed primarily of crinoidal grainstone and microbialite containing peloids. The upper part of the Tuscumbia consists of crinoid-bryozoan grainstone with faint horizontal laminae and several brecciated zones. The Tuscumbia is overlain sharply by the Lewis limestone, which contains argillaeous limestone with abundant crinoids and fenestrate bryozoans.

Sponge-microbial boundstone in the lower part of the Tuscumbia core was interpreted as biohermal deposits by Kopaska-Merkel and others (2013) and constitutes the first recognized biological buildups in the formation. Dolomitization and brecciation (Figures 50, 51) indicate significant alteration of the limestone during episodes of exposure, and silicification indicates continued alteration by remobilization of silica from sponges during burial. The middle part of the limestone indicates shoal-water conditions that somehow favored preservation of microbial rock fabrics but not sponges. The low-angle laminae in the encrinite forming the upper part of the Tuscumbia is suggestive of beach-shoreface sedimentation, and the brecciated zones indicate episodic cementation, exposure, and desiccation.

The Pride Mountain Formation was cored to assess sealing potential between depths of 2,830 and 2,868 feet to analyze the sealing potential of shale (Figure 52). The shale is gray to dark gray, silty, and fissile. The lower 8 feet of the shale contains marine fossils, including ostracodes, bivalves, and an athyrid brachiopod (Figure 53A). Fissility decreases upward through the shale. The shale contains carbonized plant debris and a few slickensides between 2,850 and 2,860 feet. Irregular slickensides (Figure 53B) become increasingly abundant upward in the shale, as do

Figure 51.—Photographs of core from the Tuscumbia Limestone in the Gorgas #1 borehole. (A) Sponge-microbial boundstone containing white dolomite, gray limestone, and white chert. Note large, irregular fractures filled with calcite. (B) Breccia formed in laminated white micrite with interstices filled with brown dolostone and gray limestone similar to boundstone shown in photograph A.

siderite bands and nodules, and the upper part of the shale is non-fissile (Figure 52). Fossils in the lower part of the shale indicate deposition in marine environments, and regional facies relationships suggest sedimentation on a muddy slope (Thomas, 1972; Pashin, 1994) (Figure 21).

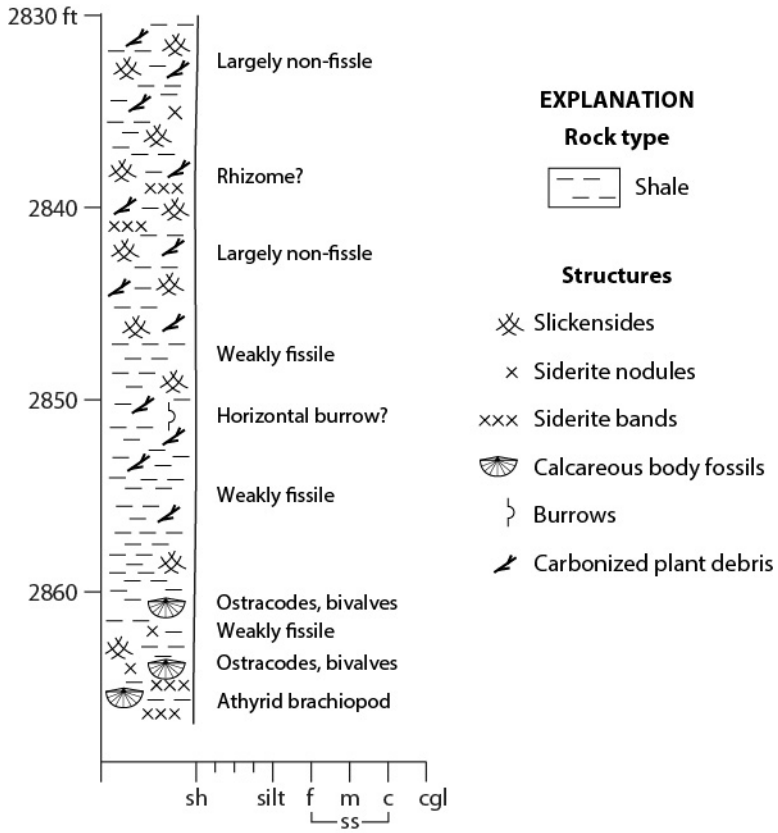

Figure 52.—Graphic core log showing characteristics of shale in the Pride Mountain Formation in the Gorgas #1 borehole.

Plant fossils and abundant irregular slickensides suggest a pedogenic origin for the upper part of the Pride Mountain core, probably in a forested area behind an ancient shoreline.

The upper part of the Pride Mountain Formation and most of the Hartselle Sandstone were cored from 2,615 to 2,733 feet to determine basic reservoir properties (Figure 54). The sandstone is highly jointed and is thus difficult to photograph. The upper Pride-Mountain Formation contains a coarsening-upward succession containing primarily thinly interbedded shale, siltstone, and sandstone with wavy and lenticular bedding. The shale contains abundant current ripples, load casts, and trace fossils. Pinstripe bedding with bundled laminae was observed at the top of the Pride Mountain. The contact between the Pride Mountain Formation and the Hartselle

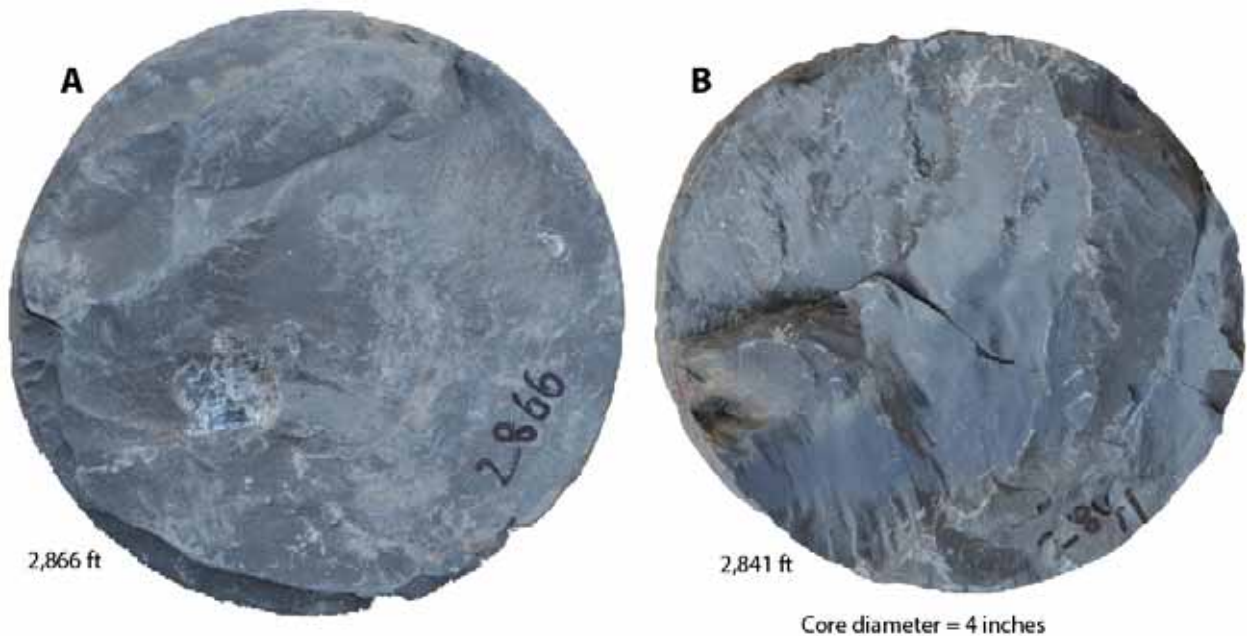

Figure 53.—Photographs of shale core from the Pride Mountain Formation in the Gorgas #1 borehole. (A) Gray shale containing an athyrid brachiopod. (B) Gray shale containing irregular pedogenic slickensides.

Sandstone is gradational. The Hartselle is composed primarily of very fine to fine-grained sandstone that has been stained yellowish-brown to brown with oil and in places black with pyrobitumen. Upon retrieval of the core, the sandstone showed a blue-white fluorescence (Figure 55), indicating API gravity of about 40°. Shale partings are common in the sandstone and decrease upward in abundance, and some shaly intervals contain flaser, wavy, lenticular, and pinstripe bedding. Sedimentary structures include current ripples and horizontal laminae, and shale intraclasts occur in several parts of the section. Cross-bedding was observed in the upper 30 feet of the core. Bioturbation consists predominantly of horizontal burrows, and crinoid ossicles are common between 2,640 and 2,649 feet. Diagenetic structures include stylolites. Concretionary carbonate cement was observed in horizontally laminated sandstone between 2,633 and 2,645 feet.

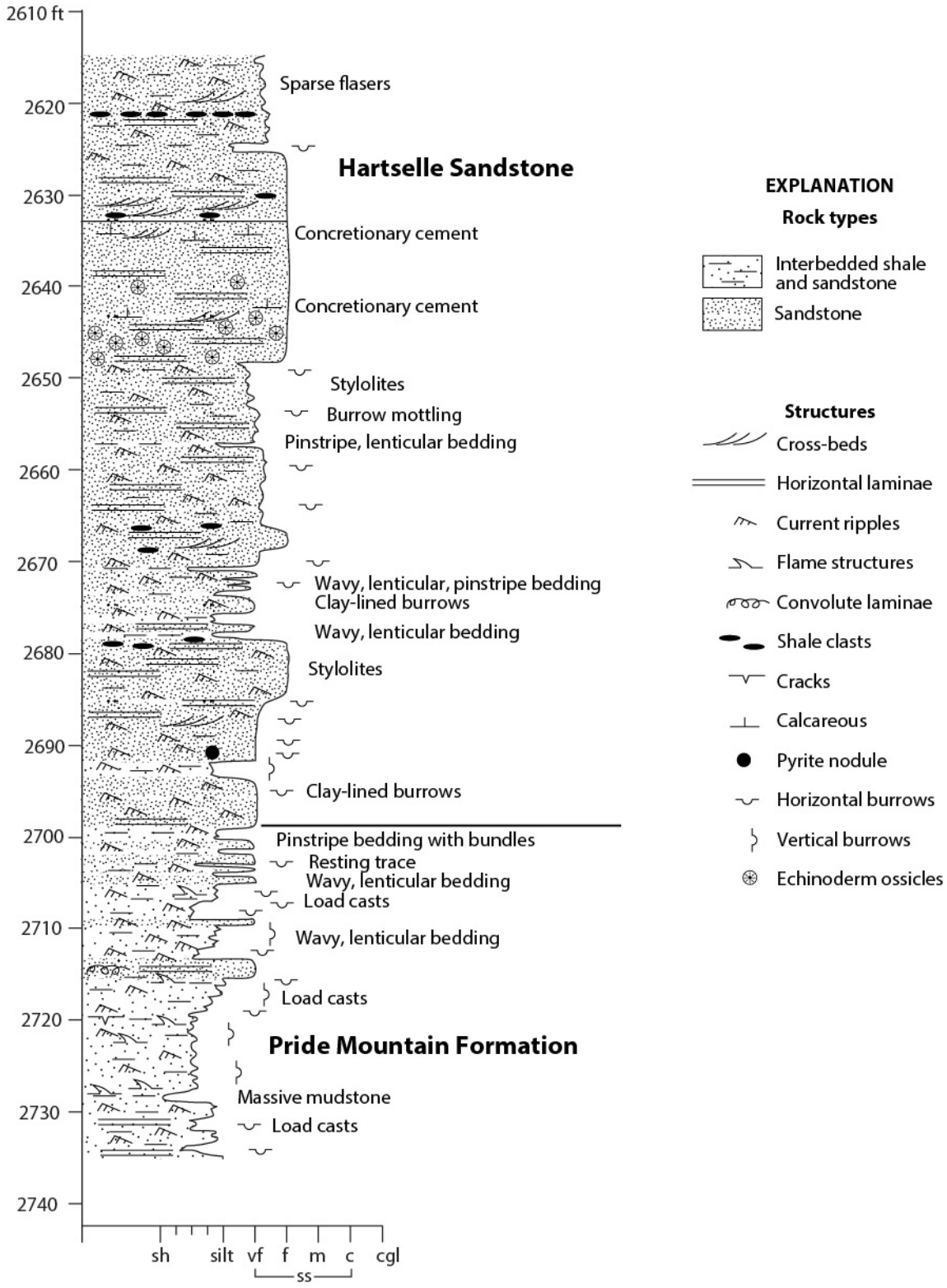

Figure 54.—Graphic core log of the upper Pride Mountain Formation and Hartselle Sandstone in the Gorgas #1 borehole.

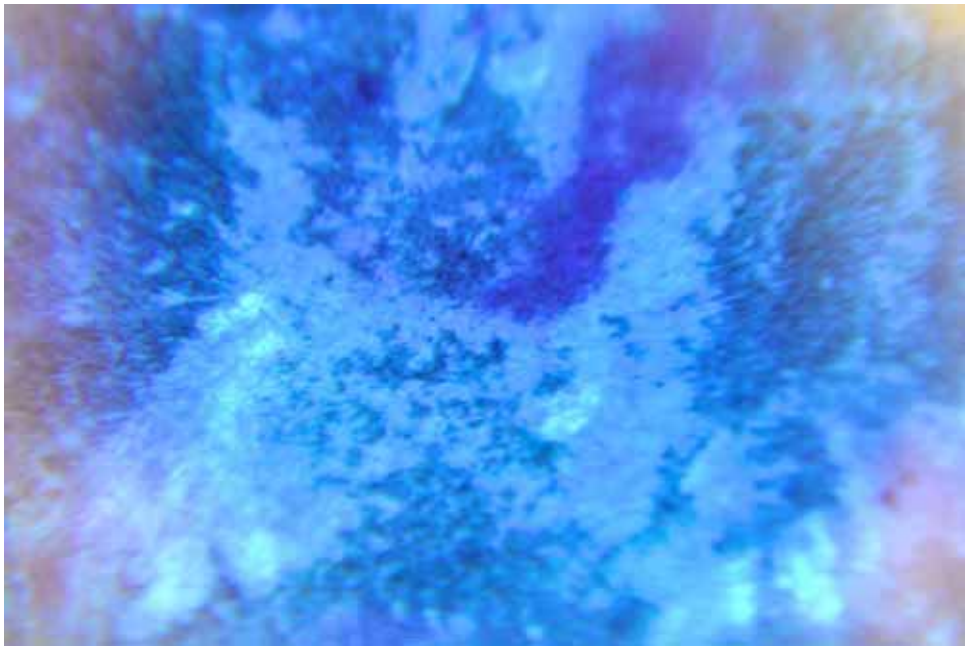

Figure 55.—Fluoroscope image showing blue-white fluorescence of oil stain in Hartselle Sandstone. Dark coloration is pyrobitumen. Sample retrieved from depth of 2,675 feet.

The overall coarsening-upward succession in the Pride-Mountain-Hartselle core (Figure 54) suggests progradational sedimentation. Wavy, lenticular, and pinstripe bedding is typical of tidal deposits, and one possibility is that the upper Pride Mountain Formation represents a back-barrier lagoon system. The predominance of horizontal laminae is consistent with the beach-shoreface interpretation proposed by Thomas and Mack (1982), and the abundance of clay partings in the sandstone is typical of beach systems in mesotidal areas, and the occurrence of crinoid debris confirms marine influence of sedimentation.

Core was taken from the Boyles Sandstone from 1,900 to 1,930 feet to assess the reservoir properties of quartzarenitic sandstone in the lower Pottsville Formation (Figures 56, 57). The sandstone forms a fining-upward succession with rock types ranging from conglomerate and coarse-grained sandstone to thinly interbedded shale, siltstone, and sandstone (Figure 56). Polymictic, clast-supported conglomerate containing large siderite and shale pebbles and small

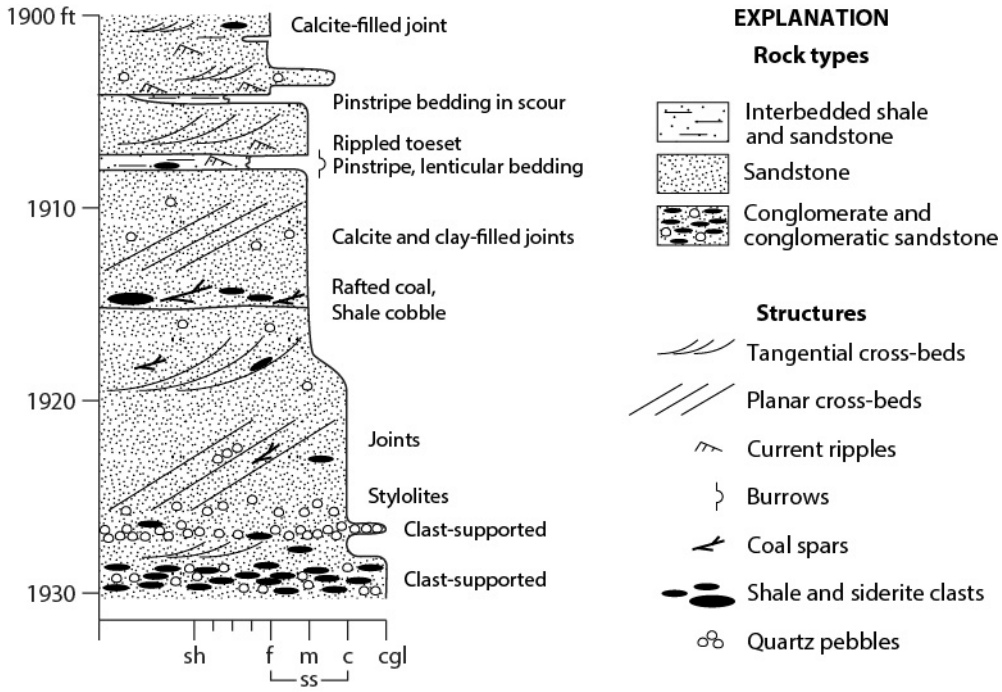

Figure 56.—Graphic core log of part of the Boyles Sandstone Member of the lower Pottsville Formation in the Gorgas #1 borehole.

quartz pebbles (Figure 57A) makes up the basal 3 feet of the core. The siderite and shale clasts are platy to subspherical and angular to well-rounded, whereas the quartz pebbles are subspherical and subangular to subround. Platy coal spars are common in the conglomerate, as are stylolitic clay partings. The lower 10 feet of the sandstone is conglomeratic and stylolitic, and quartz pebbles resembling those in the basal conglomerate are the dominant clast type (Figure 57B). The main body of the sandstone is cross-bedded, and planar and tangential forms are present. Quartz pebble lags are common on foresets, and sedimentary lithoclasts locally form lags. Shale partings are common in the upper part of the core. The thickest shale intervals contain intercalations of siltstone and very fine sandstone containing lenticles with current ripples and planar pinstripe laminae (Figure 57C). Sparse burrows were observed in the shale zones. The upper part of the sandstone is rippled and cross-bedded, and some cross-strata have micaceous clay-organic drapes and inversely graded laminae (Figure 57D).

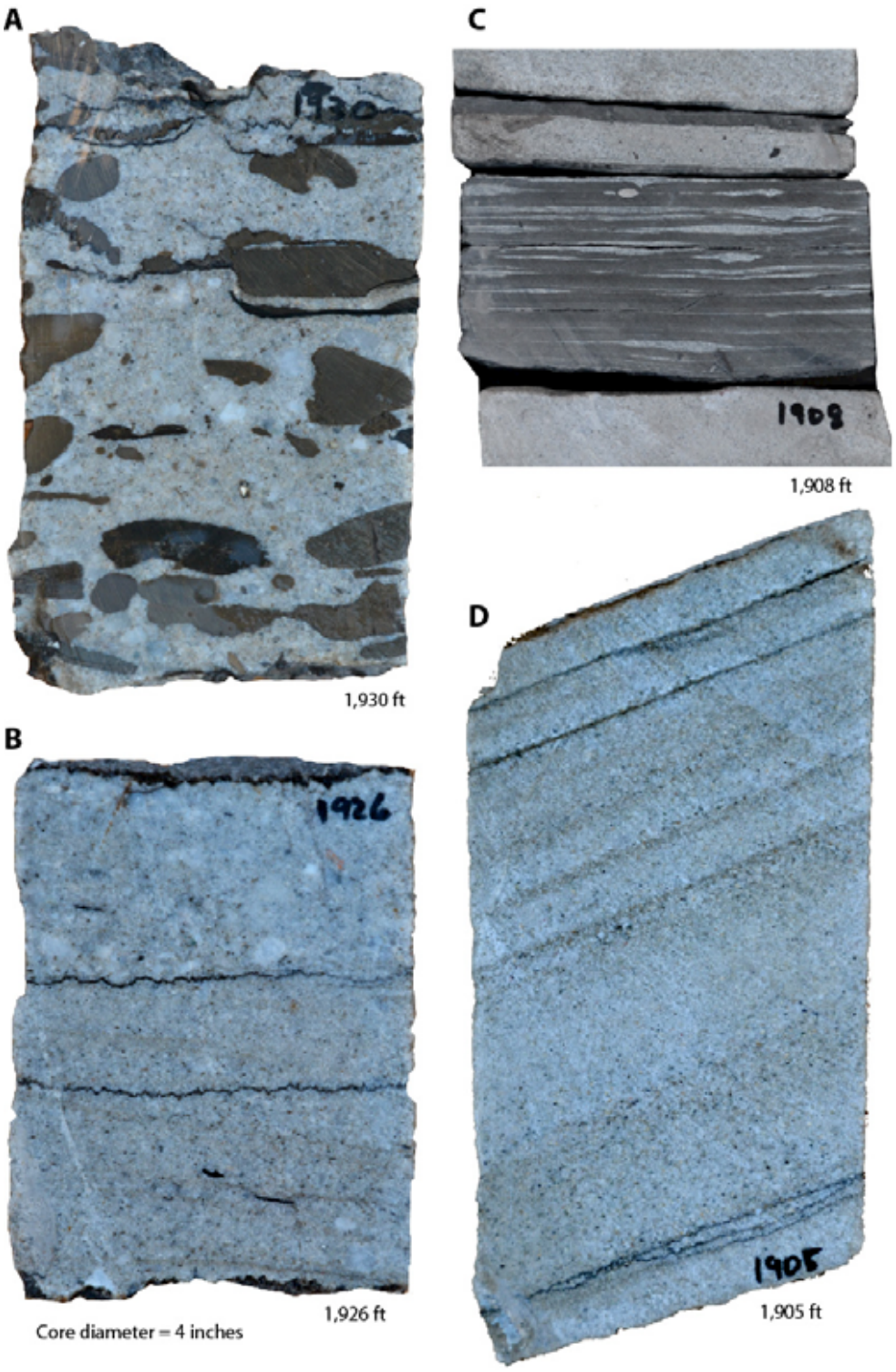

Figure 57.—Photographs of core from the Boyles Sandstone Member in the Gorgas #1 borehole. (A) Conglomerate containing pebbles of shale, siderite, coal, and quartz. (B) Conglomeratic sandstone containing quartz pebbles and clay-lined stylolites. (C) Interlaminated shale, siltstone, and very fine sandstone with pinstripe and lenticular bedding. (D) Cross-bedded sandstone with inversely graded laminae and clay-organic-mica drapes.

Hobday (1974) recognized that lower Pottsville sandstone is the product of inlet-dominated beach systems that formed in areas of high tide range, and subsequent workers have documented a large number of tidal features, such as pinstripe bedding and clay-draped cross-strata (e.g., Gastaldo and others, 1993). The fining-upward succession in the Boyles core (Figure 56) is typical of tidal channel and inlet facies in the lower Pottsville. The clast-supported conglomerate near the base of the sandstone (Figure 57A) was probably deposited on the channel floor, and the large-scale cross-strata in the middle of the core represent dunes that formed tidal shoals and filled the channel. Ripple cross-laminae and shale partings in the upper part of the core indicate lower energy sedimentation. Inverse grading in the major cross-beds indicates that some dunes migrated by traction or grainflow. Clay drapes suggest that sedimentation was episodic, which is consistent with tidal currents in shoals, channels, and inlets.

The basal shale of the Fayette cycle was cored from 1,220 to 1,280 feet to analyze seal quality in the Pottsville Formation (Figures 58, 59). The lower part 13 feet of the core is composed of thinly interbedded dark gray shale and light gray siltstone and very fine sandstone and is intensely burrow-mottled (Figure 59A). The upper 2 feet of this interval is calcareous and contains macerated mollusk and brachiopod shells and a solitary rugose coral. Vertical welling burrows are developed at the top of the interval and are up to 4 inches deep. The shelly interval is overlain by 7 feet of dark gray silty shale (fig 58). The shale is weakly laminated and contains abundant horizontal burrows (Figure 59B); the lower part of the shale has elevated radioactivity relative to the rest of the core and, and intense bioturbation gives the shale an irregular fissility. The upper 40 feet of the core contains thinly interbedded shale, siltstone, and very fine sandstone (Figure 58). This interval is intensely bioturbated, but bedding is better preserved than in the lower part of the core (Figure 59C). Trace fossils include numerous forms of feeding and

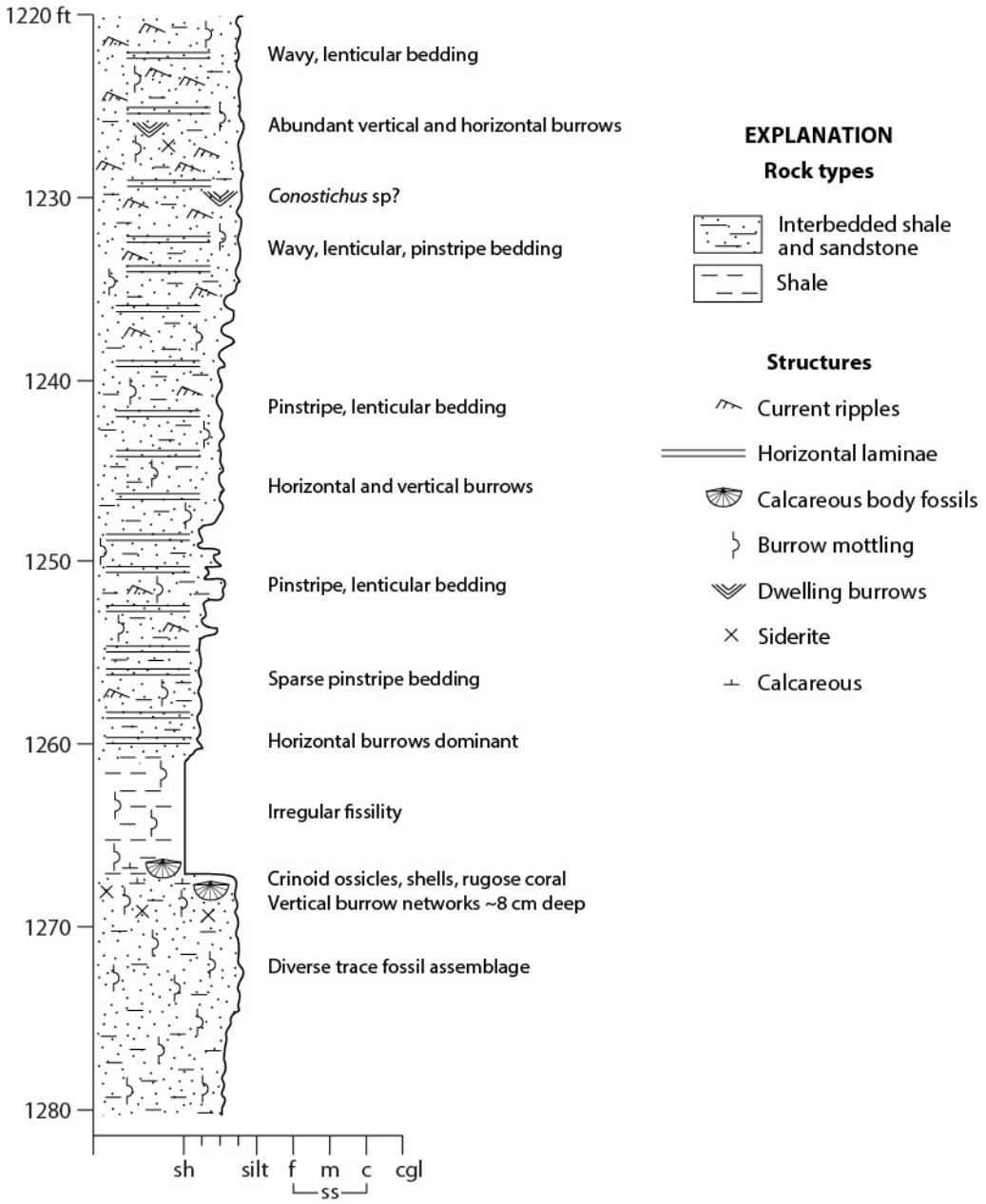

Figure 58.—Graphic core log of the basal shale of the Fayette cycle of the lower Pottsville Formation in the Gorgas #1 borehole.

dwelling traces, including conical forms resembling *Conostichus*. Wavy, lenticular, and pinstripe bedding predominate, with horizontal laminae being common throughout the interval and ripple cross-laminae increasing upward in abundance (Figures 58, 59C).

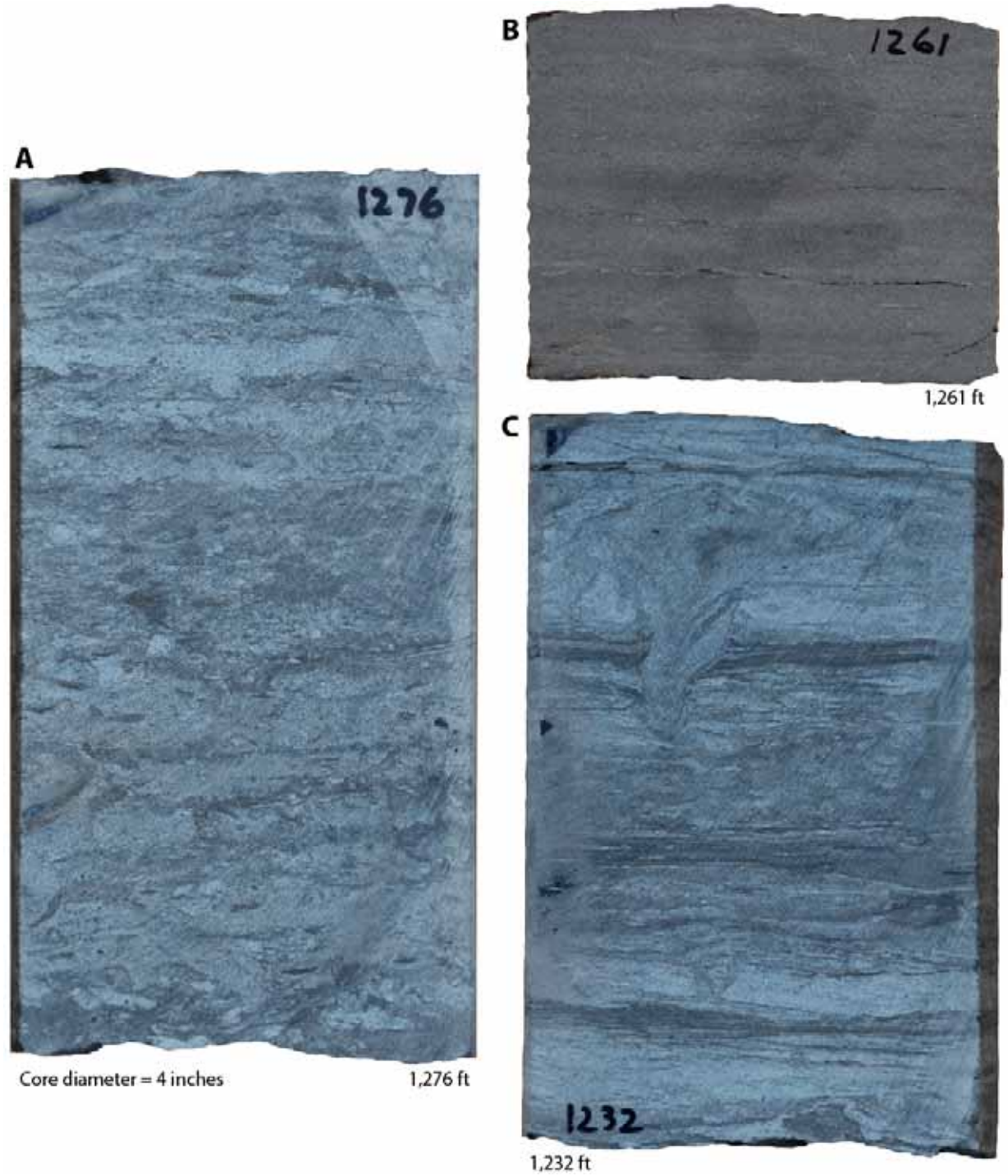

Figure 59.—Core photos of the Fayette shale the Gorgas #1 borehole. (A) Interlaminated, shale, siltstone, and sandstone with intense burrow mottling. (B) Dark gray, silty shale with bioturbation, faint laminae, and irregular platy fissility. (C) Interbedded shale, siltstone, and very fine sandstone containing current ripples, dwelling burrows, and feeding burrows.

The basal Fayette shale is one of several regionally extensive coarsening-upward shale-siltstone-sandstone successions in the Pottsville Formation (e.g., Pashin, 1994, 2004). Coarsening-upward successions indicate progradational sedimentation, and the fossil assemblages indicate marine environments. Accordingly, these types of facies have been interpreted as prodelta and delta front deposits. The lower part of the core records a minor progradational episode at the start of Fayette deposition, and intensely bioturbated intervals with calcareous marine faunas are typical of condensed sections that formed in response to marine transgression (Gastaldo et al., 1993; Pashin, 2004). The silty shale between 1,260 and 1.267 feet, therefore, overlies a marine flooding surface and is interpreted as a prodelta deposit. The upper part of the core records a transition from prodelta to delta front environments, and the predominance of wavy, lenticular, and pinstripe bedding indicates that sedimentation was driven in large part by tidal processes.

Coring results: conventional core analysis.—Conventional core analysis was performed on 192 samples, including sidewall cores and 1-inch plugs that were taken from whole cores at 1-foot intervals. Results of porosity analysis indicate that matrix porosity is low in all carbonate and sandstone units, ranging from 0.5 to 8.3 percent (Figure 60). Porosity in the Knox Group ranges from 1.2 to 4.4 percent. In the Stones River Group and Sequatchie Formation, porosity ranges narrowly from1.9 to 2.5 percent, and in the Red Mountain Formation, porosity ranges from 1.0 to 3.7 percent. The one sample taken from the Devonian limestone has a porosity value of 1.9 percent , which is similar to the values in the older formations. Average porosity in the Cambrian-Devonian section is only 2.1 percent.

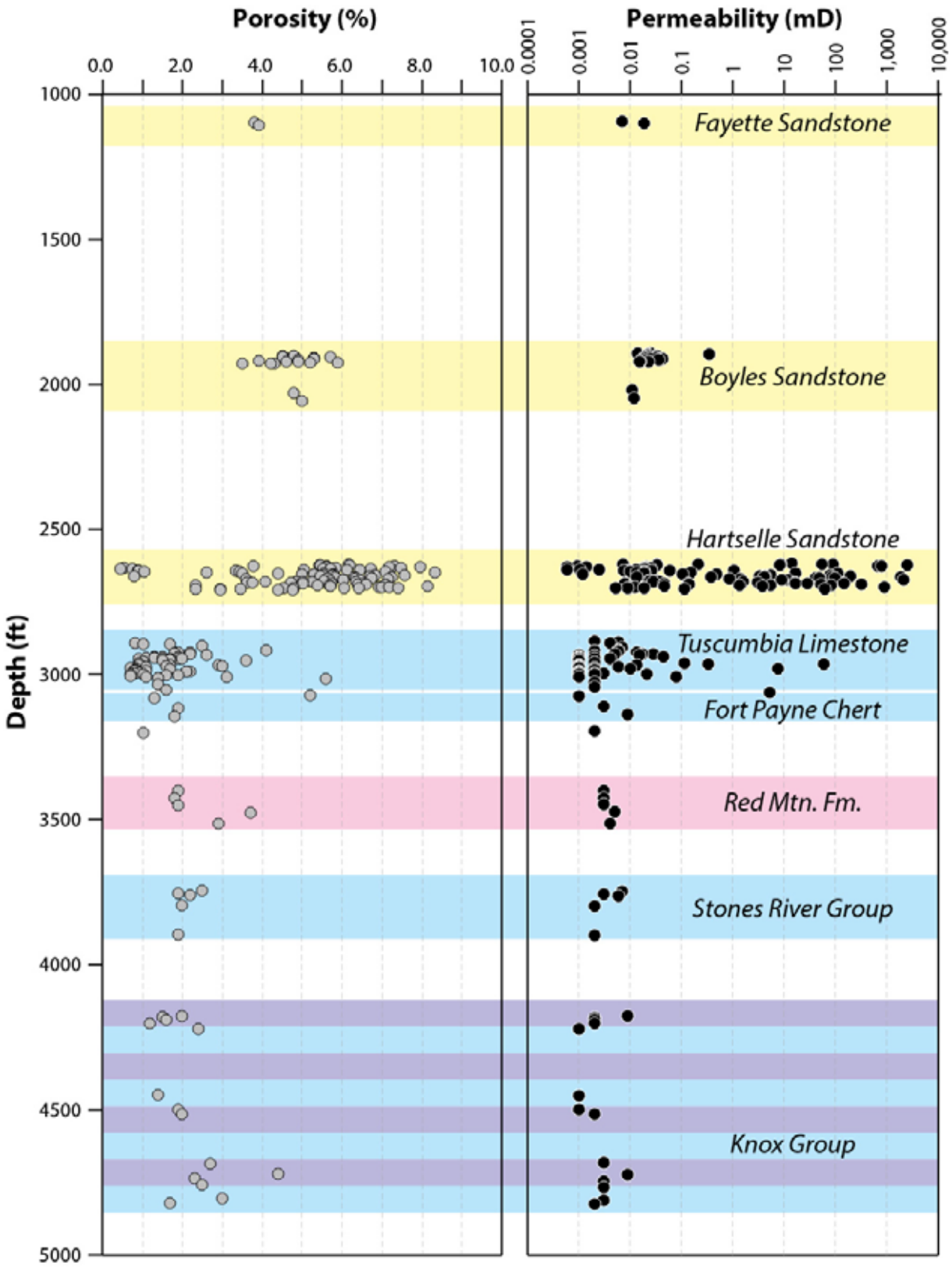

Figure 60.—Plots of porosity and permeability versus depth in the Gorgas #1 borehole based on the results of conventional core analysis.

The range of porosity is substantially greater in the Mississippian-Pennsylvanian section (Figure 60). In the Fort Payne Chert, porosity values range from 0.3 to 5.2 percent. Based on 51 analyses, porosity in the Tuscumbia Limestone ranges from 0.7 to 5.6 percent. Average porosity is only 1.7 percent, and the standard deviation is 1.0 percent. In the Hartselle Sandstone, porosity ranges from 0.5 to 8.3 percent and averages 5.2 percent. The standard deviation of porosity in the Hartselle is 1.9 percent. Values from 20 samples of lower Pottsville sandstone range from 3.5 to 5.9 percent. Average porosity is 4.7 percent, and variability is limited, with a standard deviation of only 0.6 percent.

Permeability ranges greatly from 0.6 μD to 2.4 Darcies (Figure 60). In the Cambrian-Devonian carbonate section, permeability is extremely low, ranging from 1.0 to 9.0 μD. Data from the Fort Payne Chert have the same range. Permeability is more variable in the Tuscumbia Limestone, ranging from 1.0 μD to 60.1 mD. The geometric mean for the Tuscumbia is only 4.7 μD, and values higher than 13.0 μD fall outside the log normal standard deviation. The highest and lowest values of permeability measured during this study are from the Hartselle Sandstone. The geometric mean for the Hartselle is 0.54 mD, indicating that tight sandstone predominates. In the lower Pottsville, permeability also is quite low, ranging from 7.0 to 349.0 μD with a geometric mean of 22.7 μD.

The low porosity and permeability of most strata below the Gorgas steam plant indicates a predominance of tight, low-porosity formations with microdarcy-class permeability. Samples with elevated permeability are most common in the Hartselle Sandstone, which contains abundant natural fractures. Indeed, virtually all of the samples with permeability higher than 1 mD contain natural fractures within the core plugs. Permeability in these samples was

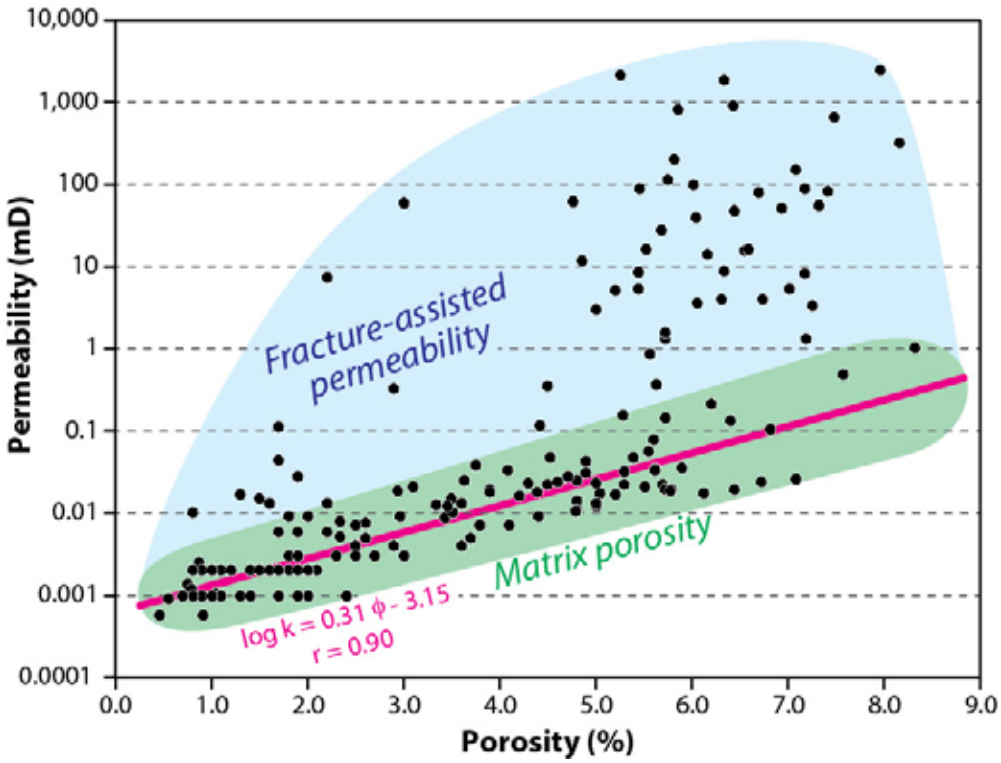

Figure 61.—Plot of permeability versus porosity in the Gorgas #1 borehole showing effect of matrix properties and natural fractures on reservoir properties.

determined under confining pressure of 800 psig, and so the results of core analysis provide insight into the impact of natural fractures on reservoir properties. Plotting porosity against permeability indicates that matrix porosity higher than 8 percent percent or higher to support permeability on the order of 1.0 mD (Figure 61). Samples containing natural fractures, by contrast, typically support effective permeability values on the order of 10 mD, and a few fractures support Darcy-class permeability.

In the Gorgas #1 borehole, porosity and permeability values are substantially lower than in equivalent strata in other parts of the basin (Figures 24, 60). Values calculated from density- and neutron-porosity logs are consistent with those determined by laboratory analysis, indicating that results are reproducible using independent methods. Comparison of well logs from Plant Gorgas with those in other areas indicates that sandstone porosity is at least 3 percent lower than is

typical of the Black Warrior Basin). Geophysical logs from nearby wells drilled into the Sequatchie anticline also show anomalously low density and neutron porosity values in sandstone and limestone, suggesting that the anticline is a site of enhanced cementation. One explanation is that cementation is a by-product of increased pressure solution of quartz and carbonate during folding (e.g., Houseknecht, 2006). Regardless, it appears that the diagenetic halo around the Sequatchie anticline extends into the Gorgas area.

Significant natural gas shows were observed periodically while drilling the Gorgas #1 borehole, but no oil shows were observed during drilling. Surprisingly, oil was observed in most core samples, and core analysis reveals that oil saturation is as high as 65.8 percent in the Hartselle Sandstone (Figure 62). Perhaps the foam drilling system coupled with low reservoir permeability masked the oil occurrences. Strata in the Knox Group are characterized by high gas saturation, and water saturation is generally lower than 8 percent (Figure 63). Oil saturation is typically low, although two samples have saturation greater than 50 percent. The Stones River Group and Sequatchie Formation samples were gas saturated with very little water or oil. Fluid saturation in the Red Mountain Formation is highly variable, and oil saturation was greater than 20 percent in some samples.

Water saturation is typically lower than 8 percent in the Fort Payne Chert and Tuscumbia Limestone. Oil saturation averages 12 percent, has a maximum value of 53 percent, and a standard deviation of 12 percent. As in the older carbonate units, gas saturation in the Tuscumbia section is high, averaging 84 percent and having a standard deviation of 13 percent.
The Hartselle Sandstone contrasts strongly with the other formations in terms of water, oil and gas saturation. Water saturation ranges from 3 to 95 percent, averages 34 percent and has a standard deviation of 21 percent. In general, water saturation decreases upward in the Hartselle

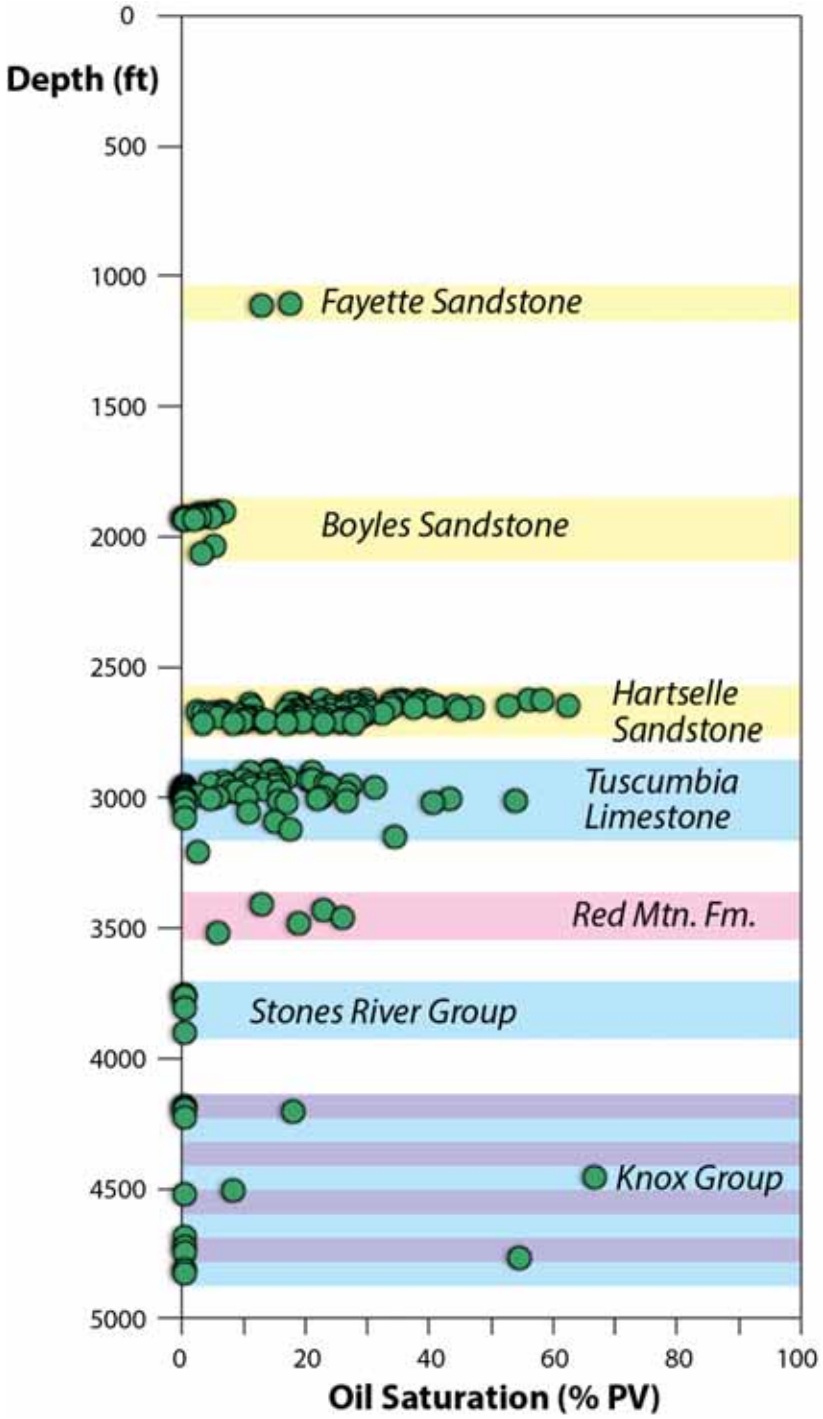

Figure 62.—Relationship between oil saturation and reservoir depth in the Gorgas #1 borehole.

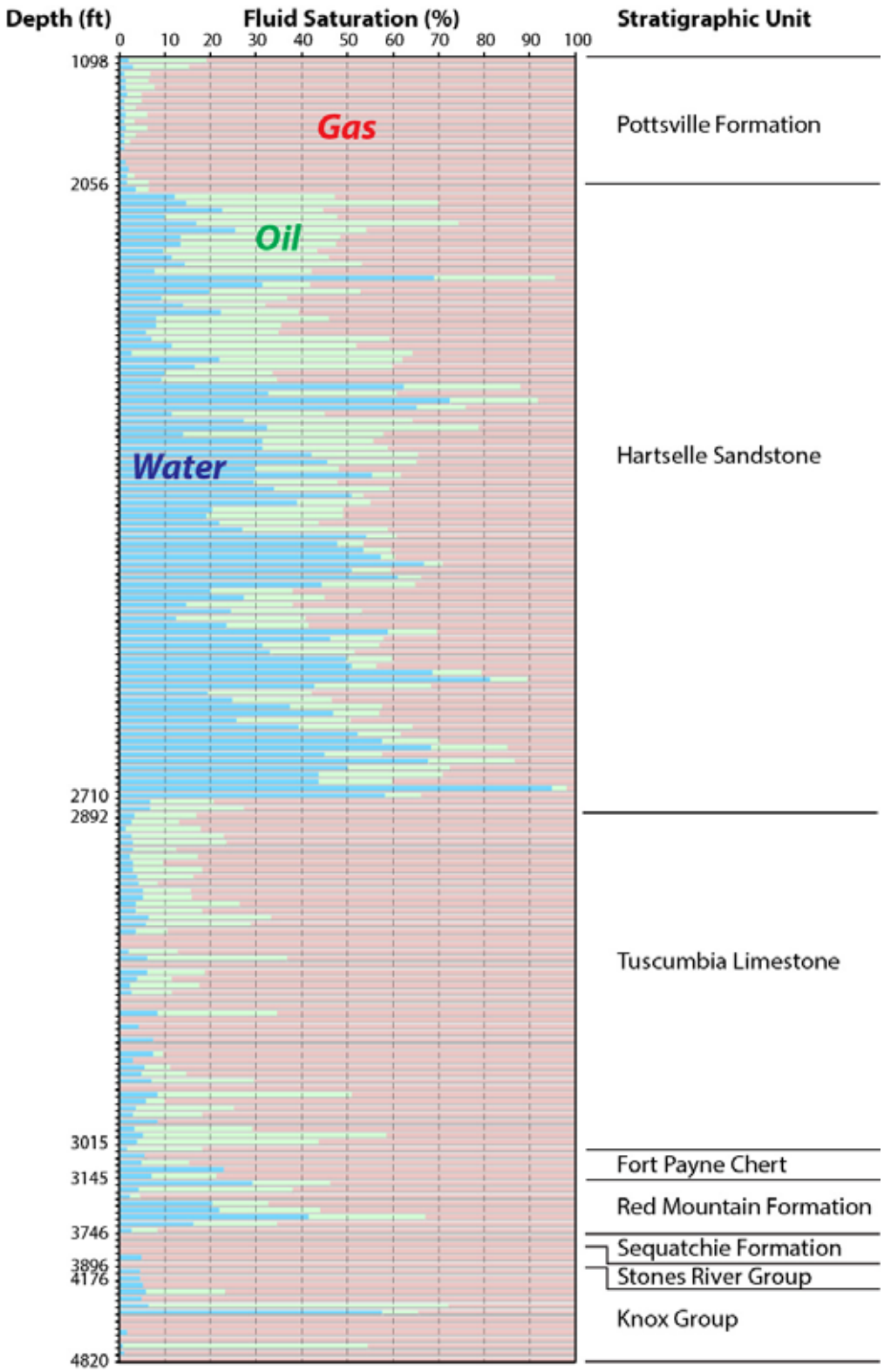

Figure 63.—Bar chart showing variability of fluid saturation in the Gorgas #1 borehole by stratigraphic unit.

section. Oil saturation ranges from 2 to 61 percent. Average saturation is 24 percent, and values have a standard deviation of 13 percent. Water and oil saturation are negatively correlated with a regression coefficient of -0.71. Gas saturation is significantly lower than in the other formations studied, ranging from 2 to 68 percent and averaging 42 percent. The standard deviation of gas saturation is 15 percent. Based on the thickness, porosity, and average oil saturation of the Hartselle Sandstone in the Gorgas #1 borehole, the amount of oil in place is estimated to be 9,000 barrels per acre, or 360,000 barrels per 40-acre tract of land.

2-D Seismic Reflection Data.—2-D seismic reflection data were collected along two 8.05 km (5 mile) lines (Rutter, 2012). The closest line (Line 201) is 1.28 km (0.795 miles) north of the well site (Figure 64). Line 101 has a north-south orientation and follows County Road 6. Line 201 is oriented northwest-southeast on State Highway 269, perpendicular to the axial trace of the Sequatchie Anticline. Seismic data were collected using three Hemi-44 Vibroseis trucks with a 19,958 kg (44,000 lb) peak force. The trucks performed four, 6 - 100 Hz, 4 -12 second sweeps at each location with a record length of 5 seconds and a sample rate of 2 microseconds (ms). The distance between shots was 36.58 m (120 ft), and the receiver interval was 3.05 m (10 ft). The receivers had a digital group formed every 12.9 m (40 ft). The maximum offset attained between source and receiver was 8,047.72 m (26,400 ft). A complete list of the acquisition parameters is given in Table 5.

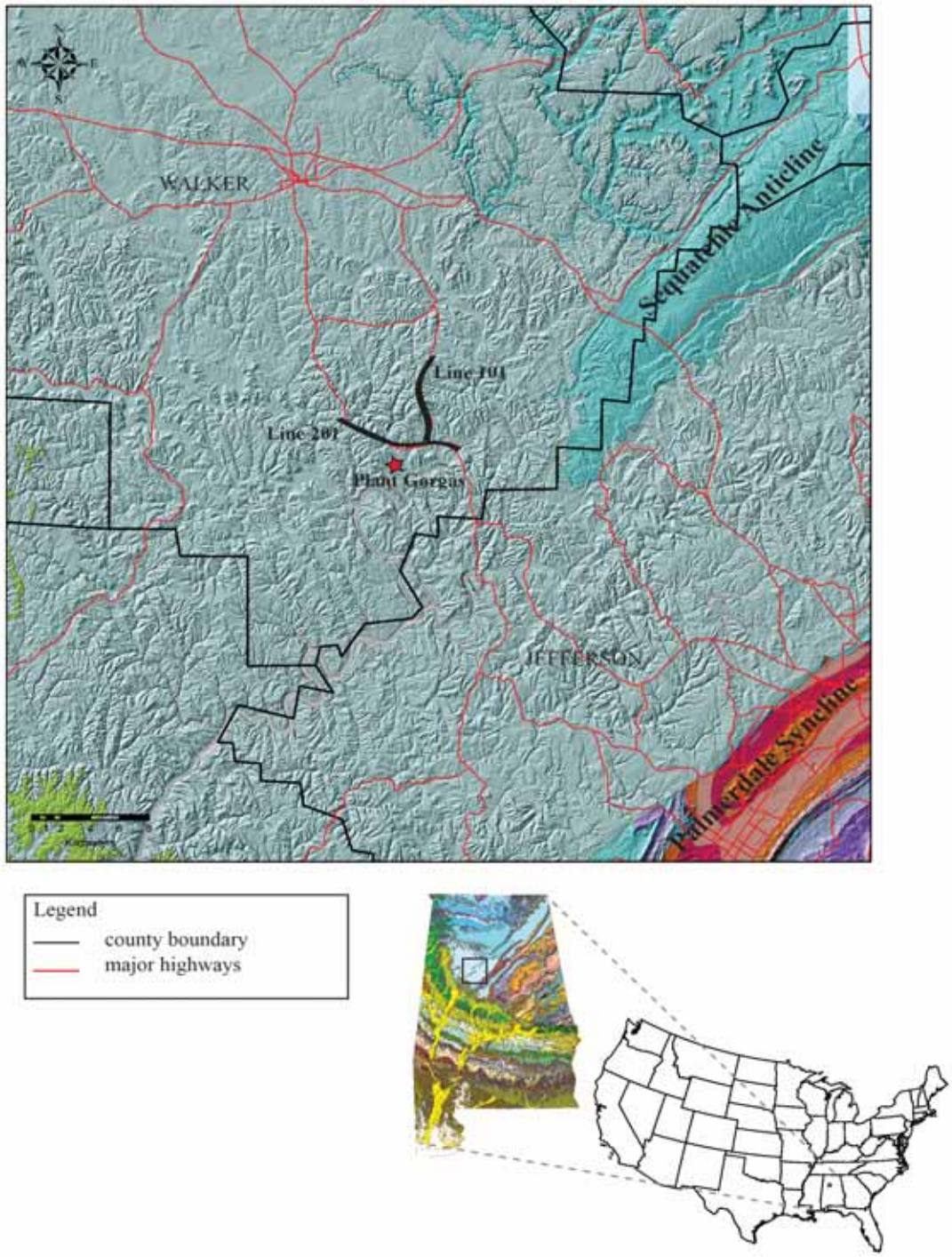

Figure 64.—Geologic map showing the location of Plant Gorgas characterization site and acquisition lines for the 2D seismic reflection survey in Walker County, Alabama. Plant Gorgas is on the eastern side of the Black Warrior Basin in close proximity to the Sequatchie Anticline. The Pennsylvanian Pottsville Formation is the only unit at the surface (grayish blue). In our study area, two five mile long lines were collected. A broadly north-south strike line (Line 101) was acquired along County Road 6. This line ends at Highway 78. A roughly east-west dip line (Line 201) was acquired along State Highway 269. Line 201 is 1.28 km (0.795 miles) north of the test well drilled at Plant Gorgas.

Seismic Studies

The seismic survey used the Schlumberger Q-land system (see Table 5 for details). This allows for the option of using single sensors rather than relying on the signal from a group of sensors. If there is noise on a single sensor, the Q-land system allows for that signal to be isolated rather than corrupting the receiver group. This method is useful for detailed static corrections where the topography is rugged. Static corrections were referenced to a seismic reference datum (SRD) at 244.844 m (800 ft) above mean sea level using a 4,572 m/s (15,000 ft/s) replacement velocity. Data processing was completed by Schlumberger (Table 6) to produce pre- and post-stack time migrated seismic sections.

The seismic data are zero-phase. Seismic data collected using a Vibrosies source is also known as a correlogram. This is derived after the sweep is cross-correlated with the data that has been recorded on the accelerometers. The cross-correlation process creates a peak at each reflection event. Interpretations of the seismic reflection profile were completed after the synthetic seismogram was generated to ensure accurate ties between depths of units interpreted from the geophysical logs and reflectors on the seismic reflection profile. Horizons were picked on peaks that corresponded with unit contacts. In some instances a trough was picked because the formation was either too thin to produce a top and bottom reflection or due to effects from tuning, which will be addressed in the results section. A topographic high in the center of Line 101 (Figure 65) is coincident with increased noise levels. This area is adjacent to vertical faces associated with coal mine high-walls adjacent to the road; this may have resulted in ray paths not accounted for in the preliminary 2-D seismic reflection processing. Two zones along Line 201 (Figure 66) at common mid-point (CMP) 237 and CMP 781 are treated with caution because bridges along the road required a gap in the receiver distribution. Anomalous dips may result

Table 5. Acquisition parameters for seismic reflection data. ITO = Intelligent Take-Out Interval, DGF = Digital Grouped Formation, PR = Point-Receiver.

Acquisition	
Source	
Source (Vibrosies)	X3 Hemi-44, 20411.65 kg (45,000 lb) trucks
Source Interval	36.5 m (120 ft)
Shot Density / sq mile	44 Vps
Receivers	
Receiver Interval	3.048 m (10 ft)
ITO Interval	36.5 m (120 ft)
DGF Interval	12 m (40 ft)
PR Density / mile	528 single sensors
DGF Density /sq mile	132 Group Formed channels
Design Patch	
Total Channels/Line	8 km (5 mile) lines all live
Design - DGF/Line	1 x All live Digital Group Formed channels
Recording Statistics	
Total Live Channels	All live point receivers
Effort	4 - 12 sec sweep per location
Sweep Type	6 - 100 Hz Phase Rotated Sweep
Record Length	5 seconds
Sample Rate	2 ms
Subsurface Statistics	
Bin Size	6 m (20 ft)
Bin Density	264 per mile
Nominal Fold	110 post DGF
Minimum Offset	6 m (20 ft)
Maximum Offset	8047 m (26,400 ft)

from locally low-fold CMPs that prelude good velocity picks and hence corrections of Normal Move Out. More detailed processing, beyond the scope of this project, will focus on improved imaging in these areas.

Table 6. Processing flow of post-stack time migrated 2-D seismic reflection profiles for Line 101 and line 201. QC = Quality control.

Convert to Internal Format

↓

Correlation

↓

Update Geometry Headers

↓

QC Geometry

↓

Diversity Sum 4 Sweeps

↓

Refraction Statics

↓

Linear Noise Attenuation

↓

Surface Consistent Deconvolution

↓

Noise Attenuation

↓

Velocity Analysis

↓

Reflection Statics

↓

Stack

↓

Migration

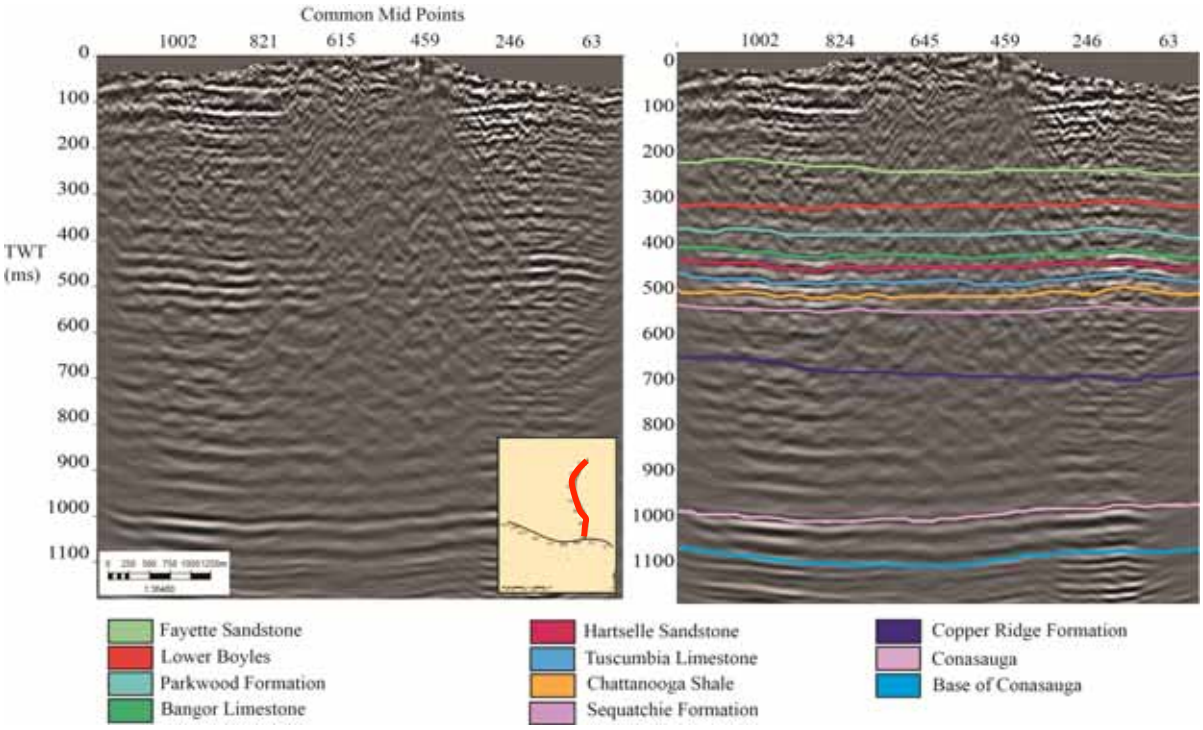

Figure 65.—Pre-stack time migrated 2-D seismic reflection profile for Line 101 prior to depth conversion. On the right side is Line 101 with formation tops interpreted. The profile is broadly oriented north to south. The CMP spacing is 6 m (20 ft). The vertical scale is in milliseconds (ms). Target reservoirs lie below the Lower Boyles Sandstone (~300 ms). The line passes over a topographic high between CMPs 896 and 288.

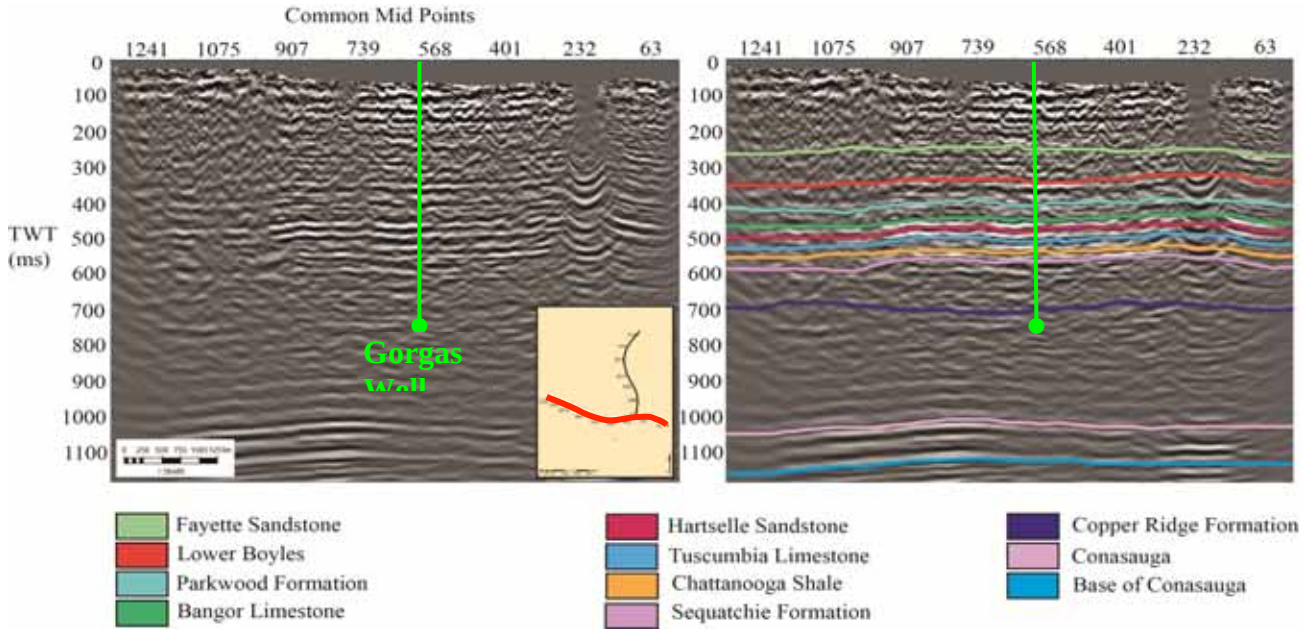

Figure 66.—Pre-stack time migrated 2-D seismic reflection profile of Line 201 prior to depth conversion. On the right side is Line 201 with formation tops interpreted. The profile is oriented west to east. The CMP spacing is 6 m (20 ft). The vertical scale is in milliseconds (ms). The well reached a total depth in the Copper Ridge Formation at approximately 4915 ft (700 ms). Reflector disturbance under CMP 232 is due to the presence of a bridge where there was a gap in accelerometer deployment.

Check-Shot Data.—Check-shots supply the most accurate time-to-depth conversion because they take a direct measurement of time for a signal at the surface to reach a receiver at a given depth in the borehole. For the check-shots, the Vibrosies source had a horizontal offset of 49 m (162 ft) to the northwest of the well, with a vertical offset of 4.18 m (13.74 ft) below the Kelly Bushing (KB; Figure 67). Measurements were taken downhole at 15 m (50 ft) intervals between 30 and 1478 m (100 - 4850 ft) depth. The Check-Shot report (Appendix I) provides depths from the KB and the seismic reference datum (SRD; 244 m (800 ft) above sea level), acoustic average velocity, root-mean-square (RMS) velocity, interval velocities calculated between each measurement level, and vertical one-way transit time corrected for source offset with static corrections applied. Correcting for a vertical well is necessary because there was a small offset

between the Vibrosies source and the well head. This was achieved by first applying a static correction to the measured depth (MD) and then finding the oblique distance between the source and down-hole receiver using MD from KB and the horizontal offset distance. The angle of the incoming ray-path was calculated, and a verticalized one-way transit time was derived using the offset angle and one-way times provided in the report. A separate velocity report (Appendix II) includes average, interval, and RMS velocities using down-hole sonic log data to interpolate between check-shot levels. A recalculation was made using the method of Linari (2004), to ensure accuracy of travel times corrected to a vertical well. Velocities were recalculated using the change in depth over the change in time ($\Delta z/ \Delta t$) for accuracy of the velocity model. These data are essential in the depth conversion of the seismic reflection data that was collected 1.28 km (0.795 miles) to the north. All travel times were calculated in relation to the seismic reference datum.

Zero-Offset Vertical Seismic Profile.—The zero-offset vertical seismic profile (VSP) was acquired simultaneously with the check-shot survey. Acquisition was carried out using a Vibrosies truck source with 21,409.55 kg (47200 lbs) peak force and a 12 second 8 - 96 Hz sweep (Table 7). The receiver array comprised 4 receiver levels separated by 15.2 m (50ft). This was lowered to the base of the hole and progressively moved up the hole as measurements were taken. Basic data processing included stacking the data, automatic gain control, applying a band-pass filter of 5 – 100 Hz, temporal amplitude recovery, amplitude normalization RMS, applying a median velocity filter on the up-going and down-going wavefields, waveshape devonvolution. Creation of a corridor stack was accomplished using a narrow stack window of the zero phase deconvolved up-going wave-field, ensuring a multiple free 1-D response to compare side by side

with the seismic reflection data. The VSP corridor stacks have a window length of 0.100 seconds and were filtered with a band-pass filter using frequencies ranging from 8 - 40, 50, 60, and 80 Hz in order to find the best match with the frequency content of the seismic reflection data (Figure 68; Campbell et al., 2005). The best frequency match with the seismic reflection data was the 8 – 40 Hz corridor stack. Due to the shorter path length of the seismic wave in a VSP in comparison to conventional 2-D reflection seismic data, the higher frequencies provide better resolution. The interpreter can use this to evaluate stratigraphic variations and the acoustic impedance responses of target formations in greater detail. The higher frequency stacks are valuable for imaging thinner formations such as the Chattanooga Shale, which is below the resolution of the seismic reflection data.

Table 7.—Zero-Offset vertical seismic profile acquisition parameters. VSI = Virtual Seismic Imager; GAC-D = Geophone Accelerometer with Dampening.

Zero – Offset VSP	
Tool	VSI-4
Geophone	GAC-D
Sample Rate	2 ms
Receiver Range	1478.28–30.48 m (4850-100 ft)
Receiver Interval	15.24 m (50 ft)
Source Type	Vibrosies
Source Offset	49.37 m (162 ft)
Source Azimuth	345 degrees
Elevation	114.6 m (376.10 ft)

Wireline Logging Data.—The well reached a total depth of 1498 m (4915 ft) in the Upper Cambrian Copper Ridge Formation. All well logs and mud logs were used during interpretation. The gamma ray log readings were used to determine lithologic boundaries and heterogeneity within units. The sonic and density logs were used to create a synthetic seismogram. The resistivity curve values were used to create a pseudo-sonic log in areas where

sonic readings were affected by borehole breakout (rugosity along the sides of the borehole). Where the neutron and density porosity logs crossed over each other, they indicated porosity and gas effect. The logging tools that made contact with the sides of the borehole are of poor quality between 840 m (2758 ft) and 880 m (2887 ft) due to a major washout in the Pride Mountain Formation. In this interval the sonic and density logs required editing before being used to generate a synthetic seismogram in order to correct the extraneous values caused by poor coupling of the wireline tool with the borehole. The following editing techniques were applied: smoothing (triangular filter), despiking, and clipping extreme values. In addition, 3 m (10 ft) of the log between 870 to 874 m (2856 to 2867 ft) is missing. A sonic log was derived from resistivity for the 3 m (10 ft) missing section using a "scale function" (Kim, 1964) in IHS Kingdom Suite. This is a predictive method that creates a synthetic sonic log using a relationship derived between sonic and resistivity in an intact portion of the borehole (AF90; Rudman et al, 1975; Smith, 2007). This method is preferred over the more traditional Faust's formula (Faust, 1953) in cases where both the sonic and resistivity logs exist for a borehole, but the sonic log has been affected by washout zones.

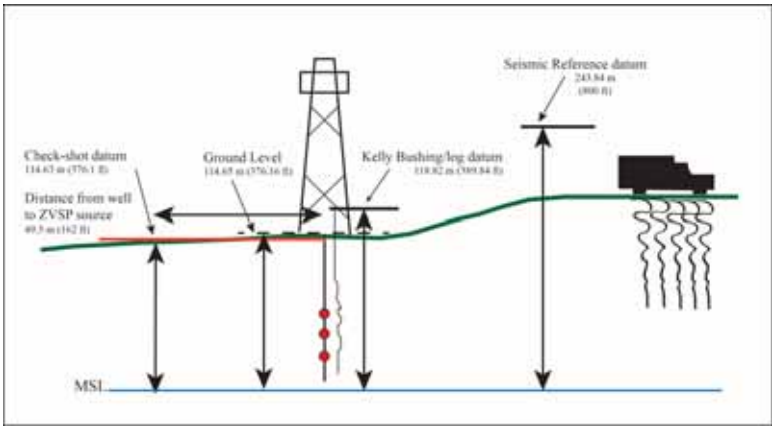

Figure 67.—Datum elevations for the 2-D seismic reflection data, check shot data, and geophysical log data. During analysis the check-shot data were corrected to the SRD to ensure proper alignment of key reflectors. The check-shot datum is slightly lower than the ground level under the Kelly Bushing because of an offset of 49.3 m (162 ft) of the Vibrosies source.

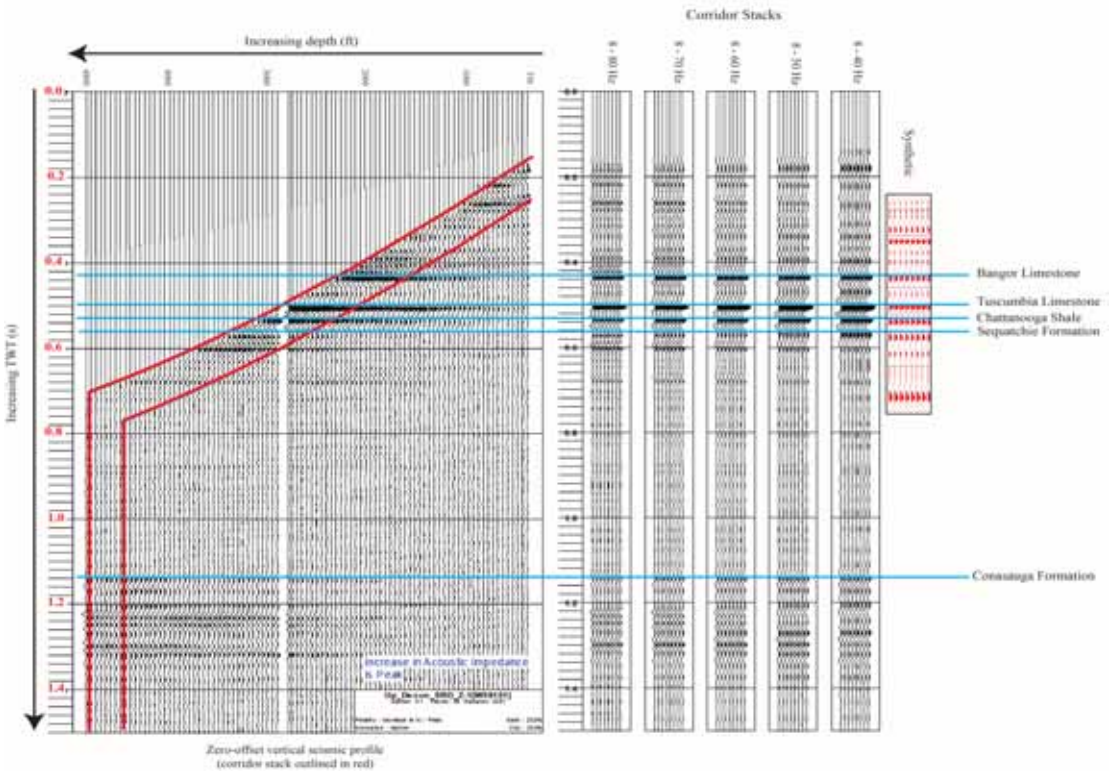

Figure 68.—ZVSP after initial processing. The panel outlined in red is the section of the data used for the corridor stack. Corridor stacks (right) are displayed for a range of frequency contents. The synthetic seismogram (red) generated from the well data is to the right of the corridor stacks. The synthetic shows the depth interval for the well compared to the deepest Conasauga Formation.

Synthetic Seismogram.—A synthetic seismogram is a simulated seismic section computed from well data, which correlates the information gained down-hole with the seismic reflection data. Generating a synthetic creates a tie between the time and depth domains (Box et al., 2004). The check-shot survey was used to calibrate the sonic data. Due to a difference in sampling interval and frequency range, down-hole logs sample the stratigraphy at a much finer scale than a seismic wavelet, so creating a time - depth relationship from the sonic velocities will result in differences between the synthetic and seismic trace (Liner, 2004). Calibration addresses this difference; it involves comparing transit times between defined intervals from the check-shot and sonic log to ensure the accuracy of a time – depth relationship.

The reflection coefficient was calculated using the edited sonic and density logs. A zero-phase wavelet was extracted from the 2-D seismic reflection data and convolved with the reflection coefficient in Petrel to create the synthetic seismogram (Figure 69). The reflection coefficient was convolved with the extracted wavelet. The resulting synthetic seismogram compares very well with the zero-offset 8 – 40 Hz ZVSP corridor stack and 2-D seismic reflection profile extracted at CMP 580 (Figure 69). All key reflectors in the 2-D seismic reflection data were interpreted based on matching the seismic character of the synthetic seismogram and the 8 – 40 Hz ZVSP corridor stack. As sonic logs and vertical seismic profiles are sparse in this part of the Black Warrior basin, this survey is essential in providing a well-seismic correlation that represents this region of the basin.

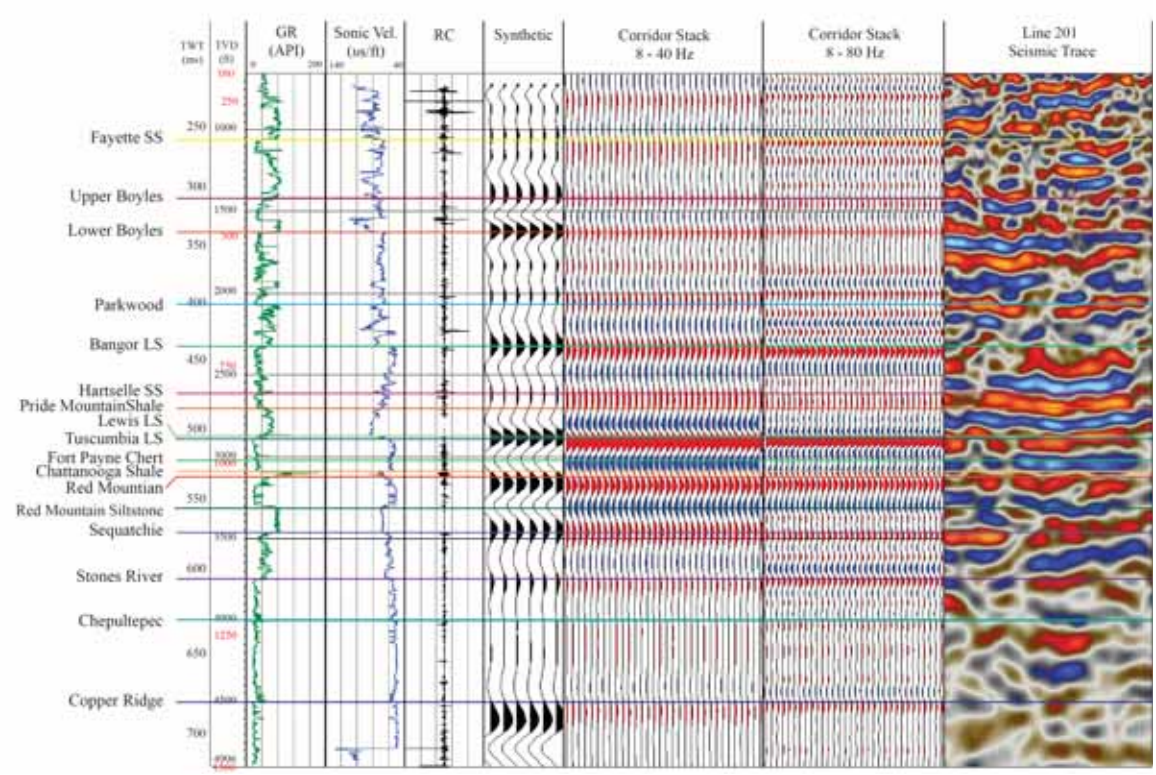

Figure 69.—Down-hole logging, synthetic seismograms, ZVSP, and seismic reflection data for the Gorgas #1 well. The scale is depth in units of feet (black), meters (red), and two way travel time (TWT). The gamma ray (GR) log (green) is a reference log useful in identifying shale units. The sonic log (blue) is especially useful in differentiating sandstones from limestone when the GR count is low. The reflection coefficient (RC; black) is convolved with a wavelet that has been extracted from the 2-D seismic reflection data to derive the synthetic seismogram (black). The synthetic correlates very well with the corridor stack (red = peak; blue = trough). Two corridor stacks are shown: (left) filtered with an 8-40 Hz Butterworth wavelet, which has a closer frequency to the surface seismic data (Table 5), making it a good tool for the well seismic tie; (right) filtered with an 8 – 80 Hz, which allows the interpreter to resolve more detail concerning the thickness variation of units and heterogeneity below the resolution of the surface 2-D seismic reflection data. As an example, in the Parkwood Formation multiple peaks and troughs can easily be identified and correlated with the GR and sonic velocity to determine heterogeneity of the formation. Both the synthetic and the corridor stack tie well with the seismic trace (red = peaks; blue = troughs), which represents 50 traces surrounding CMP 580 on Line 201

Geophysical Characterization.—The time difference between the synthetic seismogram and the 2-D seismic reflection data is less than 10 milliseconds. The well-seismic tie shows that lithologic changes observed in wireline data correspond to key reflectors from stratigraphic units

(Figure 69). Picks for unit tops in depth and time for the characterization well are shown in Table 8. Wireline readings begin at 218 m (716 ft) and stop at 1491 m (4894 ft). There are several transitions from clastic to carbonate rocks that create strong reflectors, but some units have thicknesses below the limit of vertical resolution (Table 9). Vertical resolution is the ability to resolve the top and bottom of an individual unit with reflectors on a seismic trace, and is equal to ¼ of the wavelength (Liner, 2004). Both vertical resolution limits and tuning effects can cause interference from thin beds. Tuning results when beds are approximately ¼ the seismic wavelength in thickness, and have strong enough acoustic properties that they interfere with the reflections from their upper and lower boundaries (Kallweit and Wood, 1982; Gochioco, 1991; Sheriff, 1999). This must be taken into account while doing any interpretations.

Table 8. Two-way travel time (TWT; ms), measured depth (MD) from Kelly Bushing (KB), and Seismic Reference Datum (SRD) of formation tops at Plant Gorgas.

Surface	**MD from SRD m (ft)**	**MD from KB m (ft)**	**TWT (ms)**
Mary Lee Coal	100.84 (331)	-143 (469)	168.80
Jefferson Coal	-17.16 (252)	-252 (828)	225.13
Fayette Sandstone	-87.16 (322)	-322 (1058)	260.77
Upper Boyles	-196.16 (616)	-431 (1416)	311.39
Lower Boyles	-261.16 (827)	-496 (1627)	342.10
Parkwood	-396.16 (1271)	-631 (2071)	401.21
Bangor Limestone	-472.16 (1520)	-707 (2320)	434.31
Hartselle Sandstone	-562.16 (1815)	-797 (2615)	479.28
Pride Mountain	-589.16 (1902)	-824 (2702)	479.05
Lewis Limestone	-614.16 (2074)	-876 (2874)	504.19
Tuscumbia Limestone	-645.16 (2088)	-880 (2888)	506.46
Fort Payne Chert	-685.16 (2221)	-920 (3021)	521.98
Chattanooga Shale	-706.16 (2288)	-941 (3088)	529.26
Red Mountain	-717.16 (2324)	-952 (3124)	533.10
Sequatchie Formation	-822.16 (2667)	-1057 (3467)	572.64
Stones River Group	-907.16 (2946)	-1142 (3746)	603.79
Chepultupec	-986.16 (3207)	-1221 (4007)	630.70
Copper Ridge	-1137.16 (3700)	-1372 (4500)	678.89
Conasauga*	-2585.16 (8450)	-2820 (9250)	1144.32

*Only seen on seismic

Table 9. Vertical resolution of the seismic reflection data for a representative velocity and peak frequency. The replacement velocity (15000 ft/s) is the acoustic velocity used during processing to produce static vertical shifts in seismic in order to align common elevation features. This velocity was also used in processing the ZVSP and check-shot, both of which were processed by Schlumberger.

Velocity	4572 m/s (15000 ft/s)
Peak Frequency	30 Hz
Wavelength	152.4 m (500 ft)
Vertical resolution	38 m (125 ft)

reflections from their upper and lower boundaries (Kallweit and Wood, 1982; Gochioco, 1991; Sheriff, 1999). This must be taken into account while doing any interpretations.

Seismic Reflection Signatures.—Many of the key reflectors have characteristic amplitudes on the 2-D seismic reflection, ZVSP, and synthetic data (Figure 69). Figure 69 includes reference logs, a synthetic seismogram, seismic traces, and two corridor stacks (one processed using a low frequency and one at a high frequency). The low frequency 40 Hz processed corridor stack is most representative of the overall surface 2-D seismic reflection data, which has a peak frequency of 30 Hz, and is best used for comparison with the synthetic seismic and 2-D seismic reflection traces. The higher frequency (80 Hz) stack is valuable for resolving the tops, bottoms, and the heterogeneity within the units.

The top of the Fayette sandstone coincides with a 26 m (85 ft) thick sandstone bounded by shale. The sand unit produces a single low amplitude positive reflector at 270.67 ms, 322 m (1058 ft), but the higher frequency corridor stack shows the top and bottom of the sandstone. The Boyles Sandstone is separated into an upper and lower unit by a 30 m (100 ft) thick shale that is identified by a very high spike on the gamma ray log and produces a strong negative reflector on the synthetic trace (Figure 69). Directly below is a positive, high-amplitude reflector associated with the transition into the Lower Boyles Sandstone at 352.26 ms, 496 m (1627 ft). A lithologic transition from sandstone to the underlying shale marks the top of the Parkwood Formation at 411.31 ms, 631 m (2071 ft). A single peak-trough-peak set makes up the entirety of the 76 m (250 ft) thick formation. The transition from trough to peak occurs because of a calcareous unit in the basal Parkwood that also corresponds to the top of the Bangor Limestone

reflector at 444.55 ms, 707 m (2320 ft). Multiple peaks and troughs can easily be identified and correlated with the gamma ray log and sonic velocity to show formation heterogeneity.

The Bangor Limestone is the first of a series of strong amplitude reflections corresponding to the Hartselle Sandstone, Pride Mountain Formation, Tuscumbia Limestone, Chattanooga Shale, and the Red Mountain Formation. Strong reflectors are caused by the acoustic impedance changes between limestones, shales, and sandstones. A weak positive reflector is present at 478 ms, 797 m (2615 ft) on the synthetic at the top of the hydrocarbon-rich Hartselle Sandstone. A trough follows this when the Pride Mountain Shale is encountered at 489.15 ms, 824 m (2702 ft). Three dominant high amplitude peaks are the key tie points for the synthetic seismic (Figures 68 and 69). These reflectors correspond to the top of the Tuscumbia Limestone at 516.78 ms, 880 m (2888 ft), and the upper Red Mountain limestone at 543.34 ms, 952 m (3124 ft), and the Sequatchie Formation at 582.96 ms, 1057 m (3467 ft). The Chattanooga Shale at 539.44 ms, 941 m (3088 ft), and the middle Red Mountain silty shale at 552.12 ms,1004 m (3294 ft), produce troughs in between the three main peaks. These distinct reflections result from contrasting lithologies and tuning effects.

There are significant differences in the corridor stacks between the top of the Tuscumbia Limestone and the top of the Red Mountain Formation. In the 80 Hz corridor stack, each of these formations, within that interval (e.g. Fort Payne Chert and the Chattanooga Shale), are detected. The Sequatchie Formation marks the top of a 1524 m (5000 ft) carbonate succession. Within this large unit of carbonate rocks, there is a seismic peak that corresponds to the top of the Stones River Group at 614.2 ms,1142 m (3746 ft), but the remainder of this section consists of low amplitude reflectors with good lateral continuity until the base of the Knox Group at approximately 1000 ms on the seismic reflection data. The Knox is also seen on the ZVSP at

1.14 seconds (Figure 68). It is characterized by laterally continuous, high amplitude reflectors that result from the abrupt change in acoustic impedance from dolomite to the calcareous shale of the Conasauga Formation.

Depth Conversion.—By depth converting the 2-D seismic reflection profiles, one can not only make accurate interpretations but also extend volume calculations away from the well and accurately calculate dips of beds and structures. The study area has a low structural complexity, making a velocity model with continuous horizontal layers viable. In this model, each lithologic unit is defined using a velocity relationship as a function of burial depth (Marsden, 1989) that is constrained by the check-shot results. Specific velocity intervals were chosen based on lithology including the Parkwood Formation, Hartselle Sandstone, Tuscumbia Limestone, Lower Red Mountain Formation, Sequatchie Formation, and Conasauga Formation (Figures 70 and 71). It is especially important that horizons are picked accurately as velocities in the Black Warrior Basin can change abruptly among shale, coal, sandstone, limestone, and dolostones beds.

The velocity model, created in Petrel, is based on interval velocities from the sonic log calibrated using the check-shot data. Interval velocities from the sonic log calibrated check-shots were averaged for each unit and then input to the velocity model for each surface based on interpretations (Table 10). A polygon, containing the Plant Gorgas characterization well, was created around the two seismic lines. Surfaces were extrapolated from the interpreted seismic horizons using a convergent interpolation algorithm and a grid increment of 10 by 10 meters. A qualitative match between depth converted seismic surfaces and well tops provides evidence of an accurate velocity model (Figure 72).

Table 10. Interval velocities input to the velocity model. Velocities are applied to the unit overlying the given surface.

Surface	**Velocity (m/s)**
Zero	0
Parkwood	3763
Bangor LS	4715
Hartselle SS	5419
Tuscumbia LS	4146
Lower Red Mountain	5511
Sequatchie	5091
Conasauga	6300

The first unit in the model is the heterogeneous Pennsylvanian Pottsville Formation, composed of interbedded sandstone, shale, and coal. This interval was assigned an average velocity of 3763 m/s. The underlying Parkwood Formation is composed of shale and limestone and has a velocity of 4715 m/s. The Bangor Limestone has a significantly higher velocity of 5419 m/s. The Hartselle Sandstone and Pride Mountain Shale make up 45.7 m (150 ft) of clastic material between these two limestone units and are assigned a significantly lower velocity of 4146 m/s. The Tuscumbia Limestone, Fort Payne Chert, Chattanooga Shale and upper Red Mountain Formation comprise a 128.3 m (421 ft) unit with a velocity of 5511 m/s, an increase in velocity from the overlying Hartselle/Pride Mountain unit. The Red Mountain is split into two units that are resolved on the seismic reflection data as distinct reflectors: the upper Red Mountain Formation is 33.5m (110 ft) of limestone; the lower 68.5 m (225 ft) of the Red Mountain is silty shale. A surface was interpreted for the lower Red Mountain siltstone and a velocity of 5091 m/s was applied. A single velocity was applied to all units below the Red Mountain, including the Sequatchie Formation and the Knox Group. This velocity interval consists of 1524 m (5000 ft) of limestone and dolomite that extends down to the Conasauga

Formation, a strong continuous reflector that marks the first significant shale-limestone pair after the Knox Group. A velocity cannot be calculated for this unit because of a lack of data, but previous studies (Maher, 2002; Pearce, 2002; Gates, 2006) used wells that penetrated the entirety of the Cambrian-Ordovician carbonate unit and assigned a velocity of 6100 to 6400 m/s. The

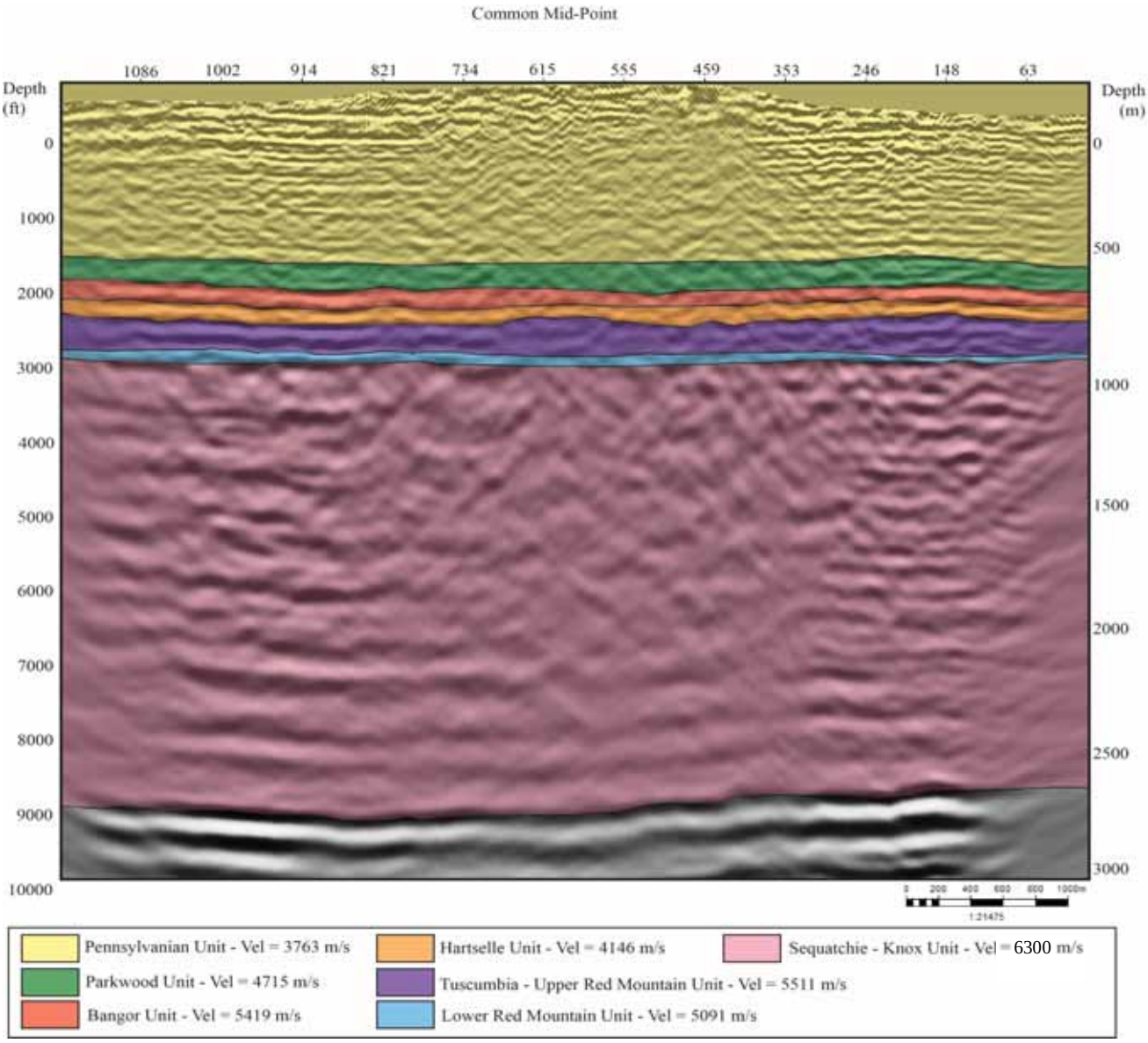

Figure 70.—Depth converted seismic reflection data for Line 101. The vertical depth scale is given in feet (left) and meters (right) relative to mean sea level. CMP number is displayed along the horizontal axis. The velocity model used to convert time to depth is overlain on top of the seismic data with the average interval velocities for each unit indicated in the legend. All velocities are in meters per second (m/s).

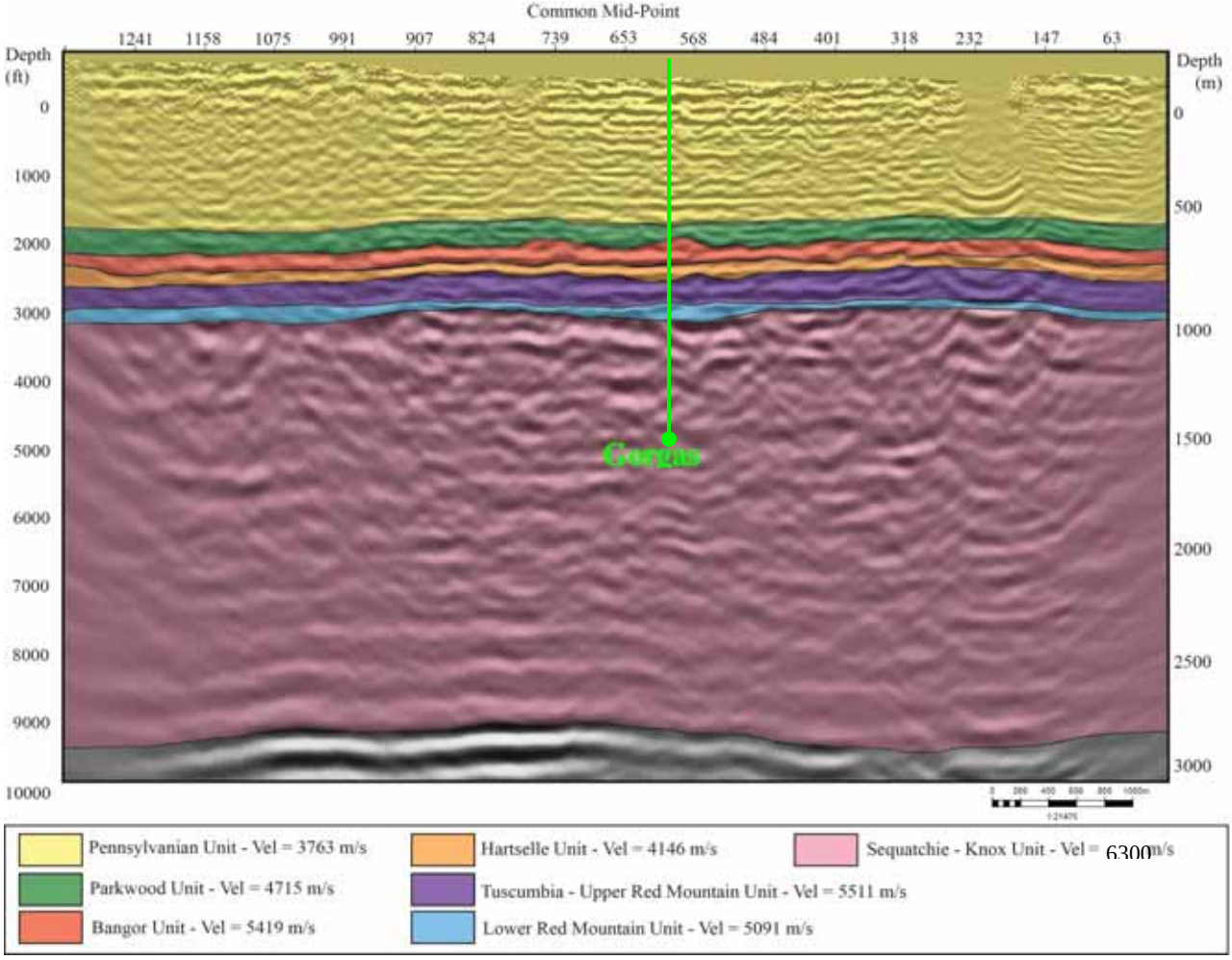

Figure 71.—Depth converted seismic reflection data for Line 201. The vertical depth scale is given in feet (left) and meters (right) relative to mean sea level. CMP number is displayed along the horizontal axis. The velocity model used to convert time to depth is overlain on top of the seismic data with the average interval velocities for each unit indicated in the legend. All velocities are in meters per second (m/s).

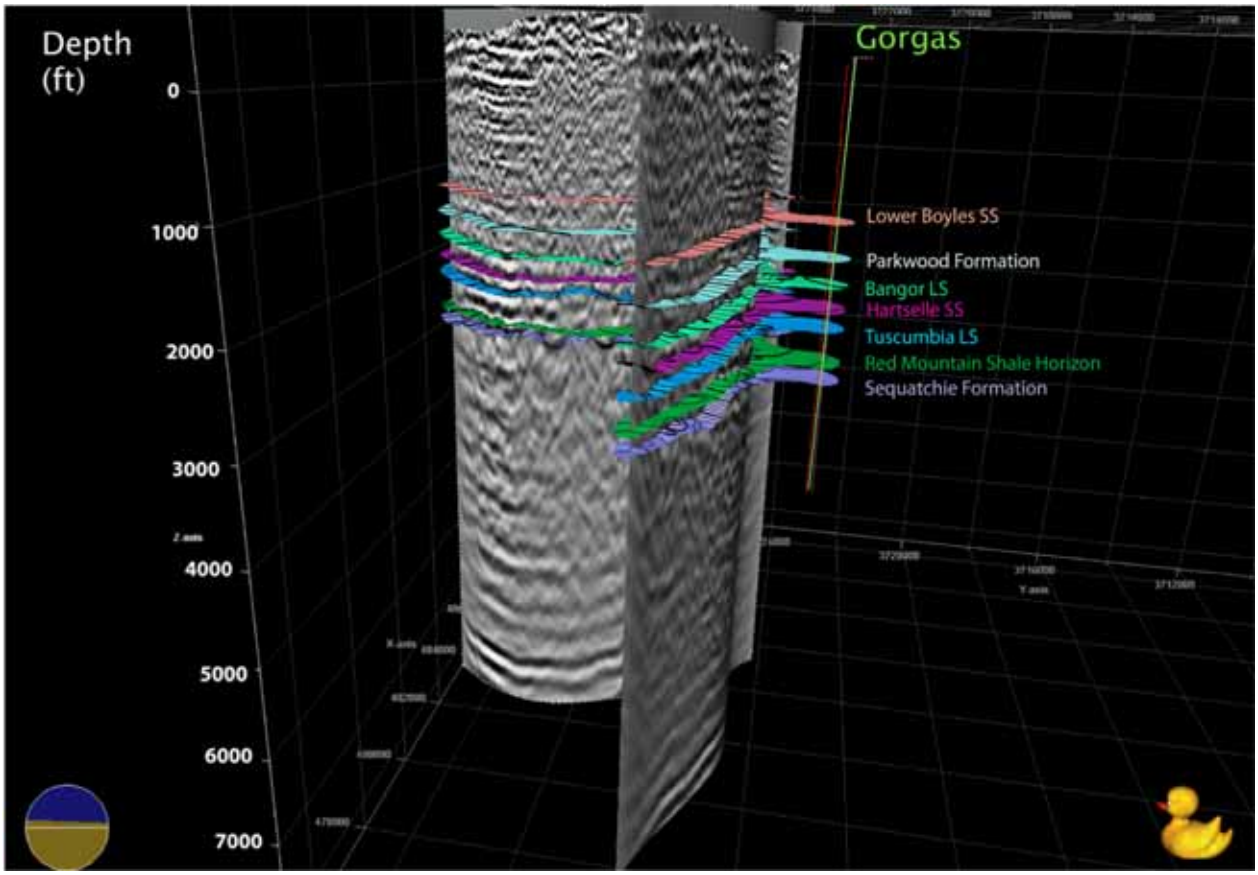

Figure 72.—Three-dimensional view of depth converted Lines 101 and 201 with Gorgas #1 borehole.

Applicability of CO_2 sequestration technology.—Many factors influence the applicability of CO_2 storage technology at the Gorgas test site, including the chemistry of formation fluids, the distribution of porosity and permeability, injectivity, and the quality of the confining units. The Safe Drinking Water Act (SDWA) provides the authority for the regulation of underground injection in the United States through the establishment of the Underground Injection Control (UIC) program. The SDWA necessitates that geologic CO_2 storage in saline formations be restricted to formations containing water with total dissolved solids (TDS) content greater than 10,000 milligrams per liter (mg/L) (Class V experimental and Class VI UIC wells). However, exceptions to this rule exist for enhanced hydrocarbon recovery (Class II UIC wells). Fresh-water plumes with less than 10,000 mg/L have been identified along the frontal structures of the Appalachians at depths greater than 2,000 feet in the coalbed methane reservoirs of the upper Pottsville Formation (Pashin and others, 1991; Pashin and others, in press).

A large number of geochemical analyses from wells completed in Mississippian and Pennsylvanian sandstone are available in the National Brine Wells Database (NETL, 2002) and in the files of the OGB and are helpful for constraining the position of the USDW in the subsurface. These data indicate that a great majority of wells are completed in saline formations with TDS between 20,000 and 100,000 mg/L (Figure 73). Only three wells completed in lower Pottsville and older strata have produced water with TDS content less than 10,000 mg/L. Two of these wells are shallower than 1,000 feet, whereas the third is deeper than 2,000 feet. No wells completed in Mississippian-Pennsylvanian sandstone deeper that 2,500 feet produced formation

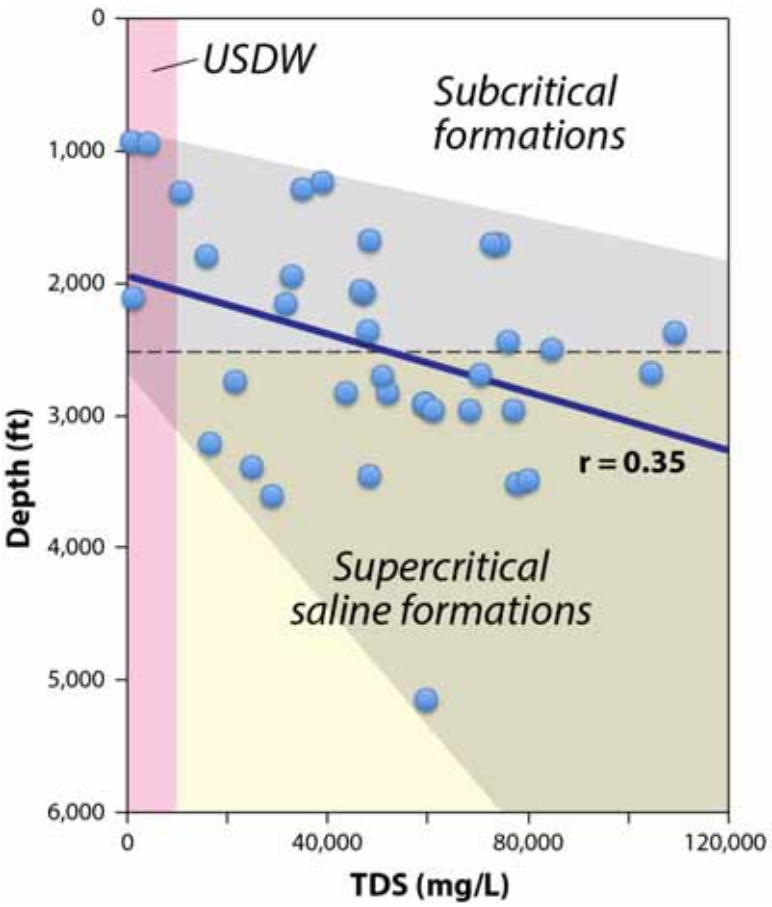

Figure 73.—Cross-plot of TDS measurements versus depth for Mississippian-Pennsylvanian sandstone units in the Black Warrior Basin.

water that is protected by the SDWA. This is important because this is the depth beyond which CO_2 can be stored in a supercritical state under normal hydrostatic pressure.

During drilling, the resistivity of the fluid returning with the cuttings was monitored, and analysis of SP and resistivity logs provided further insight into the TDS of the formation water (Figure 74). The estimated TDS content of water in the Pottsville Formation below surface casing is above 10,000 mg/L and locally exceeds 30,000 mg/L. TDS content is estimated to be between 20,000 and 30,000 mg/L in the Hartselle Sandstone and Bangor Limestone and locally exceeds

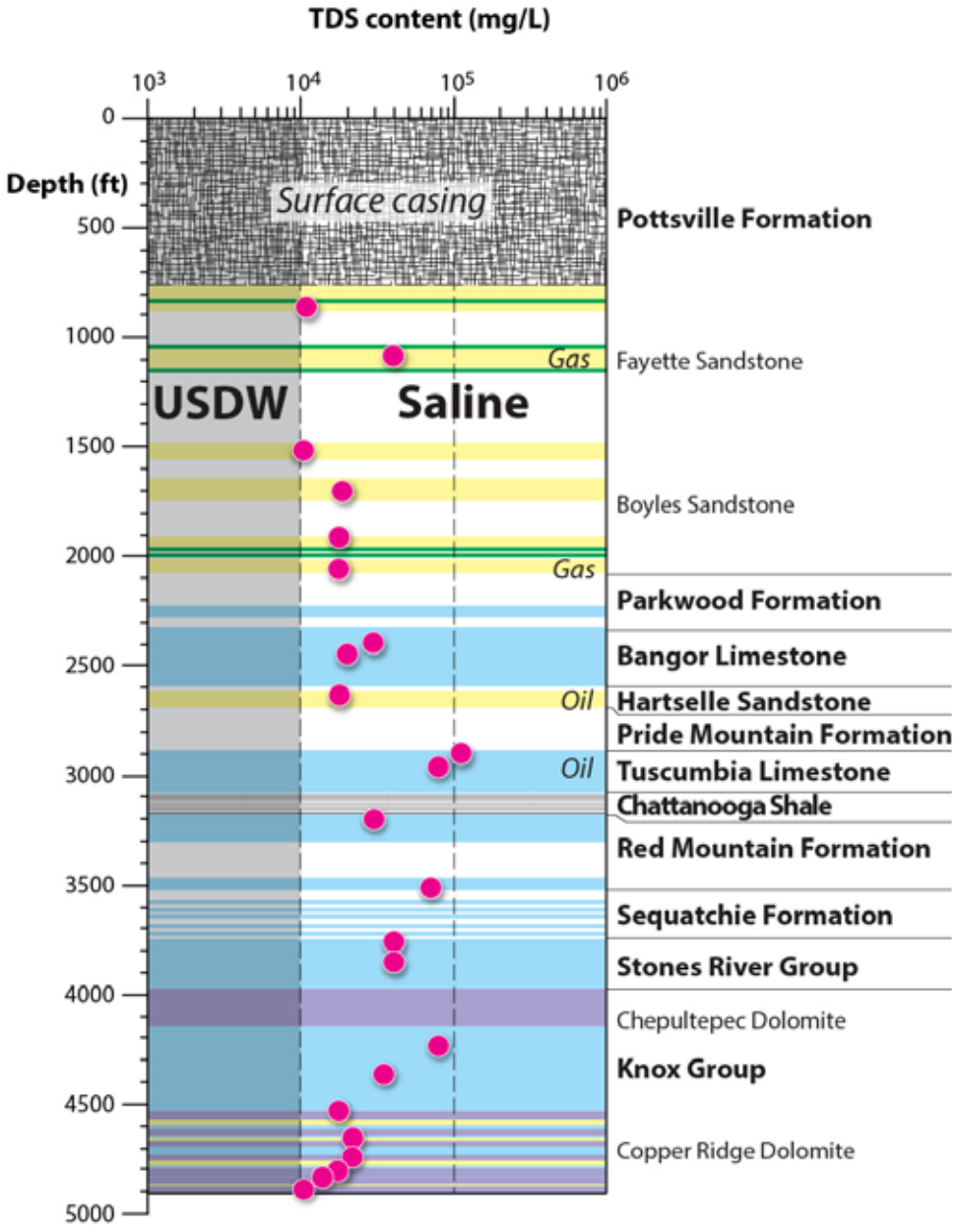

Figure 74.—Plot of estimated TDS content versus depth in the Gorgas #1 borehole.

100,000 mg/L in the Tuscumbia Limestone. Values are estimated to be between 40,000 and 80,000 in the Stones River Group, Sequatchie Formation, and Red Mountain Formation. In the Chepultipec Dolomite, TDS content appears to range from 20,000 to 80,000 mg/L. However, TDS content is generally lower than 20,000 mg/L in the upper part of the Copper Ridge Dolomite and dropped to near 10,000 mg/L as the well reached total depth. This drop in TDS

content corresponded with a major increase in formation water in the wellbore, which forced the termination of air drilling. The drill rig was switched to a mud system, and drilling ended because of slow rate of penetration and continued influx of low-TDS fluid into the wellbore.

Recent oil and gas exploration in the region provides crucial insight into the origin of low TDS formation water in the Gorgas area (Figure 75). As the Gorgas borehole was being planned in 2009, Geomet, Incorporated drilled a prospective salt-water disposal well into the Copper Ridge Dolomite in Blount County (Cullman Property Company 21-04-08 SWD; OGB permit 15854-SWD-09-02). The well encountered large volumes of fresh water, and the mud log records TDS content lower than 500 mg/L in the Copper Ridge. Accordingly, the well could not be used for brine disposal and was abandoned. An exploration well that was drilled in Cullman County in 2007 (Haynes Farms, LLC 26-08 #1; OGB Permit 15223) also encountered large volumes of water in the Copper Ridge Dolomite, although the TDS content of the water was not recorded. Multiple wells have been drilled into Cambrian-Ordovician carbonate southwest of Plant Gorgas in the Wiley Dome Field, and drilling records indicate that Copper Ridge strata contain saline water, as well as oil and gas.

The Copper Ridge Dolomite does not come to the surface in the Sequatchie anticline but is exposed along the southeastern margin in the Black Warrior Basin (Figure 75). In the Murphrees Valley anticline of Blount County, a large structural panel containing a thick Copper Ridge section is exposed at the surface and dips northwest into the Coalburg syncline (Figure 76). Meteoric recharge of the basinward-dipping structural panel helps explain the combination of fresh water and high yield of wells penetrating the Copper Ridge Dolomite in Blount and Cullman Counties. Farther southwest, Copper Ridge strata along the southeastern margin of the Black Warrior Basin are horizontal or dip southeastward into the Cahaba synclinorium. In this

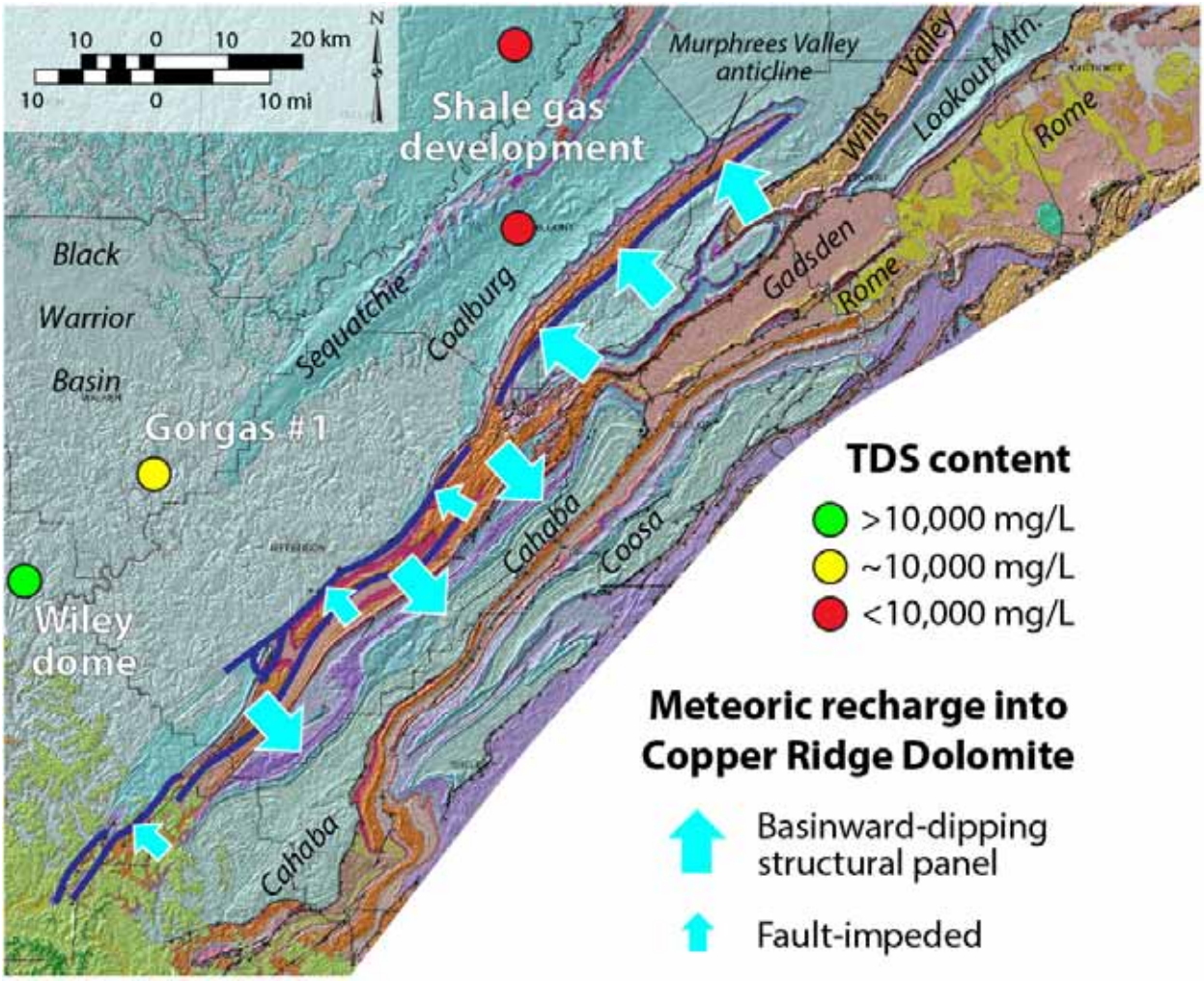

Figure 75.—Geologic map showing predicted flow directions of meteoric recharge in Cambrian-Ordovician carbonate rocks (pink and orange) along the southeastern margin of the Black Warrior Basin. Mississippian-Pennsylvanian strata shown in purple and blue.

area, thrust faults shield the Cambrian-Ordovician section in the Black Warrior basin from major fresh-water recharge, and southeastward dip favors flow away from the basin and into the Cahaba synclinorium. Regardless, it appears that Plant Gorgas lies in the transition zone between protected water and saline water in the Copper Ridge Dolomite (Figure 75). Accordingly, Copper Ridge strata are not viable geologic CO_2 storage targets in the Gorgas area, and efforts should focus on deep targets southwest of the plant where saline formation water is known to occur.

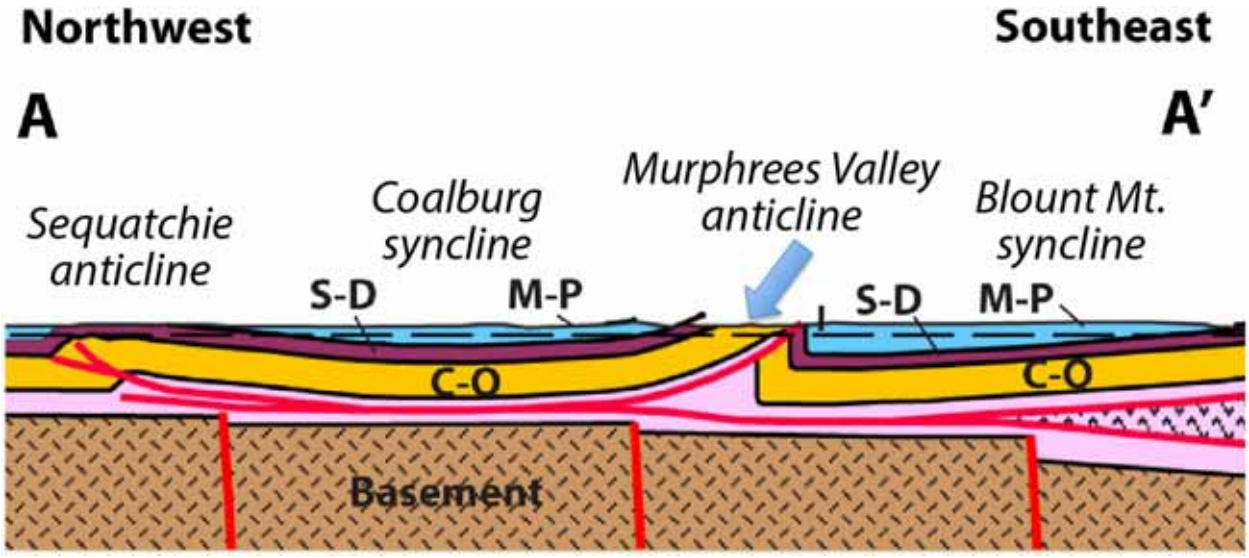

Figure 76.—Structural cross section showing basinward dipping structural panel facilitating fresh-water recharge (blue arrow) along the southeast margin of the Coalburg syncline in the Black Warrior basin (cross section modified from Thomas and Bayona, 2005).

Results from drilling the Gorgas #1 test borehole indicate that low porosity and permeability are significant impediments to conducting commercial-scale CO_2 sequestration operations in the Gorgas area. However, the Hartselle Sandstone poses a significant opportunity to apply innovative approaches to oil recovery. Although porosity and matrix permeability are low, conventional core analysis indicates that the abundant natural fractures in the reservoir locally provide Darcy-class permeability and thus could support commercial flow rates. The principal issues facing recovery of the oil are low mobility and normal reservoir pressure. Accordingly, innovative drilling, stimulation, and recovery techniques are required to develop the oil resources in the Hartselle Sandstone, and the resource estimate of 9,000 bbl/acre indicates economic potential.

Directional drilling and multi-stage stimulation have revolutionized the U.S. oil industry by enabling the recovery of oil from nanodarcy-class reservoirs, such as shale (EIA, 2013). Application of similar technology may be key for unlocking the oil resources in the Hartselle

Sandstone. Core data indicate that the oil in the Hartselle has API gravity on the order of 40°, indicating high potential for the application of miscible CO_2 flooding. Injection of CO_2 as a source of reservoir energy, moreover, may be applicable as a primary recovery technology in the Gorgas area. Therefore, the project team recommends that additional exploratory cores be drilled in this area to better characterize the oil resource and reservoir heterogeneity. Based on the results of this characterization, a pilot site can then be selected to test the most promising drilling and completion technologies, as well as the applicability of CO_2 flooding as a primary recovery technique in tight oil reservoirs.

Capacity and Injectivity

Data from the Gorgas #1 test site indicate that capacity and injectivity are limited in the Gorgas area. The high potential for water with TDS content lower than 10,000 mg/L in the Copper Ridge Dolomite precludes underground injection in the lower part of the Knox Group. Low matrix porosity and permeability precludes injection in all other formations, save for the Hartselle Sandstone, where a large oil resource may be recoverable using primary CO_2 injection and permeability is assisted by natural fractures. Formations above the Hartselle Sandstone, such as the lower Pottsville, are too shallow to be prospective for supercritical CO_2 storage. Hence, the only formation that can be considered for CO_2 storage is the Hartselle Sandstone.

Reservoir thickness and porosity data indicate that a pore volume of about 21,000 $feet^3$/acre is available for storage in the Hartselle Sandstone at Plant Gorgas. This is equivalent to 2,675 tonnes of CO_2/acre, or about 107,000 tonnes per 40-acre tract. Extrapolated to 10,000 acres in the area of Plant Gorgas, this translates to a pore volume of 27 Mt. This is equivalent to just over one year of emissions from the Gorgas and Miller steam plants. Importantly, tertiary oil recovery

operations typically sweep 2 to 4 pore volumes of CO_2 through the reservoir (ARI, 2006). What this means in terms of actual amounts of CO_2 required from the steam plants to drive operations, as well as the scale of the recycle loop needed to reinject CO_2 that has broken through to production wells, remains to be determined and is an object for further research.

Experience from brine disposal in the Black Warrior Basin indicates that natural fractures can facilitate high injectivity (Table 4). However, low matrix permeability and limited fracture connectivity results in significant buildup of back-pressure over time. Although natural fractures are expected to serve as major flow conduits in the Hartselle Sandstone, few predictions can be made without advanced simulation and well testing. This also is true for deep targets in other parts of the Black Warrior Basin, such as the Knox Group, where natural fractures are an essential part of the subsurface hydraulic architecture. Accordingly, a central objective of the simulation efforts conducted during this project was the characterization of the relationship between flow in natural fractures and rock matrix.

SIMULATION

Knox Group Fractured Carbonate Simulation

The simulation effort conducted by the GSA focused on numerical modeling of flow transport of supercritical CO_2 injected into deep saline formations of the Knox Group in the Black Warrior Basin. The work is composed of two major areas of research: (1) fracture permeability characterization and (2) multiphase flow modeling of CO_2 injection. Novel methods for fracture permeability characterization and multi-dimensional directional flux weighting were developed during this study. These new methods enable stochastic reservoir characterization and simulation of injection and transport of CO_2 highly heterogeneous fractured reservoirs. The

resulting models facilitate simulation of fractured media in areas with hundreds of thousands of fractures, which can not be achieved by either traditional continuum or DFN methods alone.

The transmissivity of a fracture is usually much larger than that of rock matrix. Consequently, fluid will flow preferentially through fractures, provided that the fractures are interconnected at the reservoir scale (Snow, 1969; Lee et al, 2001). The permeability of a fractured formation is a nonlinear function of matrix permeability, fracture size (i.e., aperture, length, and height), fracture spacing, fracture orientation, and (Long and others, 1985; Dershowitz and Einstein, 1988; Anderson and Dverstrop, 1987; Cacas and others, 1990). Accurate modeling of effective permeability in fractured reservoirs has been challenging because fracture networks may significantly alter the hydrologic properties of the reservoir. Numerical models for fluid flow and transport in fractured media can be divided into continuum and DFN models (Lee and others, 2001; Teimoori and others 2003). In continuum models, such as dual porosity-permeability models, fractures are assumed to be infinitely long and distributed in a regular pattern. This approach ignores the geologic variability of basic fracture properties and thus results in ineffective simulation of fracture-related heterogeneity. Calculation of an effective permeability tensor is an effective way to represent permeability in fractured formations (Teimoori and others 2003). According to this approach, effective permeability is defined for a fractured medium that is statistically homogeneous at a large scale. The minimum volume at which a reservoir volume can be simulated as homogeneous is called the reservoir equivalent volume (REV) (Pouya and Fouche, 2008) (Figure 77).

DFN) modeling is a stochastic approach that utilizes the probabilistic density functions of fracture properties, which can be measured in outcrops, cores, and geophysical well logs (e.g., Long and others, 1985; Dershowitz and Einstein, 1987). Multiple realizations of a DFN model

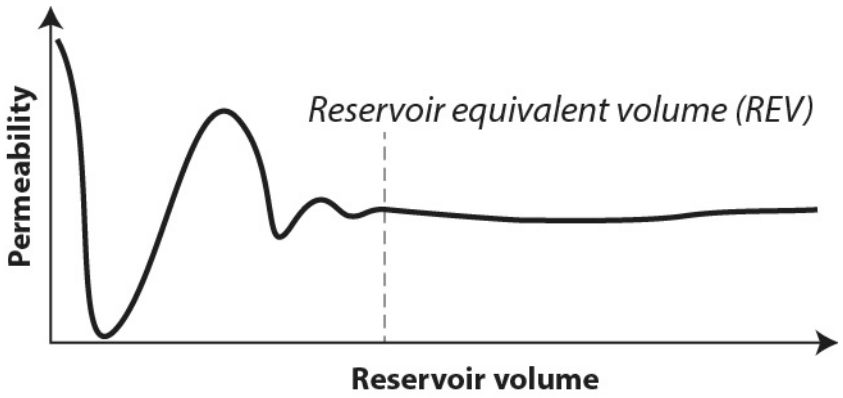

Figure 77.—Diagram showing relationship of reservoir equivalent volume (REV) to permeability and reservoir grid cell volume. Cell volumes larger than REV treat the reservoir as homogeneous, whereas smaller volumes preserve heterogeneity. Resolution of heterogeneity increases as cell volume decreases.

can be generated stochastically if the statistical characteristics of fracture orientation, size, and connectivity are known. In this approach flow is modeled by treating each simulated fracture individually in a discretized spatial domain. Theoretically, the DFN approach is the most realistic model for predicting the fluid flow and transport through the fractured geometric media. One disadvantage, however, is that these models simulate the characteristics of fracture populations rather than the precise locations of actual fractures in nature. Another disadvantage is the computationally-intensive nature of these models. Our experience with developing DFN models is that, while it is possible to develop large geologic simulations of natural fracture systems, modeling flow through systems with hundreds of thousands of fractures having different properties is computationally infeasible given current desktop computing technology (Pashin and others, 2004, 2008).

Simulation workflow.—The approach used to calculate the effective permeability for fractured Knox strata by integrating DFN and continuum method in a way that honors the geometry and flow properties of each modeled fracture based on field and subsurface data. A

mathematical permeability matrix can be expressed as a 2nd rank tensor. Each fracture is defined as a finite crack between two parallel planes (i.e., parallel plate theory). The transmissivity of a fracture obeys the cubic law that is generally accepted for Newtonian flow. The permeability tensor of a fracture is defined as:

$$K_f = \frac{A_f}{V} \bullet \frac{b^3}{12} \bullet \begin{bmatrix} 1-n_1n_1 & -n_1n_2 & -n_1n_3 \\ -n_1n_2 & 1-n_2n_2 & -n_2n_3 \\ -n_1n_3 & -n_2n_3 & 1-n_3n_3 \end{bmatrix} \quad (1),$$

where A_f is the area of the fracture, *b* is the aperture, V is the volume of the element containing the fracture, and *n* is the normal to the fracture plane. In equation (1), the permeability tensor is composed of three terms, namely the fracture size, aperture, and orientation. The equivalent permeability of an element is the sum of the permeability tensor of each fracture contained in equation (1).

For stochastic characterization of the fractured Knox reservoirs, we have established a workflow that emphasizes data collection, stochastic representation, model realization, and permeability mapping (Figure 78). This workflow permits rapid evaluation of the equivalent fracture permeability based on multiple realizations of a DFN model and to optimization of the grid size of the flow model to achieve accurate and efficient modeling of multiphase flow systems.

Knox DFN model.—The DFN model was built upon the stratigraphic information based on the SP, mud log, and gamma ray log from Gorgas #1 borehole. Ortiz and others (1993) have studied the well test data in brine disposal wells that penetrated the Knox Group, and this

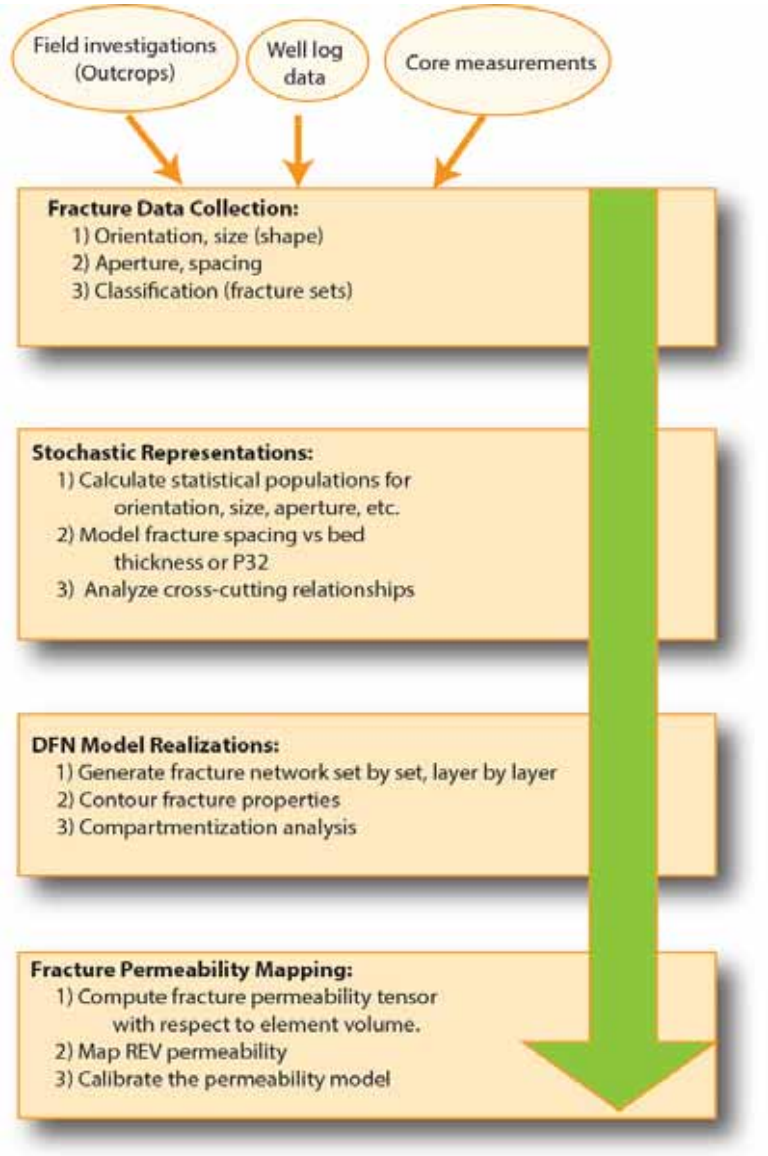

Figure 78.—Diagrammatic workflow used to characterize fracture permeability for CO_2 injection, flow, and transport modeling.

information was vital for developing the reservoir model. Analysis of the FMI log from the Gorgas #1 borehole reveals numerous natural fractures that are open and have imageable aperture (Figure 79). In carbonate rocks, open fractures have low resistivity and thus image as black lines, whereas calcite cemented fractures have high resistivity similar to that of the host

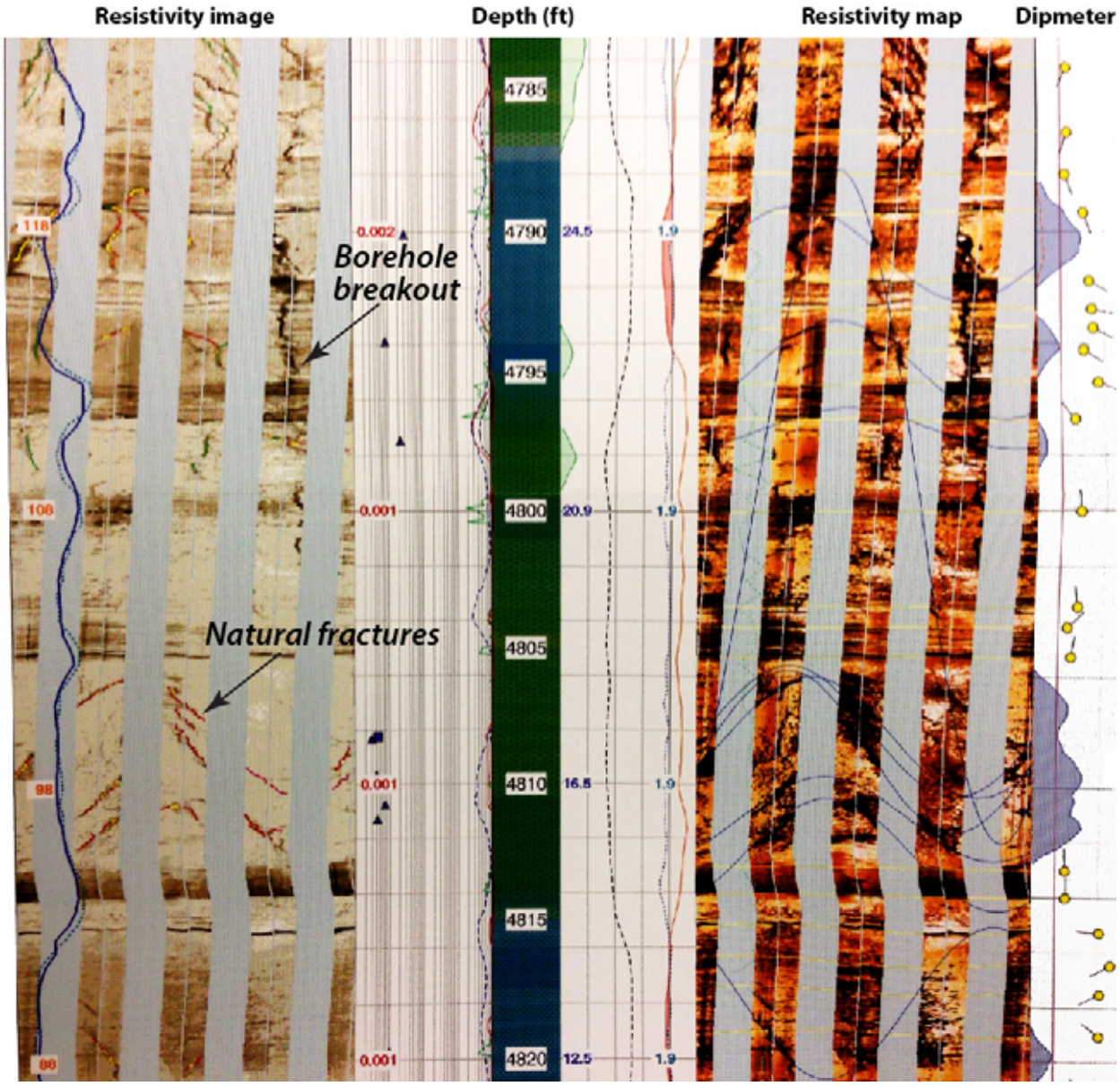

Figure 79.—FMI log showing interpreted natural fractures and borehole breakouts in the Knox Group, Gorgas #1 borehole.

limestone or dolostone. In the excerpt of the FMI log shown here, dipping natural fractures are imaged at 4,810 feet, and a borehole breakout that formed during drilling is imaged at 4,795 feet.

Analysis of the FMI log resulted in the recognition of three major zones of fracturing in the Knox Group (Figure 80). Identified natural fractures were plotted to show vertical locations with strike and dip information. A total of 75 fractures were identified and classified as joints,

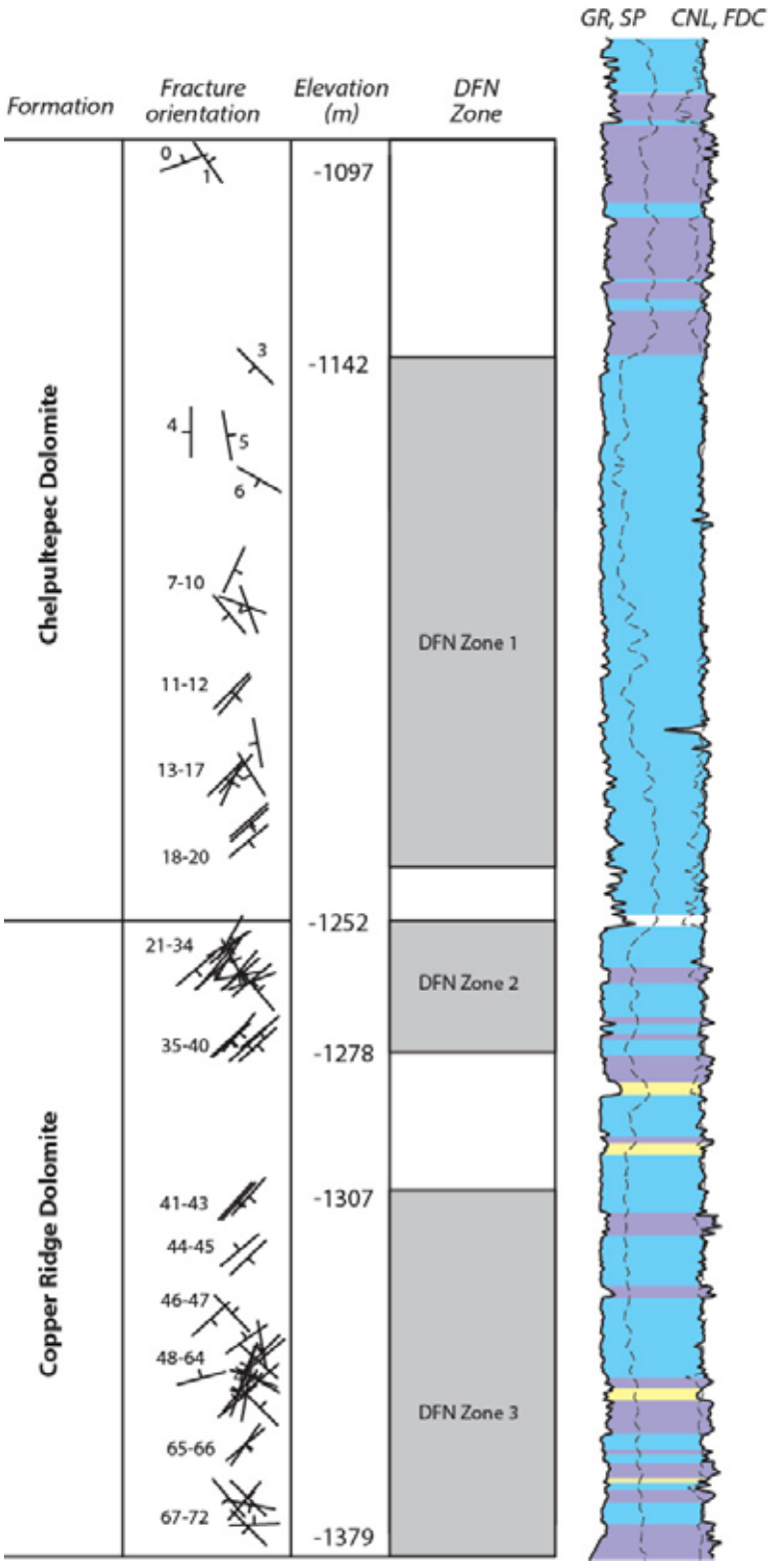

Figure 80.—Interpretation of joint distribution and orientation in the Knox Group of the Gorgas #1 borehole. Clustering of readings was used to define thee fracture zones for DFN modeling.

drilling-induced fractures, and shear fractures, and the dominant systematic fracture azimuth is about 45°. Few fractures were identified in two intervals, one near the top of Chepultepec Dolomite, and the other in the upper part of the Copper Ridge Dolomite. Overall, fracture abundance increases with depth. The fracture population was subdivided into three zones based on visual clusters, and each zone represents a stratigraphic layer in the DFN models. Results of statistical analysis of each DFN zone is summarized in Table 11. Since there are no direct measurements of fracture aperture, values are based on Schlumberger's interpretation of the FMI logs. Stratigraphic and structural data were entered into DFNModeler to develop a multilayer realization of Knox fracture architecture, and multiple realizations were made using different fracture seed values. Each realization was visually similar and simulates near-vertical joints in classic orthogonal networks (Figure 81).

Determining the effective permeability of the fracture networks is required to translate the DFN model to a REV model. To analyze REV in the Knox Group, permeability tensors were calculated for each DFN realization using 10 different grid element sizes (Figure 82). Permeability values oscillate strongly where the element size is less than 150 meters. However, when the element size is greater than 200 meters, the permeability tensor is relatively stable, which effectively determines the REV of the Knox Group. Calculated REV permeability tensors from 10 different realizations of DFN zone 1 of the Knox Group show similar results (Figure 83). The important thing to note is that grids equal to or larger than the REV effectively treat the model area as homogeneous, whereas progressively smaller grids capture increasing amounts of fracture-related reservoir heterogeneity. Ultimately, the lower limit of grid size is determined by the amount of computational power and the efficiency of the modeling code that is deployed.

Table 11. Summary of statistical analysis of fracture networks in the Knox Group, Gorgas #1 borehole.

DFN Zone	Formation	Interval	Thickness	NE Fracture Set						NW Fracture Set					
				Mean Direction		P32	Aperture*	Size	Termination frequency (%)	Mean Direction		P32	Aperture*	Size	Termination frequency (%)
		(m)	m	Strike	Dip		Mean (m)	(m)		Strike	Dip		Mean (m)	(m)	
Zone 1	Mid-lower Chepultepec	-1142 -1253	110.73	40.7	78.6	0.10	6.43E-05	200	0	132.5	82.1	0.05	3.20E-05	30	100
Zone 2	Upper Copper Ridge	-1253 -1278	25.27	48.7	83.8	0.11	6.43E-05	200	0	139.4	87.6	0.06	3.20E-05	30	80
Zone 3	Lower Copper Ridge	-1307 -1379	72.00	48.4	83.8	0.12	6.43E-05	200	0	139.4	87.6	0.07	3.20E-05	30	80

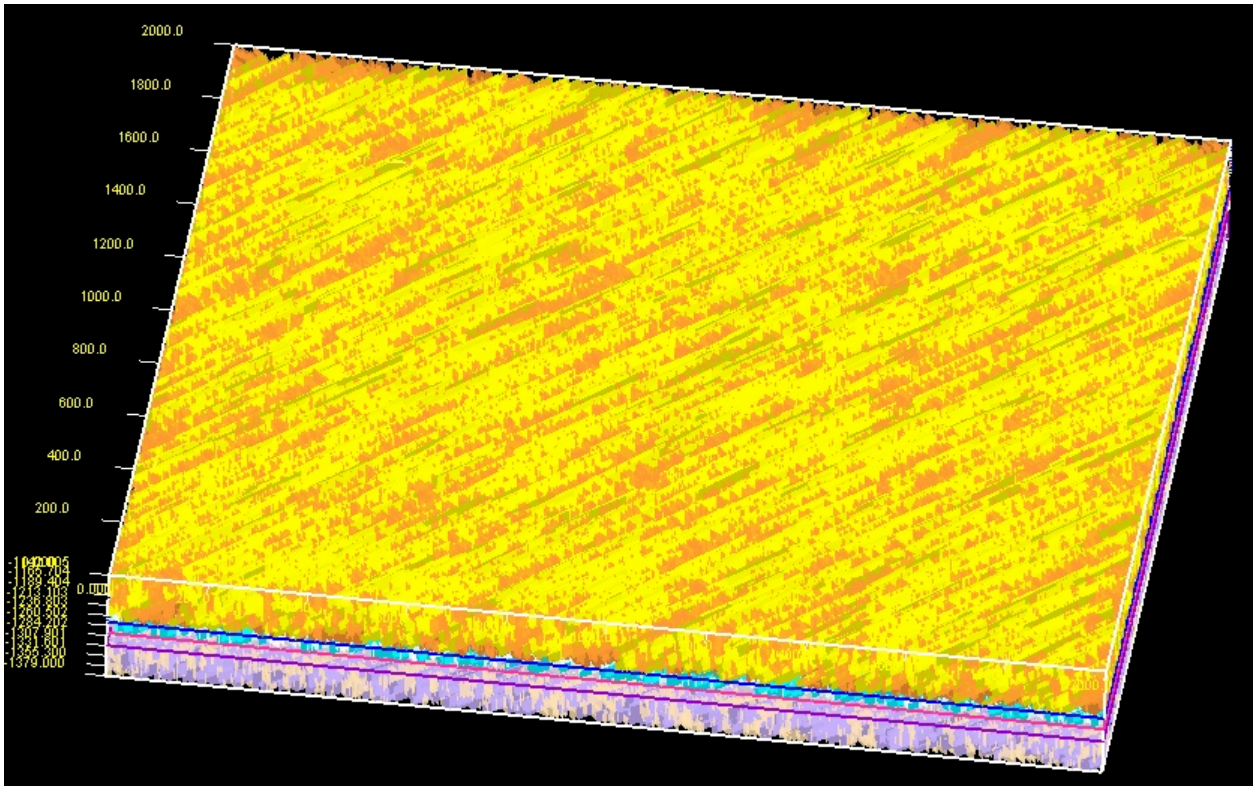

Figure 81.—DFN model simulating orthogonal joint networks in the Knox Group in the Gorgas #1 borehole. The upper layer of the model depicts northeast-striking systematic joints in yellow and cross-joints in orange.

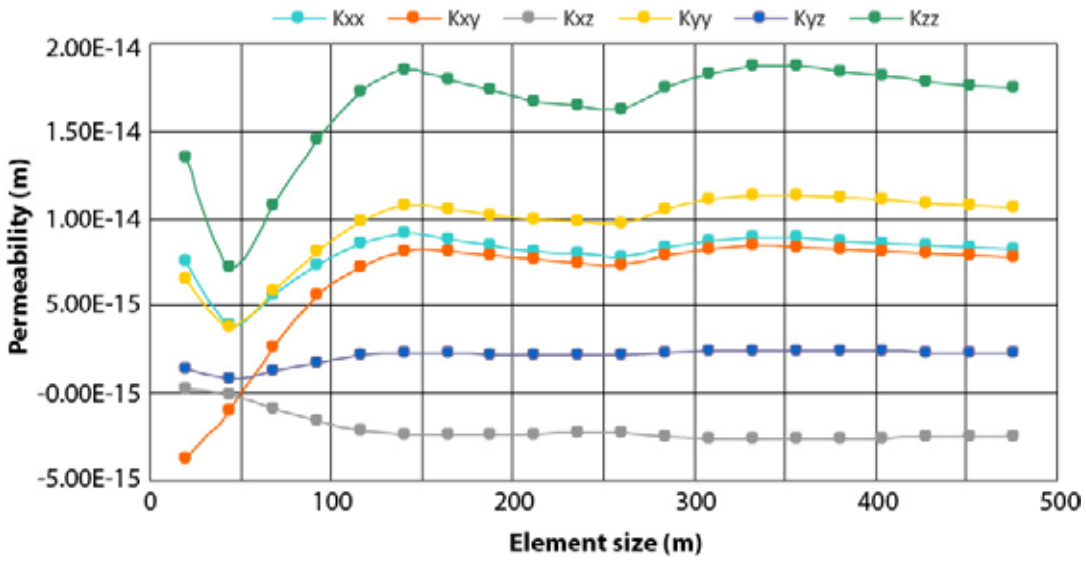

Figure 82.—Plot of permeability tensors at different grid cell (element) sizes. This plot suggests that the REV is about 150 meters.

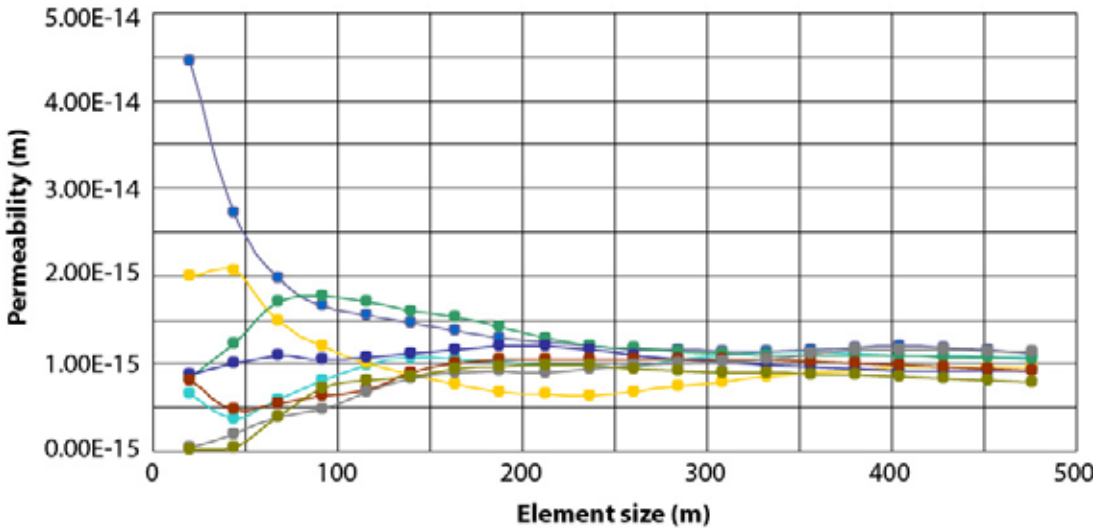

Figure 83.—Diagrammatic workflow used to characterize fracture permeability for CO_2 injection, flow, and transport modeling.

The calculated average REV tensor for DFN zone 1 based on 10 realizations is:

$$K = \begin{bmatrix} 7.5E-15 & 7.02E-15 & -2.2E-15 \\ 7.02E-15 & 9.66E-15 & 2.07E-15 \\ -2.2E-15 & 2.07E-15 & 1.59E-14 \end{bmatrix} \quad (2)$$

The non-zero values in equation (2) indicate the permeability tensor ellipsoid is not aligned with the geographic reference axes (east, north, and vertical). The corresponding principal permeability ellipsoid is

$$K_p = \begin{bmatrix} 8.53E-16 & 0 & 0 \\ 0 & 1.55E-14 & 0 \\ 0 & 0 & 1.63E-14 \end{bmatrix} \quad (3)$$

with the respective principal axis oriented in the direction (direction cosine)

$$Axis_p = \begin{bmatrix} -.75 & -.66 & 0.06 \\ .64 & -.74 & -0.22 \\ -.19 & .13 & 0.97 \end{bmatrix} \quad (4)$$

with the first column corresponding to the first axis. The orientation of the REV permeability ellipsoid derived from equation (4) can be visualized as an oblate disk that is closely aligned with the strike of the systematic regional fractures, which is the expected result.

In order to verify our calculation of the fracture permeability tensor, we used a two-phase model simulating water injection to compare model results with real-world well test results as reported by Ortiz and others (1993). We used data from the first 6 months of injection for comparison and validation, because injectivity was relatively stable during that time (Figure 84). Results indicate that injectivity can be modeled that is representative of the observed injectivity in the Knox Group.

Models of CO_2 injection.—Numerical modeling of multi-phase, multi-component flow is of fundamental importance for understanding the dynamics of fluid transport in porous media. The overarching principles governing numerical simulation of multiphase flow in porous media are the conservation of mass and energy in keeping Darcy's law. These principles can be simulated with a set of second-order partial differential equations (PDEs) (Peaceman 1977; Helmig, 2007). The PDEs are commonly approximated by numerical approaches with set boundary conditions, such as finite difference method, finite element method, finite volume method, and mixed methods.

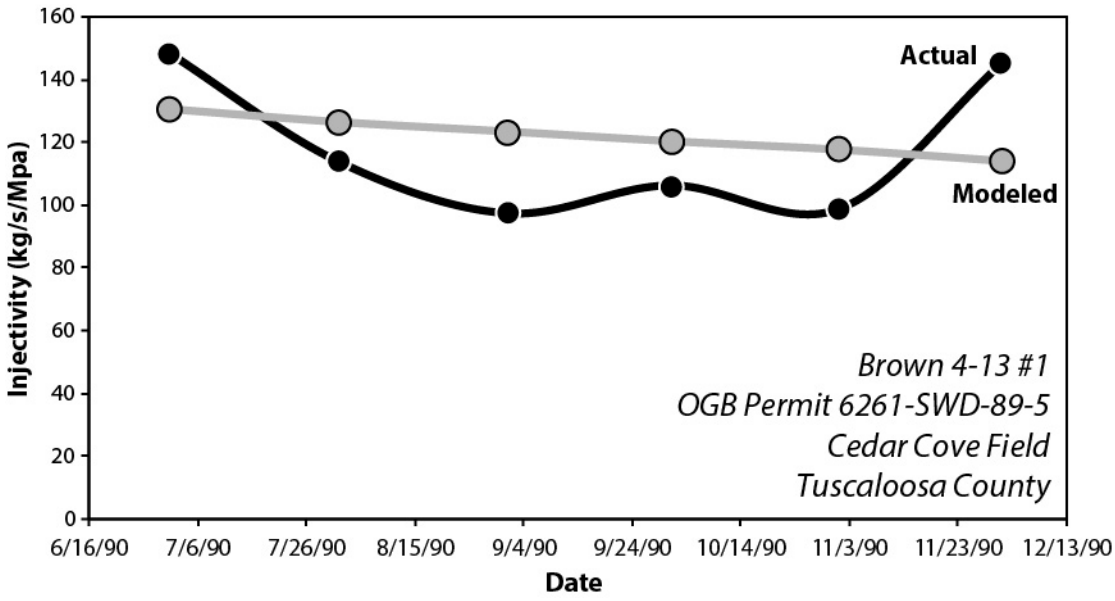

Figure 84.—Plot showing relationship between actual and modeled injectivity in a brine disposal well, Knox Group, Cedar Cove Field, Black Warrior Basin.

Numerical modeling of multiphase flow poses many computational challenges. First, the inherently tight coupling and strong non-linear nature of the governing equations require novel algorithms to reduce computational load and numerical errors, especially for transient problems. Numerical instability and spurious oscillations will arise from complex geologic reservoirs where rock properties, such as porosity and permeability, can vary by several orders of magnitude (Edward and Zheng, 2010; Gerritsen and Durlofsky, 2005; Huber and Helmig, 2000). The existence of gravitational and capillary forces together with strong viscosity differences can lead to countercurrent flow, which is responsible for non-physical saturation solutions and imposes severe restrictions on the numerical methods (Geiger and others, 2004; Kozdon and others, 2011). This complexity is partially responsible for the grid orientation effect (GOE) in multiphase numerical modeling (Todd and others, 1972; Aziz and Settari, 1979). Various upwind weighting techniques have been proposed in an effort to reduce GOE, and this is still a subject of intensive study. Most reservoir simulators use a first-order single point upstream weighting

(SPU) method in which relative phase mobility is interpolated from the upstream cell according to either pressure difference or the sign of phase velocity along grid lines (Brenier and Jaffré, 1991; Kwok and Tchelepi, 2007). This practice seems to be one of the main sources of GOE, especially in higher dimensions where the directional fluxes are oblique to the grid lines (Lamine and Edwards, 2010).

The simulation team has developed a new upwind weighting scheme that utilizes multipoint flux-based approximations (MPFAs) to minimize the grid orientation effects that are inherent in the SPU method (Figure 85). MPFAs employ the characteristic flow information to develop a multipoint stencil for transport, as opposed to merely considering the sign of the phase velocity as in the SPU method. The resulting numerical simulator employs a hybrid finite element-finite volume method (FEM-FVM) that includes a detailed upwind weighting scheme.

Multiphase CO_2 injection modeling was first performed on simple models simulating DFN zone 1 in the Chepultepec Dolomite (Figure 86). Rock matrix was populated with the permeability values determined by conventional core analysis. The physical properties of supercritical CO_2 and H_2O brine that were used for modeling are summarized in Table 6. Boundary conditions are summarized as follows:

- *Boundary conditions*
  - No-flow boundaries: top, bottom
  - Hydrostatic boundaries: left, right, front, back

- *Initial conditions*
  1. All layers are initially saturation with saline water
  2. All layers are pressured under hydro-static condition
  3. Injection of CO_2 occurs at the center of the model at various depth interval(s) based on specific model setup

The first model developed contains only DFN zone 1 in the Knox Group and has X-Y dimensions 2,000 by 2,000 meters and a Z dimension of 111 meters. The permeability tensor was

Table 12. Fluid properties used for simulation of CO_2 injection into Knox carbonate.

Fluid	Density* (kg/m^3)	Viscosity (kg/ms)
Saline H_2O	998.4	0.00382
Supercritical CO_2	600	0.0002

Calculations performed at reservoir temperature (50°C) and salinity >10,000 mg/L TDS.

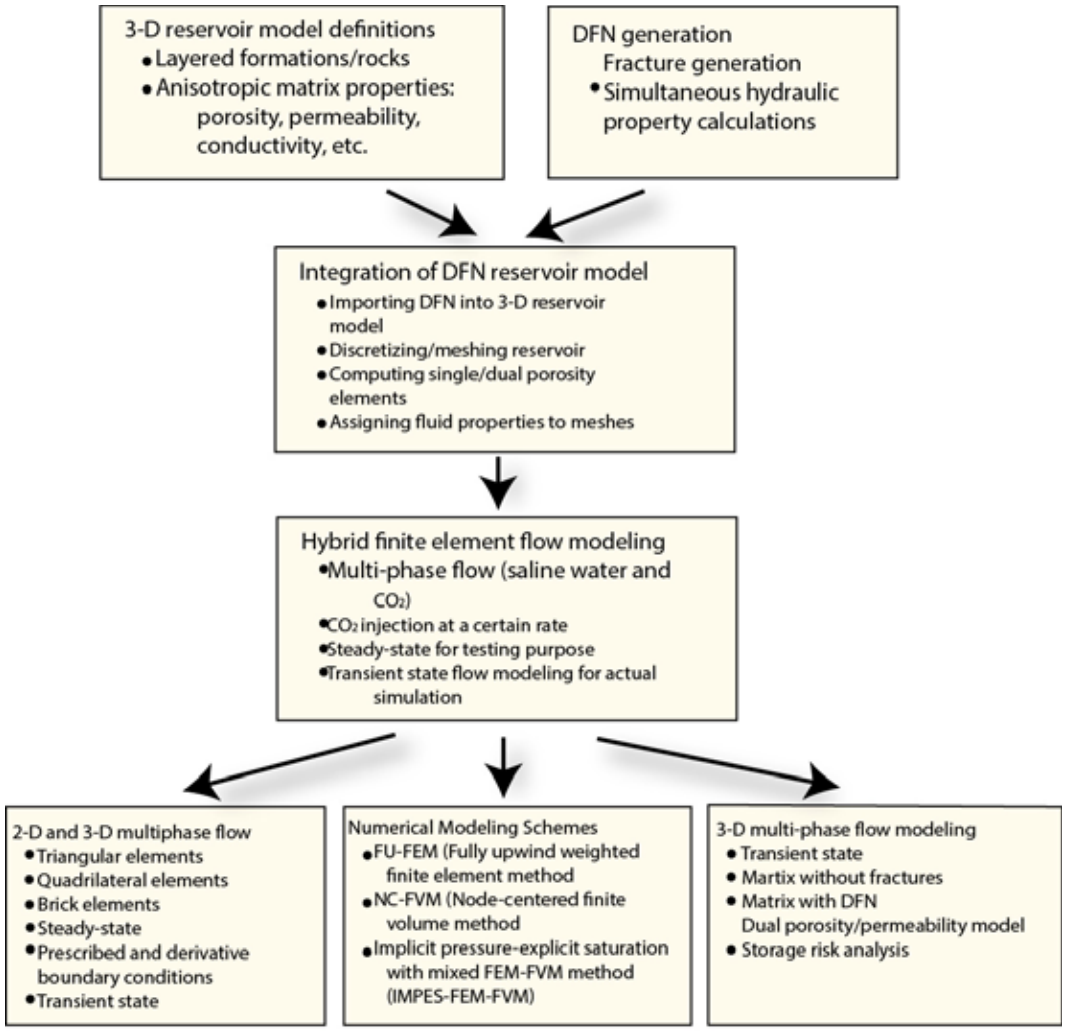

Figure 85.—Flow chart sowing procedure used for multiphase finite element-finite volume modeling of CO_2 injection into a fractured saline formation.

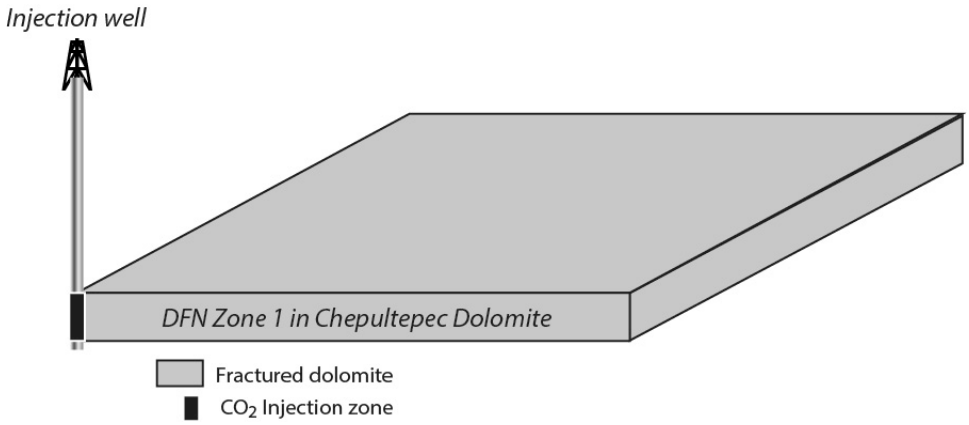

Figure 86.—Diagrammatic representation of the modeling setup used to simulate injection, flow, and transport of CO_2 in Knox Group saline formations.

calculated and contoured for each element. The model was discretized using 50 x 50 x 5 grid elements. The horizontal dimension for each element is 40 meters, which is much less than the minimum REV size (200 meters). Thus the permeability values vary greatly from element to element, indicating that a portion of the fracture heterogeneity was captured.

The CO_2 injection rate was simulated at 475,200 kilograms per day. This model shows the CO_2 saturation after 1.5 years of injection, indicating strong northeastward preferential migration, which is well aligned with the principal permeability tensor ellipsoid direction (Figure 87). The CO_2 also tends to accumulate in cells with high permeability elements, thus creating localized islands of CO_2 saturation. The model also shows the viscous fingering effects of diffusive CO_2 migration occurs at the frontal margin of the CO_2 plume. This effect is commonly observed in highly heterogeneous geological media. A plan view of the CO_2 saturation contour at the top of DFN zone 1 illustrates the geometry of the plume (Figure 88). The total phase pressure contour shows elevated pressure in the vicinity of the injection well (Figure 89). It also suggests that the pressure footprint is elongate.

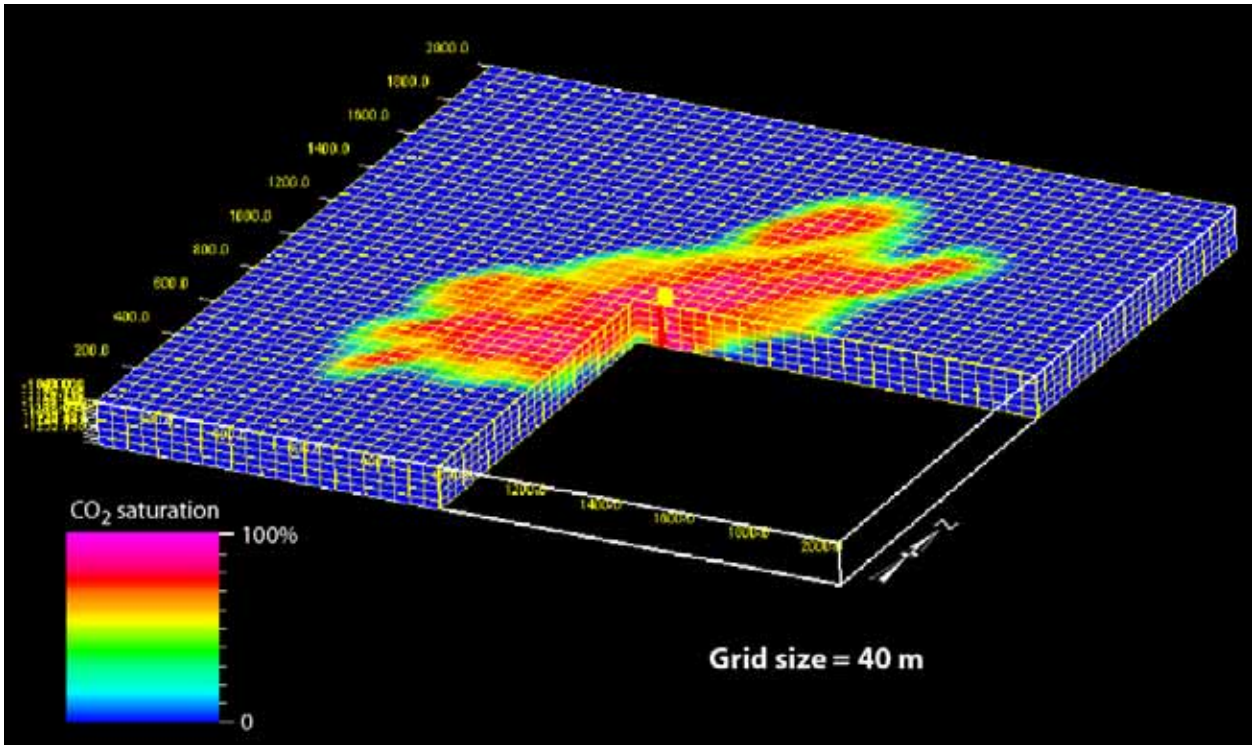

Figure 87.—Color contoured model of CO_2 saturation in DFN zone 1 after 1.5 years of injection. Model area = 2 square kilometers.

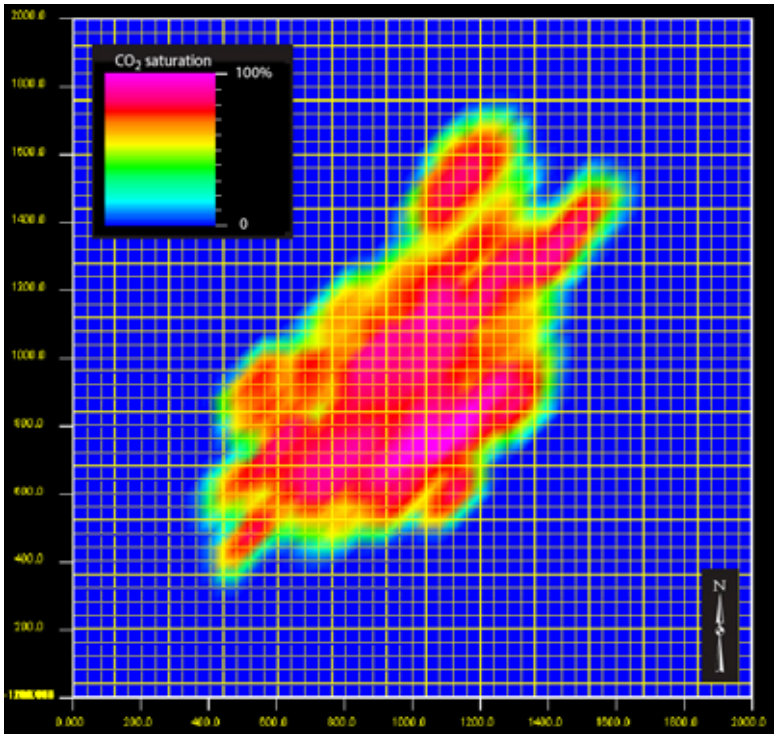

Figure 88.—Plan-view model of CO_2 saturation in DFN zone 1 after 1.5 years of injection.

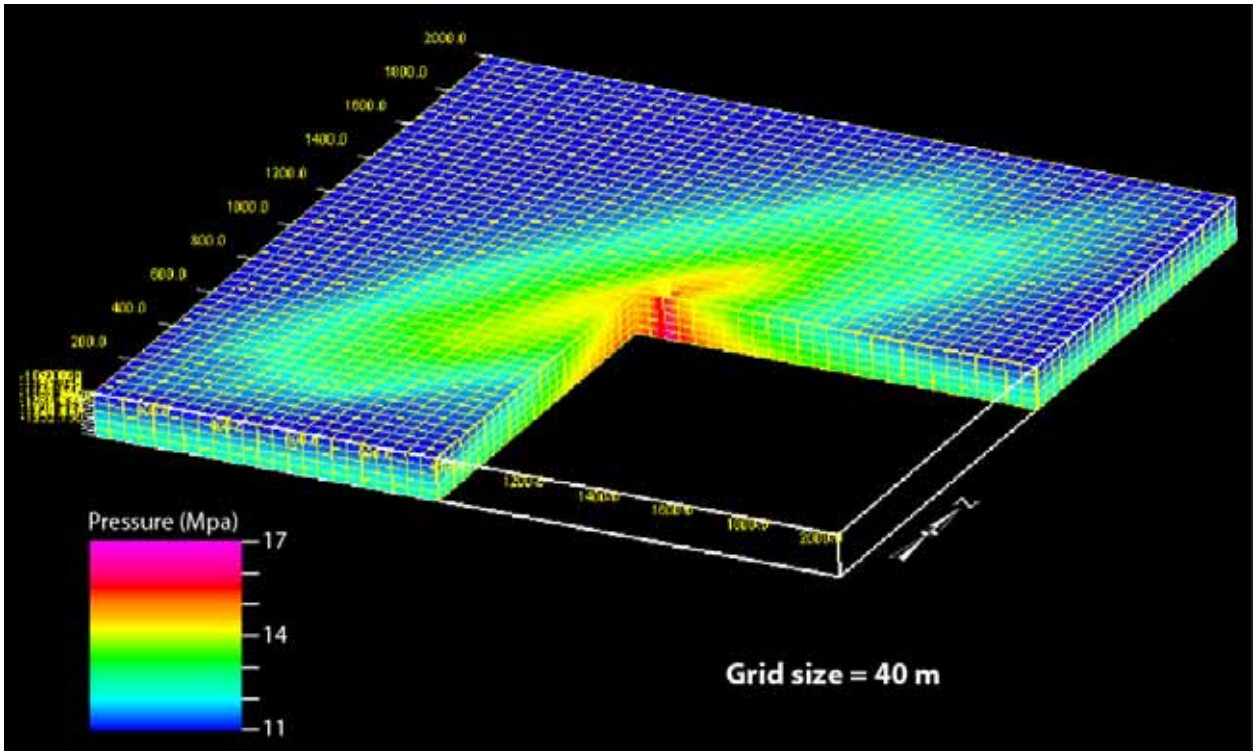

Figure 89.—Model of the pressure footprint at the end of 1.5 years of CO_2 injection into DFN zone 1 of the Knox Group.

The CO_2 injection modeling was performed using a variety of grid sizes to investigate the consistency of modeling results using the same basic parameters (Figure 90). The larger grid, by comparison shows no effects of fracture heterogeneity. The smaller grid size results in a robust model of saturation showing the effects of heterogeneity expressed as viscous fingering near the plume front. Despite of these differences, the overall shape and area of CO_2 plume remains similar and the total CO_2 volumes in the two models are the same. Similar models were developed for the other DFN zones, and the models yield comparable results with plume size and geometry reflecting differences in reservoir architecture (Figure 91). An interesting outcome of these models, moreover, is that Knox carbonate lacking natural fractures appears to have significant sealing capacity, at least relative to the short-term models shown herein. These results

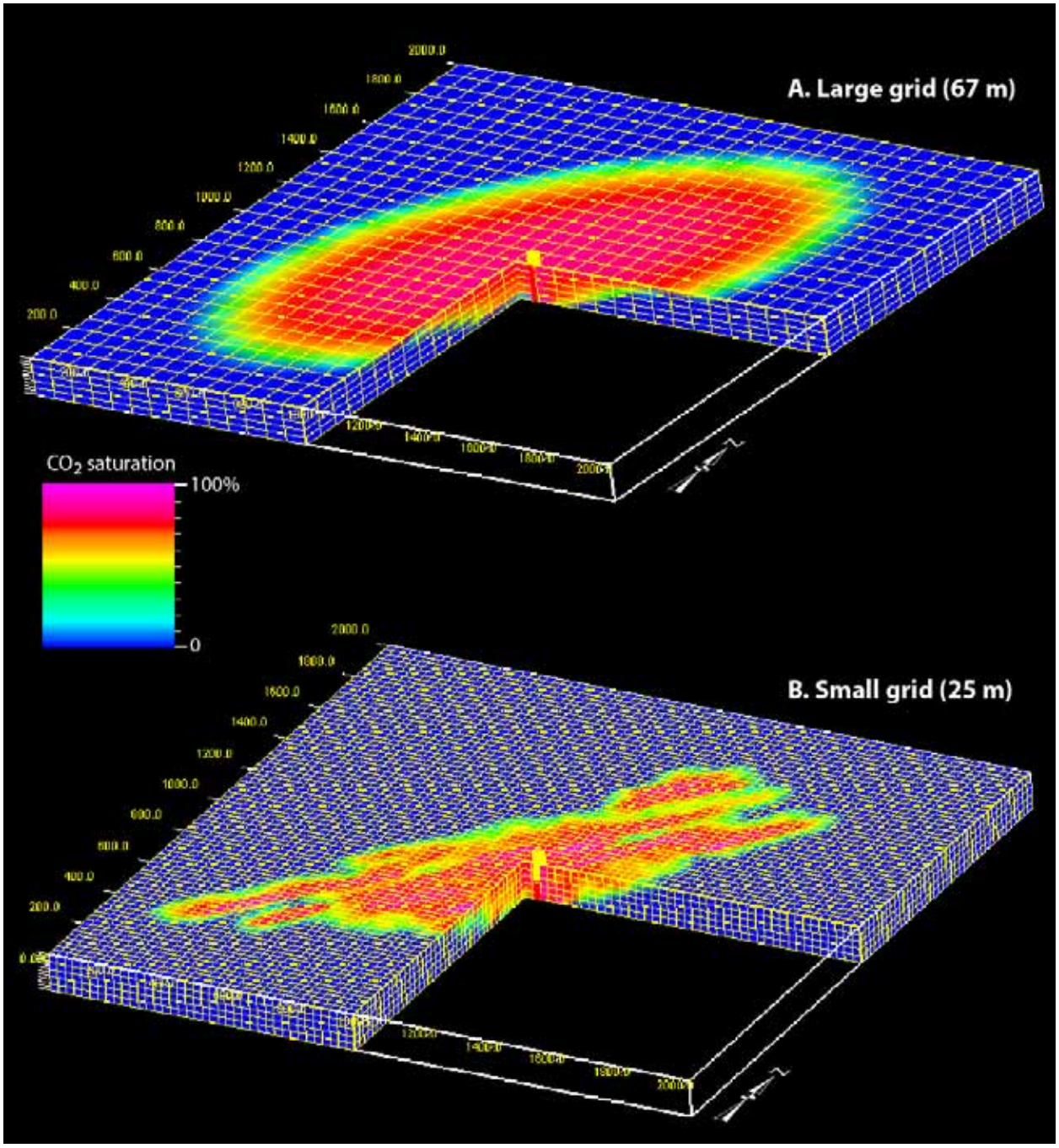

Figure 90.—Different models using identical parameters showing the effect of grid cell size on model results. (A) Model employing cell volume approaching REV that is volumetrically correct but does not simulate heterogeneity. (B) Model showing grid size that is substantially below REV that provides a high-resolution simulation of a heterogeneous CO_2 plume.

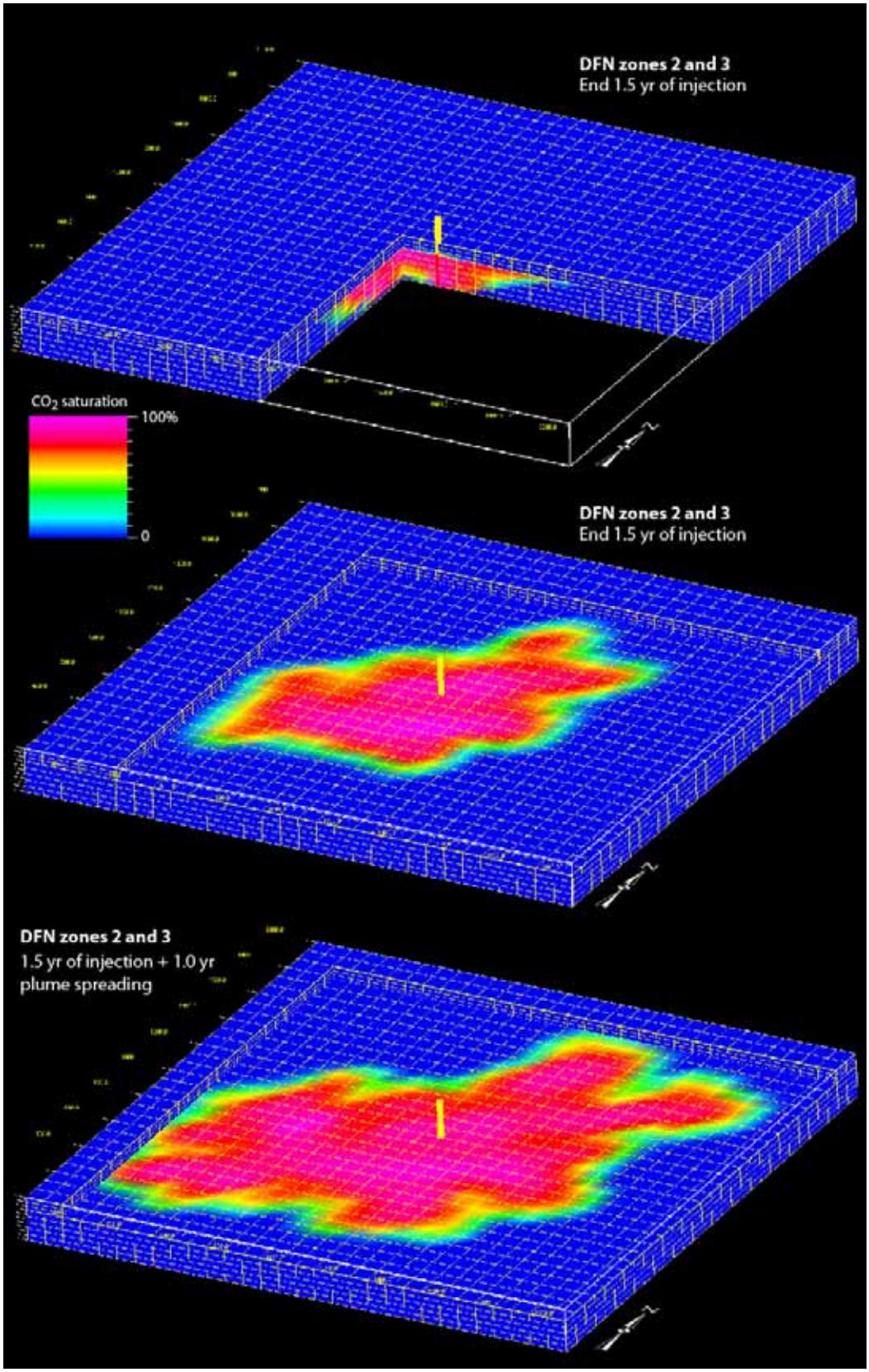

Figure 91.—Models of CO_2 saturation showing modeled plume geometry in DFN zones 2 and 3.

suggest that the technique developed during this study to calculate the permeability tensor is valid and that the algorithm used is stable.

Large-Scale Simulation Results: Lower Pottsville Sandstone

We have performed a number of large-scale simulation runs for CO_2 injection into the Boyles Sandstone, which can also be applied to other units, such as the Hartselle Sandstone. These runs use a hypothetical area of 10 miles by 12 miles for a 320-foot heterogeneous zone. This section begins by summarizing the geologic models and correlations used. Next, simulation results are given for a hypothetical case similar to those encountered at the Gorgas test site that confirm our assumptions that the Boyles Sandstone would be a poor target for sequestration at the site. The final section, however, presents simulation results that suggest that the same stratigraphic unit with reservoir properties more representative of the region could actually be suitable.

All of the simulation runs used our in-house, soon-to-be-released simulator, nSpyres, and all of the runs used a grid with 7.5 million cells. The grid was uniform, with cell size of 264 feet by 264 feet by 2 feet. All of the wells were set to inject at a constant pressure of 1.0 psi/foot times the depth to the injector top. Finally, the bounds of the grid were set to zero flow, meaning the domains were all finite.

Geologic Model Summary.—We successfully generated simulation grids based on porosity characteristics provided by the geology team. For the creation of simulation grids, we must have information that allows us to assign porosity and permeability for each grid cell. Unfortunately, there is insufficient core data with this information available on a broad scale. In almost all cases, the best that we can do are estimates of porosity values inferred from well logs. The best

we can do for permeability estimation is to make use of the available core data from the basin for the development of correlations between permeability and porosity. In this case, a representative sample of available core data is plotted as red circles in Figure 92 and the model used to describe the general trends is shown with the dashed green line. For our initial simulation runs, we wanted to get by with a single equation that could adequately predict permeability from porosity without the need to characterize the rock as either shale or sandstone. To accomplish this goal, we simultaneously manually picked control points and fit those points with the spline until we had the solid curve shown in the figure. We then fit our control points, and not the actual data points, to the model to estimate parameters. The correlation is

$$\log_{10}(K)=2.786-.3949*\exp(-17.07*(phi-.2048)) \qquad (5)$$

as shown in the figure, where K is the permeability in millidarcies, and “phi” is the fractional porosity.

The geology team provided us with log-estimated porosity as a function of depth at one half foot intervals for nine wells, located as shown by the well labels on the left side of Figure 93. The data set identified the depth to the top of the Upper Boyles Sand and corresponding surface elevations for each well. The left side of Figure 93 shows a contour plot of subsea elevation (indicating no relative highs or lows and a nearly uniform rise from south to north), and the top of Figure 94 is a depiction of porosity as a function of depth relative to the top of the formation. Although it is not necessary for the simulator, we decided to adjust the locations of some of the wells for the sole purpose of giving us a rectangular boundary area. The bounding perimeter on the left-hand side of 6ure 93 does not really represent a physical boundary, so we are choosing to

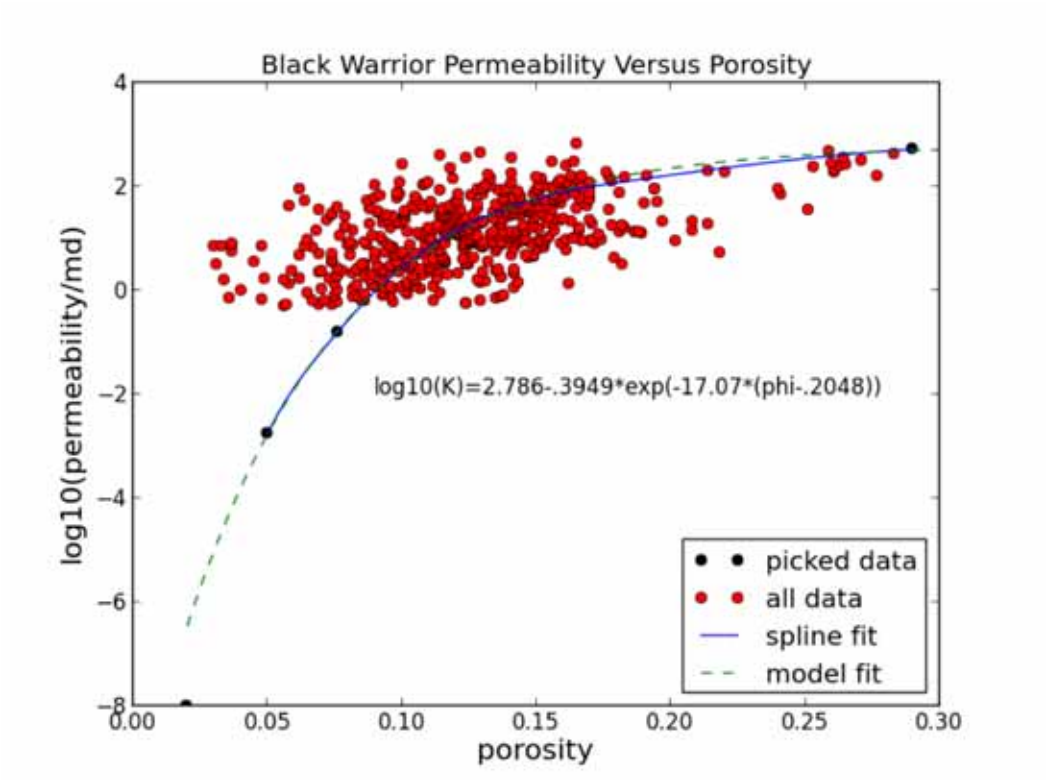

Figure 92.—Permeability versus porosity fit for the Black Warrior Basin.

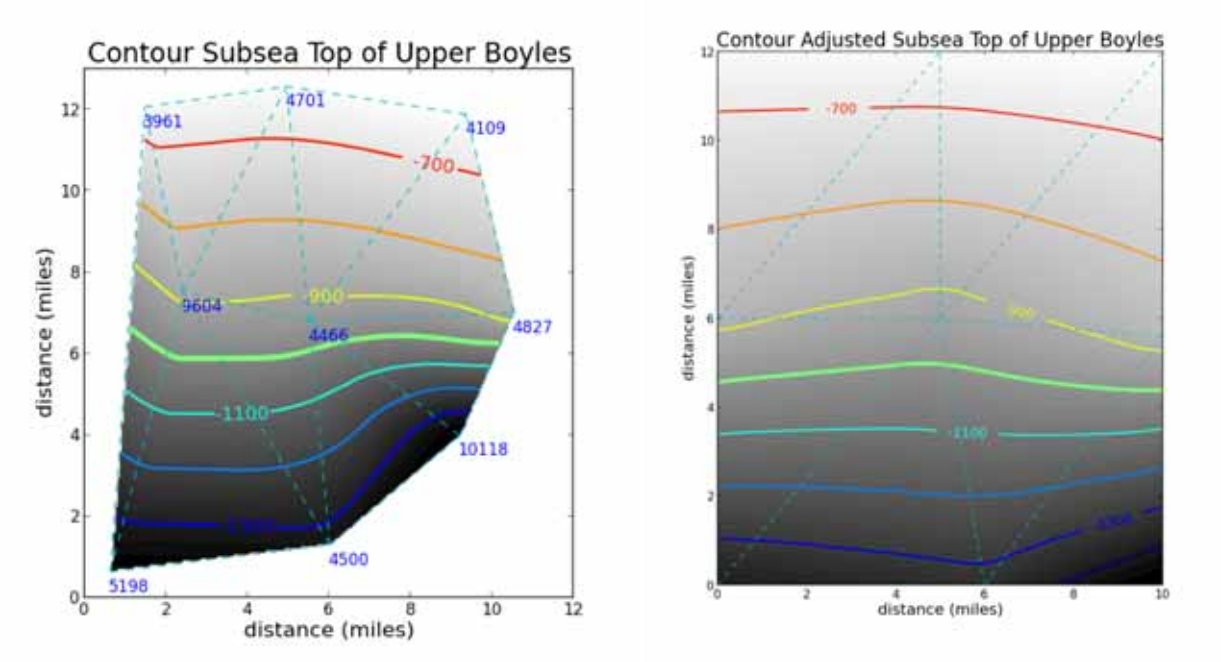

Figure 93.—Original well locations (labeled at cyan line vertices) and contours of the top of Upper Boyles (left) and adjusted well locations and tops used for the reservoir simulation grid(right) – vertical axis is oriented North-South.

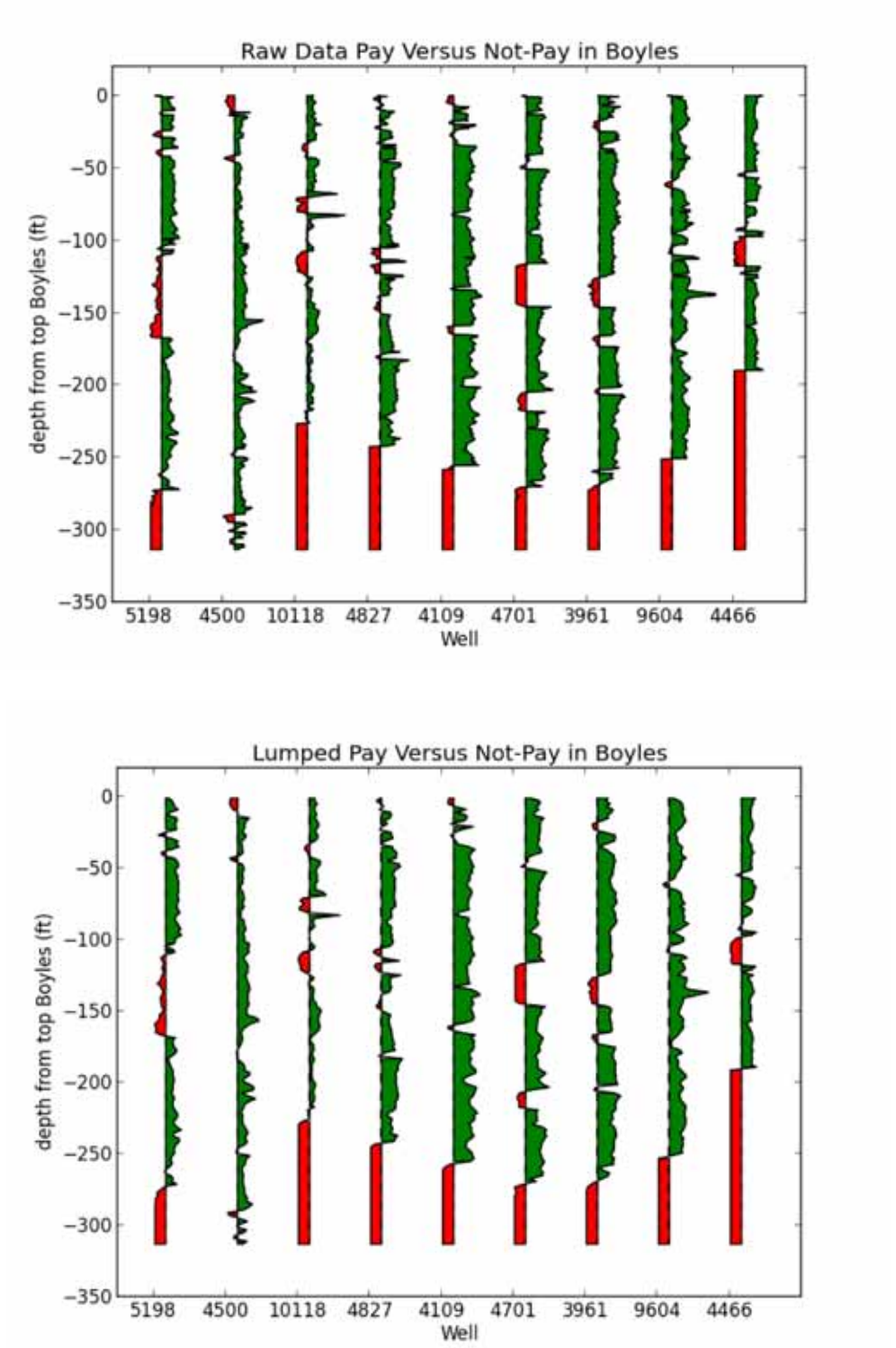

Figure 94.—Porosity of the Upper Boyles formation at the control wells, coloring based on 5% porosity cutoff. The top is the raw data based on .5 foot intervals, and bottom is based on arithmetically lumped 2-foot samples from the finer intervals

expand the region and regularize the geometry. The porosity data was provided at a slightly finer interval than we needed at this point, so we decided to lump together these data into 2 foot intervals, with the result as shown at the bottom of Figure 93. A comparison of the top and bottom of Figure 93 show very few differences due to the lumping.

The image sequences shown in the last two figures are views of the bounding isosurfaces for various qualities of sand. In Figure 95, the same bounded volume is shown from a variety of angles. Everything that is inside the box but not inside one of the isosurfaces is extremely tight rock. An examination of the figure shows a number of areas in the field where substantial continuity of impermeable regions exists. Each image of the sequence shown in Figure 96 is taken from approximately the same viewpoint. For this figure, every image shows the bounding surfaces for regions of different porosities, and from this figure is clear that high-capacity thief zones exist in the region.

The generation of the data values for the isosurfaces used the lumped data from Figure 94, the adjusted spatial locations from the right side of Figure 95, and multi-linear interpolation of the data evaluated at the cell center locations. For this particular case, a Scientific Python interpolation package (LinearNDInterpolator) was available that worked well. It took 16 seconds to calculate the results on 16 million cells which is quite fast for a sequential algorithm. Unfortunately, on tests with many more locations, the routine was very slow. For finer grids or for systems with data from many wells, a modified procedure will be necessary. For us, for now, this standard multi-linear interpolator is exactly what we need.

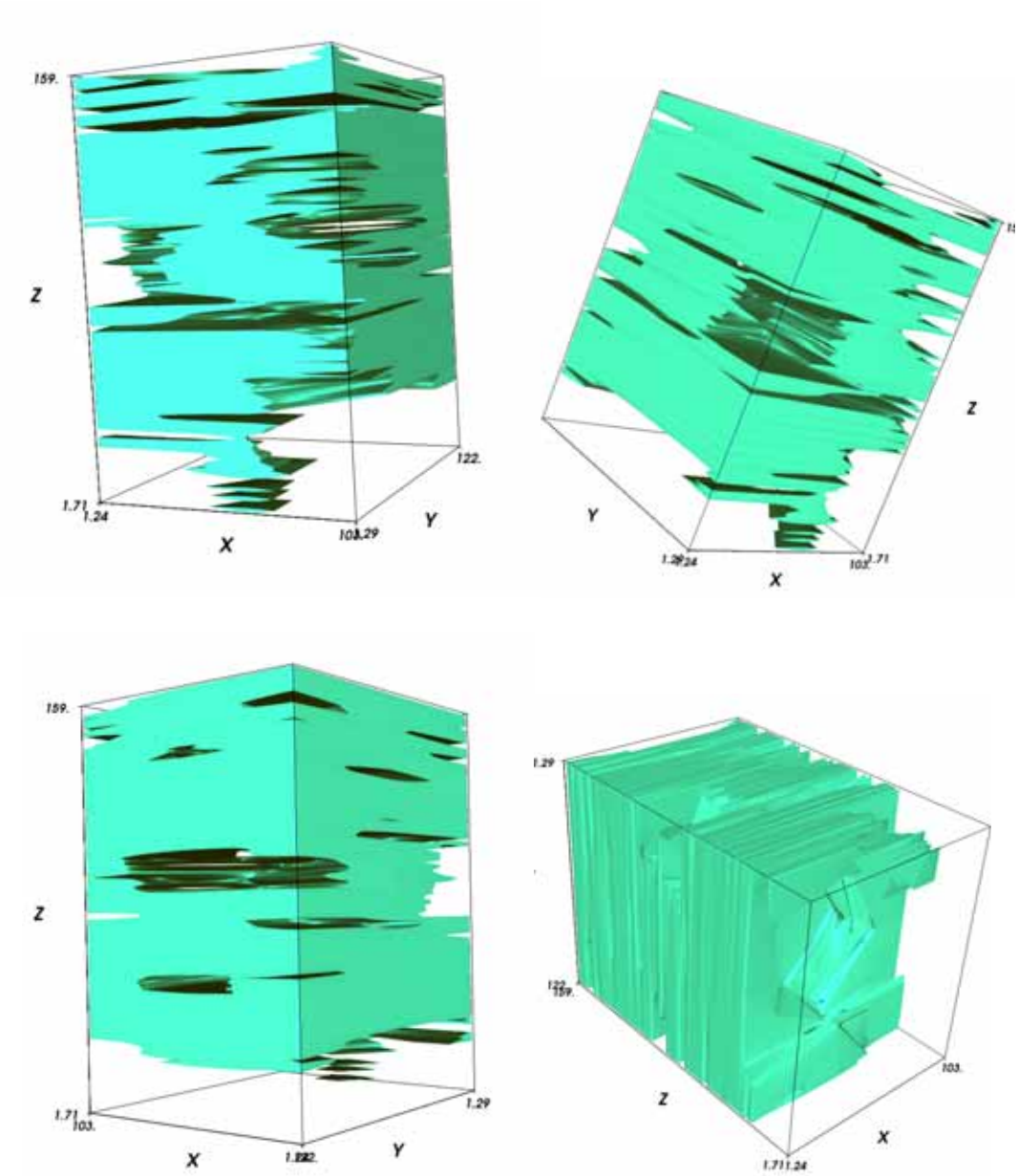

Figure 95.—Bounding regions (not to scale for stratigraphic emphasis) for porosity >.05 in an Upper Boyles sand simulation grid, as viewed from four angles – Top left from Southeast, top right from Southwest, lower left from Northwest, lower right is bottom.

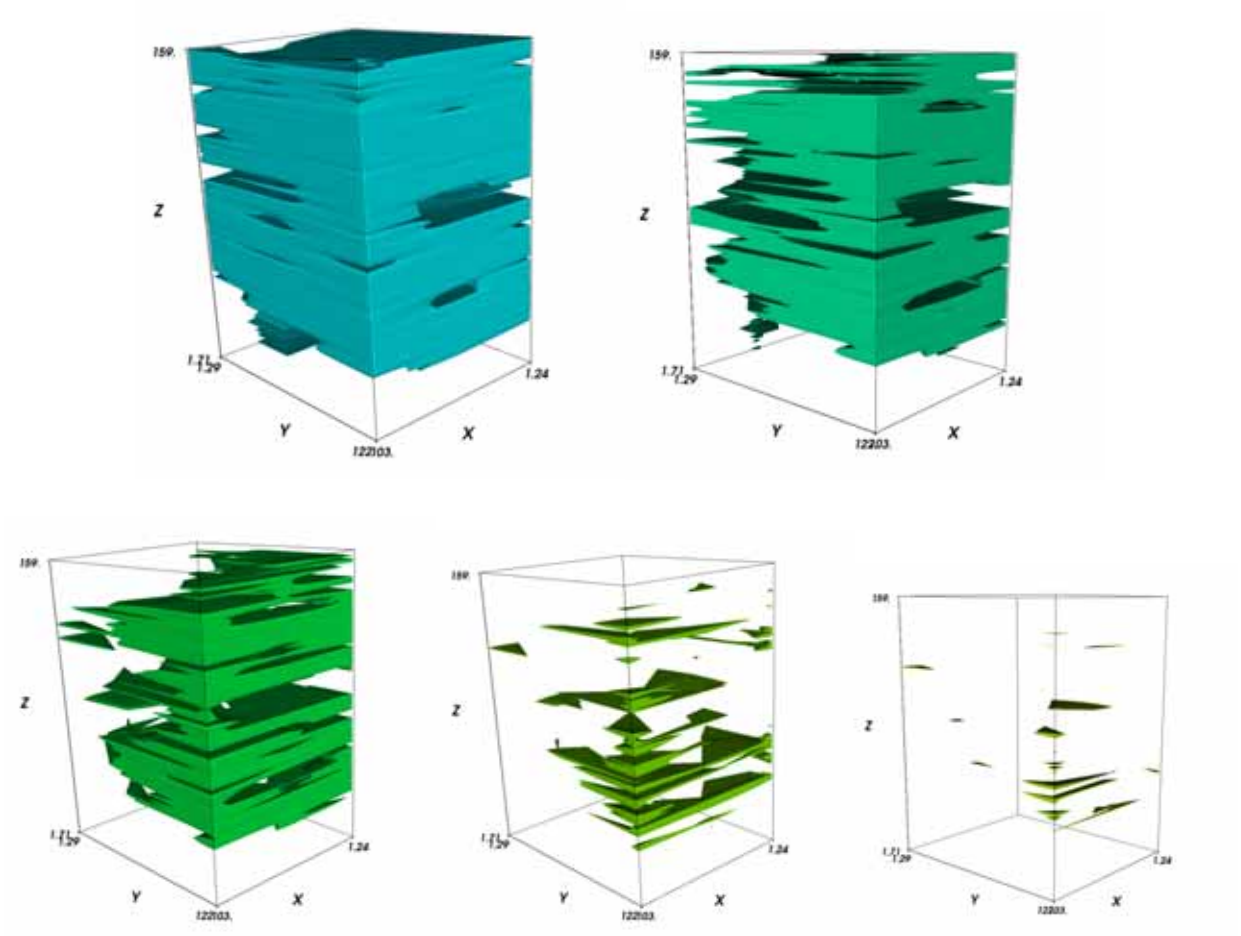

Figure 96.—Porosity bounding surfaces (not to scale for stratigraphic emphasis, all views from Southeast) for an Upper Boyles simulation grid - top left has porosity>.05, top right porosity>.08, bottom left porosity>.10, bottom middle porosity>.12, and bottom right porosity>.13.

Results of Test-Hole Condition Simulation.—Although we knew that results would be uninspiring, we ran a number of simulations for conditions as they exist at the test hole. Some sample results are presented in Figure 97 through Figure 99. In Figure 97, injection rates are shown for 6 different cases. In the first column are results for a somewhat restrictive vertical permeability of 1% of horizontal permeability ($K_v = K_h/100$), and in the second column $K_v=K_h/10$. Each row concerns use of different numbers of wells, in this case one, three, and seven wells, respectively. The images of Figure 98 present the pressure distributions after 10

years of production for the "Low K_v" cases with one, three and seven wells. Finally, the images of Figure 99 present the CO_2 saturation distributions after 10 years of production for the "Low K_v" cases with one, three and seven wells.

For this shallow formation, all the results show very poor injection performance. This is due in part to a small injection pressure, but probably even more likely due to the very low associated CO_2 density. In the best of cases, the maximum total injection rate for all wells is on the order of 100 tons per day. The figures show a substantial drop in injection rate for the best wells that may not actually occur, but the overall maximum rates should be very accurate.

In all three of the cases shown in Figure 98, the pressure isosurfaces have cylinder-like shapes around the wells, but plane-like surfaces away from the wells. The cylindrical surfaces are expected as a result of the injection, but these planar surfaces only reflect that the pressure has changed little from initial conditions. After ten years, so little CO_2 has been injected that it barely has an impact on the system pressures.

Despite the very small densities for the CO_2, the saturation isosurfaces are demonstrating only local vertical movements of the plume. Despite vertical permeability being 1% of horizontal permeability, that should be sufficient to allow for mass vertical movement. In fact, the presence of impermeable streaks severely restricts the vertical movement. Almost all of these streaks would be averaged out using more traditional simulation strategies with coarser grids.

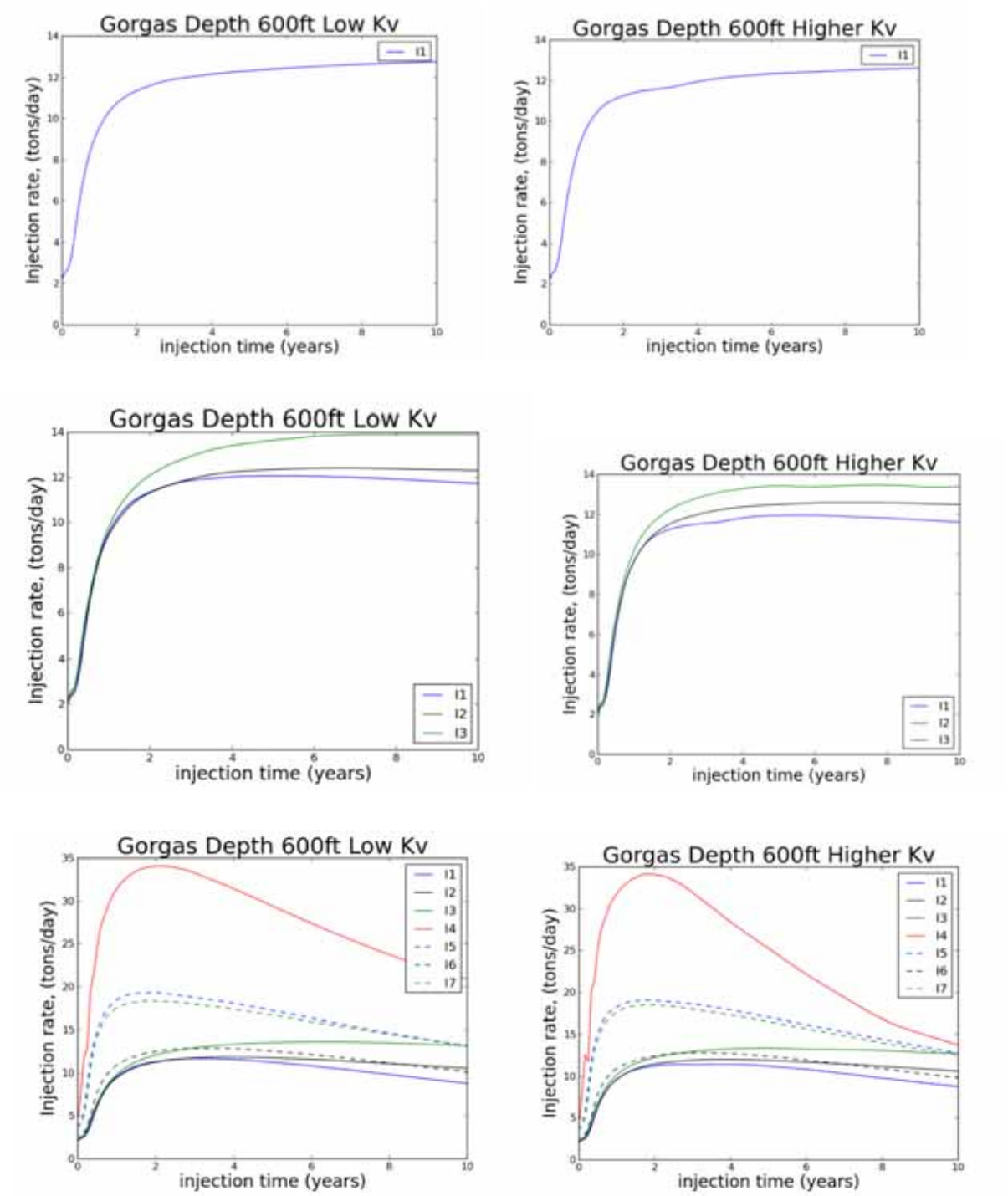

Figure 97.—Simulated CO_2 injection rates for various scenarios associated with a minimum depth of 600 feet. The left column cells are results for a low vertical permeability, and the right side is for a higher vertical permeability. Each row of the table shows different numbers of wells used (1,3, and 7 wells respectively) in a particular run.

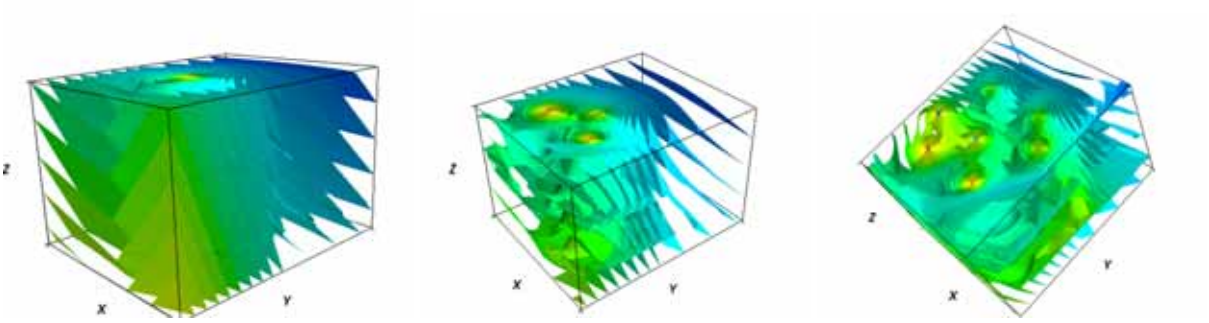

Figure 98.—Isosurfaces for simulated pressure at ten years for 1-,3-, and 7-well cases from left to right, with minimum depth of 600 feet.

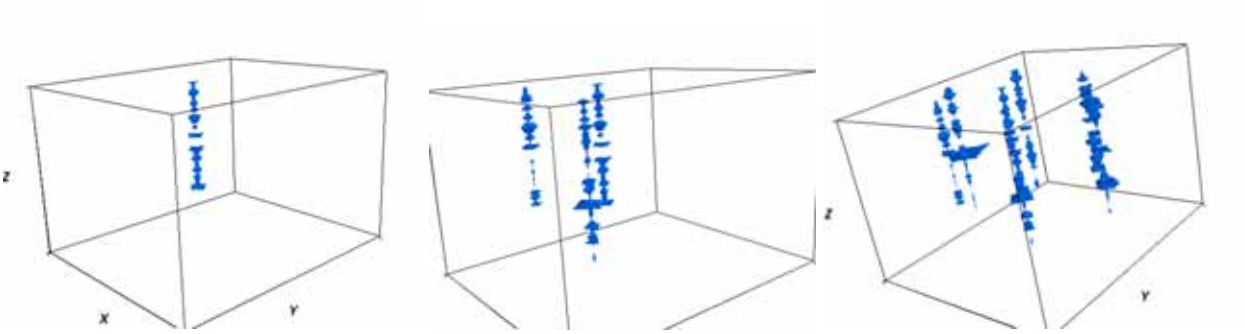

Figure 99.—Isosurfaces for simulated CO_2 saturation at ten years for 1-,3-, and 7-well cases from left to right, with minimum depth of 600 feet.

Summary of the 6,000-foot Cases.—The structure may be overly simple, but the overall property distributions depicted in Figure 95 and 96 are quite plausible for any number of areas. We ran many cases at various depths. Some sample results for a minimum depth of 6000 feet are presented in Figure 100 through Figure 102. In Figure 100, injection rates are shown for 6 different cases. In the first column are results for a somewhat restrictive vertical permeability of 1% of horizontal permeability (Kv = Kh/100), and in the second column Kv=Kh/10. As in Figure 97, each row concerns use of different numbers of wells, in this case one, three, and seven wells, respectively. The images of Figure 101 present the pressure distributions after 10 years of production for the “Low Kv” cases with one, three and seven wells. Finally, the images of Figure

102 present the CO_2 saturation distributions after 10 years of production for the “Low Kv” cases with one, three and seven wells.

For this deeper formation, we see substantially improved performance over the shallow case. This is due in part to a larger injection pressure, but probably even more likely due to the much higher CO2 (supercritical) density. In the best of cases, the maximum total injection rate for all wells is on the order of 1.3 million tons per year.

The figures show a substantial drop in injection rate for the best wells. In this case, this drop in injection is expected because the pressures have built up substantially and the wells, despite being miles apart, begin to interfere with each other after many years.

In all three of the cases shown in Figure 98, the pressure isosurfaces have cylinder-like shapes around the wells, but surfaces begin to conform to the distribution of wells. Unlike the shallow case, there is little remaining evidence of the original planar isosurface, and the interference noted by inference in the previous paragraph is becoming more obvious.

The density of supercritical CO_2 is substantially still substantially smaller than water, so the CO_2 should want to move vertically. Once again, the local impermeable streaks are sufficient to restrict this movement. In all the cases, the primary distribution of the CO_2 remains around the wells.

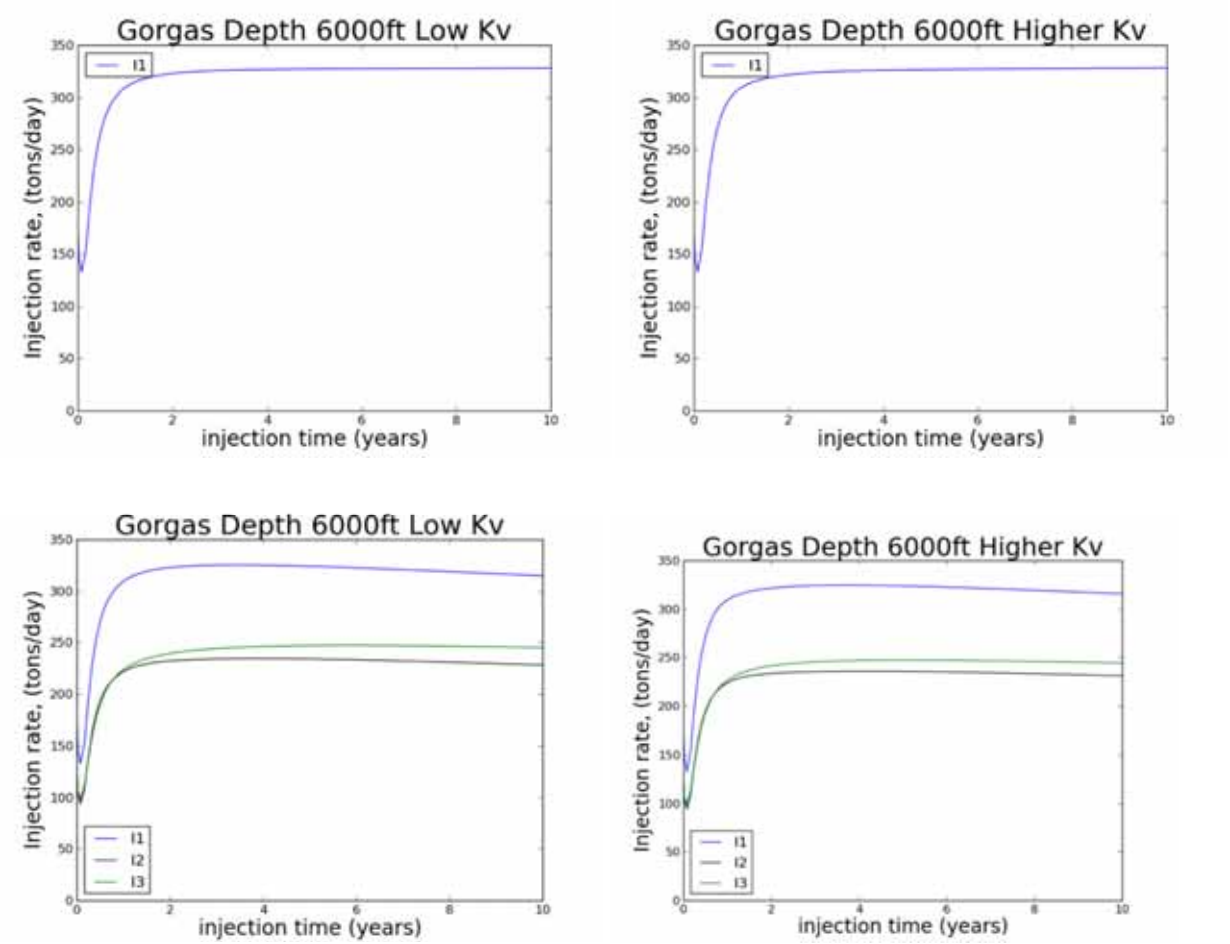

Figure 100.—Simulated CO_2 injection rates for various scenarios associated with a minimum depth of 6000 feet. The left column cells are results for a low vertical permeability, and the right side is for a higher vertical permeability. Each row of the table shows different numbers of wells used (1,3, and 7 wells respectively) in a particular run.

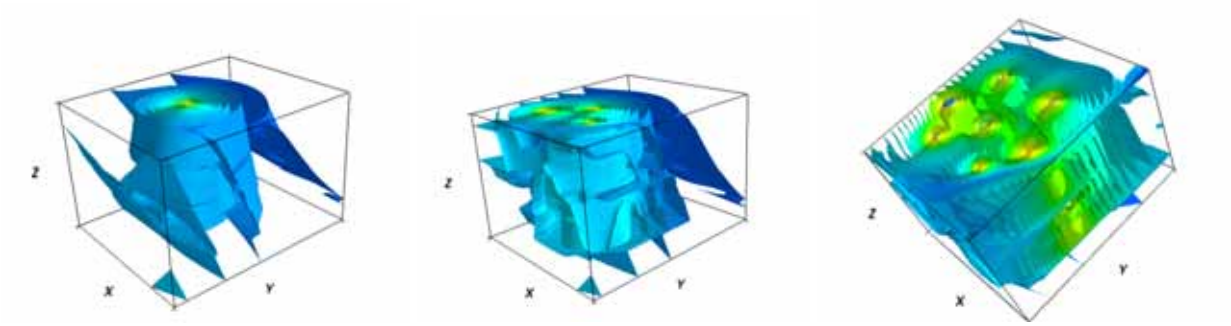

Figure 101.— Isosurfaces for simulated pressure at ten years for 1-,3-, and 7-well cases from left to right, with minimum depth of 6000 feet.

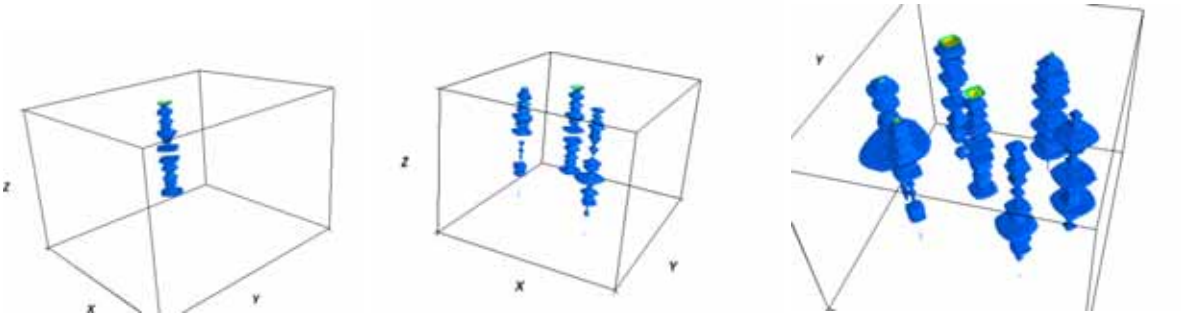

Figure 102.—Isosurfaces for simulated CO_2 saturation at ten years for 1-,3-, and 7-well cases from left to right, with minimum depth of 6000 feet.

CONTAINMENT ANALYSIS

Seal Analysis

Regional analysis indicates that gigatonne-class sequestration capacity exists in the Cambrian-Devonian carbonate section and in Mississippian-Pennsylvanian sandstone units (Table 3). For storage to be successful, confining strata must be present that ensure safe CO_2 storage over geologic time and ensure protection of the USDW. The principal confining strata in the Black Warrior Basin are carbonate and shale units. Reservoir modeling in the Knox Group indicates that the low-permeability strata between the major fractured horizons can confine CO_2 over the short term (Figure 91). The long-term confining capacity of carbonate strata in the Black

Warrior Basin is uncertain because none of these strata are significant hydrocarbon reservoirs or direct reservoir seals. Hence, it is probably best to consider the carbonate units as important baffles and barriers to cross-formational flow and not to rely on these units as major seals that provide storage security at the scale of geologic time.

Virtually all commercial conventional reservoirs in the Black Warrior Basin are in sandstone that is sealed by shale. The preponderance of natural gas in the commercial reservoirs indicates, moreover, that these seals are capable of confining gas that is otherwise mobile and buoyant. Laboratory analysis of shale provides crucial insight as to how shale units function as seals for CO_2. Shale represents a low-permeability, dual porosity system in which gas is stored in free and adsorbed states (e.g., Soeder, 1988; Kuuskraa and others, 1992; Montgomery and others, 2005; Ross and Bustin, 2008). Research in the Black Warrior Basin and the adjacent Appalachian thrust belt has focused on organic-rich shale formations that are prospective natural gas reservoirs (Pashin, 2008, 2009; Pashin and others, 2010, 2011), and new data from the Gorgas #1 borehole provide critical information on the basic properties of non-reservoir shale.

Analysis of core samples from the Gorgas #1 borehole indicates that shale composition varies significantly (Table 11). A composite analysis of sidewall core samples of Red Mountain shale contains 49 percent quartz, 14 percent feldspar, 5 percent pyrite, and incidental amounts of other non-clay constituents. Clay makes up the remaining 29 percent and is dominated by illite, chlorite, and kaolinite. Expandable clay only makes up 2 percent of the clay fraction, and illite-smectite expandability is only 25 percent. Total organic carbon (TOC) content is only 0.04 percent in the composite sample.

Pride Mountain shale contains 14 to 38 percent quartz (Table 11). Feldspar content ranges from 5 to 11 percent, and one sample contains 37 percent calcite and 10 percent dolomite. Clay content ranges from 27 to 70 percent, and is dominated by illite, with lesser amounts of kaolinite

Table 12. Summary of mineralogy of shale units inthe Gorgas #1 borehole.

Depth (ft)	Formation	Quartz	K-Feldspar	Plagioclase feldspar	Calcite	Siderite	Ankerite, Fe Dolomite	Dolomite	Pyrite	Fluorapatite	Barite	Magnetite	TOTAL NON-CLAY	Smectite	Illite/Smectite	Illite + Mica	Kaolinite	Chlorite	TOTAL CLAY	Total expandable clay (% of clay fraction)	% Illite/Smectite expandability
1221.0	Pottsville	48	3	10	1	2	0	0	0	1	1	0	**66**	0	4	14	5	12	**35**	1	35
1230.5	Pottsville	55	2	10	0	1	0	0	0	0	2	0	**69**	0	3	13	4	12	**31**	1	35
1241.5	Pottsville	44	3	9	0	2	0	1	0	0	0	1	**60**	0	4	18	7	12	**40**	1	30
1251.0	Pottsville	46	6	8	1	2	0	0	0	0	1	0	**63**	0	5	15	4	14	**37**	1	25
1261.0	Pottsville	34	4	6	4	2	0	0	0	0	2	0	**52**	0	2	27	6	14	**48**	1	35
1264.0	Pottsville	19	9	5	2	3	0	1	1	0	1	0	**41**	0	8	25	9	18	**59**	2	30
1271.0	Pottsville	63	2	7	2	1	3	0	1	1	0	0	**79**	0	1	7	3	10	**21**	0	25
1280.0	Pottsville	50	3	6	1	1	2	0	1	0	2	0	**64**	0	4	17	6	9	**36**	1	35
2842.0	Pride Mtn.	29	1	7	1	2	0	0	0	1	1	0	**42**	1	16	28	7	7	**58**	10	55
2845.0	Pride Mtn.	32	3	4	2	1	0	0	0	0	1	0	**43**	0	15	27	9	5	**57**	8	50
2852.5	Pride Mtn.	38	1	7	1	3	1	1	1	0	1	0	**52**	1	13	22	7	5	**48**	8	50
2856.5	Pride Mtn.	36	1	10	0	2	1	0	0	0	0	0	**51**	1	12	26	5	5	**49**	7	50
2863.0	Pride Mtn.	21	3	2	1	1	1	0	1	0	1	0	**30**	1	16	37	12	4	**70**	10	55
2890.5	Pride Mtn.	14	6	0	37	0	3	10	3	0	0	0	**73**	1	7	18	0	1	**27**	4	50
3290.0-3375.0	Red Mtn.	49	6	8	1	0	2	0	5	0	1	0	**71**	0	9	12	3	6	**29**	2	25

and chlorite. Expandable clay constitutes 4 to 10 percent of the clay fraction, and illite-smectite expandability is 50 to 55 percent. TOC ranges from 0.09 to 0.80 percent.

Pottsville shale samples are from the basal shale of the Fayette cycle (Table 11). The shale contains 19 to 69 percent quartz and 9 to 14 percent feldspar. Carbonate minerals make up no more than 4 percent of the shale. Total clay content is 21 to 59 percent. Illite and mica form the bulk of the clay fraction, and chlorite content is between 9 and 18 percent. Expandable clay constitutes 0 to 2 percent of total clay, and illite-smectite expandability is 25 to 35 percent. TOC is between 0.36 and 0.74 percent.

The results of mineralogical analysis indicate that all the shale units analyzed are composed principally of quartz and illitic clay and contain very little organic matter. Clay expandability is very low in the Red Mountain and Pottsville samples, indicating low fluid sensitivity. Pride Mountain shale, by comparison, is much richer in expandable clay than the other formations and thus appears to be highly fluid-sensitive, especially for a Paleozoic shale unit in a thermally mature sedimentary basin like the Black Warrior.

The shale samples exhibit a range of porosity, permeability, and fluid saturation (Table 13). Porosity ranges from 1.0 to 6.3 percent, and no obvious differences exist among the three formations. Water saturation is quite variable, ranging from 1 to 78 percent. Water saturation is significantly higher in the Pride Mountain Formation than the other formations, which reflects the difference in bulk mineralogy. In the Pottsville Formation, however, water saturation is extremely variable. Gas saturation ranges from 15 to 98 percent and is inversely correlated to water saturation ($r = -1.00$), indicating that the native fluid system is effectively binary. Some oil, however, is present in the system, and saturations range from 1 to 9 percent.

Table 13. Results of core analysis in prospective sealing shale formations, Gorgas #1 borehole.

Depth (ft)	Formation	Effective Porosity (%)	Water Saturation (%)	Gas Saturation (%)	Oil Saturation (%)	Pressure-Decay Permeability (μD)
1221.0	Pottsville	2.08	4.27	91.46	4.27	0.037
1230.5	Pottsville	2.00	3.94	91.64	4.43	0.042
1241.5	Pottsville	0.96	9.26	81.49	9.26	0.055
1251.0	Pottsville	1.87	4.74	90.52	4.74	0.062
1261.0	Pottsville	1.49	23.13	70.93	5.95	0.072
1264.0	Pottsville	2.09	63.03	32.73	4.23	0.059
1271.0	Pottsville	4.08	1.17	90.63	8.20	0.053
1280.0	Pottsville	1.70	10.23	84.66	5.11	0.056
2842.0	Pride Mtn.	2.58	62.14	34.53	3.33	0.086
2845.0	Pride Mtn.	1.51	78.43	15.78	5.79	0.080
2852.5	Pride Mtn.	2.49	45.36	51.18	3.46	0.087
2856.5	Pride Mtn.	1.51	69.85	24.27	5.88	0.075
2863.0	Pride Mtn.	6.27	76.56	22.12	1.33	0.048
2890.5	Pride Mtn.	2.03	14.59	82.98	2.43	0.060
3290.0-3375.0	Red Mtn.	1.84	1.07	97.86	1.07	0.060

Pressure-decay permeability was measured parallel to bedding. Permeability perpendicular to bedding tends to be lower than that parallel to bedding by an order of magnitude (e.g., Young and others, 1964; Kwon and others, 2004), and so for seal evaluation, the values reported here should be considered as minima. Permeability is low in all shale samples from the Gorgas #1 well, ranging narrowly from 0.037 to 0.087 μD (Table 10). No significant correlation exists between porosity and permeability (r = -0.24) in the Gorgas samples. Plotting porosity and permeability from all the available core analyses in the Black Warrior Basin yields similar results (r = 0.11) (Figure 103). It is not clear what controls permeability in the Gorgas samples, although analysis of the regional dataset indicates that no significant correlation exists between permeability and clay content (Figure 104) and that a significant correlation exists between permeability and TOC (r = 0.86) (Figure 105).

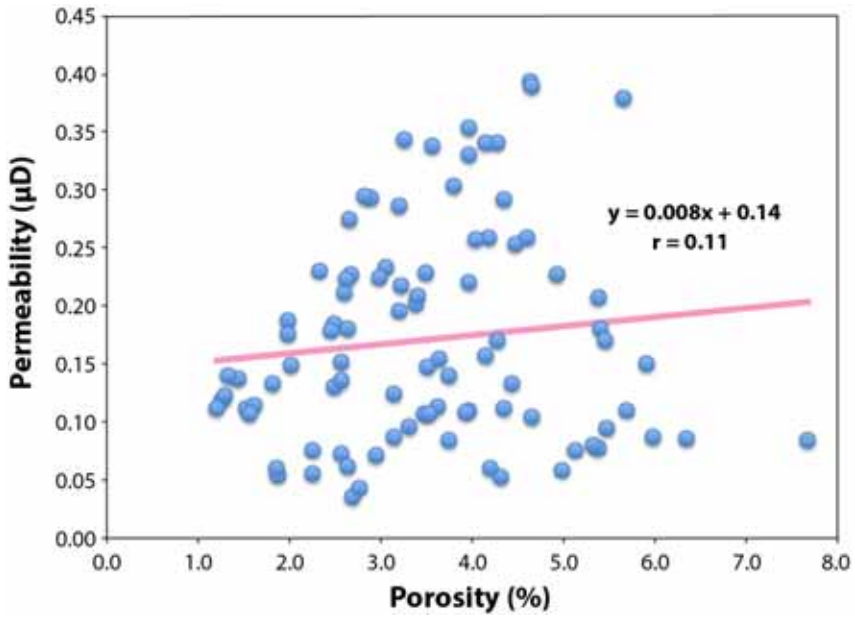

Figure 103.—Scatterplot of permeability versus porosity in shale formations of the Black Warrior Basin and Appalachian thrust belt.

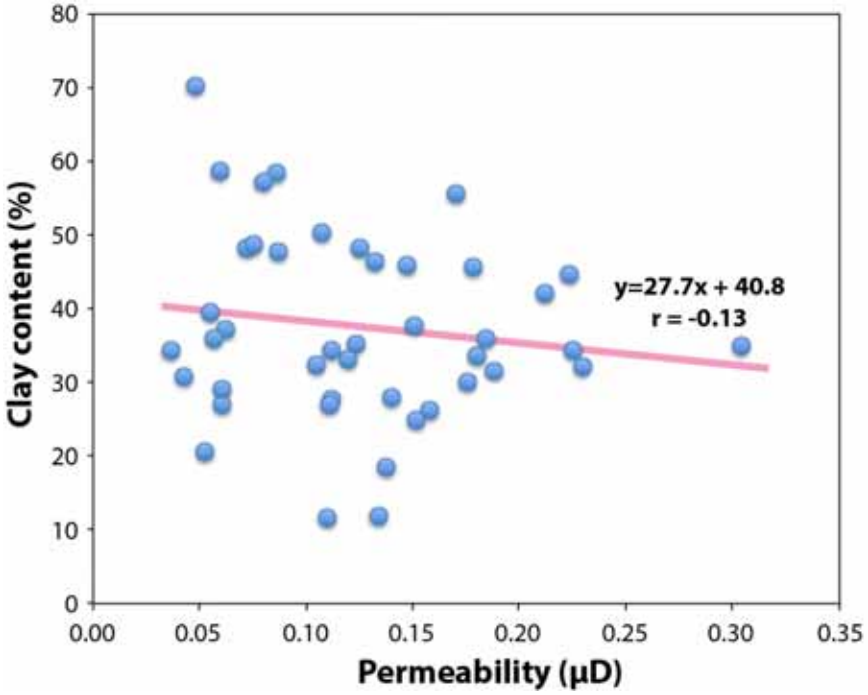

Figure 104.—Scatterplot of permeability versus total clay content in shale formations of the Black Warrior Basin and Appalachian thrust belt.

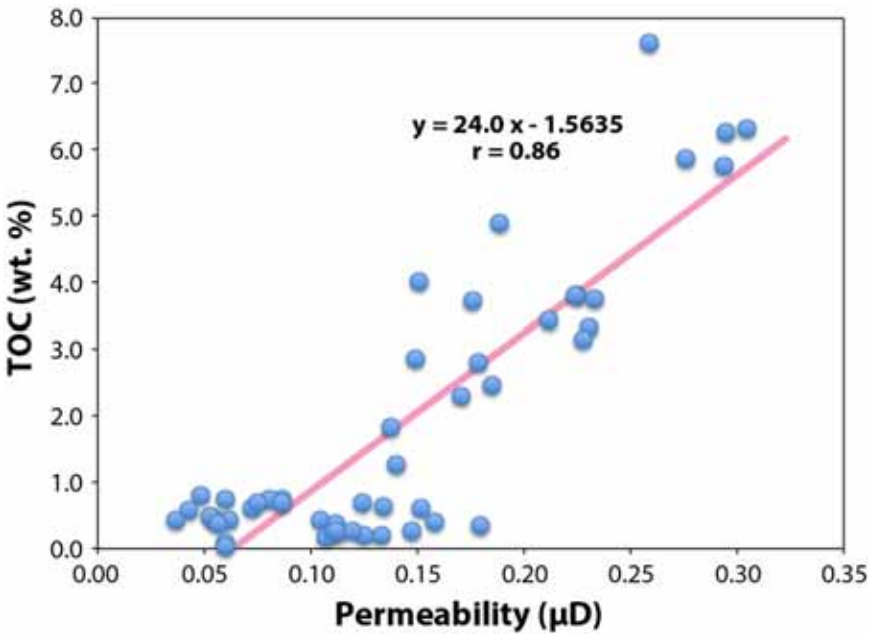

Figure 105.—Scatterplot of permeability versus TOC in shale formations of the Black Warrior Basin and Appalachian thrust belt.

Adsorption isotherms for CO_2 were derived at reservoir temperature for 14 shale samples, and the samples were evaluated in terms of Langmuir volume, Langmuir pressure, TOC, inherent moisture, and clay content (Table 14). Langmuir volume, which is the calculated sorption capacity of the shale at infinite pressure, ranges from 17.3 to 76.6 scf/t. Langmuir pressure, which is the pressure at which CO_2 capacity is 50 percent of Langmuir volume, ranges from 257 to 406 psia. Langmuir pressure is an indicator of the shape of the isotherm. Low values indicate that isotherms flatten at elevated pressure, whereas high values indicate that isotherms maintain slope at elevated pressure.

Regression analysis indicates that Langmuir pressure does not correlate with any of the analytical parameters used in this study. Langmuir volume, however, correlates with TOC, moisture, and clay content (Figure 106). The correlation with TOC is weakened by two samples with anomalously low TOC; without these samples, the regression coefficient would be 0.88.

Similarly, the correlation with moisture is weakened by a sample with anomalously high moisture content. Without this sample, the coefficient of regression would be 0.95. Correlating Langmuir volume with clay content yields a regression coefficient of 0.88. No outlier clay content data were identified, and it is unclear whether the outliers for TOC and moisture owe to analytical error or some unknown compositional factor. Pashin and others (2010, 2011) identified a strong correlation between gas adsorption and TOC in a variety of Paleozoic shale formations in Alabama, and even with low TOC, the shale from the Gorgas #1 borehole is no exception. The strong correlation of CO_2 sorption with clay content is surprising and is difficult to explain on the basis of surface area alone. Indeed, the correlation with inherent moisture indicates that hydrolysis of CO_2 is an important storage mechanism in shale. Total clay content

Table 14. Results of CO_2 isotherm analysis for shale samples from the Gorgas #1 borehole.

Depth (ft)	Formation	Temperature (°F)	Langmuir Volume (scf/t)	Langmuir Pressure (psia)	TOC (%)	Moisture (%, ar)	Total Clay (%)
1221.0	Pottsville	82.4	28.8	363	0.44	0.44	35
1230.5	Pottsville	82.4	25.8	278	0.58	0.33	31
1241.5	Pottsville	82.4	33.8	304	0.45	0.39	40
1251.0	Pottsville	82.4	27.5	291	0.43	0.33	37
1261.0	Pottsville	82.4	35.1	242	0.61	0.48	48
1264.0	Pottsville	82.4	76.6	348	0.74	0.85	59
1271.0	Pottsville	82.4	17.3	314	0.49	0.18	21
2842.0	Pride Mtn.	98.6	56.5	359	0.75	1.93	58
2845.0	Pride Mtn.	98.6	62.4	406	0.76	1.63	57
2852.5	Pride Mtn.	98.6	54.2	265	0.70	2.02	48
2856.5	Pride Mtn.	98.6	50.4	257	0.70	1.51	49
2863.0	Pride Mtn.	98.6	72.9	351	0.80	2.54	70
2890.5	Pride Mtn.	98.6	43.7	395	0.09	0.74	27
3290.0-3375.0	Red Mtn.	103.5	28.8	281	0.04	0.16	29

correlates strongly with inherent moisture (r = 0.81) and clay-bound water (r = 0.89) in the samples, indicating that clay-bound water provides most sites for hydrolysis of CO_2.

Laboratory analysis indicates that the shale formations in the Black Warrior Basin have strong sealing capacity, especially considering that permeability perpendicular to bedding is probably an order of magnitude lower than the tens of nanodarcies reported here. Permeability data indicate that shale formations with low TOC make better seals than the organic-rich shale that is prospective as hydrocarbon source and reservoir strata (Figure 105). In addition to pure sealing capacity, adsorption and hydrolysis of CO_2 in shale provides storage capacity that acts as a buffer, particularly in reservoirs that lie above capillary entry pressure.

Hence, the principal geologic containment risks in the Black Warrior Basin are posed by natural fractures and faults. Analysis of fracture networks in the Pottsville Formation indicates that joints are dominantly strata-bound, which limits fracture connectivity from bed to bed and leads to hydraulic compartmentalization (Pashin and others, 2004, 2008). The abundant normal faults in the basin cut across bedding; some fault networks are detached in basement, whereas others are detached in the lower Pottsville Formation (Pashin and Groshong, 1998; Groshong et al., 2010). Subsurface mapping indicates that four-way structural closures are rare in the Black Warrior Basin. Rather, three-way closures are common in the hanging-wall blocks of the major normal faults (Figure 5). Widespread porosity zones typically do not trap commercial quantities of hydrocarbons in these structures. Indeed, a stratigraphic trapping component typically provides the fourth direction of closure, which favors trapping in lensoid Mississippian sandstone units (e.g., Pashin, 1993; Pashin and Rindsberg, 1993). Accordingly, true fault seals appear to be few in the basin, except for some cases where sandstone-shale juxtapositions facilitate localized traps. Because of this, CO_2 storage operations should avoid faults, and a

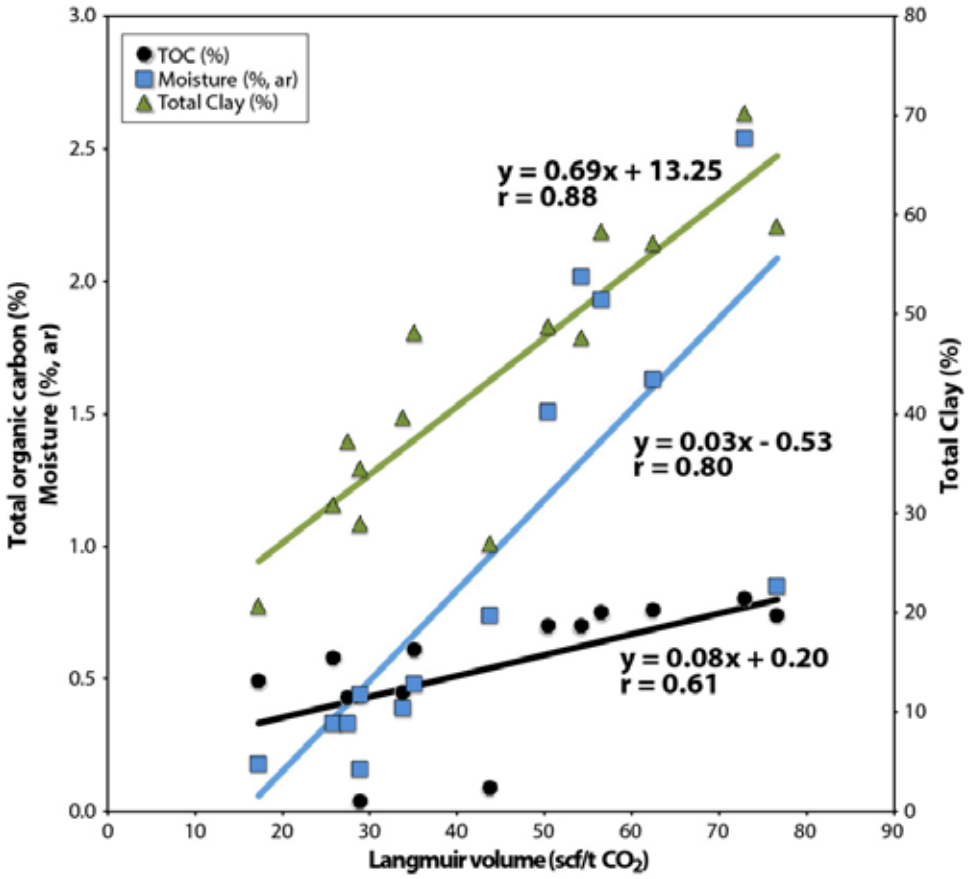

Figure 106.—Relationship of CO_2 adsorption to TOC, inherent moisture, and clay content in shale samples from the Gorgas #1 borehole.

careful assessment of sealing risk needs to be performed when siting projects in the area of conventional oil and gas production in Lamar, Fayette, and Pickens Counties.

Mineralization

Underground injection of acid gas has been performed for years for enhanced oil applications. This study presents a discussion on the expected changes to the near well bore mineralogy in carbonate formations, which commonly comprise at least part of the locations targeted for CO_2 injection. This research will simulate mineral and acidic brine interactions similar to those at a pilot scale injection into a carbonaceous saline aquifer located near the site

of a coal fired power facility in the Black Warrior Basin of Alabama. The objective of this study is to investigate the impact of surface treatments on dissolution kinetics during the brine/mineral interaction that follows injection of CO_2 into a geologic formation.

Calcium carbonate, ground and sieved to ~250μm, was used to study the impact of acidified (pH~3) brine on carbonate formation material similar to near well bore conditions. Because of the high solubility of calcium carbonate at pH~3, a protective surface coating was desired to preserve mineral integrity. As suggested in the literature, some acids can form “armoring” on carbonates exposed to low pH solutions.

The results of batch experiments conducted herein show that a meso tartaric acid solution at pH 3 will form coating over the calcite in-situ, dramatically reducing the overall dissolution of the carbonate mineral. SEM images and aqueous analysis show the fastest layer formation at the highest tested concentration of 0.15 M meso tartaric acid, with similar but less inhibition observed at 0.08M and 0.015M treatment levels. Additionally, fluoride at pH 3 showed a similar response in early reaction times, but a column experiment showed particular promise due to the distinct surface morphology of the formed coating. For each system, the $SI_{Calcite}$ <<0 confirms the system was in equilibrium with the precipitated calcium/acid anion coating rather than calcite.

Background.—Reactive transport simulation of the injection process suggests that there will be a total loss of carbonate mineral near the wellbore, followed by a re-precipitation of the dissolved ions with distance from the injection well as the formation conditions return to rock dominated (Knauss, 2005; Langmuir 1997; see Figure 107). A technique to stabilize the near well bore carbonate minerals would benefit the CO_2 capture and containment process by assuring

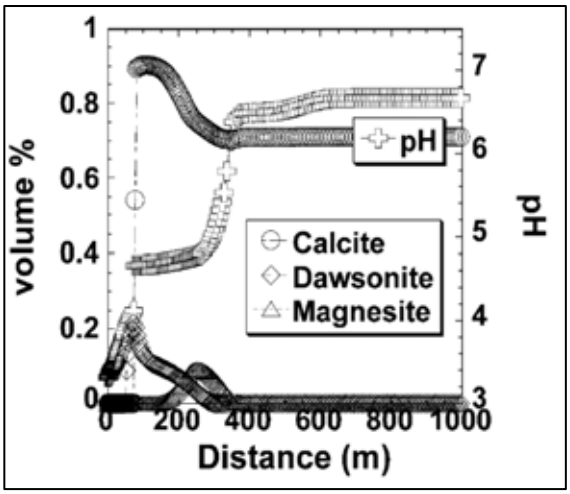

Figure 107.—CRUNCH reactive transport simulator predicted mineralogical changes following 5 years of CO_2 injection into a saline formation (Knauss, 2005).

structural integrity of the rock, as well as reduce the risk associated with mineral re-precipitation, which may reduce formation porosity.

Because earlier experiments conducted during this study found polymers and other surface-active agents to be ineffective carbonate dissolution inhibitors at low pH, an inorganic, acid insensitive, surface coating was explored. Several references in the literature describe natural surface coatings formed on carbonate minerals following exposure to an acid. First, in the field of monument preservation, oxalic acid was determined to form a natural protective coating on calcite. This phenomenon was observed on stone substrate of several ancient monuments in the Mediterranean region, including the Parthenon (Liebig, 1853). Calcium oxalate was the only substance consistently identified on preserved carbonate stone structures (Wilkins et al., 2001b). It come to be known as Mediterranean patinas (Garcia-Valles, 1998). Composition of these films was determined based on the presence of calcium oxalate ($CaC_2O_4 \cdot nH_2O$), gypsum ($CaSO_4 \cdot 2H_2O$), calcite ($CaCO_3$), and silicates in various amounts, with some additional minerals present as well in smaller fractions (Rampazzi et al., 2004). Calcium oxalate films are very

stable, less soluble, and hardly affected by atmospheric pollution encountered in an urban environment.

Also, in the field of acid mine drainage treatment, carbonate minerals (limestone) in contact with sulfuric acid have also been observed to create a natural passivation layer (Huminicki and Rimstidt, 2008). Acid mine drainage management requires clean-up and maintenance in order to attain the effluent limits recommended by the EPA; this can cost on the order of $1 million per day (Perry, 1992). Naturally existing limestone formations or crushed packed beds may provide a cheaper solution to remediation. However, precipitated coatings on the limestone have been observed to hinder acid neutralization. Recommended remedy for this problem is dilution of the influent acid stream (Huminicki and Rimstidt, 2008).

Laboratory studies on this subject were conducted by Wilkins et al. (2001b). These authors pretreated calcite crystals with various acids, including oxalic acid, in an effort to form the protective coating observed in nature. The solids were pretreated for 1, 5 or 24 hours; then a pH 2 HCl solution was run over the crystals and dissolution was observed; significant reductions in calcite dissolution were observed. Booth et al. also confirmed that exposing a calcite crystal, cast into a resin block, to a 0.1M sulfuric solution created a fully passivated surface (Booth et al., 1997; Wilkins et al., 2001a). Detection of the coating by these authors was primarily by atomic force microscopy (AFM). These authors determined that in these scenarios, only some acids precipitate a stable, epitaxial mineral coating; epitaxial growth is characterized by the crystal lattice of the substrate and coating matching to form an adherent layer (Booth et al., 1997; Hammarstrom et al., 2003).

The objective of this research was to use the concept of naturally forming mineral coatings in the presence of certain acids, to generate a protective coating for near well bore mineral

stabilization. Treatment screening was presented in previous reports, but experiments run with the final acid choices and conclusions are presented here.

Materials and Methods.—Because carbonate reservoirs typically contain calcite, Iceland spar was chosen as the mineral for experimentation purposes. Iceland spar is commonly used in experimentation throughout the literature because of its high purity (>99.9%) (Plummer and Wigley, 1976; Plummer et al., 1978; Pokrovsky et al., 2005). See Figure 108. The rhombohedral cleavage is consistent at any size scale; this is a characteristic of a mineral.

The Iceland spar was ground using a mortar and pestle; stacked sieves were used to obtain the desired size fraction (212-250μm). Then, the mineral was washed with a dilute acetic acid wash solution to remove fines remaining on the surface after grinding, as well as create an even surface for reaction after the grinding process; surface preparation can significantly impact dissolution rates (Macinnis and Brantley, 1992). Washing was performed expecting about 5% weight loss of the solid. The ground and washed sample was oven dried for 24 hours at 70ºC. Surface area of the particles was determine by BET surface analysis as well as geometric calculation (See Table 15) based on SEM imaging similar to that in Figure 108. The BET surface area determination technique is ideal for high specific surface area solids, these large ground particles have small specific surface area and the geometrically calculated surface area should be used for further calculations.

a. b.

Figure 108. A photo of the Iceland spar used throughout experimentation. (a) Bulk (b) SEM images of ground calcite used in column at 1720x magnification.

Table 15. Surface area of Iceland spar calcite used in experiments.

SSA determination method	***Calculated SSA(cm^2/g)***
BET	130
Geometric Calculation	105

All experiments were conducted with brines prepared using lab-purified water, composed of Rice University groundwater deionized by ion-exchange, then purified by either a Millipore Mili-Q water system (18.2 MΩ-cm) or by reverse osmosis followed by a 4-stage Barnstead filter. Solutions were prepared with ACS-grade chemicals from Fisher or Sigma Aldrich. Solution preparation using this technique required a set of volumetric flasks.

Glassware was washed with soap containing no phosphates, to avoid interference with inhibitor experiments. After washing with soap and water, it was rinsed at least two times with tap water, then once with DI water. Teflon covered stir bars were used to stir and homogenize the solutions.

A Perkin Elmer 4300 Inductively Coupled Plasma – Optical Emission Spectrometer (ICP-OES) was used for analysis of elements in the parts per million range (mg/l). The calibration

solutions were acidified to 1% by volume with trace metal grade HNO_3. An internal standard of yttrium was prepared by volume dilution of a 1,000 mg/l Y standard solution (Perkin Elmer) into Mili-Q water with 1% by volume trace-metal-grade HNO_3. Standard solutions were remade whenever the correlation coefficient, R^2, dropped below 0.9999.

SEM images were taken throughout these experiments using a PhonomWorld desktop SEM. This touch screen monitor instrument allows non-gold coated samples to be examined, quickly reducing the time needed to image. The sample stage is adjusted to an approximate working distance, and the instrument can auto-focus and auto-contrast further.

Visual Minteq (Gustafsson, 2009) and ScaleSoft Pitzer (Tomson and Kan, 2011) were used to determine predict solution characteristics such as speciation and saturation. Visual Minteq is a free software downloadable from the internet that performs many equilibrium calculations such as solubility, speciation, sorption, titrations, and many other things. The software was built on the USEPAs MINTEQA2. It uses the tableau method to simultaneously solve equations and generate useful information for both experimentalists and industry. The specific ion interaction theory (SIT) (Guggenheim and Turgeon, 1955) method was chosen for activity coefficient calculations involving higher ionic strengths, given the known discrepancies resulting from Davies and Debye Huckle methods. Scalesoft Pitzer is a similar solution calculator produced for the Brine Chemistry Consortium at Rice University, mainly used by consortium members and related research conducted at Rice University. This software performs equilibrium calculations such as solubility and inhibitor calculations. Pitzer theory was used in the development of this software, which has been found to be the most accurate method for solutions up to 6M salinity (Elizalde and Aparicio, 1995).

Tartaric Acid at pH 3.—Experiments studying the inhibitory effects of tartaric acid were conducted with meso-tartaric acid at three concentrations (0.015 M, 0.08 M, and 0.15 M). Barwise studied the calcite inhibitory effectiveness of d-,l- tartarate dianions compared to meso tartaric dianions (Barwise, 1990). These authors found that mesotartrate dianions acid showed better dissolution inhibition, and may be related to the internally reflective molecular structure on the ability of the molecule to adsorb to the dislocation sites. Meso tartaric acid has an eclipsed structure of both the hydroxyl groups and the carboxyl groups, which the d-, or l- does not display. See Figure 109.

The four experiments exploring effects of this treatment were conducted in a system similar to that seen in Figure 110. See

Table 16 for experiments conducted. During each experiment, a 500mL plastic bottle was filled with 1 M NaCl, various weights of solid meso tartaric acid were added and the solution was stirred, the solution was adjusted to pH 3 with solid NaOH. As shown in Figure, the pH near wellbore is projected to be approximately 3. A Teflon coated stirbar was used to mix the solid and solution rapidly. 10 grams of the ground calcite was added at the start of the reaction.

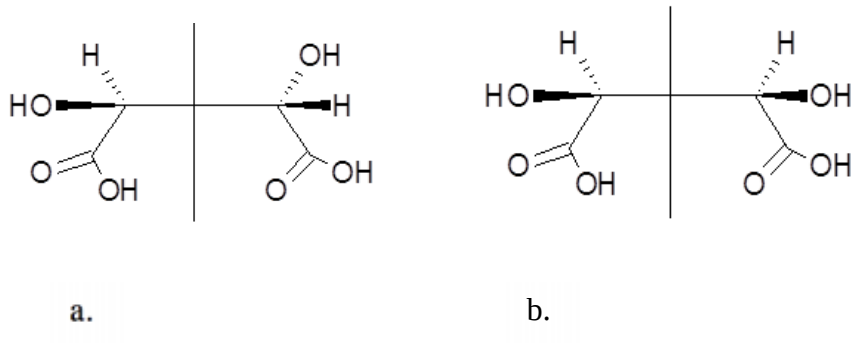

Figure 109.—Most stable conformations of a.) DL-tartaric acid b.) meso- tartaric acid (structures discussed in Ascenso and Gil, 1980).

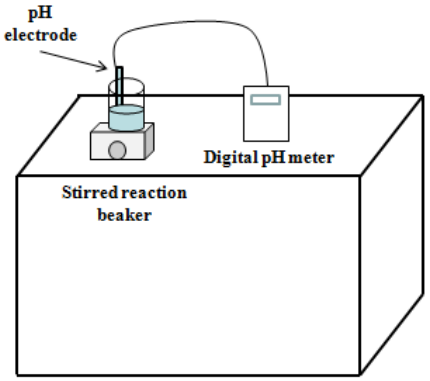

Figure 110.—Stirred batch reactor for acid induced surface treatment screening, acid provided by various concentrations of tartaric acid in brine.

Table 16. Meso tartaric acid experiments conducted.

Meso tartaric acid treatment	***Stirred batch***	***Stirred batch continued with 1 atm CO_2 bubbled***
0.015 M	Experiment 1	-
0.08 M	Experiment 2	-
0.15M	Experiment 3	Experiment 4

The initial pH was recorded and the reaction progress was monitored by tracking pH and taking aqueous samples to measure calcium and tartaric acid content. Development of the surface coating was observed by SEM of samples, which were taken throughout the experiment. A small amount of solid was retrieved from the experimental vessel by a plastic pipette. The solid was dropped onto a glass dish and dried in the oven before mounting on an SEM stub for observation.

Tartaric acid content was measured using a TOC analyzer. Samples were diluted into the ideal range for the instrument using deionized water.

Fluoride at pH 3.—Three different apparatuses were used during these experiments. The acid induced pre-coating of the calcite surface reactions were conducted in a stirred batch reactor. See Figure 110. Various amounts of fluoride were added as reagent grade NaF_{solid}, followed by various amounts of concentrated HCl used to adjust the pH of the reaction solution to the appropriate pH 4. The initial pH was recorded and the reaction progress was monitored by tracking pH and taking aqueous samples to measure calcium and fluoride. Development of the surface coating was observed by SEM images as well.

Feasibility of acid induced calcium fluorite coating of calcite was also tested in a flow through column apparatus. Fresh ground calcite was packed into column in the apparatus in Figure 111. The solid was packed into a column and flowed over with 1 M NaCl containing 0.3 M fluoride. The effluent pH, Ca, and F were monitored to determine the effectiveness of the surface coating. SEM images were taken of the calcite following the column tests.

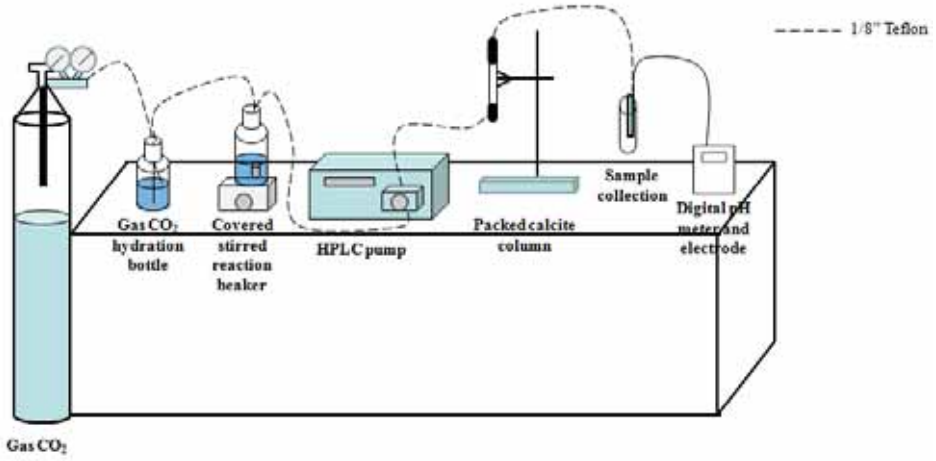

Figure 111.—Packed column apparatus used to test the feasibility of surface coating formation in a different hydrodynamic environment.

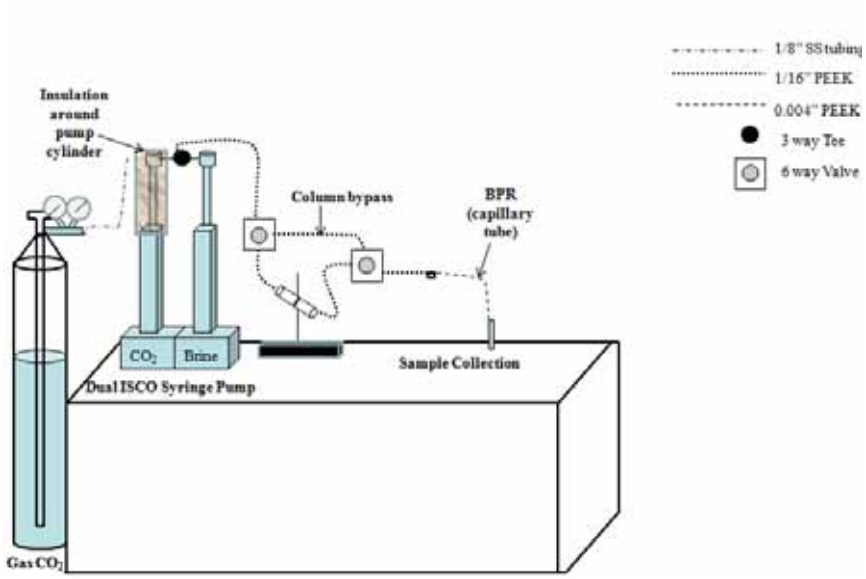

Figure 112.—High-pressure column apparatus flowing liquid CO_2 and brine used to test the pre-treated solid under high CO_2 content field conditions.

Table 17. Acidified fluoride experiments conducted.

Acidified fluoride treatment	***Stirred batch***	***Low pressure column***	***High pressure column***
0.015 M	Experiment 1	-	-
0.3M	Experiment 2	Experiment 3	Experiment 4*

* solid had already been coated with calcium fluorite in an experiment similar to Experiment 3.

Lastly, a previously developed (See previous reports) high-pressure column apparatus was used to test the successful results in the batch and low-pressure column system. Solid pre-treated in an experiment similar to the low pressure column test was performed to prepare the solid, which was then packed into a high-pressure column for testing with brine saturated at 1500 psi of CO_2 rather than 14.7psi.

Aqueous fluoride was determined using a Cole Parmer ion specific electrode. Samples were taken and combined with an equal volume of total ion strength adjustment buffer I (TISAB I). This buffer is used to moderate the ionic strength contributed by the experimental solution, as well as de-complex fluoride with any calcium or magnesium ions in the solution. A standard curve was prepared over the broad range of fluoride concentrations and experimental concentrations were determined.

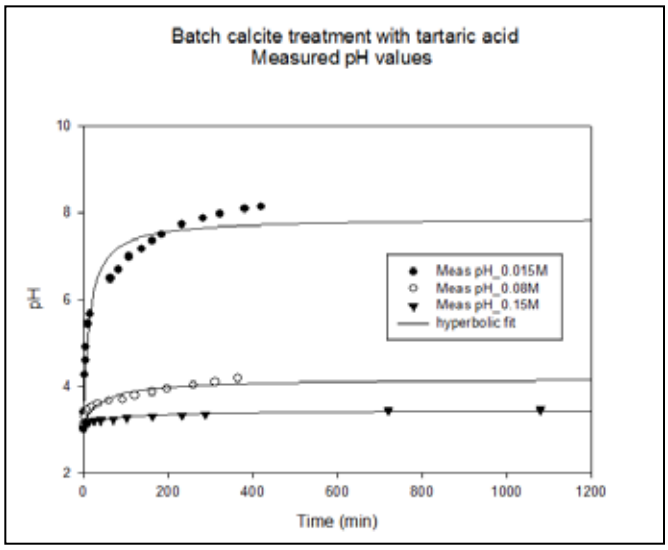

Figure 113.—Summary of the recorded pH values during the progression of the tartaric acid treatment.

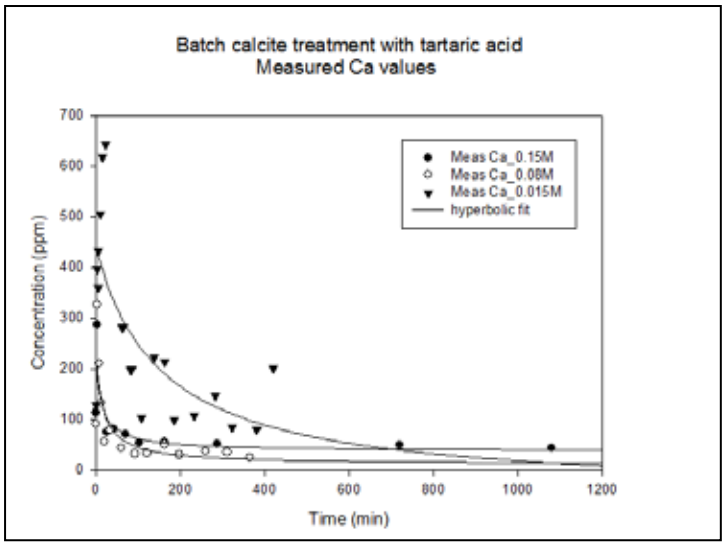

Figure 114.—Summary of the measured calcium values during the progression of the tartaric acid treatment.

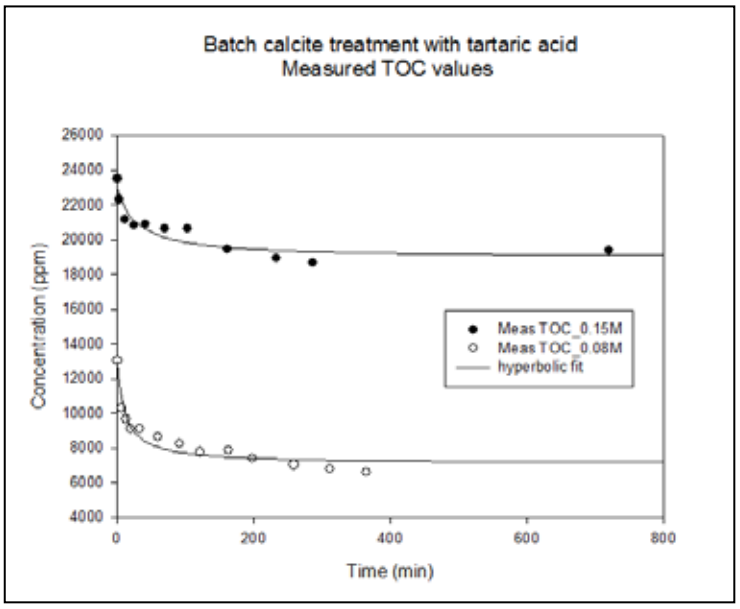

Figure 115.—Summary of the measured calcium values during the progression of the tartaric acid treatment.

Mineralization Results and Discussion

Tartaric Acid at pH 3.—Changes in surface morphology and composition of the solution served as indicators of the treatment effect. The changes in pH with time can be seen in Figure

113, aqueous calcium concentrations in Figure 114, and tartaric acid concentrations for the two higher treatment levels in Figure 115.

The pH of the reactor was observed to change very little with the higher acid concentrations, indicating little calcite dissolution. A small amount of calcium is observed to be release by the calcite at the start of the reaction, probably before full surface coverage is obtained. Also, the relatively constant tartaric acid concentrations suggest the system becomes stable quickly. These observations were supported by SEM images taken of the solid throughout the experimental progress; seen in

Figure 116 through Figure 118. As one may expect, the solid showed rapid

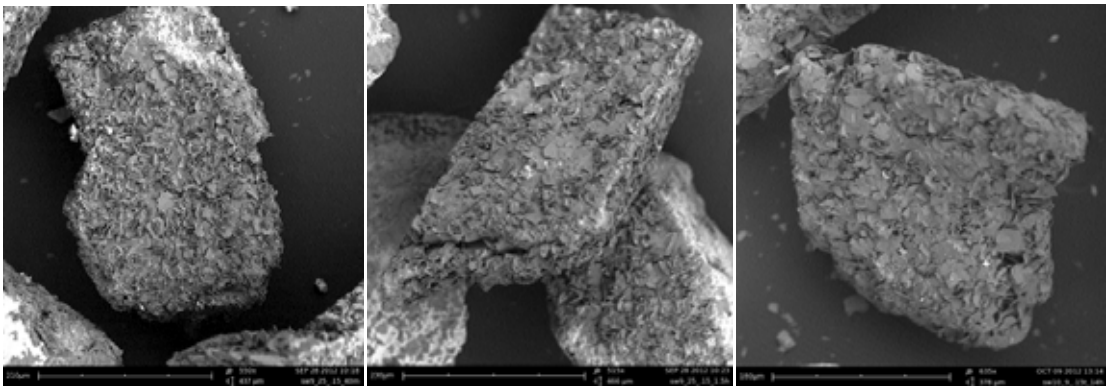

a. b. c.

Figure 116.—Surface coating development in the 0.15 M tartaric acid treatment run at pH 3 (a) 40 minutes (b) 1 hour 30 minutes (c) 15 hours.

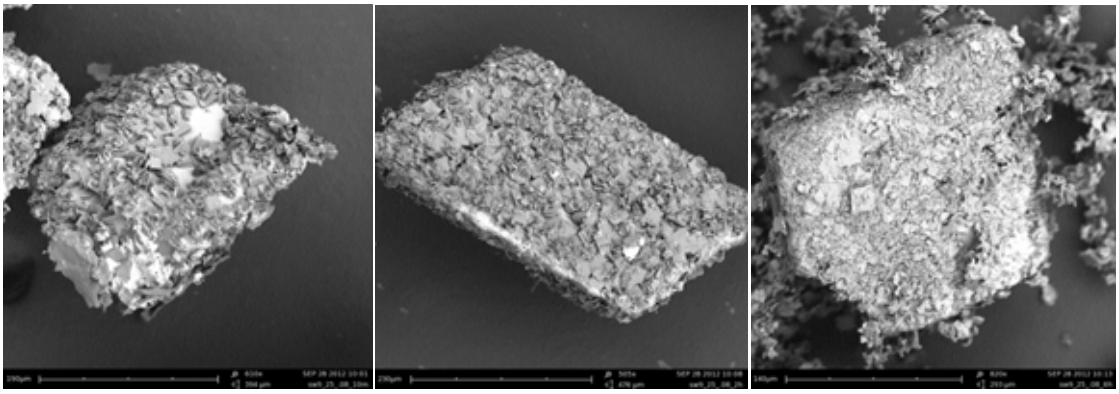

a. b. c.

Figure 117.—Surface coating development in the 0.08 M tartaric acid treatment run at pH 3 (a) 10 minutes (b) 2 hours (c) 6 hours

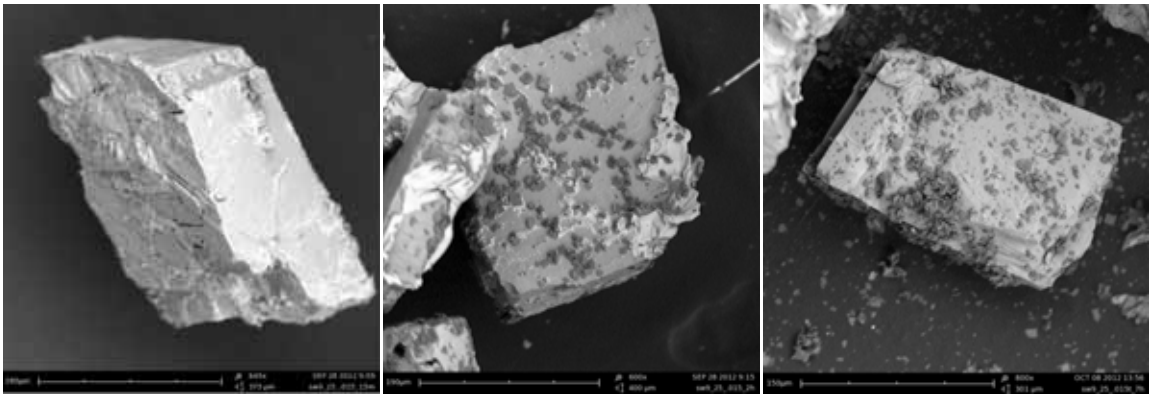

a. b. c.

Figure 118.—Surface coating development in the 0.015 M tartaric acid treatment run at pH 3 (a) 15 minutes (b) 2 hours (c) 7 hours.

surface coating in the two higher treatments, while the lowest treatment level showed little formation of a surface coating and likely explains the rapid climb to equilibrium pH.

The solid and solution from the 0.15 M meso tartaric acid treatment (i.e. the highest concentration treatment) in the previous experiments was used for a longer test in which CO_2 was bubbled into the reactor to increase the aqueous CO_2 concentration. This test allowed the pre-formed surface coating to be tested for stability in the stirred batch reactor environment,

while being exposed to a higher CO_2 content environment. Again, measured pH, aqueous calcium, and tartartic acid concentration were monitored during the reaction. Results are seen in Figure 119 and Figure 120. Accompanying SEM images are seen in Figure 121. Calcium, tartaric acid and pH remain relatively stable during the experiment. Slightly increasing pH, and calcium concentrations may be associated with regeneration of the surface coating in the hydrodynamically violent batch environment.

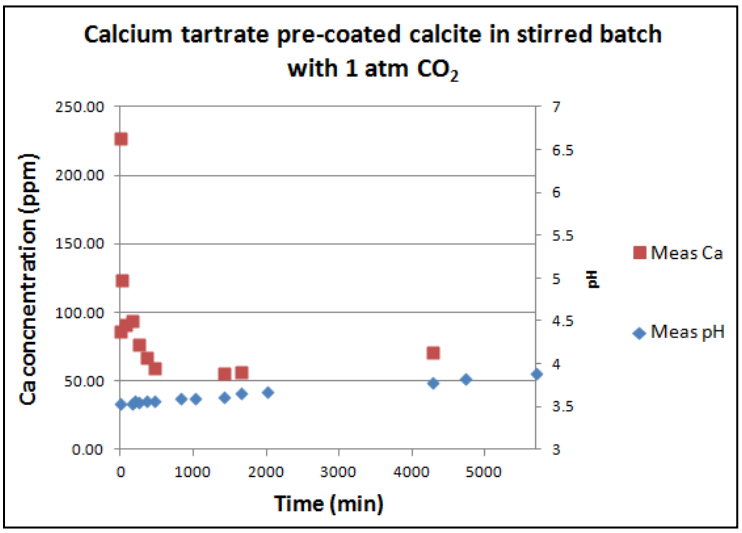

Figure 119.—Aqueous calcium and pH during the CO_2 sparged stirred batch reaction of pre-coated calcite and tartaric acid with excess tartaric acid in solution.

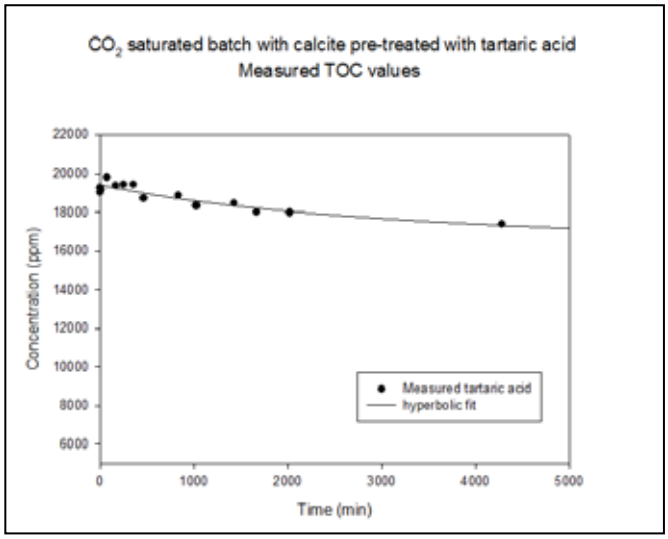

Figure 120.—Aqueous tartaric concentration during the CO_2 sparged stirred batch reaction of pre-coated calcite and tartaric acid with excess tartaric acid in solution.

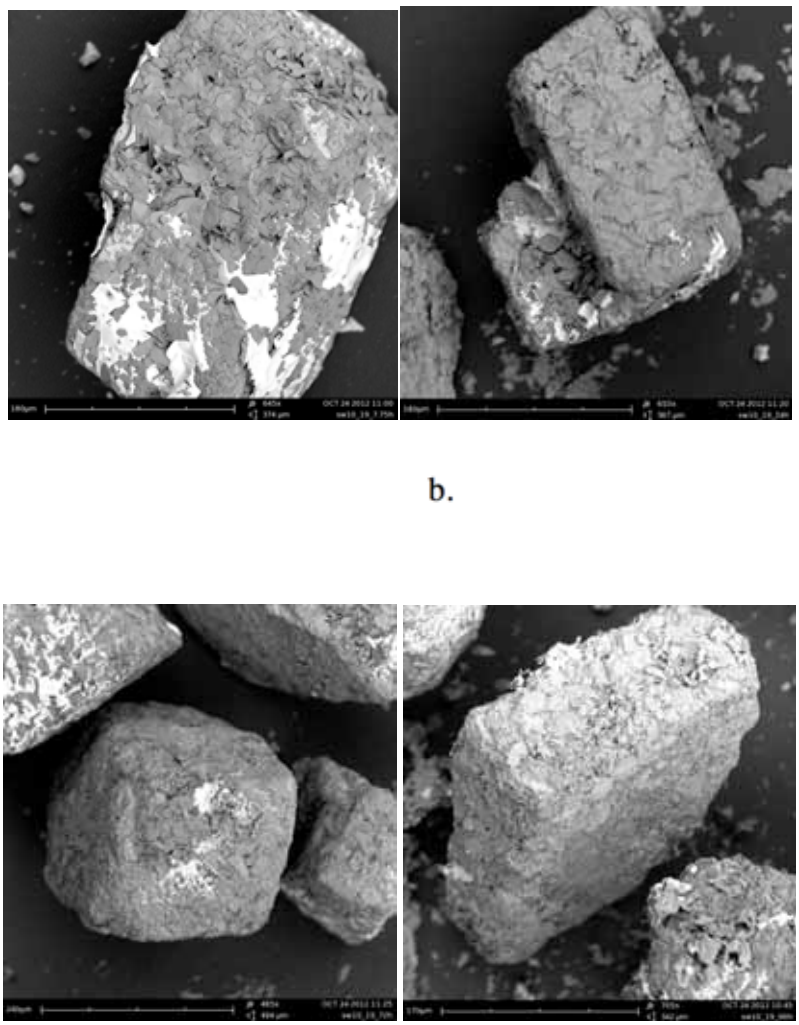

a. b.

c. d.

Figure 121.—Reaction of pre-coated solid with 1atm CO_2 sparged brine with excess tartaric acid present (a) 7 hours 45 minutes (b) 24 hours (c) 72 hours (d) 96 hours.

With the measured pH, and aqueous calcium and tartaric acid concentrations, saturation index (SI) values can be calculated for the two mineral phases present. Data shown in Figure 122 demonstrates the surface coating adequately protects the calcite from the acid and calcium

tartrate is in equilibrium with the solution rather than calcium carbonate, even after nearly 4 days of vigorous stirring in the batch reactor.

$$SI_{Calcite} \equiv Log_{10}\left\{\frac{a_{Ca^{2+}} a_{CO_3^{2-}}}{K_{sp,Calcite}(T,P)}\right\} = Log_{10}\left\{\frac{K_2 a_{Ca^{2+}} a^2_{HCO^-_3}}{K_{sp,Calcite} K_1 K_{H_2CO_3} P_{CO_2} \gamma^{CO_2}_{gas}}\right\}$$

$$SI_{CaTartrate} = Log_{10}\left\{\frac{a_{Ca^{2+}} \cdot a_{Tartrate^{2-}}}{K_{sp,CaTartrate}(T,P)}\right\}$$

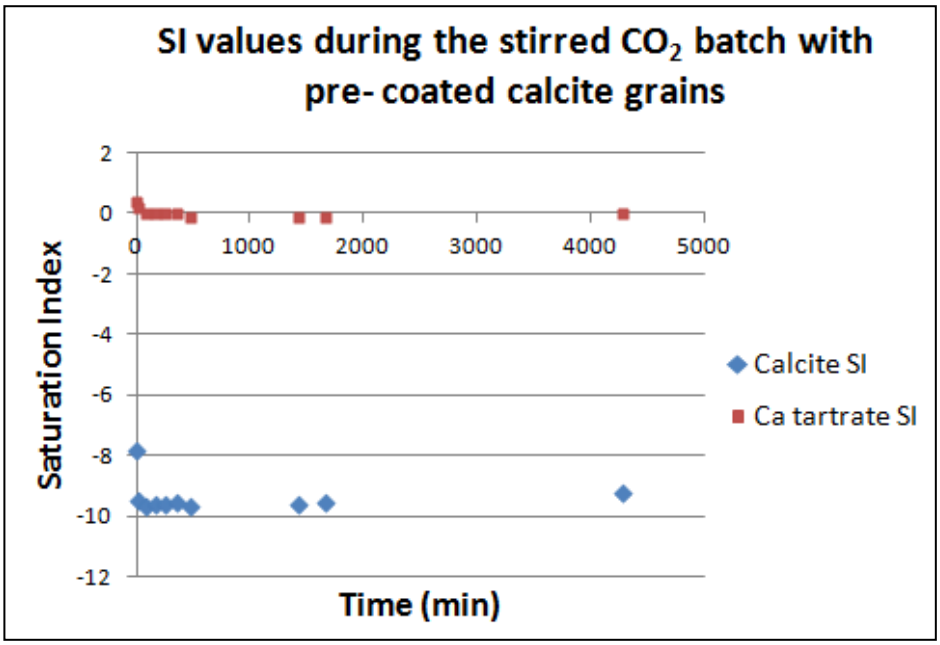

Figure 122.—Saturation index (SI) values calculated with Visual Minteq demonstrates the system is at equilibrium with calcium tartrate rather than calcite.

Fluoride at pH 3.—Measured pH during calcite surface treatment experiments run at pH 4 with two fluoride concentrations present. See Figure 123. Measured effluent fluoride and calcium concentrations during calcite dissolution experiments run at pH 4 with two fluoride treatments present can be seen in Figure 124. pH 4 was chosen because it gave an acidic environment, while still allowing a majority of the fluoride to be in the free form measurable with the fluoride ion specific electrode.

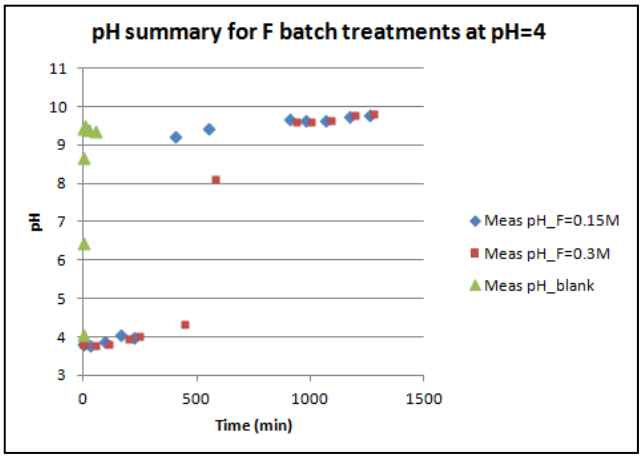

Figure 123.—Measured pH during calcite pre-coating experiment.

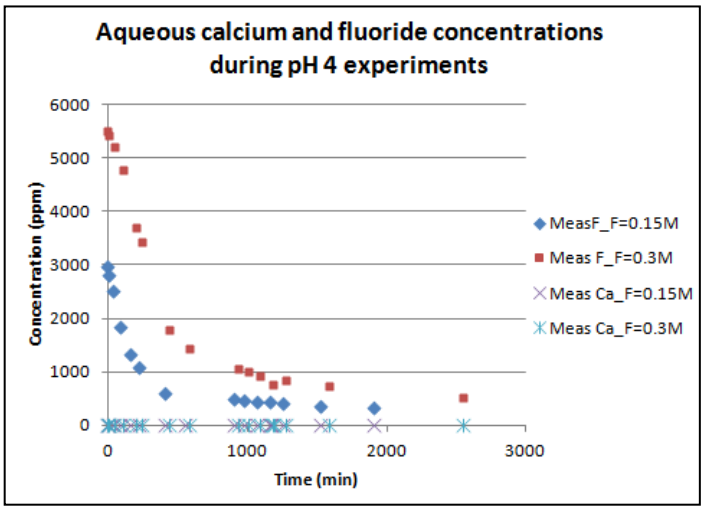

Figure 124.—Measured calcium and fluoride concentrations during calcite pre-coating experiment.

Once the calcium and fluoride concentrations were determined, the saturation index (SI) of calcite and fluorite were calculated. See Figure 125. Measured pH values were also used in the calculation of calcite saturation index to generate the carbonate term. Literature accepted K_{sp} values are shown in Table 17. SI values in 4.2.20 were calculated using the following equations:

$$SI_{Calcite} \equiv Log_{10}\left\{\frac{a_{Ca^{2+}}a_{CO_3^{2-}}}{K_{sp,Calcite}(T,P)}\right\} = Log_{10}\left\{\frac{K_2 a_{Ca^{2+}}a^2_{HCO^-_3}}{K_{sp,Calcite}K_1K_{H_2CO_3}P_{CO_2}\gamma^{CO_2}_{gas}}\right\}$$

$$SI_{Fluorite} = Log_{10}\left\{\frac{a_{Ca^{2+}}\cdot a^2_{F^-}}{K_{sp,Fluorite}(T,P)}\right\}$$

Table 18.—Literature accepted K_{sp} values for calcite and fluorite at 298°K.

Mineral phase	***Literature accepted log K_{sp}***	***K_{sp} value source***	***Implications of the K_{sp} value***
Calcite ($CaCO_3$)	-8.48	Plummer and Busenberg, 1982 NIST 46.7	At low pHs (i.e. low free CO_3 values) calcite is very soluble Solubility is a weak function of pH
Fluorite (CaF_2)	-10.5		

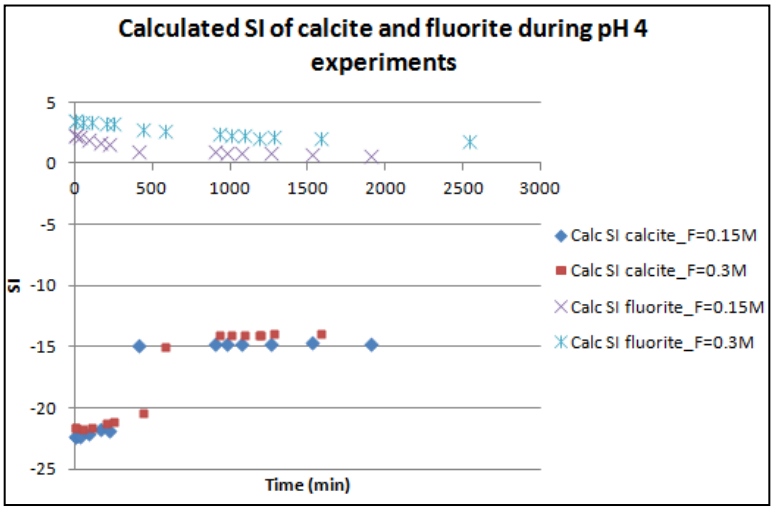

Figure 125. Calculated calcite and fluorite calcium and fluoride concentrations during calcite pre-coating experiment.

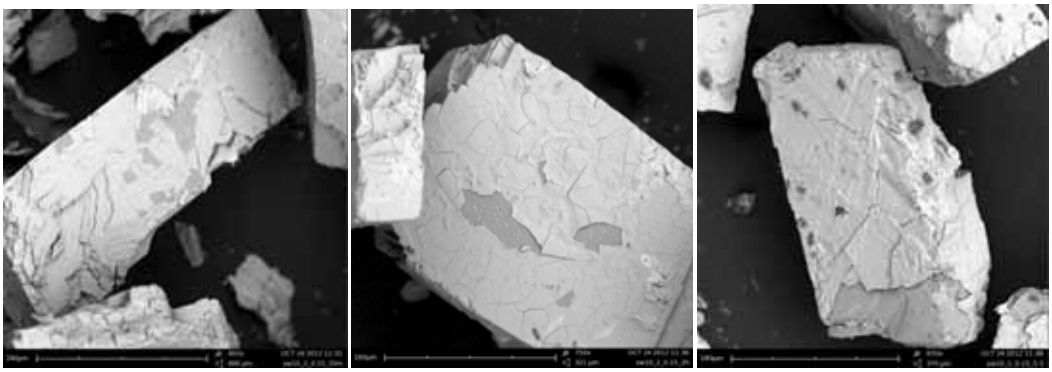

a. b. c.

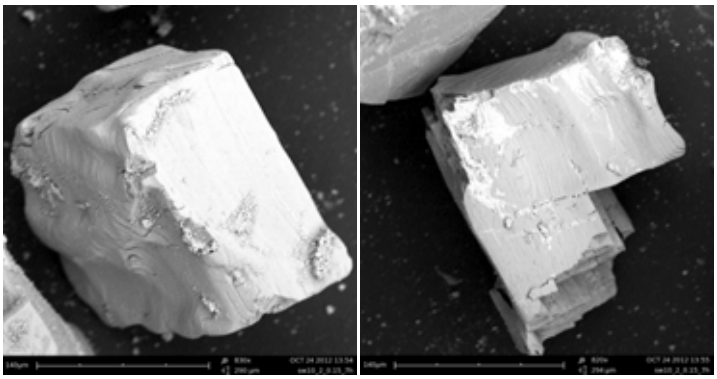

d. e.

Figure 126.—Stirred batch reaction of calcite with 0.15 M fluoride in 1 M NaCl at pH 4 adjusted by HCl a.) 33minutes b.) 2 hours c.) 5 hours 30 minutes d.) 7 hours e.) 7 hours.

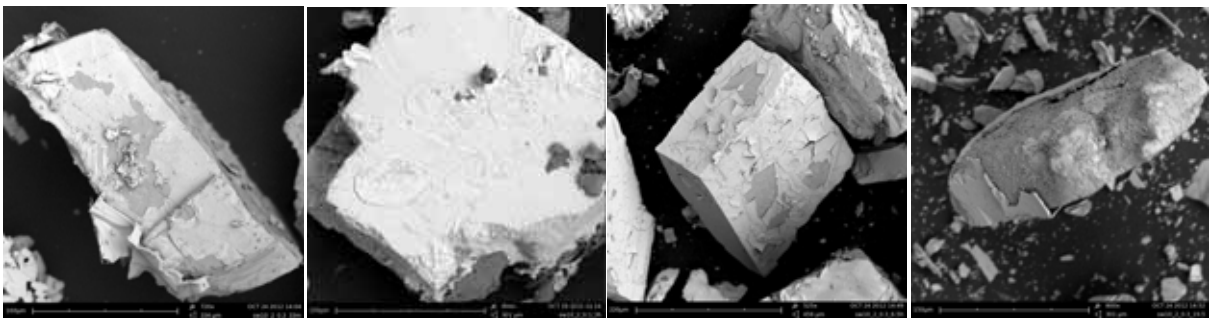

a. b. c. d.

Figure 127.—Stirred batch reaction of calcite with 0.3 M fluoride in 1 M NaCl at pH 4 adjusted by HCl a.) 33minutes b.) 3 hours c.) 6 hours 30 minutes d.) 19.5 hours.

Packed column surface coating.—This phenomenon was also tested in a column. Fresh calcite material was packed into a column and CO_2 saturated brine with excess fluoride was flowed over it to determine if a similar surface coating would form on the calcite under different hydrodynamic conditions. Also, at various times CO_2 was bubbled into the solution. Two relevant flow rates tested 0.65mL/min= 100 ft/day; 0.1mL/min=15 ft/day.

Table 19. Low pressure column experimental description and data.

Experimental description					***Effluent Analysis***		
$pH_{influent}$	***F^- (ppm)***	***Volumetric flow rate (mL/min)***	***1 atm CO_2***	***Approx PV flowed until sampled***	***Ca (ppm) Calculated****	***F (ppm) Measured***	***Measured pH***
3.64	4626	0.1	Y	14.2	3.9×10^{-4}	4394	3.84
		0.1	N	94.9	4.77×10^{-4}	3980	3.704
		0.65	Y	54.6	7.89×10^{-4}	3043	3.67
		0.65	N	243.8	8.38×10^{-4}	2948	3.67

* calcium concentration was calculated using Scalesoft Pitzer software assuming fluorite was at equilibrium in the system.

After the column experiment was conducted, the column material was carefully unpacked and SEM images of the calcite were taken. Calcite grains from near the column inlet, outlet, and middle (linear) of the column were taken. See Figure 128. The images suggest that the coating occurs evenly on the particles as well as evenly throughout the column. With very good coating obtained in the column studies, this calcite coating technique shows promise for field application.

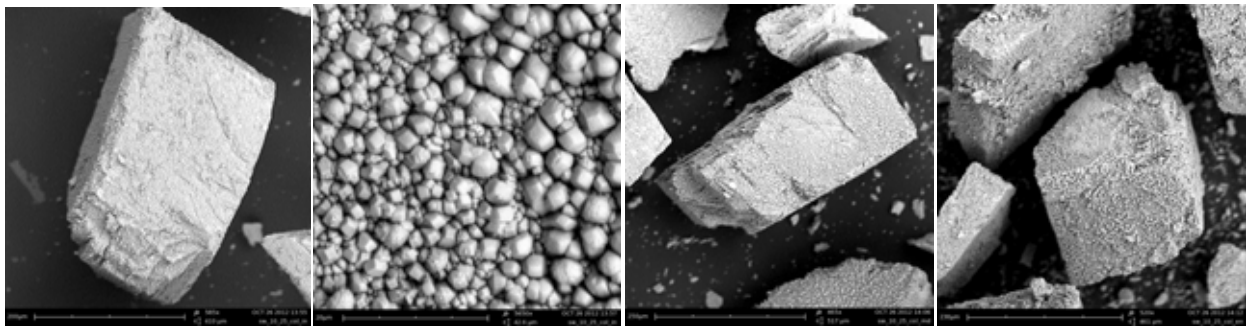

a. b. c. d.

Figure 128. Calcite obtained from the column coating study with 0.3 M fluoride in 1 M NaCl at pH 4 adjusted by HCl a.) near column inlet b.) zoom of coating on grain near column inlet c.) near column middle d.) near column outlet.

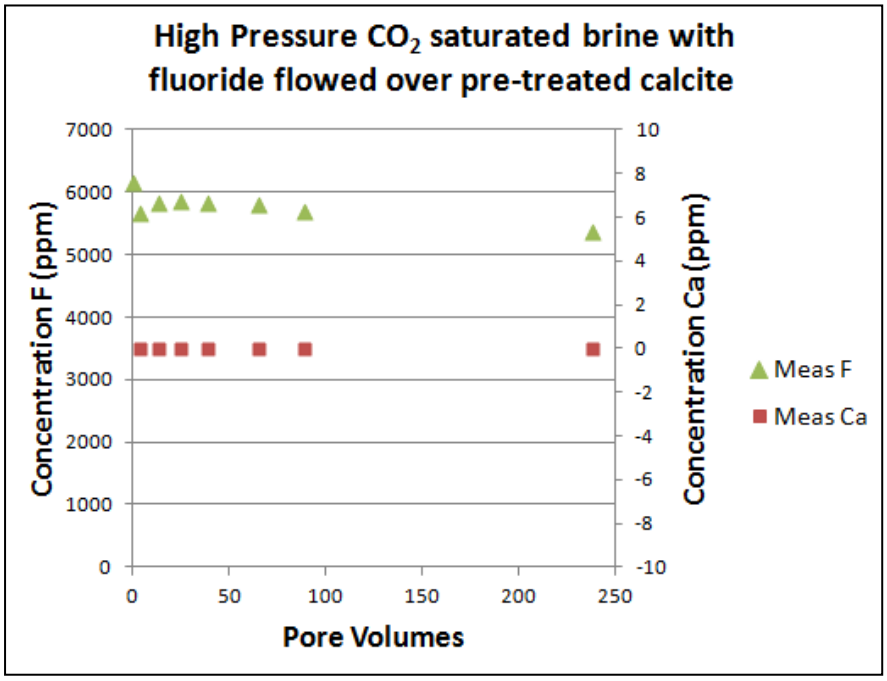

Figure 129. Summary of pre-coated calcite flowed with 1 M NaCl saturated with liquid CO_2 at 100 ft/day, 1500psi, calculated pH=2.8, calculated $CO_{2,\,aq,}$ =1.22M

Table 20. Properties of several of the acid possibilities, and the characteristics of the resulting solids coatings.

Acid tested				*Precipitated Surface Coating*			
Acid Name	***pKa 1***	***pKa 2***	***pKa 3***	***Solid Name***	***Solid Formula***	***Molar volume (mol/cm^3)***	***pK_{sp}***
No treatment	-	-	-	Calcite	$CaCO_3$	0.027	8.5
No treatment	-	-	-	Dolomite	$CaMg(CO_3)_2$	0.015	16.5
Sulfuric Acid	-3	1.99	-	Anhydrite	$CaSO_4$	0.022	4.14
Sulfuric Acid	-3	1.99	-	Gypsum	$CaSO_4 \cdot 2H_2O$	0.014	4.5
Hydrofluoric	3.2	-	-	Fluorite	CaF_2	0.041	10.5
Oxalic Acid	1.25	4.14	-	Ca Oxalate	CaC_2O_4	0.015	8.63
Tartaric Acid	3.22	4.85	-	Ca Tartrate	$CaC_4H_4O_6$	0.007	7.7
Phosphoric Acid	2.15	7.19	12.38	Brushite	$CaHPO_4 \cdot 2H_2O$	0.029	2.41

An experiment was carried out to test this treatment under more field-like conditions. Previous experiments were run at a field relevant pH, i.e. pH 3 to 4, but a high CO_2 content was not simulated. The effluent was collected after the backpressure regulator; calcium and fluoride were measured. See Figure 129.

RISK ASSESSMENT

A systematic assessment was performed to evaluate geologic risks associated geologic carbon storage in the Black Warrior Basin. Risks were evaluated in terms of likelihood and severity and plotted on a matrix, which provides a visual representation of what the risks are and how they interrelate (Figure 130). Likelihood was ranked in five classes from improbable to probable, and severity was ranked in five classes from light to multi-catastrophic. Where likelihood is improbable to unlikely or severity is light to serious, reservoirs are considered viable, although operations should proceed carefully and strive continually for improvement. Where likelihood is possible and severity is major, risks require major consideration, and

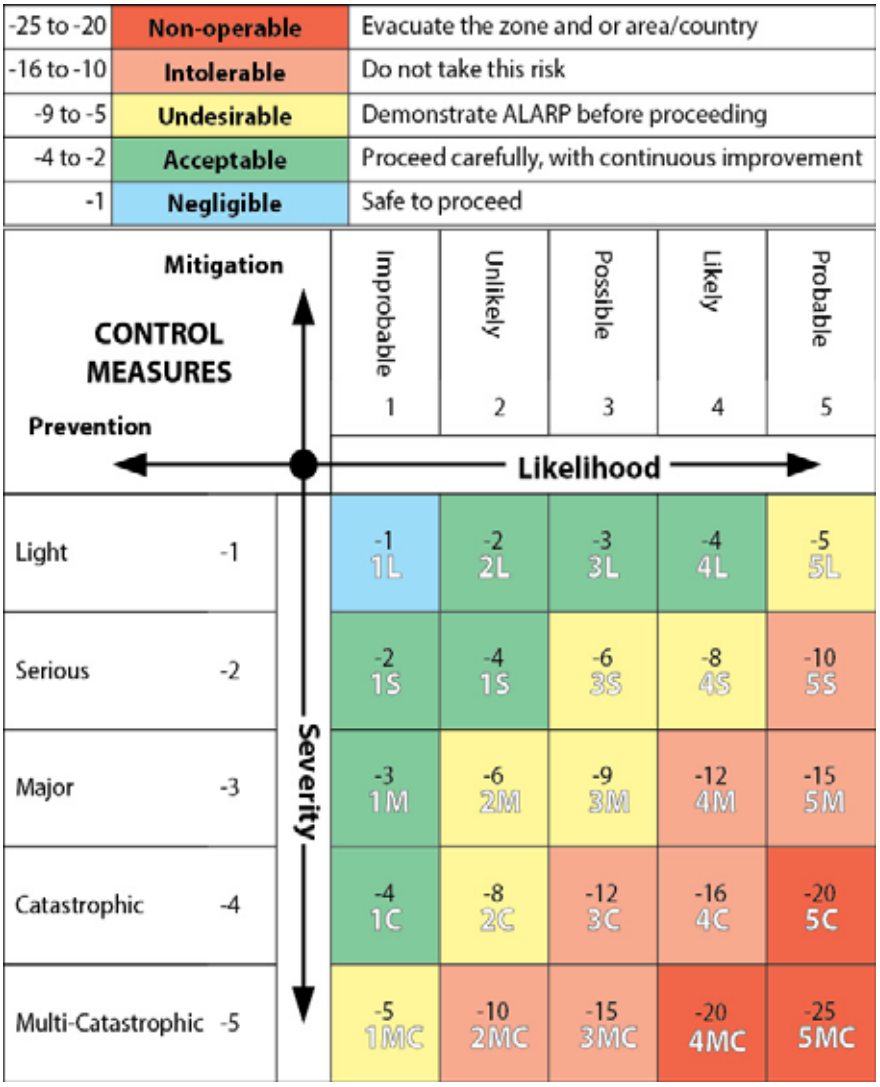

Figure 130.—Risk analysis matrix used to evaluate CO_2 storage opportunities in the Black Warrior Basin. Based on matrix in Schlumberger Hazard Analysis and Risk Control Standard 20.

operations should commence only after risks are demonstrated to be as low as reasonably practicable (ALARP). In cases where likelihood ranks as likely to probable or severity is catastrophic to multi-catastrophic, the risk simply should not be taken. If a risk is identified with high likelihood or severity, one option is to evaluate possibilities for mitigation that reduces likelihood or severity to acceptable levels.

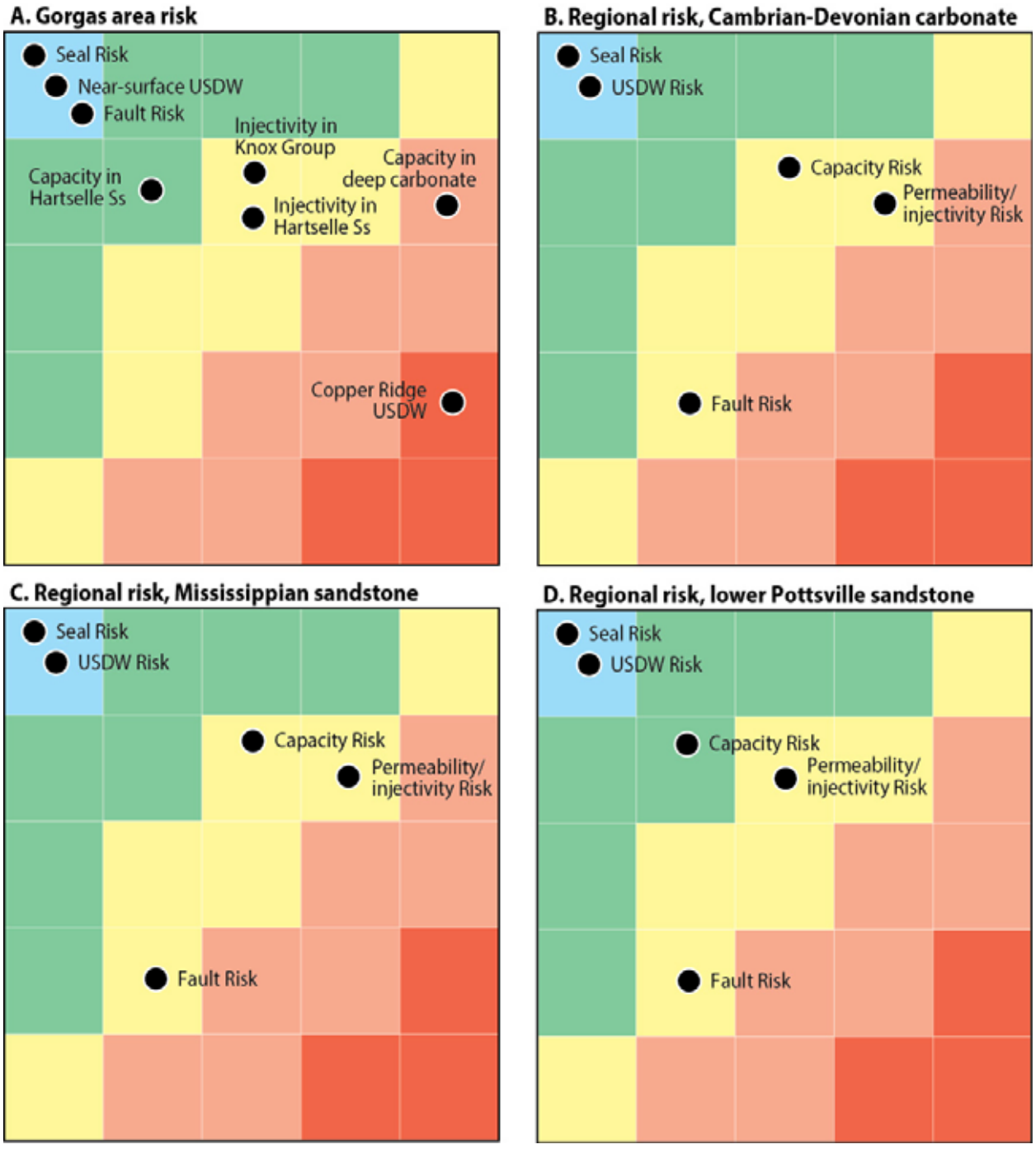

Figure 131.—Risk matrices showing relationships among geologic risks associated with CO_2 storage in the Black Warrior Basin.

Based on the evaluation of the Black Warrior basin and the Gorgas test site, five major classes of geological risk need to be evaluated: (1) capacity risk, (2) permeability and injectivity risk, (3) sealing risk, (4) fault risk, and (5) risks to USDWs. The risk of high-magnitude natural seismicity in the Black Warrior Basin is low, and careful monitoring of injection operations should be sufficient to minimize the risk of induced seismicity. One matrix was developed to evaluate opportunities in the Gorgas area, and three matrices were developed to evaluate opportunities elsewhere in the region, one for Cambrian-Devonian carbonate, one for Mississippian sandstone, and another for lower Pottsville sandstone (Figure 131). In the following paragraphs, the results of risk analysis are discussed for each matrix.

In the Gorgas area, the identified risks are highly varied (Figure 131A). Capacity in Cambrian-Devonian carbonate is limited by the low porosity and permeability determined by core analysis (Figure 60). However, the abundant and open natural fractures in the Knox Group helps provide access to what storage is available and can support high injectivity, at east early in the development lifecycle (Figure 84; Table 4). Seal quality appears to be a negligible issue for injection into the Knox Group. Reservoir models indicate that carbonate lacking natural fractures has some sealing capacity (Figure 91), and the middle Red Mountain shale forms a widespread topseal that overlies the Cambrian-Ordovician carbonate section with close proximity. Widespread shale and tight carbonate formations in the Mississippian-Pennsylvanian units provide additional storage capacity, thus making the likelihood of long-range leakage extremely low. Seismic data indicate that no imageable faults are present in the Knox Group, and the known faults in the upper Pottsville Formation are thin-skinned structures that apparently do not extend below the lower Pottsville sandstone section (Pashin and Groshong, 1998; Groshong and others, 2010). The occurrence of numerous widespread, high-quality reservoir seals (Tables 7-9)

poses negligible danger to near-surface USDWs in the Gorgas area. However, the discovery of water with TDS content close to 10,000 mg/L in the upper part of the Copper Ridge Dolomite (Figures 75, 76) effectively renders the possibility of commercial CO_2 storage in the Knox Group inoperable. Indeed, it is highly likely that fresh water that is protected by the SDWA exists in the lower part of the Copper Ridge and, as a consequence, that a Class VI UIC permit cannot be secured.

The Hartselle Sandstone presents an unusual opportunity for CO_2 storage in the Gorgas area, and the risk matrix indicates that operations are viable, but not without technological hurdles (Figure 131A). Reservoir thickness is great in the Hartselle Sandstone, although capacity is limited by low porosity compared to the sandstone in other regions (Figures 24, 60). Regardless, the high oil saturation (Figures 62, 63) indicates that a large oil resource exists in the Hartselle, and the volume of oil in place makes commercial development possible with unconventional production techniques. In essence, the Hartselle can be considered as a tight oil play. Matrix properties of the sandstone indicate significant injectivity risk, but this risk is mitigated by abundant natural fractures and the prospects for tight reservoir development (Figure 61). The extent to which the fractures will facilitate injection and oil recovery, however, requires further testing. Sealing and fault risks are considered negligible and are quite similar to those in the deep carbonate section. Risk to USDWs also is negligible, and injection operations appear viable with drilling, production, and Class II UIC permits administered by the OGB.

Aside from the Hartselle Sandstone, all commercial CO_2 storage potential is remote to the Gorgas area. As in the Gorgas area, the risk profile of the regional opportunities is varied, and individual risk elements can be expressed in diverse ways. In the Cambrian-Devonian carbonate section, capacity risk is variable, and so the reservoir must be approached with a degree of

caution (Figure 131B). Porosity is low in most intervals and tends to be highest in the Devonian limestone. Capacity is high in the Knox Group, but this is more because of great formation thickness rather than high matrix porosity. Permeability appears to be low in all of the carbonate intervals, and experience from brine injection operations indicates that natural fractures provide significant storage that is not apparent in standard geophysical log suites (Ortiz and others, 1993). Natural fractures, moreover, are required to support long-term injectivity. Experience from brine injection further indicates that formations can have vastly different performance in different areas, making identification of viable injection zones difficult in advance of drilling. Seal risk is negligible because fracturing is stratigraphically heterogeneous and the carbonate section is overlain by numerous regionally extensive shale units in the Mississippian-Pennsylvanian section. Leakage along faults is a significant risk in the Black Warrior Basin (Figure 5). Because reliable fault seals are not known in the region, care must be taken to site wells in the large, structurally coherent panels between faults. Plume geometry and migration need to be modeled and understood to ensure that CO_2 will not migrate to faults in less than a millennium. The Copper Ridge Dolomite contains saline water to the west and southwest of Plant Gorgas, and so the risk of injection to the deep USDW is negligible. As long as fault risk is controlled, then the danger posed to shallow USDWs by commercial CO_2 storage operations in Cambrian-Devonian carbonate is negligible.

The risk matrix for Mississippian sandstone is identical to that for the Cambrian-Devonian carbonate (Figure 131C). Capacity is limited by variable porosity (Figure 24), and development potential is restricted to the area of conventional oil and gas development in Fayette, Lamar, and Pickens Counties (Figures 25, 32, 37). Accordingly, any commercial injection operations will focus mainly on depleted oil and gas reservoirs. Core analyses and geophysical well logs indicate

that Mississippian sandstone reservoirs are highly heterogeneous, and injectivity is limited not only by this heterogeneity, but by the discontinuous, lensoid nature of the sandstone bodies. That being stated, brine disposal and underground natural gas storage have been successful in depleted Mississippian reservoirs, and so careful evaluation of opportunities and the development of technologies focused on heterogeneous geologic formations can unlock the storage potential. Numerous reservoir seals that have trapped natural gas over geologic time are present in the Mississippian section, and additional shale units in the Pennsylvanian section provide additional storage security. Leakage along faults is a significant risk in the conventional development area, and this risk can be minimized by focusing on reservoirs with known hydrocarbon accumulations that do not close against faults. Again, as long as fault risk is addressed, the threat of CO_2 storage operations to USDWs is negligible.

The risk matrix for lower Pottsville sandstone is similar to that for Mississippian sandstone (Figure 88D). The main difference between the matrices is that capacity and permeability/injectivity risk are reduced because of higher porosity and permeability (Figure 24). Lower Pottsville sandstone units, moreover, have higher storage capacity than Mississippian sandstone units because quartzose Pottsville sandstone bodies are thicker and more widespread. The many thick, regionally extensive marine shale units in the Pottsville Formation make seal risk negligible, and fault risk is similar to that in deeper formations. Because the Pennsylvanian sandstone units are more widespread than the Mississippian units, reservoir heterogeneity and plume migration need to be understood to ensure that CO_2 does not migrate into fault zones. As is the case with all of the other prospective geologic carbon sinks in the basin, proper management of fault risk effectively negates risk to USDWs.

The results of this analysis indicates that geologic risk in the Black Warrior Basin is varied. Tight and heterogeneous reservoir is a significant factor affecting the applicability of CO_2 sequestration technology to the basin. Many of the candidate geologic sinks, moreover, need to be characterized as dual porosity systems containing abundant natural fractures which are the principal determinants of injectivity. Tight carbonate units act as significant baffles and barriers to flow and appear to have significant sealing capacity. Numerous widespread shale units occur in Silurian through Pennsylvanian strata, and many of these units are proven reservoir seals. Normal faulting poses the most significant geologic containment risk in the basin because proven fault seals are few and far between. Hence, careful evaluation of fault risk is required to develop successful carbon storage programs. A deep USDW in the Copper Ridge Dolomite of the Knox Group was identified in the northeastern part of the basin and precludes deep development in that area. Shallow USDWs are protected by the widespread shale seals in the Mississippian-Pennsylvanian section, and avoiding the leakage risk posed by faults is the key to effective aquifer protection.

BEST PRACTICES AND LESSONS LEARNED

Geologic evaluation of saline formations and mature conventional oil and gas reservoirs in the Black Warrior Basin indicates that diverse techniques spanning a range of geologic disciplines are required to determine the CO_2 sequestration potential. Knowledge of the regional geologic framework and the location of injectivity data from brine disposal operations is essential for identifying the best opportunities for geologic storage. Constructing the framework requires assembly of all the available well logs and core analysis, as well as a comprehensive knowledge of the literature on the regional subsurface framework. Critical factors that must be

analyzed include stratigraphy, depositional architecture, structure and tectonics, basic reservoir properties, and seal properties. Assembly of these data using GIS packages enables rapid subsurface mapping and calculation of reservoir volumetrics. The resulting maps and volumetric calculations can then be used to identify the locations of prospective geologic sinks and their relationships to major sources of anthropogenic CO_2 emissions.

Development of the Gorgas test site provided crucial information on geologic storage potential that could not have been obtained from other sources. Site selection required a decision on whether to drill at Plant Gorgas or Plant Miller (Figure 47). This decision was informed by a simple screening procedure that identified obvious geological containment risk related to Appalachian folding and fracturing at the Miller steam plant. Risk was determined to be minimal at Gorgas, and so the site was developed. Geophysical well logs, cores, and seismic data were indispensible for characterizing local geology and determining the composition, facies characteristics, petrophysical properties, continuity, and geological integrity of candidate storage zones and reservoir seals.

The most valuable well logs that were run were Schlumberger's basic triple combo suite (Figure 48), which yielded accurate information on bulk rock composition, porosity, and the conductivity of formation water. Computed logs, such as the ELAN suite, helped facilitate rapid interpretation of the log results and identification of the relationship between log signature and rock type. The FMI log was indispensible because it provided vital information on fracture architecture in the Gorgas #1 borehole (Figure 79). Indeed, relying on matrix property data alone would have resulted in a major mischaracterization of reservoir properties in the Gorgas area.

Laboratory core analysis was critical for characterizing rock matrix and the contained fluids (Figures 60-63). Core analysis confirmed that implementing commercial sequestration programs

in the Gorgas area requires the application of drilling and completion technology that is tailored to tight, naturally fractured reservoirs. Rotary sidewall cores provided invaluable confirmation of well log interpretations, and whole core enabled detailed characterization of prospective sandstone and carbonate reservoirs, as well as shale seals. Analysis of fluorescence and fluid saturations (Figures 55, 62, 63) revealed significant quantities of oil throughout the Paleozoic section at Plant Gorgas and enabled quantification of what appears to be a potential oil resource in the Hartselle Sandstone. Importantly, no oil shows were observed during drilling. Hence, the importance of a robust coring program cannot be overemphasized.

Discovery of an apparent USDW in the Copper Ridge Dolomite precludes the application of commercial CO_2 injection technology to saline formations in the Knox Group, and characterization of the regional hydrogeologic framework provided insight into the origin of the deep, low-TDS formation water (Figures 66, 67). Core data reveal that a significant opportunity for geologic carbon storage exists in the Hartselle Sandstone at Plant Gorgas. The driver for this opportunity, however, is not large-scale storage capacity. Instead, the driver is the opportunity to use CO_2 injection as a potentially miscible reservoir drive mechanism to commercialize the oil recovery potential in the Hartselle Sandstone in the Gorgas area. With an estimated 450 million barrels of oil in place on the 50,000 acres around the plant, the recoverable fraction of this resource provides impetus for the installation of CO_2 separation technology at Gorgas. Infrastructure for CCUS at Gorgas can further serve as a gateway to the gigatonne-class geologic carbon sinks that exist southwest of the plant in the Knox Group and the lower Pottsville Formation.

Computer simulation of CO_2 injection is a fundamental tool for understanding reservoir volumetrics and the fate of injected and displaced fluid. A central challenge of this project was

developing a simulation engine that is capable of modeling flow in naturally fractured porous media. This was achieved through combining continuum reservoir modeling techniques with DFN modeling techniques. DFN models can simulate complex reservoir systems containing hundreds of thousands of fractures (Figure 81), but modeling flow in these models is too computationally intensive for current desktop computing hardware. A method was developed to assess fracture heterogeneity and identify model cell sizes that preserve fracture-related reservoir heterogeneity while facilitating rapid and efficient generation of numerical models for flow and transport. The results indicate that fractures in the Knox Group facilitate the development of elongate CO_2 plumes with sharp fronts (Figures 78-82). Results also indicate that weakly fractured carbonate has significant sealing capacity, at least at the scale of injection.

Analysis of shale properties was important for identifying factors that influence geologic containment of injected CO_2. Results indicate that shale seals in the Gorgas area have a range of compositional, porosity, and fluid saturation values (Tables 7, 8). Pressure-decay permeability determinations indicate that the shale units have nanodarcy-type permeability and thus major sealing capacity. The principal factor influencing shale permeability is TOC, and organic-lean shale units, like those in the Red Mountain, Pride Mountain, and Pottsville Formations form better reservoir seals than the organic-rich shale units that are prospective for oil and natural gas (Figures 83-85). Sealing capacity is further enhanced by adsorption of CO_2, which helps sealing strata serve as buffers where formations lie above capillary entry pressure. Regression analysis confirms that adsorption capacity correlates positively with TOC (Figure 106). Surprisingly, CO_2 adsorption capacity was found to correlate most strongly with clay content and inherent moisture, indicating that hydrolysis of CO_2 by clay-bound water is an important storage mechanism in sealing strata.

Risk assessment is a key step for determining the viability of geologic sequestration in saline formations and at candidate storage sites. Five basic geologic risk factors were identified for the Black Warrior Basin: capacity, injectivity, seals, faults, and risk to USDWs (Figure 131). Although capacity in the region is high, it is concentrated in low-porosity formations with low permeability. Indeed, natural fractures are required to support injectivity in most formations. Multiple widespread shale units make seal risk negligible in the Black Warrior Basin, and normal faults pose the principal containment risk in the region. Hence, sequestration wells should be located in internally coherent structural panels, and plume modeling should be used to ensure that CO_2 does not migrate into fault zones at the millennial time scale. Identification of the deep USDW in the Copper Ridge Dolomite precludes commercial injection in the Cambrian-Ordovician carbonate in the Gorgas area, but opportunities exist farther southwest where Knox strata contain saline fluid. The widespread shale units in the Mississippian-Pennsylvanian section are proven reservoir seals the protect shallow USDWs. Hence, minimizing fault risk is a central aspect of aquifer protection in the Black Warrior basin.

SUMMARY AND CONCLUSIONS

The Black Warrior Basin of Alabama contains two coal-fired power facilities that emit more than 27 Mt of CO_2 annually. Options for management of these emissions include the implementation of CCUS technology, and so the a multi-year evaluation of the geologic storage potential in the basin was conducted. Activities included regional evaluation of capacity, the development of an exploratory borehole and test site at the Gorgas steam plant, reservoir simulation, containment analysis, and risk assessment. Results of this program were synthesized

to identify best practices that can be applied to sedimentary basins in similar geologic settings, particularly the Paleozoic basins of the eastern United States.

Opportunities for geologic storage exist in Cambrian through Devonian carbonate rocks and in Mississippian-Pennsylvanian siliciclastic rocks. Volumetric assessment of storage capacity indicates that the basin has gigaton-class storage potential. The P_{50} storage estimate for carbonate rocks of the Cambrian-Ordovician Knox Group is about 650 Mt, and an additional 812 Mt of capacity was assessed in Ordovician-Devonian carbonate rocks of the Stones River Group, Red Mountain Formation, and an unnamed Devonian limestone interval. About 380 Mt of capacity was identified in Mississippian sandstone and carbonate that includes the major conventional oil and gas reservoirs in the basin. Nearly half of the capacity in the basin is in Pennsylvanian-age sandstone units of the lower Pottsville Formation, which is estimated to P_{50} capacity exceeding 1,350 Mt. Although regional capacity is high, however, widespread implementation of CCUS technology will need to employ drilling and well completion techniques designed for tight, heterogeneous formations in which natural fracture systems account for a significant portion of the available storage and injectivity.

The Gorgas #1 borehole was drilled to a depth of 4,915 feet and reached total depth in the Copper Ridge Dolomite of the Knox Group. A diverse geophysical log suite was obtained from the well, and sidewall cores and whole cores were retrieved from selected intervals in the Cambrian-Pennsylvanian section. Results of core analysis indicate that porosity and permeability are anomalously low in the Gorgas area. Low-TDS water was discovered at depth, indicating that a USDW may exist in the Copper Ridge Dolomite that was fed by meteoric recharge in the Appalachian thrust belt. However, analysis of reservoir fluids indicates that saline water is present in younger strata and that a large oil resource in the Hartselle Sandstone. In addition, the

cores revealed many open natural fractures in the Hartselle, which can be characterized as a fractured tight oil prospect. Oil saturation of the Hartselle Sandstone in the Gorgas #1 borehole, the amount of oil in place is estimated to be 9,000 barrels per acre, or 360,000 barrels per 40-acre tract of land. Directional drilling may be help unlock this oil resource, and CO_2 flooding may be promising as a technology that can mobilize the oil.

Simulation activities focused on modeling CO_2 injection in the Knox Group. A combination of continuum and DFN modeling was used, and new techniques were developed to merge discrete element models with cellular flow models. Results indicate that natural fracturing is a major source of permeability anisotropy in the Knox Group. This anisotropy affects the geometry of the injected CO_2 plume, as well as the pressure footprint associated with the plume. Zones containing weakly fractured carbonate function as confining units at the scale of the injection modeling, although the sealing integrity of these zones over geologic timespans is unknown.

Analysis of shale properties helped identify factors that influence geologic containment of CO_2. Shale seals in the Gorgas area have a range of compositional, porosity, and fluid saturation values; the shale units have nanodarcy-type permeability and thus major sealing capacity. The principal factor influencing shale permeability is TOC, and organic-lean shale forms better reservoir seals than organic-rich shale. Sealing capacity is enhanced by adsorption, which serves as a buffer where formations lie above capillary entry pressure. An important outcome of this research is that hydrolysis of CO_2 by clay-bound water augments monolayer storage by adsorption.

Five basic geologic risk factors were identified for the Black Warrior Basin. These are capacity, injectivity, seals, faults, and risk to USDWs. Although regional capacity is high, it is concentrated in tight formations in which natural fractures support injectivity. Multiple

widespread shale units make seal risk negligible in the Black Warrior Basin, and normal faults pose the most serious containment risk in the region. Therefore, sequestration wells should be located in internally coherent structural panels, and plume modeling should be used to ensure that CO_2 does not migrate into fault zones at the millennial time scale. Identification of the deep USDW in the Copper Ridge Dolomite precludes commercial injection in the Cambrian-Ordovician carbonate in the Gorgas area, but opportunities exist farther southwest where Knox strata contain saline fluid. The widespread shale units in the Mississippian-Pennsylvanian section are proven reservoir seals the protect shallow USDWs. Hence, minimizing fault risk is a central aspect of aquifer protection in the Black Warrior basin.

REFERENCES CITED

Anderson J. and Dverstrop, B. 1987, Conditional simulation of fluid flow in three-dimensional networks of discrete fractures: Water Resources Research, v. 23, p. 1876-1886.

ARI, 2006, Ten basin oriented strategies for CO_2 enhanced oil recovery: An analysis by Advanced Resources International, Arlington, Virginia, for the U. S. Department of Energy, Office of Fossil Energy, http://www.fossil.energy.gov/ programs/oilgas/eor/Ten_Basin-Oriented_CO_2-EOR_Assessments.html

Bearce, D. N., 1973, Origin of conglomerates in the Silurian Red Mountain Formation of central Alabama; their paleogeographic and tectonic significance: American Association of Petroleum Geologists Bulletin, v. 57, p. 688-701.

Box, R., L. Maxwell and D. Loren, 2004, Excellent synthetic seismograms through the use of edited logs: Lake Borgne Area, Louisiana, U.S.: TLE, v. 23, no. 3, p. 218–223.

Brenier, Y., and Jaffré, J., 1991, Upstream differencing for multiphase flow in reservoir simulation: Journal of Numerical Analysis v. 28, p. 685–696.

Cacas M.C., Ledoux, E., de Marsily, G., Title, B., Barbreau, A., Durand, E., Feuga, B., and Peaudecerf, P., 1990, Modeling fracture flow with a stochastic discrete fracture network: Calibration and validation 1, Flow model: Water Resources Research, v. 26, p. 479-489.

Campbell, A., A. Fryer, and S. Wakeman, 2005, Vertical seismic profiles – more than just a corridor stack: TLE, v. 24, no. 7, p. 694 – 697.

Chowns, T. M., 2006, Sequence Stratigraphy of the Red Mountain Formation; Setting for the Origin of the Birmingham Ironstones, *in* Chowns, T. M., ed., Birmingham Ironstone; Sequences, Deposition, and Mining History: Alabama Geological Society 43rd Annual Field Trip Guidebook, p. 1-30.

Cleaves, A. W., 1983, Carboniferous terrigenous clastic facies, hydrocarbon producing zones, and sandstone provenance, northern shelf of Black Warrior basin: Gulf Coast Association of Geological Societies Transactions, v. 33, p. 41-53.

Cleaves, A. W., and Broussard, M. C., 1980, Chester and Pottsville depositional systems, outcrop and subsurface, in the Black Warrior basin of Mississippi and Alabama: Gulf Coast Association of Geological Societies Transactions, v. 30, p. 49-60.

Dershowitz, W. S., and Einstein, H. H., 1988, Characterizing rock joint geometry with joint system models: Rock Mechanics and Rock Engineering, v. 1, p. 21-51.

DNV, 2003, Risk analysis of geologic sequestration for carbon dioxide: Høvik, Norway, Det Norske Veritas, Report R249, 109 p.

Edwards, M. G., and Zheng, H., 2010, Double-families of quasi-positive Darcy-flux approximations with highly anisotropic tensors on structured and unstructured grids: Journal of Computational Physics, v. 229, p. 594-625.

EIA, 2013, Annual Energy Outlook 2013 with Projections to 2040: U.S. Department of Energy, Energy Information Administration report DOE/EIA-0383(2013), 233 p. http://www.eia.gov/forecasts/aeo

Elizalde, M.P., Aparicio, J.L., 1995. Current theories in the calculation of activity coefficients—II. Specific interaction theories applied to some equilibria studies in solution chemistry. Talanta, 42(3): 395-400.

Faust, L. Y., 1953, A Velocity Function Including Lithologic Variation: Geophysics, v. 18, p. 271-297.

Gastaldo, R. A., Demko, T. M., and Liu, Y., 1993, Application of sequence and genetic stratigraphic concepts to Carboniferous coal-bearing strata: An example from the Black Warrior Basin, USA: Geologische Rundschau, v. 82, p. 212-226.

Gates, M. G., 2006, Structure of Wills Valley Anticline in the vicinity of Mentone, Alabama, Master's thesis, The University of Alabama, Tuscaloosa, AL, 46 p.

Geiger, S., Roberts, S., Matthai, S. K., Zoppou, C., and Burri, A., 2004, Combining finite element and finite volume methods for efficient multiphase flow simulations in highly heterogeneous and structurally complex geologic media: Geofluids, v. 4, p. 284-299.

Gerritsen, M., and Durlofsky, L., 2005, Modeling fluid flow in oil reservoirs: Annual Review of Fluid Mechanics, v. 37, p. 211-238.

Gochioco, L. M., 1991, Tuning effect and interference reflections from thin beds and coal seams: Geophysics, v. 56, no. 8, p. 1288-1295.

Groshong, R. H., Jr., Hawkins, W. B, Jr., Pashin, J. C., and Harry, D. L., 2010, Extensional structures of the Alabama promontory and Black Warrior foreland basin: Styles and relationship to the Appalachian fold-thrust belt, *in* Tollo, R.P., Bartholomew, M.J., Hibbard, J. P., and Karabinos, P. M., eds., From Rodinia to Pangea: The Lithotectonic Record of the Appalachian Region: Geological Society of America Memoir 206, p. 579-605.

Guggenheim, E.A., Turgeon, J.C., 1955. Specific interaction of ions. Trans. Faraday Soc., 74: 747-761.

Gustafsson, J.P., 2009. Visual MINTEQ, Stockhom, Sweden.

Helmig, R., 1997, Multiphase flow and transport processes in the subsurface: A contribution to the modeling of hydrosystems: Berlin, Springer-Verlag, 367 p.

Hobday, D. K., 1974, Beach and barrier island facies in the Upper Carboniferous of northern Alabama: Geological Society of America Special Paper 148, p. 209-224.

Houseknecht, D. W., 2006, Intergranular pressure solution in four quartzose sandstones: Journal of Sedimentary Research, v. 58, p. 228-246.

Huber, R., and Helmig, R., 2000, Node-centered finite volume discretizations for the numerical simulation of multiphase flow in heterogeneous porous media: Computational Geoscience, v. 4, p. 141-164.

IEA, 2009, A review of the international state of the art in risk assessment guidelines and proposed terminology for use in CO_2 geological storage: London, International Energy Agency Greenhouse Gas Programme Report 2009/TR7, 79 p.

I.P.C.C., 2005. IPCC special report on carbon dioxide capture and storage. Cambridge: Cambridge University Press for the Intergovernmental Panel on Climate Change.

Jewell, J. W., 1969, An oil and gas evaluation of North Alabama: Alabama Geological Survey Bulletin 93, 65 p.

Kallweit, R. S. and L. C. Wood, 1982, The limits of resolution of zero-phase wavelets: Geophysics, v. 47, no.7, p. 1035-1046.

Kidd, J. T., 1975, Pre-Mississippian stratigraphy of the Warrior Basin: Gulf Coast Association of Geological Societies Transactions, v. 25, p. 20-39.

___1976, Configuration of the top of the Pottsville Formation in west-central Alabama: Alabama State Oil and Gas Board Oil and Gas Map 1.

Kim, D. Y., 1964, Synthetic velocity log: 33rd Annual International SEG Meeting, New Orleans, LA, abstract.

Kopaska-Merkel, D. C., Mann, S. D., and Pashin, J. C., 2013, Sponge-microbial mound facies in Mississippian Tuscumbia Limestone, Walker County, Alabama, *in* Mancini, E. A., ed.,

Microbial Carbonate Hedberg: American Association of Petroleum Geologists Bulletin, v. 97, p. 1871-1893.

Kuuskraa, V. A., Wicks, D. E., and Thurber, J. L., 1992, Geologic and reservoir mechanisms controlling gas recovery from the Antrim Shale: Society of Petroleum Engineers, Annual Technical Conference and Exhibition, SPE Paper 24883, p. 209-224.

Kwok, F., and Tchelepi, H., 2007, Potential-based reduced Newton algorithm for nonlinear multiphase flow in porous media: Journal of Computational Physics, v. 227, p. 706–727.

Kwon, O., Kronenberg, A. K., Gangi, A. F., Johnson, B., and Herbert, B. E., 2004, Permeability of illite-bearing shale: 1. Anisotropy and effects of clay content and loading: Journal of Geophysical Research, v. 109, DOI:10.1029/2004JB003055.

Lamine, S., and Edwards, M. G., 2010, Higher order multidimensional upwind convection schemes for flow in porous media on structured and unstructured quadrilateral grids: Journal of Scientific Computing, v. 32, p. 1119–1139.

Langmuir, D., 1997. Aqueous Environmental Geochemistry. Prentice-Hall, Upper Saddle River.

Lee S. H., Lough, M. F., and Jensen, C. L., 2001, Hierarchical modeling of flow in naturally fractured formations with multiple length scales: Water Resources Research, v. 37, p. 443-455.

Linari, V., 2004, A practical approach to well-seismic data calibration: The Leading Edge, vol. 23, p. 774-755.

Liner, C. L., 2004, Elements of 3D Seismology, Second Edition: Tulsa, OK, PennWell Corporation, 608 p.

Long J. C. S., Gilmour, P., and Witherspoon, P. A., 1985, A model for steady fluid flow in random three-dimensional networks of disc-shaped fractures: Water Resources Research, v. 21, p. 1105-1115.

Macinnis, I.N., Brantley, S.L., 1992. The role of dislocations and surface morphology in calcite dissolution: Geochimica Et Cosmochimica Acta, 56(3): 1113-1126.

Maher, C. A., 2002, Structural deformation of the southern Appalachians in the vicinity of the Wills Valley Anticline, Northeast Alabama, Master's thesis, The University of Alabama, Tuscaloosa, AL, 45 p.

Marsden, D., 1989, I. Layer cake depth conversion: The Leading Edge, v. 8, p. 10-14.

Montgomery, S. L., Jarvie, D. M., Bowker, K. A., and Pollastro, R. M., 2005, Mississippian Barnett Shale, Fort Worth Basin, north-central Texas: Gas shale play with multi-trillion cubic foot potential: American Association of Petroleum Geologists Bulletin, v. 89, p. 155-175.

Neathery, T. L., and Copeland, C. W., 1983, New information on the basement and lower Paleozoic stratigraphy of north Alabama: Alabama Geological Survey open-file report, 28 p.

NETL, 2002, U. S. National Brine Wells Database: U. S. Department of Energy, National Energy Technology Laboratory, unpaginated CD-ROM.

NETL, 2010, Carbon Sequestration Atlas of the United States and Canada (3rd edition): U.S. Department of Energy, National Energy Technology Laboratory, 160 p.

NETL, 2013, Risk Analysis and Simulation for Geologic Storage of CO_2—2013 Revised Edition: U.S. Department of Energy, National Energy Technology Laboratory, Report DOE/NETL-2013/1603, 67 p.

Ortiz, I., Weller, T. F., Anthony, R. V., Frank, J., Linz, D., and Nakles, D., 1993, Disposal of produced waters: Underground injection option in the Black Warrior Basin: Tuscaloosa, University of Alabama, 1993 International Coalbed Methane Symposium Proceedings, p. 339–364.

Osborne, W.E., and Raymond, D.E., 1992, The Knox Group in the Appalachian Fold-Thrust Belt and Black Warrior Basin of Alabama: Stratigraphy and petroleum exploration: Alabama Geological Survey Circular 162, 34 p.

Pashin, J. C., 1993, Tectonics, paleoceanography, and paleoclimate of the Kaskaskia sequence in the Black Warrior basin of Alabama, *in* Pashin, J. C., ed., New Perspectives on the Mississippian System of Alabama: Alabama Geological Society 30th Annual Field Trip Guidebook, p. 1-28.

___1994, Cycles and stacking patterns in Carboniferous rocks of the Black Warrior foreland basin: Gulf Coast Association of Geological Societies Transactions, v. 44, p. 555-563.

___2004, Cyclothems of the Black Warrior basin in Alabama: eustatic snapshots of foreland basin tectonism, *in* Pashin, J. C. and Gastaldo, R. A., eds., Sequence stratigraphy, paleoclimate, and tectonics of coal-bearing strata: American Association of Petroleum Geologists Studies in Geology 51, p. 199-217.

___2007, Hydrodynamics of coalbed methane reservoirs in the Black Warrior Basin: key to understanding reservoir performance and environmental issues: Applied Geochemistry, v. 22, p. 2257-2272.

___2008, Gas shale potential of Alabama: Tuscaloosa, Alabama, University of Alabama, College of Continuing Studies, 2008 International Coalbed & Shale Gas Symposium Proceedings, paper 0808, 13 p.

___2009, Shale gas plays of the southern Appalachian thrust belt: Tuscaloosa, Alabama, University of Alabama, College of Continuing Studies, 2009 International Coalbed & Shale Gas Symposium Proceedings, paper 0907, 14 p.

Pashin, J. C., Grace, R. L. B., and Kopaska-Merkel, D. C., 2010, Devonian shale plays in the Black Warrior basin and Appalachian thrust belt of Alabama: Tuscaloosa, Alabama, University of Alabama, College of Continuing Studies, 2010 International Coalbed & Shale Gas Symposium Proceedings, paper 1016, 20 p.

Pashin, J. C., and Groshong, R. H., Jr., 1998, Structural control of coalbed methane production in Alabama: International Journal of Coal Geology, v. 38, p. 89-113.

Pashin, J. C., Guohai Jin, Chunmiao Zheng, Song Chen, and McIntyre, M. R., 2008, Discrete fracture networks for risk assessment of carbon sequestration in coal: Final Technical Report, U.S. Department of Energy, National Energy Technology Laboratory, Award DE-FC26-05NT42435, 118 p.

Pashin, J. C., Kopaska-Merkel, D. C., Arnold, A. C., and McIntyre, M. R., 2011, Geological foundation for production of natural gas from diverse shale formations: Research Partnership to Secure Energy for America (RPSEA) Final Report 07122.17.01, 156 p.

Pashin, J. C., and Kugler, R. L., 1992, Delta-destructive spit complex in Black Warrior basin: facies heterogeneity in Carter sandstone (Chesterian), North Blowhorn Creek oil unit, Lamar County, Alabama: Gulf Coast Association of Geological Societies Transactions, v. 42, p. 305-325.

Pashin, J. C., and Kugler, R. L., 1996, Heterogeneity in delta-destructive oil reservoirs: deposition and diagenesis of the Carter sandstone (Upper Mississippian), Black Warrior basin, Alabama, *in* Johnson, K. S., ed., Deltaic Reservoirs in the Southern Midcontinent, 1993 Symposium: Oklahoma Geological Survey Circular 98, p. 279-285.

Pashin, J. C., McIntyre, M. R., Carroll, R. E., Groshong, R. H., Jr., and Bustin, R. M., 2009, Carbon sequestration and enhanced recovery potential of mature coalbed methane reservoirs in the Black Warrior basin, *in* Grobe, M., Pashin, J. C., and Dodge, R. L., eds., Carbon dioxide sequestration in geological media: State of the science: American Association of Petroleum Geologists Studies in Geology 59, in press.

Pashin, J. C., McIntyre, M. R., Mann, S. D., Kopaska-Merkel, D. C., Varonka, M., and Orem, W., in press, Relationships between Water and Gas Chemistry in Mature Coalbed Methane Reservoirs of the Black Warrior Basin: International Journal of Coal Geology, http://dx.doi.org/10.1016/j.coal.2013.10.002.

Pashin, J. C., and Payton, J. W., 2005, Geological sinks for carbon sequestration in Alabama, Mississippi, and the Florida panhandle: Alabama Geological Survey, Final Report to Southern States Energy Board, Subgrant SSEB-NT41980-997-GSA-2004-00, unpaginated CD-ROM.

Pashin, J. C., and Rindsberg, A. K., 1993, Origin of the carbonate-siliciclastic Lewis cycle (Upper Mississippian) in the Black Warrior basin of Alabama: Alabama Geological Survey Bulletin 157, 54 p.

Pashin, J. C., Ward, W. E., II, Winston, R. B., Chandler, R. V., Bolin, D. E., Richter, K. E., Osborne, W. E., and Sarnecki, J. C., 1991, Regional analysis of the Black Creek-Cobb coalbed-methane target interval, Black Warrior basin, Alabama: Alabama Geological Survey Bulletin 145, 127 p.

Peaceman, D. W., 1977, Fundamentals of numerical reservoir simulation: Amsterdam, Elsevier, 190 p.

Pearce, P. J., 2002, Seismic interpretation and structural restoration of a transect from Murphree's Valley to the Talladega National Forest: The Appalachian Valley and Ridge of Alabama, Master's thesis, The University of Alabama, Tucsaloosa, AL, 51 p.

Plummer, L.N., Wigley, T.M.L., 1976. Dissolution of calcite in CO2-saturated solutions at 25 degrees C and 1 atm total pressure. Geochimica Et Cosmochimica Acta, 40(2): 191-202.

Pokrovsky, O.S., Golubev, S.V., Schott, J., 2005. Dissolution kinetics of calcite, dolomite and magnesite at 25°C and 0 to 50 atm pCO_2. Chemical Geology, 217(3-4): 239-255.

Rheams, K. F., and Neathery, T. L., 1988, Characterization and geochemistry of Devonian oil shale, north Alabama, northwest Georgia, and south-central Tennessee (a resource evaluation): Alabama Geological Survey Bulletin 128, 214 p.

Rodgers, John, 1950, Mechanics of Appalachian folding as illustrated by the Sequatchie anticline, Tennessee and Alabama: American Association of Petroleum Geologists Bulletin, v. 34, p. 672-681.

Ross, D. J. K., and Bustin, R. M., 2008, Characterizing the shale gas resource potential of Devonian-Mississippian strata in the Western Canada sedimentary basin: Application of an integrated formation evaluation: American Association of Petroleum Geologists Bulletin, v. 92, p. 87-125.

Rudman, A. J., J. F. Whaley, R. F. Blakely, and M. E. Biggs, 1975, Transformation of resistivity to pseudo velocity logs: American Association of Petroleum Geologists Bulletin, v. 59, p.1151-1165.

Rutter, R.S., 2012, A geophysical characterization of stratigraphy in the eastern Black Warrior Basin underlying Gorgas Power Generation plant, Walker County, Alabama, Master's thesis, The University of Alabama, Tuscaloosa, AL, 46 p.

Sheriff, R. E., 1999, Encyclopedic Dictionary of Exploration Geophysics, Third Edition: Society of Exploration Geophysicists, 384 p.

Smith, J. H., 2007, A method for calculating pseudo sonics from e-logs in a clastic geologic setting: Gulf Coast Association of Geological Societies Transactions, v. 57, p. 1-4.

Snow, D. T., 1969, Anisotropic permeability of fractured media: Water Resources Research, v. 5, p. 1273-1289.

Soeder, D. J., 1988, Porosity and permeability of eastern Devonian gas shale: SPE Formation Evaluation, March 1988, p. 116-124.

Teimoori A., Chen, Z., and Rahman, S., 2003, Calculation of permeability tensor using boundary element method provides a unique tool to simulate naturally fractured reservoirs, Society of Petroleum Engineers Paper 84545, 8 p.

Thomas, W. A., 1972, Mississippian stratigraphy of Alabama: Alabama Geological Survey Monograph 12, 121 p.

___1974, Converging clastic wedges in the Mississippian of Alabama: Geological Society of America Special Paper 148, p. 187-207.

___1972, Mississippian stratigraphy of Alabama: Alabama Geological Survey Monograph 12, 121 p.

___1985, The Appalachian-Ouachita connection: Paleozoic orogenic belt at the southern margin of North America: Annual Review of Earth and Planetary Sciences, v. 13, p. 175-199.

___1988, The Black Warrior basin, in Sloss, L. L., ed., Sedimentary cover — North American craton: Geological Society of America, The Geology of North America, v. D-2, p. 471-492.

___1995, Diachronous thrust loading and fault partitioning of the Black Warrior foreland basin within the Alabama recess of the Late Paleozoic Appalachian-Ouachita thrust belt: Society of Economic Paleontologists and Mineralogists Special Publication, v. 52,p. 111-126.

___2001, Mushwad: Ductile duplex in the Appalachian thrust belt in Alabama:American Association of Petroleum Geologists Bulletin, v. 85, p. 1847-1869.

Thomas, W. A., and Bayona, G., 2005, The Appalachian thrust belt in Alabama and Georgia: thrust-belt structure, basement structure, and palinspastic reconstruction:Alabama Geological Survey Monograph 16, 48 p.

Thomas, W. A., and Mack, G. H., 1982, Paleogeographic relationship of a Mississippian barrier-island and shelf-bar system (Hartselle Sandstone) in Alabama to the Appalachian-Ouachita orogenic belt: Geological Society of America Bulletin, v. 93, p. 6-19.

Tomson, M., Kan, A., 2011. ScaleSoft Pitzer.

Tsang, C., Doughty, C., Rutqvist, J., Xu, T., 2007. Modeling to Understand and Simulate Physico-Chemical Process of CO2 Geological Storage. In: Carbon Capture and Sequestration: Integrating Technology, Monitoring and Regulation.

Young, A., Low, P. F., and McLatchie, A. S., 1964, Permeability studies of argillaceous rocks: Journal of Geophysical Research, v. 69, p. 4237-4245.

APPENDIX A

CHECK-SHOT REPORT

SRD = Seismic Reference Datum, OWT = One-way travel time, KB = Kelly Bushing, RMS = Root mean squared.

Client and Well Information
Company: Alabama Power Company
Well: Gorgas#1
Field: Wildcat
County: Walker
State: Alabama
API Number: NA
Logging Date: 20-Sep-2011

Survey Information
SRD: 800.0 ft **KB elevation:** 389.84 ft **GL elevation:** 376.16 ft
Source Type: Vibrosies
Source Depth below KB: 13.74 ft
Source Distance from Wellhead: 162.0 ft
Source Azimuth from North: 345.0 deg
Velocity of Medium (Source to Sensor): 15000 ft/s
Velocity of Medium (Source to SRD): 15000 ft/s

LEVEL NUMBER FROM SRD	**VERTICAL** DEPTH FROM (owt)	**MEASURED** DEPTH KB (owt)	**OBSERVED** TRAVEL TIME	**VERTICAL** TRANSIT TIME-SRD	**ACOUSTIC** AVERAGE VELOCITY	**ACOUSTIC** RMS VELOCITY
ft	ft	s	s	ft/s	ft/s	ft/s
1	0	-484	0			
2	833.9	349.9	0.0517	0.0798	10456	10456
3	883.9	399.9	0.0546	0.0835	10585	10602
4	933.9	449.9	0.0582	0.0877	10648	10667
5	984	500	0.0619	0.0919	10709	10731
6	1034	550	0.0656	0.096	10776	10801
7	1084	600	0.0689	0.0995	10893	10934
8	1134	650	0.0724	0.1033	10974	11021
9	1184	700	0.0759	0.107	11069	11126
10	1234	750	0.0799	0.1112	11100	11156
11	1284	800	0.0838	0.1152	11148	11205
12	1334	850	0.0878	0.1193	11180	11235
13	1384	900	0.0914	0.123	11252	11314

14	1434	950	0.0951	0.1268	11306	11369
15	1483.9	999.9	0.0989	0.1307	11351	11415
16	1533.9	1049.9	0.1027	0.1346	11392	11456
17	1583.9	1099.9	0.1063	0.1383	11455	11524
18	1633.9	1149.9	0.1097	0.1418	11524	11599
19	1683.9	1199.9	0.1132	0.1453	11590	11669
20	1733.9	1249.9	0.1165	0.1486	11664	11752
21	1783.9	1299.9	0.12	0.1522	11719	11810
22	1833.9	1349.9	0.1235	0.1557	11776	11871
23	1883.8	1399.8	0.1271	0.1593	11823	11919
24	1933.8	1449.8	0.1306	0.1629	11868	11965
25	1983.8	1499.8	0.1342	0.1665	11913	12012
26	2033.8	1549.8	0.1379	0.1703	11942	12039
27	2083.9	1599.9	0.1416	0.174	11978	12076
28	2133.9	1649.9	0.1452	0.1776	12015	12113
29	2183.9	1699.9	0.1485	0.181	12068	12170
30	2233.9	1749.9	0.1518	0.1842	12126	12233
31	2284.1	1800.1	0.1548	0.1873	12192	12308
32	2334.1	1850.1	0.1582	0.1907	12241	12359
33	2384.1	1900.1	0.1612	0.1938	12303	12428
34	2434.1	1950.1	0.1646	0.1972	12343	12469
35	2483.5	1999.5	0.168	0.2005	12384	12512
36	2533.5	2049.5	0.1713	0.2039	12423	12553
37	2583.5	2099.5	0.1748	0.2075	12453	12582
38	2633.5	2149.5	0.1779	0.2106	12508	12642
39	2683.8	2199.8	0.1816	0.2142	12528	12660
40	2733.8	2249.8	0.1847	0.2174	12577	12714
41	2784.1	2300.1	0.1882	0.2209	12605	12741
42	2834.1	2350.1	0.1911	0.2238	12665	12810
43	2884.1	2400.1	0.194	0.2267	12723	12875
44	2934.1	2450.1	0.1965	0.2292	12799	12969
45	2984	2500	0.1993	0.232	12860	13039
46	3033.8	2549.8	0.2022	0.2349	12916	13101
47	3084	2600	0.2053	0.238	12959	13147
48	3134	2650	0.2082	0.241	13006	13197
49	3184	2700	0.2115	0.2442	13036	13227
50	3234	2750	0.2146	0.2474	13074	13266
51	3269.1	2785.1	0.217	0.2498	13088	13278
52	3384	2900	0.2263	0.2591	13061	13246
53	3434	2950	0.2293	0.2621	13104	13292
54	3484	3000	0.232	0.2648	13157	13352

55	3534	3050	0.2346	0.2674	13218	13425
56	3584	3100	0.2373	0.2701	13267	13480
57	3634	3150	0.24	0.2728	13323	13545
58	3684	3200	0.2429	0.2758	13359	13583
59	3734	3250	0.2456	0.2784	13411	13641
60	3783.9	3299.9	0.2484	0.2813	13453	13686
61	3833.9	3349.9	0.2513	0.2841	13495	13732
62	3884	3400	0.2543	0.2872	13524	13761
63	3934	3450	0.2574	0.2902	13555	13793
64	3983.9	3499.9	0.2603	0.2931	13590	13829
65	4033.9	3549.9	0.2632	0.296	13626	13867
66	4083.9	3599.9	0.266	0.2989	13664	13907
67	4133.9	3649.9	0.2687	0.3016	13708	13955
68	4183.9	3699.9	0.2715	0.3044	13746	13996
69	4233.9	3749.9	0.2741	0.307	13790	14046
70	4283.9	3799.9	0.2769	0.3098	13829	14088
71	4333.9	3849.9	0.2794	0.3123	13877	14142
72	4384	3900	0.2819	0.3148	13925	14198
73	4434	3950	0.2844	0.3173	13973	14253
74	4484	4000	0.287	0.3199	14019	14305
75	4534	4050	0.2894	0.3223	14066	14358
76	4584	4100	0.2919	0.3248	14111	14410
77	4634	4150	0.2943	0.3272	14162	14470
78	4684	4200	0.2968	0.3297	14207	14521
79	4734	4250	0.2991	0.332	14258	14581
80	4784	4300	0.3015	0.3344	14306	14637
81	4834	4350	0.3039	0.3368	14353	14691
82	4884	4400	0.3063	0.3392	14399	14743
83	4934	4450	0.3087	0.3417	14441	14791
84	4984	4500	0.3112	0.3441	14484	14839
85	5034	4550	0.3136	0.3466	14526	14885
86	5084	4600	0.316	0.3489	14570	14935
87	5134	4650	0.3183	0.3512	14618	14991
88	5184	4700	0.3206	0.3535	14663	15044
89	5234	4750	0.3229	0.3559	14708	15094
90	5284	4800	0.3253	0.3582	14750	15142
91	5334	4850	0.3276	0.3606	14793	15191

Appendix B

VELOCITY REPORT

SRD = Seismic Reference Datum, OWT = One-way travel time, KB = Kelly Bushing, RMS = Root mean squared

Client and Well Information
Company: Alabama Power Company
Well: Gorgas#1
Field: Wildcat
County: Walker
State: Alabama
API Number: NA
Logging Date: 20-Sep-2011

Survey Information
SRD: 800.0 ft **KB elevation:** 389.84 ft **GL elevation:** 376.16 ft
Source Type: Vibrosies
Source Depth below KB: 13.74 ft
Source Distance from Wellhead: 162.0 ft
Source Azimuth from North: 345.0 deg
Velocity of Medium (Source to Sensor): 15000 ft/s
Velocity of Medium (Source to SRD): 15000 ft/s

TWO WAY TRAVEL TIME FROM SRD (ms)	MEASURED DEPTH FROM KB (ft)	VERTICAL DEPTH FROM SRD (ft)	AVERAGE VELOCITY SRD/GEO (ft/S)	RMS VELOCITY (ft/s)	INTERVAL VELOCITY (ft/s)
0	-410.2	0	10153	10153	10153
10	-359.4	50.8	10153	10153	10153
20	-308.6	101.5	10153	10153	10153
30	-257.9	152.3	10153	10153	10153
40	-207.1	203.1	10153	10153	10153
50	-156.3	253.8	10153	10153	10153
60	-105.6	304.6	10153	10153	10153
70	-54.8	355.4	10153	10153	10153
80	-4	406.1	10153	10153	10153
90	46.7	456.9	10153	10153	10153
100	97.5	507.7	10153	10153	10153
110	148.3	558.4	10153	10153	10153
120	199	609.2	10153	10153	10153
130	249.8	660	10153	10153	10153

140	300.6	710.7	10153	10153	10215
150	351.6	761.8	10156	10157	12927
160	416.3	826.4	10331	10354	11925
170	475.9	886.1	10424	10453	12157
180	536.7	946.9	10520	10554	13590
190	604.6	1014.8	10682	10737	13294
200	671.1	1081.3	10812	10879	12687
210	734.5	1144.7	10902	10974	12311
220	796.1	1206.3	10966	11041	13062
230	861.4	1271.6	11057	11140	12724
240	925	1335.2	11126	11212	12584
250	988	1398.1	11185	11271	12574
260	1050.8	1461	11238	11327	14774
270	1124.7	1534.9	11369	11474	14458
280	1197	1607.1	11479	11595	14279
290	1268.4	1678.5	11576	11700	12725
300	1332	1742.2	11614	11738	13538
310	1399.7	1809.9	11676	11801	14065
320	1470	1880.2	11751	11879	14573
330	1542.9	1953	11837	11970	11817
340	1602	2012.1	11836	11966	14797
350	1676	2086.1	11921	12058	15933
360	1755.6	2165.8	12032	12183	15117
370	1831.2	2241.4	12116	12272	15922
380	1910.8	2321	12216	12382	14520
390	1983.4	2393.6	12275	12444	15970
400	2063.3	2473.4	12367	12545	15116
410	2138.8	2549	12434	12615	14554
420	2211.6	2621.8	12485	12667	15032
430	2286.8	2696.9	12544	12733	16820
440	2370.9	2781	12641	12845	19290
450	2467.3	2877.5	12789	13024	17628
460	2555.5	2965.6	12894	13143	16418
470	2637.6	3047.7	12969	13222	15886
480	2717	3127.1	13030	13284	13607
490	2785	3195.2	13042	13292	11655
500	2843.3	3253.5	13014	13261	13265
510	2909.6	3319.8	13019	13274	19201
520	3005.6	3415.8	13138	13413	18124
530	3096.2	3506.4	13232	13517	17084

540	3181.7	3591.8	13303	13593	19468
550	3279	3689.2	13415	13723	16533
560	3361.7	3771.8	13471	13780	15905
570	3441.2	3851.4	13514	13820	17503
580	3528.7	3938.9	13582	13893	18185
590	3619.6	4029.8	13661	13977	18629
600	3712.8	4122.9	13743	14067	18742
610	3806.5	4216.7	13825	14157	19823
620	3905.6	4315.8	13922	14267	19669
630	4004	4414.1	14013	14369	20234
640	4105.1	4515.3	14110	14479	20493
650	4207.6	4617.7	14209	14591	20979
660	4312.5	4722.6	14311	14709	20600
670	4415.5	4825.6	14405	14814	19738
680	4514.2	4924.3	14484	14898	20772
690	4618	5028.2	14575	15000	21209
700	4724.1	5134.2	14669	15107	21204
710	4830.1	5240.3	14762	15210	